Robot Confidence Modeling and Role Change in Physical Human-Robot Collaboration

by

Antony Tran

A thesis submitted in partial fulfilment of the
requirements for the degree of Doctor of Philosophy

at the
Centre for Autonomous Systems
Faculty of Engineering and Information Technology
University of Technology Sydney

March 2019

Certificate of Original Authorship

I certify that the work in this thesis has not previously been submitted for a degree nor has it been submitted as part of the requirements for a degree except as fully acknowledged within the text.

I also certify that this thesis has been written by me. Any help that I have received in my research work and the preparation of the thesis itself has been acknowledged. In addition, I certify that all information sources and literature used are indicated in the thesis.

This research is supported by the Australian Government Research Training Program

Signed: Production Note:
Signature removed prior to publication.

Date: 21/02/2019

Robot Confidence Modeling and Role Change in Physical Human-Robot Collaboration

by

Antony Tran

A thesis submitted in partial fulfilment of the requirements for the degree of Doctor of Philosophy

Abstract

In physical Human-Robot Collaboration, the human is generally in control of the interaction while the robot provides assistance to its human co-worker. However, with the increasing level of intelligence of robot co-workers, peer-to-peer interaction is expected and believed to be an ideal approach to collaboration between the human and the robot in a collaborative activity. In the peer-to-peer collaboration, the human and its robot co-worker would observe each other's actions and intervene if one detects changes of their counterpart during the interaction which could negatively impact the task. Current research on safe pHRC only considers role change to be initiated from the human's perspective, not from the robot's perspective. This thesis aims to address three research challenges in pHRC: the robot's perception of its human co-worker during pHRC, modeling the robot's confidence in its human co-worker and how a robot would decide whether and when it should intervene (by taking control) in its human co-worker's actions during pHRC.

This research first developed effective methods that enable the robot's perception of its human co-worker during pHRC. The human's grasping pattern and grasping strength on a handlebar, the commonly used interface in pHRC, are used by the robot to identify the orientation of the human co-worker's hand and monitor the human's reaction to unexpected events. A method for identifying the human's hand orientation and detecting the human's reaction to unexpected events was developed by analyzing the human's grasping pattern and grasping strength.

The thesis then explored how the robot's confidence in its human co-worker during pHRC can be modeled. A novel robot confidence framework was developed for modeling the robot's confidence using the robot's perception of the human's performance. The framework was evaluated in a number of pHRC case studies where a robot and its human co-worker worked collaboratively.

Finally, this thesis explored how the robot's confidence in its human co-worker can be used to decide whether and when the robot should initiate a role change. A confidence-based role change method was developed. Experimental verification of the role change method was conducted in a collaborative grit-blasting operation between a human and a robot. The results demonstrated that the method successfully identified the points during a pHRC where the robot should initiate a role change and take the control away from its human co-worker.

Acknowledgements

I would like to take this opportunity to acknowledge and give thanks for those who have stuck by me and assisted me throughout my candidature. Without their support and encouragement this work would not have been possible.

Firstly would like to thank my supervisor Prof. Dikai Liu who started me on the path of robotics research many years ago. Without the opportunity that he provided me and the direction and support he has given me over the years this work would not have been possible.

I would also like to thank my co-supervisor Dr. Ravindra Ranasinghe and Dr. Marc Carmichael who provided their technical expertise and advice during my candidature. The work in this thesis may not have gone as smoothly as it had if it were not for the both of you.

To the professors, researchers, engineers and students at the Center for Autonomous systems at the UTS, I give my thanks for giving me inspiration for being there when I needed someone to bounce some crazier ideas off.

Finally, I'd like to thank my family for their love and support over the last four years. Without you I would not be who and where I am today.

Contents

List of Figures

List of Tables

Acronyms & Abbreviations

CAS	Centre for Autonomous Systems
UTS	University of Technology, Sydney
pHRI	physical Human-Robot Interaction
HRI	Human-Robot Interaction
HHI	Human-Human Interaction
HCI	Human-Computer Interaction
ANBOT	Assistance-as-Needed-roBOT
FSPN	Fluid Stochastic Petri Net
SVM	Support Vector Machine
pHRC	physical Human-Robot Collaboration
TMMAS	Thrumode Matrix Array Sensor
PCA	Principal Component Analysis
LoA	Level of Autonomy
ARMAV	Auto-Regressive Moving Average Vector Form

Nomenclature

	General Formatting Style
$\sum\{\cdot\}$	Summation.
$\prod\{\cdot\}$	Product.
$\dot{\square}$	First derivative.
$\ddot{\square}$	Second derivative.
$\lvert\square\rvert$	Absolute value.
$\bar{\square}$	Average.
σ	Standard Deviation.
	Human Grasping
P	Pressure applied to a single cell in the TMMAS where $0 \leq P \leq 127$.
LF-SX	Grasping dataset at fixed orientations around the handlebar collected in the lab for Subject X.
LR-SX	Grasping dataset at random orientations around the handlebar collected in the lab for Subject X.
F_H	The force applied by the human measured using a load cell.
F_R	The virtual guidance force applied by the robot.
F_G	The grasping force applied by the human measured using the TMMAS.
	Confidence Based Role Change
	Performance Model
A	Generic task component.

ϕ_A	The robot's perception of the human's performance in task component A.
$\frac{\phi_A}{dt}$	The instantaneous change in the robot's perception of the human's performance.
$\phi_{A,0}$	The robot's initial perception of the human's performance in task component A.
$P_{p_1}(p_1)$	Penalty dependent on the observation p_1.
$R_{r_1}(r_1)$	Reward dependent on the observation r_1.
τ	Maximum reward or penalty in a single time step.
G_{p_1}	Enabling function for Penalty P_{A,p_1}.
G_{r_1}	Enabling function for Reward R_{A,r_1}.
B	Enabling condition which define situations where fluid is allowed to flow through the fluid arc.

Confidence Model

$\phi_{A,c}$	The robot's perception of the human's performance in a generic critical component A.
$\phi_{A,n}$	The robot's perception of the human's performance in a generic non-critical component A.
γ_A	The weighting of a non-critical component A.
C_{min}	The minimum confidence if the robot in the human if the human's performance in the critical components is at its maximum value.
C	The robot's current confidence in its human co-worker.

Control Model

t_H	A previous time horizon.
t_{step}	The time between each update of the robot's confidence in the human.
Ω	The control value which determines whether a role change is initiated.
ω_1	The second derivative of confidence component of Ω.
ω_2	The first derivative of confidence component of Ω.
ω_3	The confidence component of Ω.
$\bar{C}$	Average value of confidence in the time interval t_H.

$\bar{\dot{C}}$	Average value of the first derivative of confidence in the time interval t_H.
$\bar{\ddot{C}}$	Average value of the second derivative of confidence in the time interval t_H.
$\bar{C}_{thresh}$	The confidence threshold under which the value of ω_3 will be negative.
$\omega_{1,max}$	The maximum value of ω_1.
$\omega_{2,max}$	The maximum value of ω_2.
$\omega_{3,max}$	The maximum value of ω_3.
$\lambda_{\dot{C}}$	The sensitivity of ω_2 to changes in $\bar{\dot{C}}$.
$\lambda_{\ddot{C}}$	The sensitivity of ω_1 to changes in $\bar{\ddot{C}}$

Chapter 1

Introduction

Robots were initially incorporated in the industrial sector as a means to automate physically demanding or repetitive tasks in isolated environments. Through advancements in robotic technology, the intelligence of the robots increased and the role that the robots played in industry began to change. Robot co-workers are the result of an emerging field of robotics which aims to integrate robots into the human workspace. These robot co-workers are able to complete tasks autonomously as well as adapt to the intentions of their human co-workers. In physical Human-Robot Collaboration (pHRC), the human physically interacts with the robot as they work collaboratively towards a shared goal. A collaborative Human-Robot interaction is defined as one where only both the human and the robot make meaningful decisions during the interaction. Examples of collaborative robots designed for industrial applications are shown in Figure 1.1

In pHRC, the human would generally be in control of the interaction while the robot provides assistance to its human co-worker. This is partially due to the human's ability to quickly assess and react appropriately to any situations that may transpire during pHRC. With the increasing level of intelligence of robot co-workers, peer-to-peer interaction is expected and believed to be an ideal approach for the collaboration between the human and the robot in a shared activity. In peer-to-peer collaboration, the human and its robot co-worker would observe each other's actions and intervene if one detects changes in their counterpart during the interaction which could negatively impact the task. Current research for safe pHRC only considers role change to be initiated from the human's perspective and not from the robot's perspective. However, in these situations there

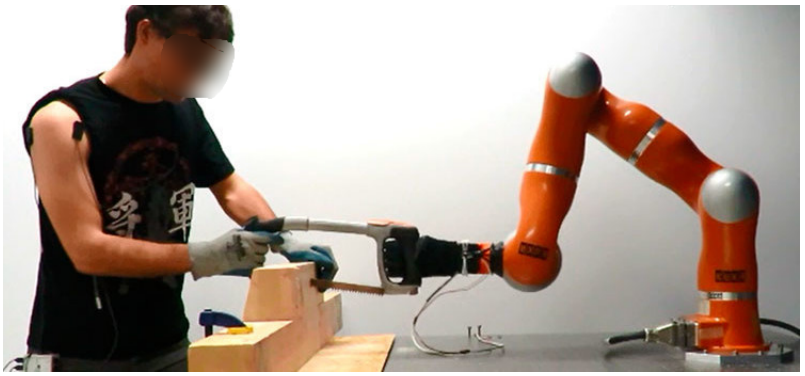

(a)

(b)

FIGURE 1.1: Examples of pHRC. (a) A collaborative robot arm designed to assist its human co-worker perform a sawing task [1]. (b) A robotic exoskeleton that augments the strength of its human co-worker during pHRC [2]

.

should be a mechanism which would allow the robot co-worker to take the initiative and intervene in the pHRC.

This thesis explores effective methods of enabling the robot's perception of its human co-worker's intention during pHRC and aims to address the question of how a robot co-worker would decide whether and when it should intervene in its human co-worker's actions and initiate a role change during pHRC. One factor that determines whether a human intervenes in its robot co-worker's actions is the human's self-confidence and the human's confidence in its robot co-worker. By

using the robot's confidence in its human co-worker to determine whether the robot should initiate a role change, a reciprocal interaction dynamic between the human and the robot can be created which may result in a more intuitive peer-to-peer interaction.

This thesis presents a method for using the grasping pattern and grasping strength of the human hand for determining the human co-worker's hand orientation and monitoring the human's reaction to unexpected events during pHRC. A confidence-based role change method for determining whether and when the robot should intervene in the actions of its human co-worker during pHRC is also presented. The method utilizes a robot confidence framework that uses the robot's perception of the human's actions and performance during pHRC to quantify the robot's confidence in its human co-worker. The robot's perception of its human co-worker's performance during pHRC is obtained by comparing the robot's observations of the human's actions during the pHRC with the robot's expectations of the task. If the human's actions are within the robot's expectations, the robot's perception of the human's performance will increase. If the human's actions deviate from the robot's expectations, then the robot's perception of the human co-worker's performance will decrease based on the difference between the robot's observations and the robot's expectations. The robot uses its confidence in its human co-worker to determine whether it should initiate a role change or if it should allow the human co-worker to continually take control during pHRC.

1.1 Background and Motivation

Robots have been used for many years to provide physical assistance to humans in physically demanding tasks. However, it has only been in recent times that robots have been able to interact directly with humans. Traditional industrial robots, like those seen in Figure 1.2a, generally do not physically interact with humans but perform physically intensive or repetitive tasks in isolated environments due to the safety risks associated with heavy payloads and the lack of compliancy in the robot.

Technological advances in the field of robotics such as compliant actuators [21], improved sensing technology [22, 23] and safe control algorithms [24, 25] have allowed robots to slowly transition out of their isolated environments and into the human workspace. One recent example is the Sawyer robot produced by Rethink Robotics (Figure 1.2b) which boasts a number of cameras that

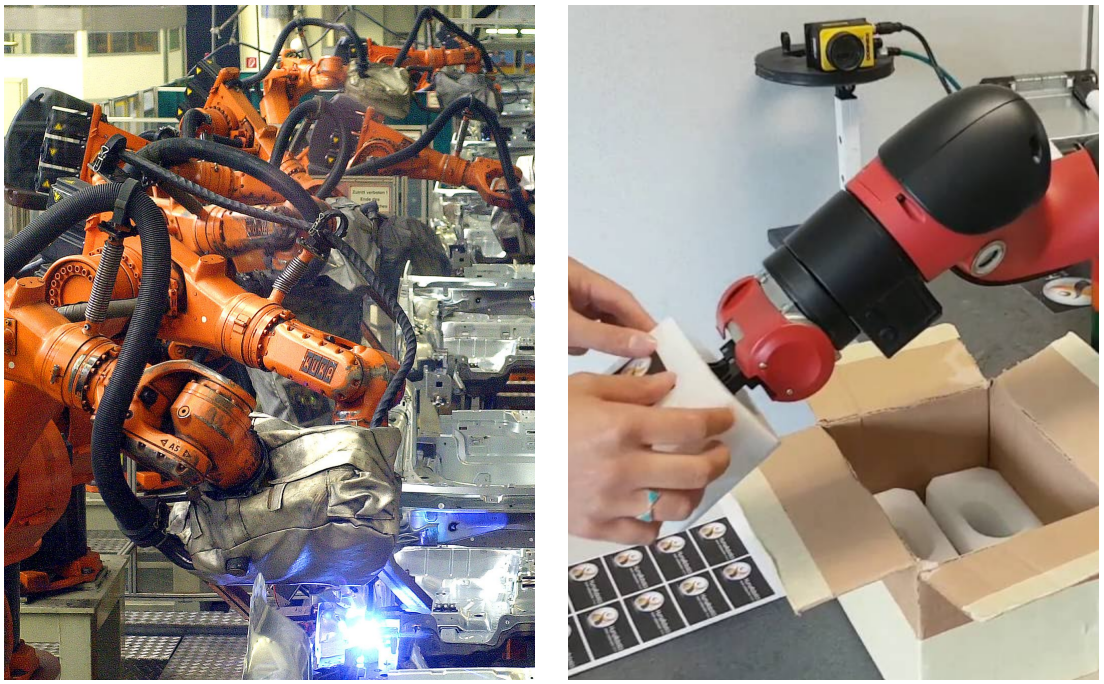

(a) (b)

FIGURE 1.2: Examples of robotic systems. (a) Traditional industrial robot used in production lines [3]. (b) Collaborative robot arm used for pHRC [4].

it uses to observe the environment and its human co-worker and elastic actuators allowing the Sawyer robot to instantly come to a halt when a collision is detected during pHRC. However, the decreased distance between the human and the robot during the interaction introduces the risk of the human suffering physical injuries. Although there has been a lot of research into safety paradigms which can be implemented in pHRC to mitigate some of the risks towards the human co-worker [26], the safety risks cannot be completely removed from the interaction.

In the industrial sector which includes fields such as aerospace, defense, industrial machinery, tools, construction and metal fabrication [27], one of the ways that safety risks have been mitigated is to automate as much of the task as possible and reduce the amount of contact between the human and the robot. An example of a field which has embraced the assistance provided by robots is the grit-blasting industry where autonomous grit-blasting robots such as those seen in Figure 1.3a are used [28, 29].

However, in more complex environments where objects may obstruct the robot's sensors or the environment undergoes constant change, having a human operator in the loop can improve the

(a)

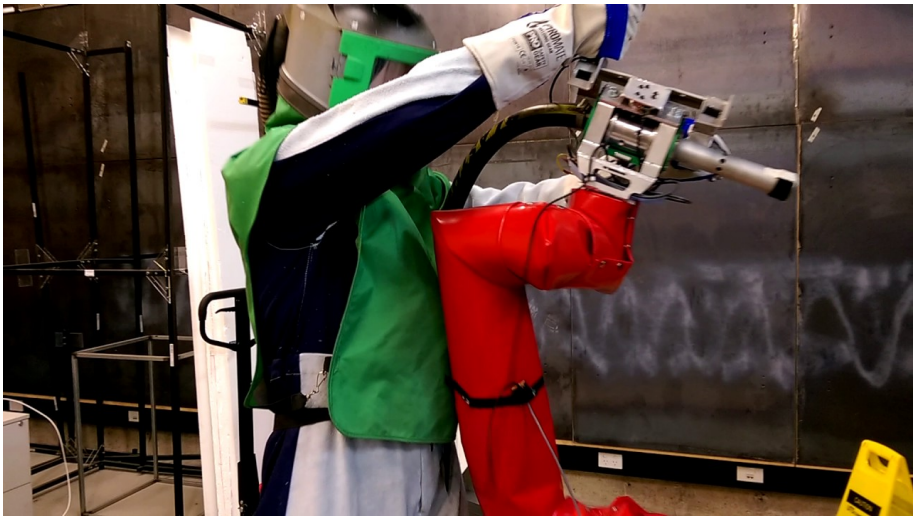

(b)

FIGURE 1.3: Robotic grit-blasting. (a) The SABER robot used for autonomous grit-blasting on the Sydney Harbour Bridge. (b) The ANBOT, a grit-blasting robot designed for pHRC.

.

safety of the task and the robot's ability to complete the task [30]. Robots designed for Human-Robot collaboration, or Cobots, have broadened the research field of Human-Robot Interaction (HRI) or more specifically physical Human-Robot Interaction (pHRI) where the human comes into direct physical contact with the robot and pHRC which is a subset of pHRI where the human and robot work collaboratively to complete a task. The Assistance-as-Needed-roBOT (ANBOT) shown in Figure 1.3b is an example of a robot designed for pHRC. With a human in the loop, the expertise of the grit-blaster can be taken advantage of and the variety of applications that the robot can be used for increases. When a human works collaboratively with the ANBOT, the human

is generally in control and responsible for the safety aspects of the interaction while the robot provides physical assistance to its human co-worker and monitors the human's performance.

Another sector which has seen an increase in the number of collaborative robots is the healthcare sector which specializes in products and services related to health and medical care [31]. The healthcare sector has been trying to use robots as a means to cope with the aging population. In Australia, there were approximately 2.8 million people (13.4% percent of the population) aged 65 or older in 2007. The population projections, shown in Figure 1.4, estimate that the population over 65 years of age will nearly triple to 7.2 million (25.3% of the population) by the year 2047 [5]. In 2016, there were 3.67 million people aged 65 years and over in June 2016, accounting for over 15.2% of the total population [32]. With the decreasing working population unable to handle the pressure created by the aging population requiring increased medical services [33], robots present a possible solution to the problem.

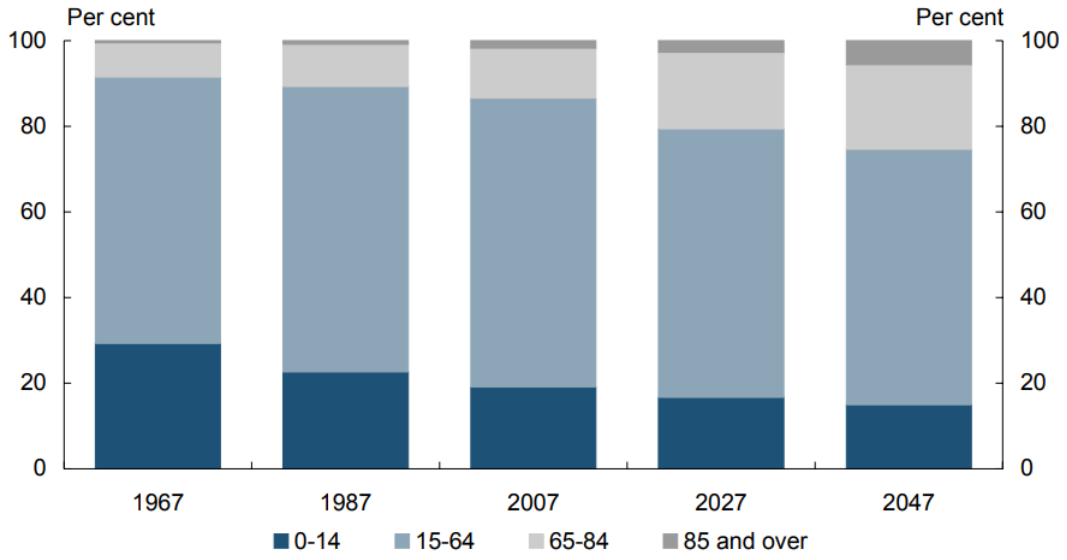

FIGURE 1.4: A projection for the age of the Australian population by 2047. Reproduced from Intergenerational Report of 2007 [5].

Although the introduction of robots into the healthcare sector provides many benefits, it also introduces robots into an environment where the robot would come into contact with those who may not be familiar with robots and how robots operate such as the elderly. In the industrial sector, the people who physically interact with a robot would have received training in how to operate the robot and the required safety precautions that must be observed when interacting with the robot.

The purpose of the training is not only to teach the functionality of the robot but also to familiarize the human operators with the appropriate actions to take when problems arise.

Without the required training, the risk of accidents involving robots occurring in the workplace increases. These accidents can be caused by factors such as the inexperience or the negligence of the human co-worker or unrelated personnel coming into contact with the robot. The consequences of these accidents on the environment and the human co-worker may be more severe as those who work in the healthcare sector may not know the appropriate response to take or the environment may be more complex or chaotic. This is especially true in pHRC where the human is in physical contact with the robot while completing a task. Generally, the human is the one who is responsible for managing the safety aspects of a pHRC. However, if a situation arises where the human does not know how to react, cannot react in time or their performance during the task is brought into question, the robot should have a method for intervening in the pHRC to protect the human and the environment.

1.2 Research Question

This thesis aims to answer the research questions raised when considering the robot perceives its human co-workers intentions during pHRC and how a robot co-worker would determine whether and when it should intervene in the actions of its human co-worker and initiate a role change during pHRC. The first research question explores how the robot perceives the human's intention in pHRC. The second research question explores how the robot's confidence in its human co-worker during pHRC can be modeled. The final research question explores how the robot's confidence can be used to decide whether it should initiate a role change during pHRC.

To determine whether the robot should intervene during pHRC, the robot must have strong situational awareness, a clear understanding of the task goals and must be able to identify actions or events which have a negative influence on the task outcomes. For a human, this knowledge is ingrained through the accumulation of their past experiences and the lessons they have learned. Therefore, it would be difficult for a robot to perfectly replicate a human's understanding of the pHRC. This is especially true if the robot has a limited number of sensors which is often the case in some pHRC scenarios where the robot must infer the human's intention through a handlebar which

is a commonly used interface in pHRC. The work in this thesis explores how information such as the grasping pattern and the grasping strength of the human hand on a handlebar during pHRC can be used to further the robot's understanding of the task and its human co-worker's intentions.

Once a model of the robot's perception of a task is obtained, the robot must consider the human's actions and intentions in the context of the task being performed. In pHRC, the human generally intervenes in its robot co-worker's actions when the human's trust or confidence in the robot's ability to complete the task decreases or the human believes that they are better equipped to complete the task [34, 35]. Confidence and trust are both considered to be subjective measures which makes accurately modeling the robot's trust or the robot's confidence in its human co-worker a difficult task. Given that the trust or confidence of two human observers may differ, attempting to create an absolute measure of robot's trust or confidence in its human co-worker which could be applied to any pHRC would be unfeasible in practical applications. Therefore, a generic framework for modeling the robot's trust or confidence in its human co-worker which can be adapted to any pHRC is required. Most definitions of confidence agree that measures of confidence are relative to the observer's understanding of a task [36]. Therefore, the solution is to model the robot's expectations of the human co-worker's actions during pHRC and use it to calculate the robot's confidence for a specific task or operation. Although the expected performance in some aspects of pHRC are subjective, factors such as industry standards or the quality of the end result are objective. By measuring the human's performance relative to a baseline performance in a task, an objective measure of the robot's confidence in its human co-worker during pHRC can be obtained.

The decision of whether to initiate a role change during pHRC can be difficult to model. This is especially true considering that the decision of whether to initiate a role change is based on the robot's confidence in its human co-worker. The ideal confidence-based role change method should not only consider the robot's current confidence in the human when deciding whether to initiate a role change but also how the robot's confidence in its human co-worker has changed during the pHRC. The previous actions of the human should have some influence on whether the role change is initiated as it adds context to the robot's decision of whether it should intervene.

1.3 Scope

This thesis investigates a method for using the grasping pattern and grasping strength of the human hand to improve the robot's understanding of its human co-worker's intention during pHRC and a method for determining whether and when a robot should intervene in the actions of its human co-worker and initiate a role change. The work presented in this thesis focuses on pHRC where the human co-worker physically controls the robot and the robot observes the actions of its human co-worker as the human and robot work collaboratively to complete a task. The confidence-based role change method presented in this work utilizes a robot confidence framework and a method for using the robot's confidence in its human co-worker to determine whether the robot should initiate a role change during pHRC.

In most pHRC scenarios presented in this thesis, the interaction between the human and the robot occurs through a handlebar. The method for exploring the use of the human hand's grasping information during pHRC utilizes a cylindrical handlebar which is a common interface in pHRC. The grasping pattern and grasping strength of the human hand is gathered using a flexible pressure sensor array wrapped around the handlebar. The grasping pattern and grasping strength of the human hand are used to identify the orientation of the human hand around the cylindrical handlebar and to detect the changes in the human's grasping in reaction to unexpected events during pHRC. The method for identifying the orientation of the human hand only considers the static grasping scenario where the human has a firm grip on the handlebar. The dynamic aspects of grasping during pHRC are not explored in this thesis but are considered in a future work.

The robot confidence framework presented in this thesis is comprised of a performance model and a confidence model. The framework is used to quantify the robot's confidence in its human co-worker during pHRC. The performance model quantifies the robot's perception of its human co-worker's performance in task components using the robot's observations of its human co-worker and its expectations of the pHRC. The robot's expectations of the pHRC are generally defined by creating a baseline for performance in aspects of the task which the robot can perceive using its sensors. Factors such as social or cultural norms which may bias the robot's perception of the human's performance in a task component are not addressed in this work but are considered in a future work. The confidence model utilizes the robot's perception of its human co-worker's

performance in the task components and the relative importance of the task components to determine the robot's confidence in its human co-worker in real-time. The more important the task component to the integrity of the task or the safety of the human or the robot, the larger impact the task component has on the robot's confidence in its human co-worker.

This thesis also presents a method that utilizes the robot's confidence in its human co-worker to determine whether and when the robot should intervene in its human co-worker's actions and initiate a role change to take the control away from the human. In this thesis, the pHRC scenarios used to verify the confidence-based role change method is limited to those where the robot has a supervising role in the pHRC and is the one who decides whether the human is in control of the pHRC or the robot is in control of the pHRC. It is understood that to have a truly reciprocal peer-to-peer interaction dynamic between the human and the robot, whether the role change occurs should be the result of a negotiation between the human's desire for role change and the robot's desire for role change. The application of the method in peer-to-peer interactions, where the human and the robot share control of the pHRC is not addressed in this work but its implementation in future works is discussed.

1.4 Contributions

The following are the main contributions from the work presented in this thesis:

- A method for identifying the orientation of a human operator's hand around a cylindrical handlebar using the grasping pattern of the human operator collected using flexible sensor array wrapped around a cylindrical handlebar (Chapter 3).
- A method for detecting the human's reaction to unexpected events during pHRC where the only point of contact between the human and the robot is a handlebar (Chapter 3).
- A robot confidence framework which calculates the robot's confidence in its human co-worker based on the robot's perception of its human co-worker's actions during pHRC. The robot confidence framework consists of a performance model and a confidence model. The performance model quantifies the robot's perception of its human co-worker's performance

in task components. The confidence model uses the human's performance in the task components and the relative importance of each task component to calculate the robot's confidence its human co-worker (Chapter 4).

- A method for using the robot's confidence in its human co-worker to determine whether and when the robot should intervene during pHRC and initiate a role change to take the control of the interaction away from its human co-worker (Chapter 5).

1.5 Publications

- Tran, A., Liu, D., Ranasinghe, R., Carmichael, M., & Liu, C. (2015). Analysis of Human Grip Strength in Physical Human Robot Interaction. Procedia Manufacturing, 3(Ahfe), 14421449. https://doi.org/10.1016/j.promfg.2015.07.320

- Tran, A., Liu, D., Ranasinghe, R., Carmichael, M., & Liu, C. (2018). A Method for Quantifying a Robot's Confidence in its Human Co-worker in Human-Robot Cooperative Grit-Blasting. International Symposium on Robotics 2018. (To be published on IEEE Xplore and Scopus following the conference in June 2018)

- Tran, A., Liu, D., Ranasinghe, R., Carmichael, M., & Liu, C. (2018). Identifying Human Hand Orientation around a Cylindrical Handlebar for physical Human-Robot Interaction. International Symposium on Robotics 2018. (To be published on IEEE Xplore and Scopus following the conference in June 2018)

- Tran, A., Liu, D., Ranasinghe, R., Carmichael, M., & Liu, C. (2018). A Robot Confidence Framework for Human-Robot Collaboration. (Under review. Submitted to IEEE Transactions on Human-Machine Systems)

- Ranasinghe, R., Dantanarayana, L., Tran, A., Lie, S., Behrens, M., & Liu, L. (2014). Smart hoist: An assistive robot to aid carers. 13th International Conference on Control ,Automation, Robotics & Vision, 2014(December), 12851291. https://doi.org/10.1109/ICARCV.2014.7064501

- Dantanarayana, L., & Ranasinghe, R. (2014). A Novel Collaboratively Designed Robot to Assist Carers. 6th International Conference, ICSR 2014, 105114. https://doi.org/10.1007/978-3-319-11973-1_11

1.6 Thesis Outline

This thesis is organized as follows:

1.6.1 Chapter 2

Chapter 2 provides a review of works related to contributions presented in this thesis. Firstly, an overview of HRI and how advancements in technology contributed to the development of the field of pHRC. A review of pHRC and its usage in the industrial and healthcare sectors is also provided.

Following this, an overview of trust and confidence and how trust and confidence contribute towards safe pHRC is discussed. Previous approaches towards modeling the trust and confidence of the human in its robot co-worker are also presented and discussed.

Finally, the concept of roles and role change in pHRC is explored. A review of different approaches used in the literature to define the role of the human and the robot during an interaction are discussed. After which, an overview of methods for initiating a role change in pHRC are also presented and discussed.

1.6.2 Chapter 3

Chapter 3 presents a method for using the grasping pattern and grasping strength of the human hand to identify the human's hand orientation around a cylindrical handlebar and to monitor the human's reaction to unexpected events in a pHRC. The human hand's grasping pattern and grasping strength is obtained using a flexible pressure sensor array wrapped around a cylindrical handlebar. The grasping pattern of the human is used to identify the human's hand orientation around the cylindrical handlebar and the hand orientation of other humans. The grasping force of the human during pHRC is also analyzed to observe the differences in the human hand's grasping strength when the human initiates a change in the task and when an unexpected event occurs during the pHRC.

1.6.3 Chapter 4

Chapter 4 introduces the robot confidence framework that quantifies the robot's confidence in its human co-worker. The framework uses the robot's perception of its human co-worker's performance in task components and the relative importance of the task components to calculate the robot's confidence in its human co-worker. The performance of the operator is modeled as a Fluid Stochastic Petri Net (FSPN) that uses the robot's observations of its human co-worker and the robot's expectations of the task component to calculate the human's performance in the task. The framework is then demonstrated using a range of pHRC case studies. Each case study explores how the pHRC can be decomposed into task components and how the robot's perception of its human co-worker's performance in each task component can be modeled. Finally, sample results from the pHRC case studies where the robot confidence framework was applied are presented and the implications and significance of the robot's confidence in these case studies is discussed.

1.6.4 Chapter 5

In Chapter 5, a method for confidence-based role change is presented which allows the robot to determine whether and when it should intervene in the human's actions and initiate a role change during pHRC. The method is verified using a collaborative grit-blasting operation where the human and the robot work collaboratively to complete a task.

1.6.5 Chapter 6

Finally, a summary of the thesis and its conclusions is presented in Chapter 6 which includes an objective discussion of its limitations and how the presented work can be expanded upon in the future.

Chapter 2

Review of Related Work

This chapter reviews work related to the work presented in this thesis. This thesis aims to answer the question of how a robot would decide whether it should intervene in its human co-worker's actions and initiate a role change during physical Human-Robot Collaboration (pHRC). The research in this thesis explores effective methods for enabling the robot's perception of its human co-worker's intention during pHRC and how the use of the robot's confidence in its human co-worker can be used as a trigger to initiate a role change and take control away from the human during pHRC.

Section 2.1 provides a review of Human-Robot Interaction (HRI) and how advancements in technology have led to the development of the field of pHRC. An overview of the robots designed for pHRC which are currently being used in the industrial sector and the healthcare sector is also provided. The focus of this section is on robotic systems where a human must physically interact with the robot and how the robot perceives the environment and the actions and intentions of its human co-worker during pHRC.

Section 2.2 provides a review of safety mechanisms which are commonly utilized in pHRC to ensure the safety of the human co-worker. The concept of trust and confidence in pHRC and the potential effect of trust and confidence on the safety of pHRC are discussed. The confidence-based role change method presented in this thesis uses robot's confidence to determine whether the robot should initiate a role change during pHRC, hence a review of the research on trust and confidence in pHRC is required.

Section 2.3 reviews role change methods in pHRC. This section focuses on how the roles of humans and robots are defined and changed over the course of a pHRC. Different approaches towards role change and their suitability for use in pHRC are discussed.

2.1 physical Human-Robot Collaboration

Robots that can work collaboratively or cooperatively with their human counterparts have gained attention in recent years. Such robots work alongside their human co-workers, providing physical assistance and sharing the workload in applications such as manufacturing, healthcare, and material handling [37–40]. Through new research innovation, the intelligence of the robot co-workers continues to increase. This allows for more complex and diverse tasks to be assigned to the robotic co-workers as well as allowing them to work in closer proximity to their human operators [41, 42]. This section presents examples of robots used for pHRC with emphasis on robots that are used in many industry sectors.

2.1.1 pHRC in Manufacturing

FIGURE 2.1: An example of an industrial robot arm [6].

Initially, traditional (industrial) robots were designed for use in the industrial sector where they would provide assistance to humans in physically demanding tasks such as construction and manufacturing. The original purpose of traditional robots was to automate manufacturing processes

in production lines which were too physically demanding for human workers [43, 44]. One of the most common robots seen in the manufacturing industry is the robot arm. In Figure 2.1, an industrial robot arm is shown performing a manufacturing task. From the figure, it can be seen that the conditions under which the robot is performing the task are unsuitable for a human co-worker. Additionally, these traditional robot arms were unsuitable for pHRC due to safety risks posed by their size, force and primitive sensing technology [45]. Robots such as these work in isolated environments to minimize the risks during the manufacturing process.

As technology advanced, the miniaturization of the traditional robot arm began and the applications that these smaller robot arms could be used for increased. With the advent of technology such as compliant joints [46–48], improved sensing and control[49–51], these smaller robot arms can now work in closer proximity to their human co-workers [52–55]. Like their larger counterparts, the human-safe robot arms are designed to provide physical assistance to their human co-workers and to automate a part of the manufacturing process. Therefore, it is not surprising that a large number of human-safe robots designed for pHRC are found in the manufacturing industry. Using cameras attached to the end-effectors of the robot arms, the robot arms are able to observe their human co-worker's actions as they assemble components [56, 57].

FIGURE 2.2: An example of a collaborative Human-Robot assembly task [7].

An example of a robot arm designed for pHRC can be seen in Figure 2.2. In the figure, the robot arm works collaboratively with its human co-worker and provides assistance by holding parts and tools that its human co-worker requires. These robots use their observations to predict the needs of their human co-workers and transfer materials to the human when needed [58]. Research has been done to optimize the handover process between the human and the robot to maximize the user experience and to ensure the safety of the human during the pHRC [59, 60].

2.1.2 pHRC in Healthcare

Robots have recently been seeing use in healthcare and aged care. The healthcare sector has seen a rise in the use of robots to assist patients with their daily living and to reduce the physical strain on healthcare workers [61–63]. Assistive robots are a subcategory of collaborative robots which have become more common place with the most well known assistive robot used in the healthcare sector being the motorized wheelchair. Motorized wheelchairs may be able to interpret the human's intention through a joystick which the human uses to control the motorized wheelchair's motion [64–66].

Advanced technologies including obstacle avoidance [64, 67], step climbing [68, 69], navigation [70–72] and hands-free driving [73–76] have started to be incorporated into motorized wheelchairs. These technologies improved the maneuverability of motorized wheelchairs and further assisted human operators in safely navigating their environment. An example of a smart wheelchair used for pHRC is shown in Figure 2.3.

FIGURE 2.3: An example of a smart wheelchair used for pHRC capable of semi-autonomous navigation [8].

The advanced technologies applied to motorized wheelchairs have also recently been incorporated into many other devices found in the healthcare sector such as in motorized walkers [77, 78] and patient hoists [79] shown in Figure 2.4. The purpose of these robots is to improve the mobility of its human operator and reduce the physical strain on the human operator during the pHRC.

(a) (b)

FIGURE 2.4: Examples of assistive devices which also have some of the technologies used in smart wheelchairs. (a) Smart walker [8]. (b) Smart Hoist.

Exoskeletons are another type of robot designed for pHRC used in the healthcare industry. Unlike industrial robot arms, exoskeletons in healthcare are normally used as a rehabilitation tool to help patients regain strength and mobility in their limbs [80, 81]. The use of a collaborative robot during rehabilitation allows the recovery exercises to be automated and adapted to each individual patient's needs [82, 83]. An example of an exoskeleton used for rehabilitation can be seen in Figure 2.5. Previous works have shown that during the rehabilitation process, the robot should not offset all the load as it would slow down muscle development in the patient [84]. By adapting the load based on the patient's strength and/or fatigue, the robot is able to monitor the human during an exercise and adjust the amount of assistance so that it would always provide the ideal amount of assistance for the human [85, 86].

FIGURE 2.5: An example of a exoskeleton used for pHRC designed to assist in the recovery of stroke patients [9].

2.2 Trust and Confidence in pHRC

This section provides an overview of how trust and confidence have been represented and used in pHRC. The human has generally been responsible for the collaborative operation and safety during pHRC [87, 88]. Based on the human's experience and knowledge, the human is able to determine the appropriate time to intervene in the actions of the robot during pHRC [34, 35]. In pHRC where the human is in physical contact with the robot, other factors need to be taken into account when determining whether the current interaction is safe for the human and the robot. De Santis [89] compiled a guide which outlined factors that need to be addressed as well as a number of benchmarks for safe pHRC. One factors that determines whether the human intervenes in the robot's actions during a pHRC is the human's trust and/or confidence in its robot co-worker [90, 91]. Previous works have shown how increased trust and/or confidence of the human in its robot co-worker has a positive effect on the interaction outcomes [92]. A human's trust and/or confidence are subjective measures which represent the human's belief about whether its robot co-worker is able to complete the task.

Most works in HRI consider trust and confidence to be equivalent; however there is an important difference between the two. The confidence of an observer is based on a specific referent. In most cases, this referent is the observer's expectation for an action or behavior during an interaction. On the other hand, trust is a more general term and is generally based on more esoteric measures and does not need to be based on observations [36]. It is possible for a human to have trust in its robot co-worker without having previously interacted with the robot. Factors such as the robot's reputation or the human's intuition will contribute to the human's initial trust in the robot [93]. Once the human begins to interact with the robot, the human's trust in the robot will increase or decrease based on whether the robot succeeds or fails at the task respectively [94–96]. A categorization of the factors which influence the human's trust in its robot co-worker can be seen in Figure 2.6. In his work, Hancock [10] performed a meta-analysis to determine the effect of each of these factors on the human's trust in its robot co-worker. It was found that the performance based factors had the largest influence on the human's trust in its robot co-worker. Therefore, based on the differences between confidence and trust, this thesis will be using the confidence of the robot in its human co-worker rather than its trust by using the robot's expectations of the pHRC

as a referent to determine the robot's confidence in its human co-worker based on the human's performance during pHRC.

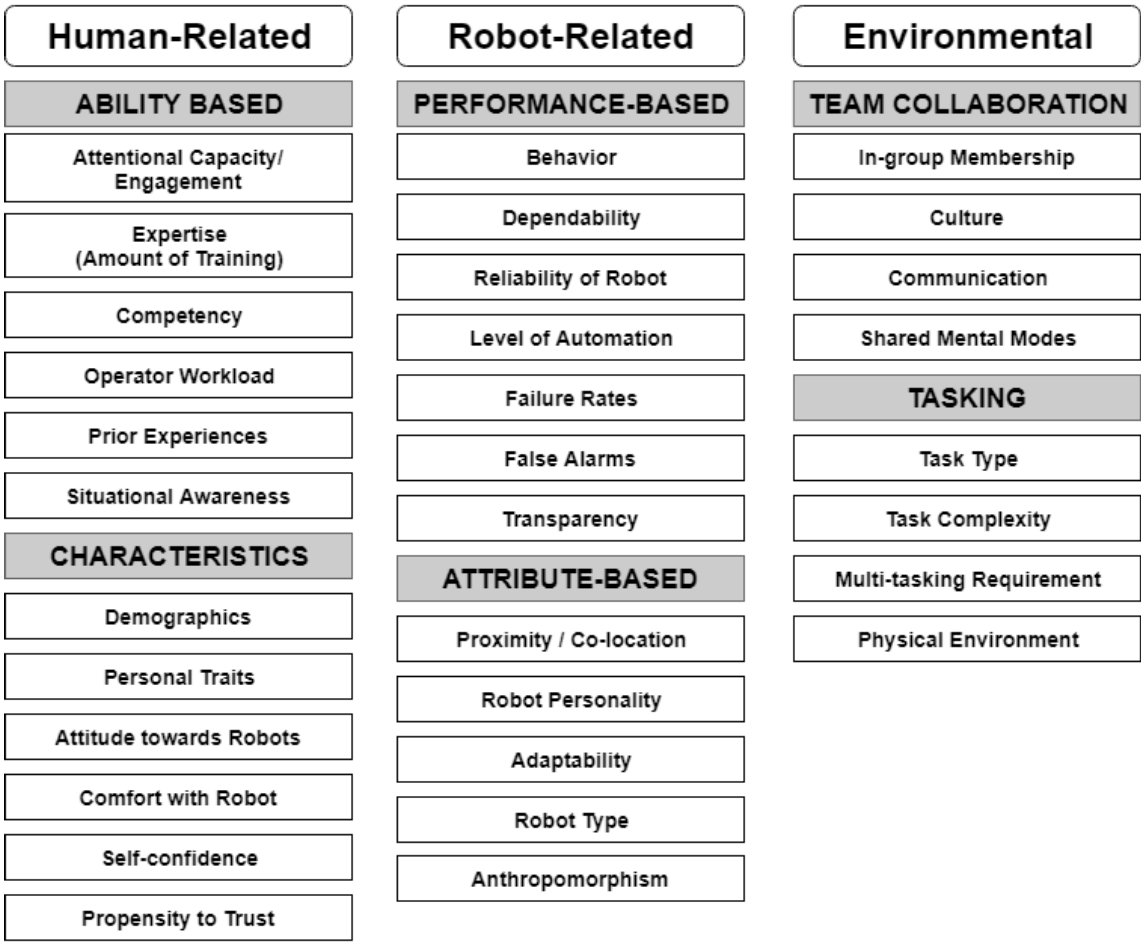

FIGURE 2.6: Factors affecting trust development in HRI [10].

The representation of trust in pHRC has generally been an inexact method. The most common approach for measuring the trust of the human is through the use of surveys which are structured using scales such as the Likert scale [97–99]. The surveys rely on the human's subjective rating of various aspects of the interaction. An example of a Likert scale used to measure the human's trust is shown in Figure 2.7 [11]. A quantitative measure of the human's trust in the robot is obtained through a statistical analysis of the survey results. Due to the nature of this approach, the human's trust in its robot co-worker is generally obtained after the task has been completed and not in real-time during the interaction [100].

As the intelligence of the robots increases, robots are expected to be able to make more nuanced

	0 %	10 %	20 %	30 %	40 %	50 %	60 %	70 %	80 %	90 %	100 %
What % of the time will this robot be . . .											
1. Considered part of the team	O	O	O	O	O	O	O	O	O	O	O
2. Responsible	O	O	O	O	O	O	O	O	O	O	O
3. Supportive	O	O	O	O	O	O	O	O	O	O	O
4. Incompetent[a]	O	O	O	O	O	O	O	O	O	O	O
5. Dependable[b]	O	O	O	O	O	O	O	O	O	O	O
6. Friendly	O	O	O	O	O	O	O	O	O	O	O
7. Reliable[b]	O	O	O	O	O	O	O	O	O	O	O
8. Pleasant	O	O	O	O	O	O	O	O	O	O	O
9. Unresponsive[a,b]	O	O	O	O	O	O	O	O	O	O	O
10. Autonomous	O	O	O	O	O	O	O	O	O	O	O
11. Predictable[b]	O	O	O	O	O	O	O	O	O	O	O
12. Conscious	O	O	O	O	O	O	O	O	O	O	O
13. Lifelike	O	O	O	O	O	O	O	O	O	O	O
14. A good teammate	O	O	O	O	O	O	O	O	O	O	O
15. Led astray by unexpected changes in the environment	O	O	O	O	O	O	O	O	O	O	O
What % of the time will this robot . . .											
16. Act consistently[b]	O	O	O	O	O	O	O	O	O	O	O
17. Protect people	O	O	O	O	O	O	O	O	O	O	O
18. Act as part of the team	O	O	O	O	O	O	O	O	O	O	O
19. Function successfully	O	O	O	O	O	O	O	O	O	O	O
20. Malfunction[a]	O	O	O	O	O	O	O	O	O	O	O
21. Clearly communicate	O	O	O	O	O	O	O	O	O	O	O
22. Require frequent maintenance[a]	O	O	O	O	O	O	O	O	O	O	O
23. Openly communicate	O	O	O	O	O	O	O	O	O	O	O
24. Have errors[a]	O	O	O	O	O	O	O	O	O	O	O
25. Perform a task better than a novice human user	O	O	O	O	O	O	O	O	O	O	O
26. Know the difference between friend and foe	O	O	O	O	O	O	O	O	O	O	O
27. Provide feedback[b]	O	O	O	O	O	O	O	O	O	O	O
28. Possess adequate decision-making capability	O	O	O	O	O	O	O	O	O	O	O
29. Warn people of potential risks in the environment	O	O	O	O	O	O	O	O	O	O	O
30. Meet the needs of the mission/task[b]	O	O	O	O	O	O	O	O	O	O	O

FIGURE 2.7: An example of a Likert scale used to determine a human's trust in its robot co-worker [11].

decisions on how to react to changes in the interaction. To improve safety in pHRC, both the human and the robot should be responsible for intervening when the other is behaving abnormally.

Although both trust and confidence in pHRC have generally been seen from the human's perspective, there have recently been works which have used the confidence of the robot in its human co-worker to affect the interaction. In his work, Sanders [101] uses the performance of the human in a navigation task to calculate the confidence of the robot in the human. He uses the calculated confidence value as a gain to scale the velocity of the wheelchair. One of the short comings of this work is that it dismisses the effects of past performance and bias on trust and confidence [102–104]. The research presented by Walker [105] and Sadrfaridpour [106] are works related to the robot confidence framework presented in this thesis in terms of using the robot's perception of its human operator to calculate its confidence in its human co-worker. It adopts the Auto-Regressive Moving Average Vector Form (ARMAV) approach of modeling trust proposed by Lee [12] and uses the human's performance, the robot's performance and the robot's previous trust to describe the dynamics of trust in a pHRC as a function of time. A block diagram of the ARMAV model can be seen in Figure 2.8.

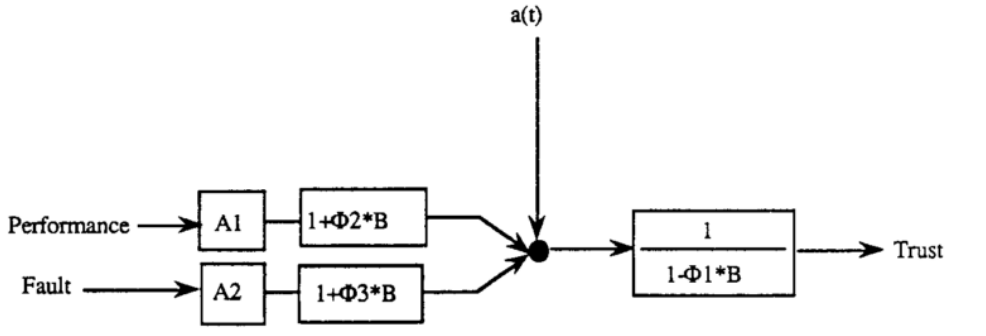

FIGURE 2.8: A visual representation of the ARMAV model [12].

Using the ARMAV model, Walker and Sadrfaridpour quantified the robot's trust in its human co-worker. The robot's trust in its human co-worker increased when the human was able to complete the handover and decreased when the human was unable to complete the handover respectively. When the trust of the robot in its human co-worker during a handover task decreased below a threshold, the pose of the robot arm would change to better accommodate its human co-worker. Although Walker and Sadrfaridpour referred to the robot's trust in their work, because they used the robot's expectations of the human's behavior as a basis of their analysis, it may be better to classify it as confidence rather than trust for their application. One of the shortcomings of the ARMAV model of trust proposed by Lee [12] is its scalability. In a pHRC, there could be a

number of components of the interaction which contribute to the robot's perception of the human's performance. As more components of the human's performance are considered when quantifying the robot's confidence using the ARMAV model, normalizing the robot's confidence in its human co-worker may result in trivializing the human's performance in some of the components due to their low weightings. Without a normalized value of confidence, determining whether a role change should occur in an interaction becomes a more difficult problem.

2.3 Role Change in pHRC

The division of roles between participants in an interaction is an increasingly important area of research in robotics. This section provides a non-exhaustive review of how the notion of roles and role change has evolved in the context of pHRC. In the past, robots would generally be operated in isolation, either performing set tasks in sectioned off areas or being controlled remotely via teleoperation. Over the years, as the intelligence of robots increased, the segregation between the human and robot decreased. As the distance between the human and the robot decreased, the safety of the human during the interaction became a pressing concern [107, 108]. The implementation of roles and role change began as a means to define the responsibilities of the human and the robot and their boundaries during an interaction [109–112].

2.3.1 The Robot's Role in pHRC

The interaction between a human and a robot can be categorized as either cooperative, collaborative or competitive [113]. In cooperative and collaborative interactions, both the human and the robot work towards the same goal. However, in a cooperative interaction, only one of the participants makes meaningful decisions about the actions being performed while the other participant takes on a purely supportive role. In collaborative interactions, both participants of the interaction contribute to the decision making process. Competitive interactions differ from cooperative and collaborative interactions in that the two participants of the interaction either do not share a goal or are antagonistic towards each other [114–116].

pHRC is a subset of HRI where the human and the robot are in physical contact and work collaboratively to complete a task. In pHRC, the robot is generally the one who takes on the supportive

role and assists the human as they work towards completing their shared goal. However, the robot may intervene when the safety of the human and the robot are at risk. Examples of robots designed for pHRC include assistive robotic devices such as the Smart Hoist [79] or exoskeletons [117–119]. In interactions involving these two types of robots, the path planning and movement of the robots is controlled by the human while the robot assists the human by reducing the physical load experienced by its human co-worker and adjusting the human's plans to avoid collisions in the case of the Smart Hoist and singularities in the case of the exoskeletons.

In this thesis, the role of the human or the robot in an interaction is defined by the responsibilities of the human or robot during the interaction. Assigning roles to the robot and the human in the interaction sets the expectations of the human and the robot for the other's behavior during the interaction [120]. These roles can be generalized into one of two categories, leader and follower [121]. In pHRC, as the robot is generally providing support to the human in the interaction, the human will generally have the leader role while the robot will have the follower role [122, 123]. Previous works [124], have stated that in an interaction between a human and robot, the human should:

- always remain in control, but should be able to experience or initiate smooth shifts between Level of Autonomy (LoA)
- receive continuous feedback about the robot's boundaries and functionality
- continuously interact with the robot
- benefit from increased performance and/or reduced workload.

The LoA of the robot has been defined as the negligence tolerance of the robot [125]. Many taxonomies have been proposed for a robot's LoA which define the relationship between the robot and the human and describe to what degree a robot can act on its own [126, 127]. A robot with a high LoA is one that does not require human intervention for a long period of time when they operate, while a robot with a low LoA requires the human to guide their actions during pHRC. As the LoA of a robot changes during an interaction, the role of the robot during the interaction also changes.

LORA	Sense	Plan	Act	Description
Manual	H	H	H	The human performs all aspects of the task including sensing the environment, generating plans/options/goals, and implementing processes.
Tele-operation	H/R	H	H/R	The robot assists the human with action implementation. However, sensing and planning is allocated to the human. For example, a human may teleoperate a robot, but the human may choose to prompt the robot to assist with some aspects of a task (e.g., gripping objects).
Assisted Tele-operation	H/R	H	H/R	The human assists with all aspects of the task. However, the robot senses the environment and chooses to intervene with task. For example, if the user navigates the robot too close to an obstacle, the robot will automatically steer to avoid collision.
Batch Processing	H/R	H	R	Both the human and robot monitor and sense the environment. The human, however, determines the goals and plans of the task. The robot then implements the task.
Decision Support	H/R	H/R	R	Both the human and robot sense the environment and generate a task plan. However, the human chooses the task plan and commands the robot to implement actions.
Shared Control With Human Initiative	H/R	H/R	R	The robot autonomously senses the environment, develops plans and goals, and implements actions. However, the human monitors the robot's progress and may intervene and influence the robot with new goals and plans if the robot is having difficulty.
Shared Control With Robot Initiative	H/R	H/R	R	The robot performs all aspects of the task (sense, plan, act). If the robot encounters difficulty, it can prompt the human for assistance in setting new goals and plans.
Executive Control	R	H/R	R	The human may give an abstract high-level goal (e.g., navigate in environment to a specified location). The robot autonomously senses environment, sets the plan, and implements action.
Supervisory Control	H/R	R	R	The robot performs all aspects of task, but the human continuously monitors the robot, environment, and task. The human has override capability and may set a new goal and plan. In this case, the autonomy would shift to executive control, shared control, or decision support.
Full Autonomy	R	R	R	The robot performs all aspects of a task autonomously without human intervention with sensing, planning, or implementing action.

FIGURE 2.9: Beer's Proposed Taxonomy of Levels of Autonomy for HRI [13]. H and R refer to which of the agents(human or robot) is responsible for the Sense, Plan and Act components of an interaction at each Level of Autonomy.

A more recent example of a taxonomy for a robot's LoA can be seen in Figure 2.9 [13]. In this taxonomy, the three components of an interaction, sense, plan and act [128] are considered. The responsibilities of the human and the robot in each of these components is assigned and a brief description of the interaction is provided. In the taxonomy of robot LoA shown in Figure 2.9, a robot's LoA during pHRC would be classified within the range Batch Processing and Executive Control where both the human and the robot contribute to the planning component of the interaction. Because the taxonomy is defining the LoA of the robot from the human's perspective, there is an exception which is not shown in the figure when considering true peer-to-peer interactions.

The exception is when the robot's LoA is Supervisory Control where the robot allows the human to perform all aspects of the task but the robot monitors the human, the environment and and the task and can intervene in the interaction to set new goals or plans.

2.3.2 Role Change in pHRC

In pHRC, where the human is in physical contact with the robot, it is necessary to establish the roles of the human and the robot during the interaction and the policy for role change during pHRC. The concept of role change (or role adaptation) was proposed as a model to help human operators adapt to changes in an environment [129]. Studies have also shown that system efficiency is higher in a collaborative interaction than in a cooperative interaction [130].

There are two general approaches towards role change in the literature. In the first approach, role change can be defined as the change in the robot's LoA during the course of an interaction [115, 131]. The second approach can be defined as the increase or decrease in the human or robot's control over the interaction [16, 132]. In Figure 2.10, a simplified representation of control between the human and the robot is shown. The change in roles can be interpreted as either a shift in the leader of the interaction or as a gradual shift in control between the human and the robot depending on the application.

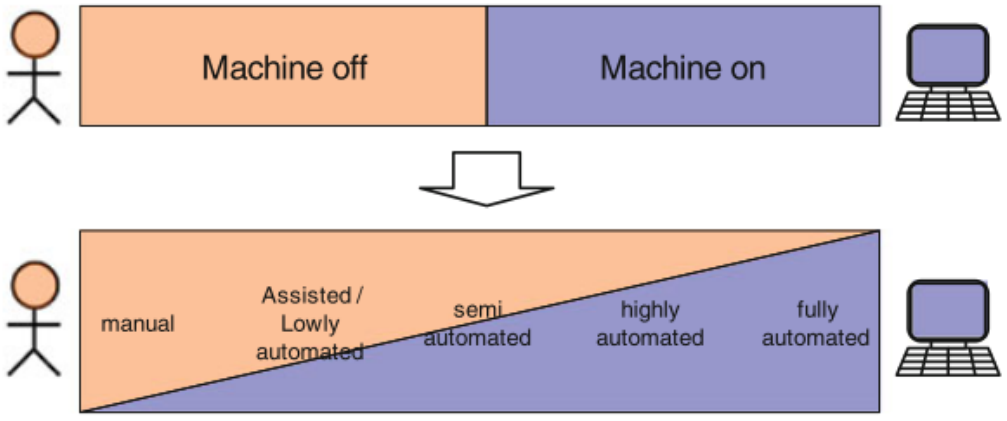

FIGURE 2.10: A simplified representation of role change [14] where the machine/robot's control over the system is represented in purple and the human's control is represented in orange.

The current trend for role change is on decision making and action selection during interactions and on how changes in the degree of control the robot and human have over the system can improve

safety during pHRC [14, 124]. One method of representing the relationship between roles and role change in pHRC used in the past was the use of state machines. In a state machine, each LoA of the robot is represented as a state and the conditions for transitioning between each state is defined. Using this method to represent the interaction dynamics makes the relationship between the human and the robot clearer. An example of this approach can be seen in Figure 2.11 [15].

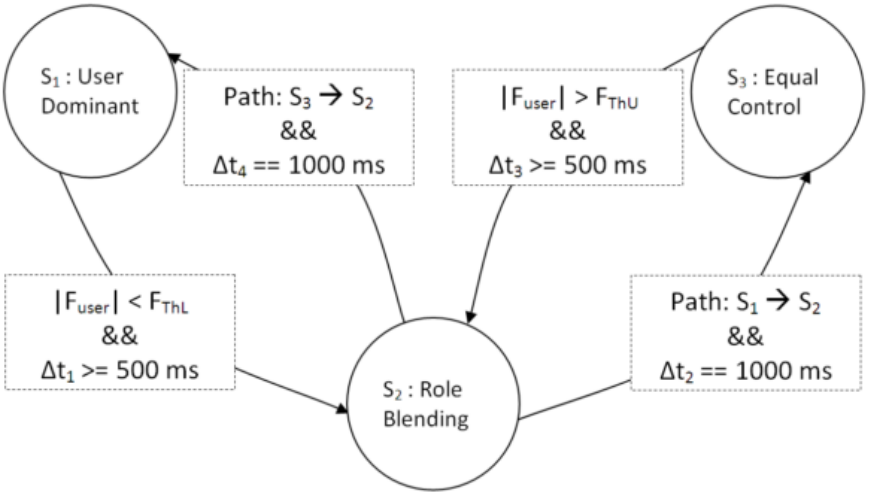

FIGURE 2.11: A representation of roles and role change using a state machine [15].

In pHRC a role change is generally triggered as a result of an event in the interaction. Emergency stops or other physical switches can be used to trigger a role change. In his work, Lyu [133] used a method for role change where the robot's behavior would change when the robot detected the presence of the human in the workspace. When the robot did not detect the human's presence, it would complete the task autonomously. However, if the robot detected the presence of the human then the robot's LoA would shift and the robot would work collaboratively with its human co-worker to complete the task. A more common approach towards role change in pHRC is to initiate a role change when the force applied by the human to the robot exceeds a predefined threshold [134].

Some researchers have adapted the force threshold method for role change and have implemented a dynamic threshold for role change that is more natural for the human during pHRC [135]. This field of research is often referred to as adaptive role change. In systems which implement adaptive role change, probabilistic models based on previous interactions are used to determine whether a role change should occur during the interaction [136, 137].

Regardless of the methods for triggering a role change, the human is generally the one who initiates the role change during pHRC. Examples in the literature where the robot intervenes in the human's actions during pHRC are generally limited to situations such as collision avoidance or singularity avoidance including the NavChair [138] and the Smart Hoist [38] where the human maneuvers the robots in cluttered environments. Whether the implementation of collision avoidance and singularity avoidance are a form of role change is ambiguous as the robot's LoA or role in the interaction must change to be considered a role change. In the Smart Hoist and and Navchair examples, a role change does occur as the robot's role in the pHRC changes from observing the human's actions in the task to creating a new path plan and implementing it to avoid collision before changing its role back to observing the human.

Flemisch in his work on autonomous driving proposed a method for determining whether a role change is initiated [16]. Inspired by the way human riders interact with their horses, H-Mode interprets the human's desire for a role change by considering the differences between tight and loose rein control of a horse which represent the rider controlling the horse's movement and allowing the horse to move freely respectively. A graphical representation of the different states is shown in Figure 2.12.

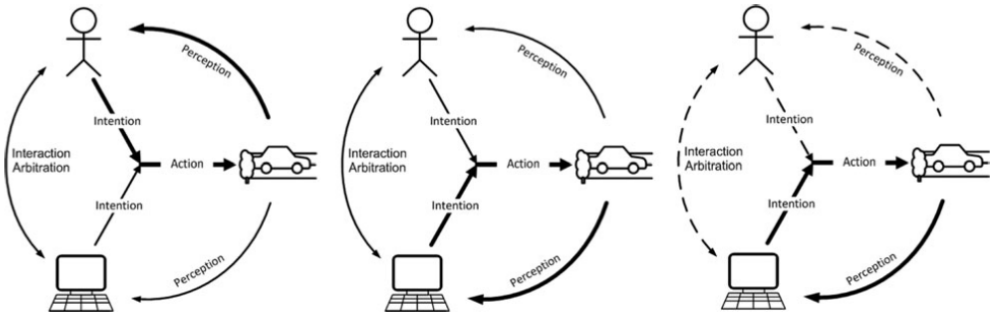

FIGURE 2.12: Left: H-Mode assisted. Middle: H-Mode highly automated (contact). Right: H-Mode highly automated (no contact) [16].

In the interaction, the robot (or vehicle) would normally operate autonomously by controlling the steering wheel and the speed of the vehicle. The human initiates a role change by resisting the change in the steering wheel's orientation. When the force resisting the steering wheel's movement surpasses a threshold, a role change is triggered which decreases the robot's LoA. When the resistance force exerted by the human decreases to a value below another threshold or the human

releases the steering wheel completely, the robot's LoA increases and the robot once again operates in an autonomous state.

Another approach focuses on a gradual shift in control between the human and the robot to facilitate a smooth transition [139, 140]. This approach is commonly referred to as shifting or sliding autonomy. In Abbink's work [124], the stiffness of the foot pedal and the steering wheel in a semi-autonomous vehicle was used to express the robot's desire for a role change. When the robot disagreed with the human driver's actions or detected an event where it should intervene to avoid collisions with other vehicles, the stiffness of the foot pedal and the steering wheel would increase. The increase in the stiffness would resist the human driver's actions as they control the vehicle and if the stiffness of the foot pedal and steering wheel increased to the point where the human cannot override the stiffness, the robot is considered to have transitioned into an autonomous state.

Although Abbink's work was on semi-autonomous vehicles, it is possible to transfer the model to other applications. In this model, the robot is an autonomous vehicle with collision avoidance capabilities. Unlike previous examples where the robot will automatically take control of the system in order to avoid collisions, this model makes the robot's intention to avoid collision known to the human operator (driver) by increasing the stiffness of the foot pedal and steering wheel. When the human can no longer overcome the stiffness of the robot, then a role change is considered to have occurred as the LoA of the robot changed from Shared Control with Human Initiative to Full Autonomy.

In a more recent work, Whitsell [135] took the concept of role change a step further when he proposed the use of the method referred to as shared responsibility. Shared responsibility considers that the robot and the human are simultaneously leaders and followers in the interaction. This was done by decomposing interaction into subtasks. Whether the robot or the human is the leader or the follower in a subtask is independent of their role in the other subtasks. When the human initiates a role change in the interaction, the human takes the leader role in one of the subtasks away from the robot. In return, the human relinquishes the leader role in one of the subtasks to the robot so that the number of subtasks that the human has a leader role in remains the same. This is in line with Long's research which defined role change as the process of relinquishing one role and assuming another [141]. In the example presented by Whitsell, the task being performed by the human and the robot is divided into two subtasks where the robot was the leader in the first subtask

while the human was the leader in the second subtask. When the human initiated a role change, the roles of the human and the robot switched resulting in the human being the leader of the first subtask while the robot became the leader in the second subtask. It is unclear from his work how the shared responsibility method of role change would change in tasks with more subtasks and whether the human or the robot must relinquish control of a subtask to becoming the leader in another subtask. When implementing the shared responsibility approach towards role change, it is possible for situations to arise where both the human and the robot attempt to take the leader role in a subtask or both the human and the robot wish to relinquish the leader role in a subtask at the same time. It is situations like these where factors for effective interaction and negotiation come into play [130, 142, 143].

A human's confidence in its robot co-worker is one of the factors determining whether the human initiates a role change. However, to date, there has yet to be a role change method which uses the confidence of the robot in its human co-worker to determine whether the robot should intervene in its human co-worker's actions and initiate a role change. The research by Sanders mentioned in Section 2.2 and Rahman [17] are to date the closest work relevant to the research presented in this thesis in terms of using the confidence or trust of the robot in its human co-worker to initiate a role change. In his work, Sanders directly uses the human's performance in doing the task to scale the gains on the robot's velocity [101]. As the human's performance decreased, the robot would decrease its maximum velocity to reduce the control the human has. In Rahman's work, the robot's trust in its human co-worker is used to determine whether a handover occurs and what type of handover will occur. The execution plan for the trust-based handover strategy proposed by Rahman is shown in Figure 2.13.

When the robot's trust in its human co-worker decreased below a threshold, the behavior of the robot would change. From this point onwards, the type of handover the robot performed would depend on the robot's current trust in its human co-worker. Based on the definition of role change used in this thesis, the robot's response to its change in trust presented in Rahman's work is not considered to be a role change. This is because the robot's LoA in the interaction does not change, nor does its role in the interaction. For all values of the robot's trust, the robot is the one who decides how the handover will proceed in the pHRC. Unlike the method presented by Rahman that only considers the robot's current trust, the confidence-based role change method presented in this thesis takes into account how the robot's confidence in its human co-worker has changed,

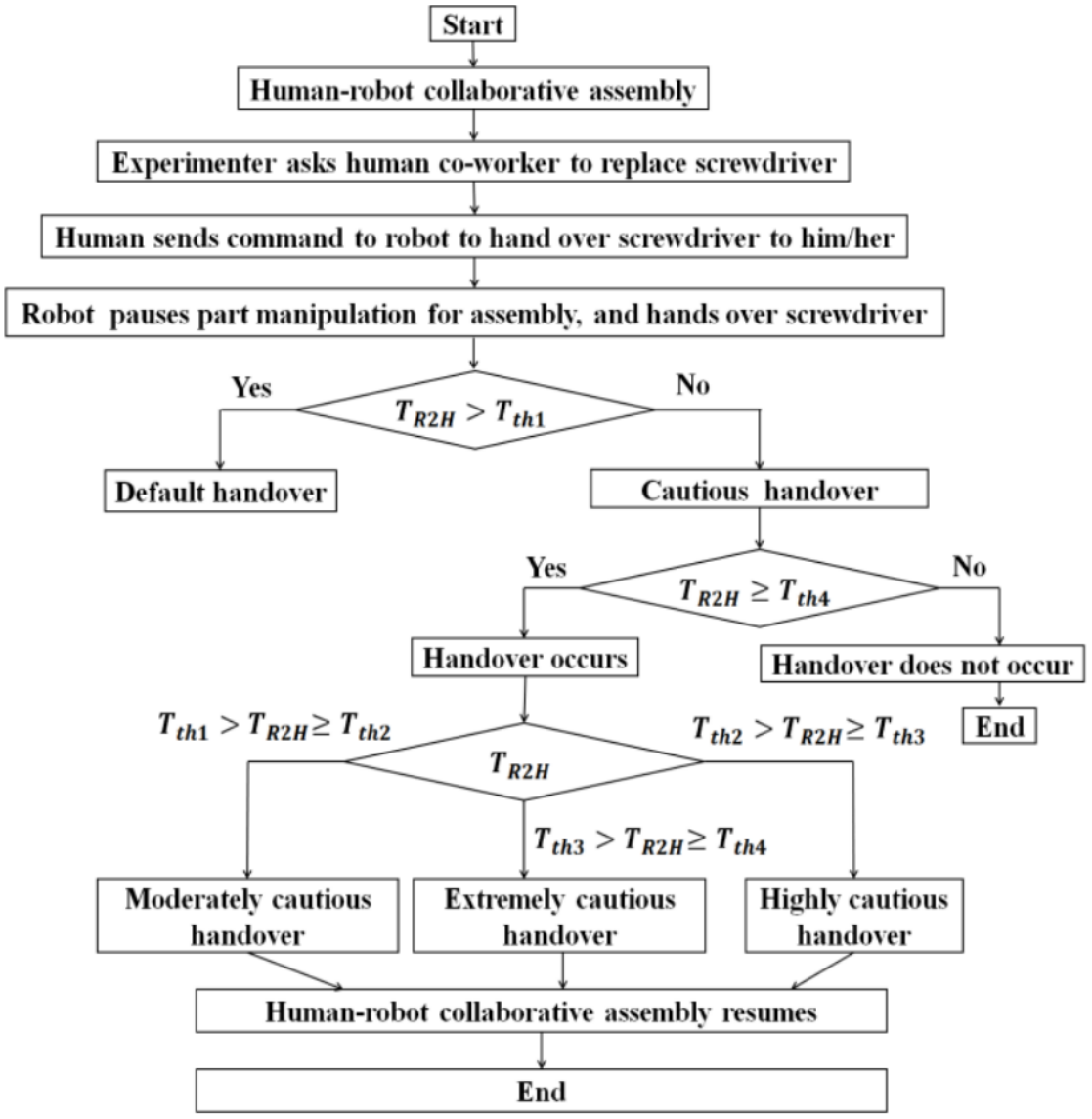

FIGURE 2.13: Execution plan for the trust-based handover strategy presented by Rahman [17].

the robot's current confidence in its human and the robot's bias when determining whether a role change should be triggered in the pHRC.

2.4 Summary

Robots designed for pHRC have been developed for a variety of applications in both the industrial and healthcare sectors. As the technology used in these robots improves, the robots are expected

to be able to make more informed and nuanced decisions on how to react to changes in the environment and its human co-worker's intentions. Previously, humans would be responsible for the safety of the interaction. However, with the increased intelligence of robot co-workers, the responsibility for maintaining the safety of the human and the robot during a pHRC can be shared. Trust and confidence are key factors in determining whether a human intervenes in the actions of its robot co-worker. Trust and confidence in pHRC is generally considered from the human's perspective. Most existing models for trust and confidence cannot be used in real-time applications as the trust and confidence of the human in its robot co-worker is obtained from a statistical analysis of survey results following the interaction. For the robot to intervene in the actions of its human co-worker, a role change must be initiated. Current models of role change in pHRC are generally focused on the forces applied by the human and how they are applied.

This thesis aims to conduct systematic research, in the context of pHRC, from methods for user intention identification in pHRC, modeling of robot confidence in its human co-worker, a general framework for interaction modeling, to a method for confidence-based role change. It also aims to verify the proposed methods through various experiments with different collaborative robots that are designed for providing physical assistance to human co-workers.

Chapter 3

Robot Perception of its Human Co-worker in physical Human-Robot Collaboration

In order for a robot to determine whether it should intervene in the actions of its human co-worker and initiate a role change during physical Human-Robot Collaboration (pHRC), one of the important capabilities the robot should have is to perceive its human co-worker's actions. A robot's perception of a pHRC is limited by the number of sensors and the type of sensors it has access to. The greater the variety in the robot's sensors, the greater the amount of information the robot can collect, allowing the robot to make more meaningful decisions.

In pHRC, the human generally interacts with the robot through a handlebar attached to the robot [87][144][79]. This handlebar is often the only point of contact between the human and the robot. The robot typically interprets the human's intention through the handlebar by either directly measuring the forces applied by the human through sensors such as load cells or strain gauges, or indirectly by sensing the changes in its joint torques [145]. These methods provide force and torque measurements but overlook information such as how the human grasps the handlebar. Incorporating the human's grasping information provides the robot with more information during pHRC, improving the robot's perception of the human's actions.

This chapter investigates the contribution the human's grasping pattern and grasping strength towards the robot's perception of the human during pHRC. A method for identifying the orientation of the human hand around a cylindrical handlebar [18] is presented (Section 3.2). Machine learning algorithms such as Support Vector Machine (SVM) and Bayesian Inference are used to classify the orientation of a human's hand during a static grasping scenario. This method is evaluated in two scenarios. In the first scenario, the training data and the test data are different but from the same subject. In the second scenario, the training data and the test data are from different subjects. The changes in grasping strength as the human co-worker works collaboratively with a robot to complete a task [19] are explored (Section 3.3). The changes in grasping strength when the robot's behavior is within the human's expectations and when the robot behaves unexpectedly are compared and contrasted. Finally, the benefits of incorporating the human's hand orientation and grasping strength in pHRC are discussed.

3.1 Human Grasping Pattern Detection

The sensor used in this thesis to detect the grasping pattern of the human co-worker is the Thrumode Matrix Array Sensor (TMMAS) shown in Figure 3.1. The TMMAS is a flexible array of 10x16 pressure sensor cells from Sensitronics [146]. When pressure is applied to any of the 160 cells of the TMMAS, the resistance of the cell changes. Each individual cell on the TMMAS is capable of measuring pressures up to $16psi$. The TMMAS was used in this thesis because it is a force sensitive resistors which was both flexible and able to record both the pressure and the location where the pressure was applied for multiple points of contact. Unlike most force sensitive resistors, the sensor reading at each individual cell of the TMMAS is independent of the pressure applied to the other cells which allows the TMMAS to simultaneously record the pressure applied at each of the 160 cells.

The average maximum grip strength of males and females between the ages of 20 and 49 is approximately $122.65lb$ and $77.1lb$ respectively under the assumption that the right and left hands of the subjects have equal strength [147]. The sensing area of the TMMAS is 2x3.5 *inches*. This results in an average pressure of approximately $17.5psi$ and $11.0psi$ on the sensing area of the TMMAS for men and women respectively. When grasping a handlebar, the grasping force applied by the human is not equally distributed over the sensing area of the TMMAS due to the distribution of

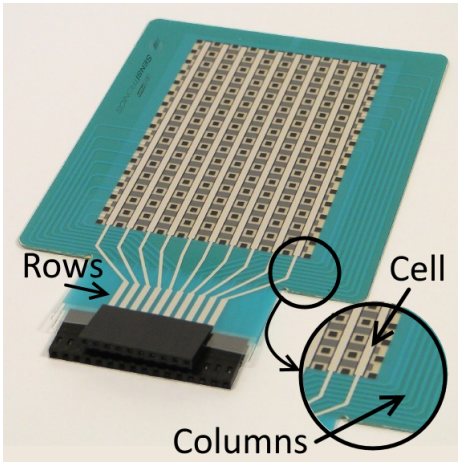

FIGURE 3.1: The Thrumode Matrix Array Sensor used in this thesis to record the grasping patterns of the human co-worker. Reproduced from [18].

muscle, fat and bone in the human hand [148][149]. Taking into consideration the sensing range of the TMMAS and the average maximum grip strengths for males and females, it is unlikely that the pressure applied during data collection would saturate the cells in the TMMAS.

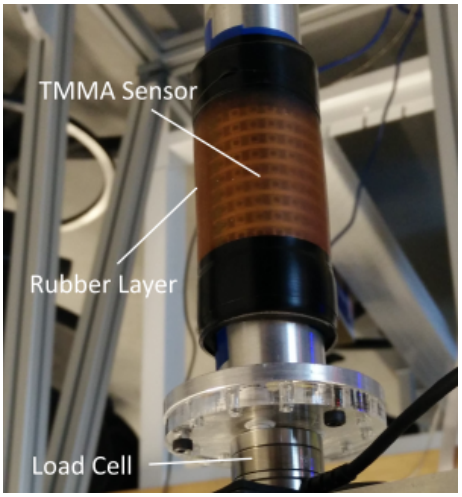

FIGURE 3.2: The Thrumode Matrix Array Sensor wrapped around a cylindrical handlebar and covered in a polyurethane compound. Reproduced from [18].

The TMMAS was wrapped around the surface of a 27*mm* outer diameter steel cylinder with a vertical slit used to feed the sensor's cables into the interior of the handlebar. The diameter of the handlebar was chosen so that the sensing area of the TMMAS would cover as much of the handlebar's circumference as possible without overlapping itself. A 3*mm* layer of polyurethane compound with a 20*A* Shore hardness was placed over the TMMAS and secured as seen in Figure 3.2.

The rubber compound increased the diameter of the handlebar closer to the optimal diameter for grasping [150] while also transferring the grasping force of the human to the TMMAS.

As the TMMAS was designed to be laid flat, wrapping the TMMAS around the handlebar introduced an initial bias to the pressure values in the sensor cells. In this thesis, the raw values of pressure (P) from the TMMAS are used. The values obtained from the TMMAS fall within the range $0 \leq P \leq 127$ where $P = 0$ represents that no pressure is being applied to the cell and $P = 127$ represents a saturated cell. It was found that the bias in the TMMAS cells generated by the vertical slit and the flexing of the sensor would generally be below $P = 25$. The sensor reading seen in Figure 3.3b depicts the pressure at each of the 160 cells of the TMMAS generated by the hand print seen in Figure 3.3a. The 160 cells of the TMMAS are sampled at a rate of $50Hz$ through a Snowboard, 3rd party data acquisition device designed specifically for the TMMAS [151].

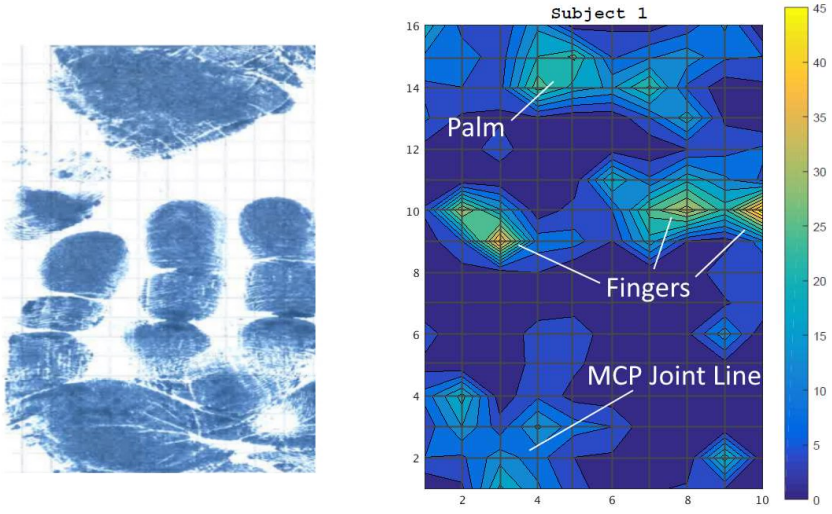

(a) (b)

FIGURE 3.3: (a) A human hand print (b) The TMMAS sensor reading generated by the grasping pattern shown in Figure 3.3a. Reproduced from [18].

3.2 Human Hand Orientation Identification

In this section, the orientation of the human hand around a cylindrical handlebar is identified using the data from the TMMAS. Recognizing the human's hand orientation around a cylindrical handlebar can contribute to the robot's understanding of how the human interacts with the robot during a pHRC.

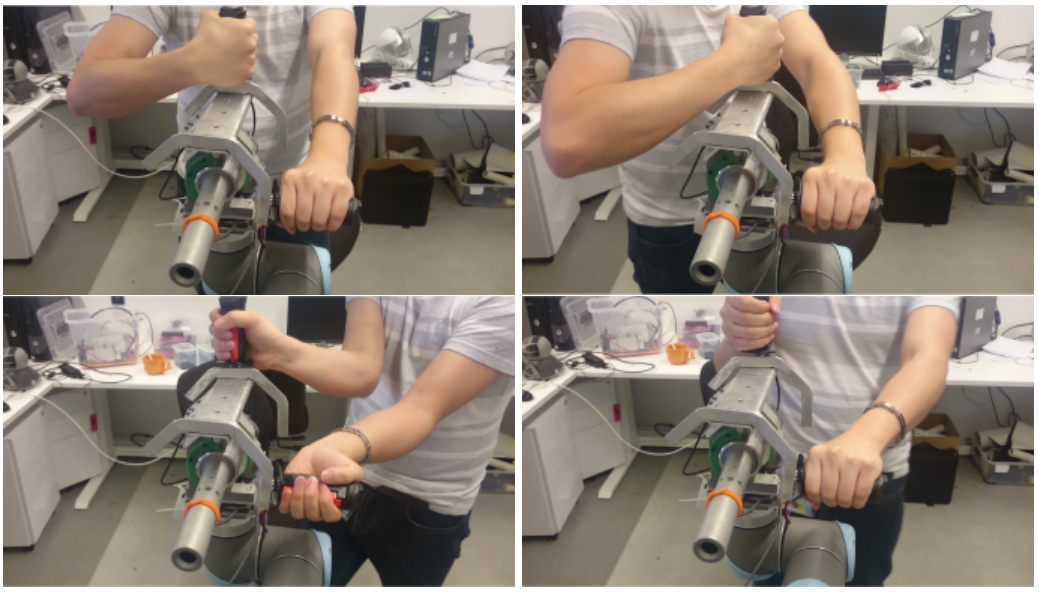

FIGURE 3.4: How changes in hand orientation can influence the pose of the human operator when the position of the hands and feet are fixed and wrist angle is approximately zero degrees.

Figure 3.4 shows an operator interacting with a robot arm designed for collaborative grit-blasting. In the images, the position of the human operator's feet are fixed and the operator's hands are placed on the handlebars with their wrist angles at approximately zero degrees. From the images, it can be seen how the operator's pose is affected by the relative orientation of the human's hands and the handlebars. Although the change in pose can be counteracted by a change in the human operator's wrist angle, having a large bend in wrist angle is unintuitive and results in increased discomfort in the operator [152]. The human's hand orientation can be used to provide insight into the human's arm posture and pose [153][154]. This information can be used in conjunction with musculoskeletal models to gain insight into the operator's strength and fatigue [155] which may be a factor in prolonged pHRC.

3.2.1 Experiment Design

For identifying the orientation of the human hand when grasping a handlebar, two different scenarios are considered as follows:

- **Scenario 1** - The training data and the test data are different but from the same subject. This is useful in applications where the robot is used by known operators who would have had

their grasping patterns recorded.

- **Scenario 2** - The training data and the test data are from different subjects. This is useful in applications where the robot can be used by any operator, even if their grasping patterns have not been recorded.

Ten subjects were asked to participate in this study. Nine of the subjects participating in the experiments were male and one was female. All of the subjects were right handed and all experiments were performed using the right hand of the subjects. The length of the subjects' right hands ranged from 167*mm* to 202*mm* measured from the tip of the middle finger to the wrist crease and the width of their right hands ranged between 77*mm* to 94*mm* measured along the metacarpal.

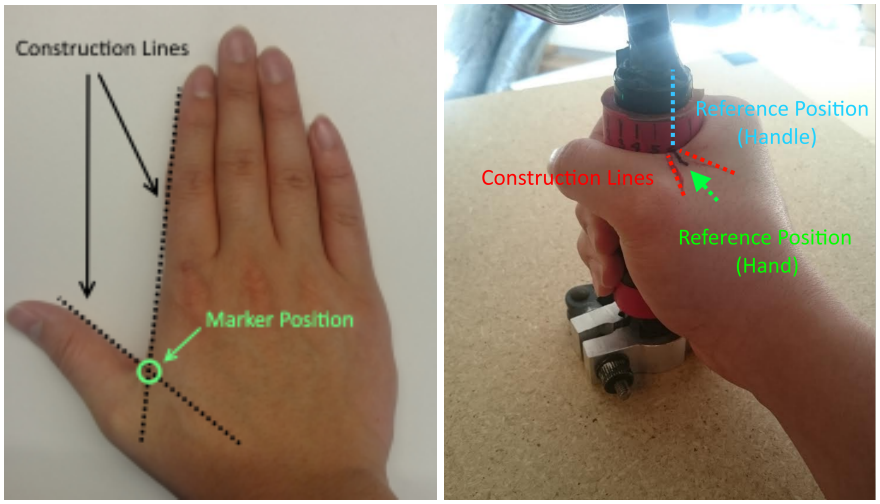

(a) (b)

FIGURE 3.5: (a) The position of the reference marker position on the subject's hand (b) A subject performing a power grip on the handlebar with the reference position on their hand aligned with a reference position on the handlebar. Reproduced from [18].

Seventeen positions were marked and numbered around the circumference of the handlebar. These marked reference positions were used to evaluate the accuracy of the identification methods. The first sixteen positions were aligned with the sixteen columns of the TMMAS, the final reference position was placed between the sixteenth and first marked positions in the small region where the TMMAS did not cover. During the data collection process, a reference marker was also placed onto the right hand of each subject between their thumb and forefinger; the position of the marker is shown in Figure 3.5a. The marker on the subject's hand serves as a reference point across all of the subjects when aligning their hands for data collection. This reference marker is used purely to

assist in labeling the grasping data and validating the test data. The error in the placement of the hand marker between subjects is estimated to be smaller than the distance between two adjacent marked regions on the handlebar.

During data collection, the subjects were seated with their elbows bent at approximately 90° and their forearms parallel with the floor. The subjects were asked to align the marker on their right hand with one of the positions marked on the upright handlebar and grasp onto the handlebar using the power grip [156] seen in Figure 3.5b.

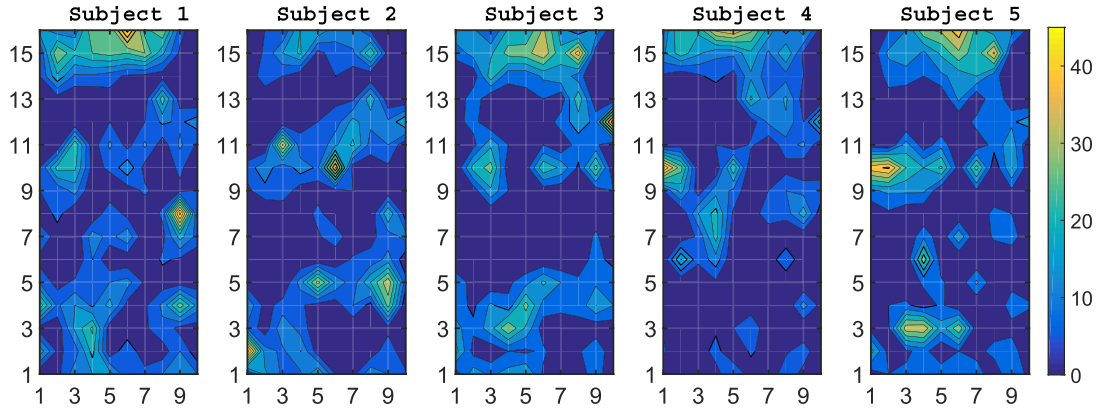

FIGURE 3.6: Comparison of the sensor readings from 5 subjects with the marker on their right hand aligned to the 2nd marked reference position. Reproduced from [18].

Figure 3.6 depicts sensor readings obtained from a single TMMAS reading for five subjects with the reference marker on their hands aligned with the 2nd marked reference position. It can be seen visually that there are similarities across all of the sensor readings. This is an expected outcome as the overall shape of the human hand is similar for all subjects. However, it can also be seen that there are variations in the sensor readings which are a result of individual differences between the subjects. Factors contributing to this include but are not limited to the difference in hand sizes, the distribution of fat, muscle and bone in each subject's right hand, how hard each subject is grasping the handlebar and the positioning of their fingers when recording the dataset [150].

In Figure 3.7, an example of the total pressure P_{total} when the pressure (P) at each of the 160 TMMAS cells are added together and the number of cells of the TMMAS with a value of $P > 25$ when a subject grasps the handlebar is shown, where $P = 25$ is the maximum bias in the pressure readings caused by wrapping the TMMAS around the cylindrical handlebar. From the figure, it can be seen that before the subject grasps the handlebar, the total bias in all 160 TMMAS cells

generated by wrapping the TMMAS around the handlebar is generally less than 800 which is an average of $P = 5$ per cell. In Figure 3.7, less than 17 cells have a reading of $P > 25$ when the human grasps the handlebar.

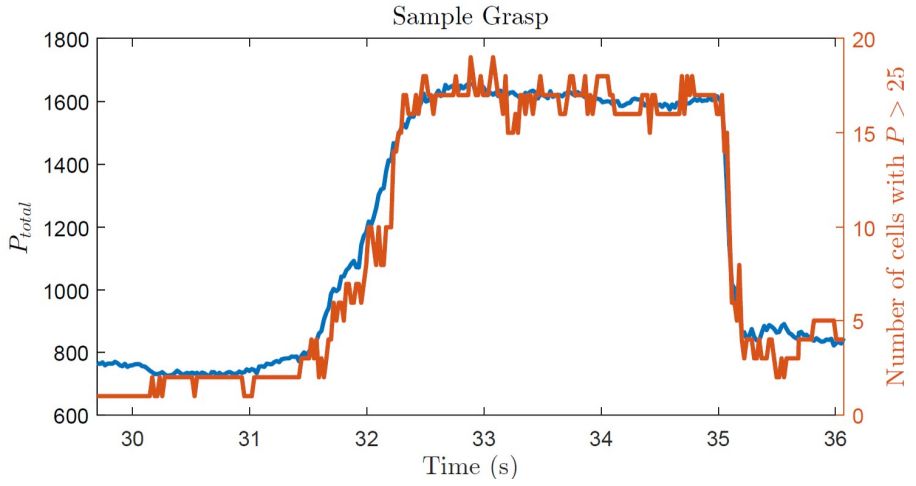

FIGURE 3.7: The total pressure applied to the handlebar and the number of cells with values over 25 as the subject grasps the handlebar. Reproduced from [18].

After the subject grasps onto the handlebar, both the P_{total} and the number of cells with values $P > 25$ increases. Following the increase in pressure, the subject's grasping force generally decreases slightly as they relax their grip to a comfortable level which is a natural reaction when grasping and picking up objects [157]. From Figure 3.6 it can be seen that when a subject grasps the handlebar only the fingers, thumb and a section of the palm are able to generate pressure values of $P > 25$ so it can inferred that $P > 25$ is a relatively high value of pressure. Therefore, when the human grasps the handlebar, although the pressure applied to each of the 160 cells of the TMMAS increases, the majority do not surpass $P > 25$. The training data was collected once the subject had maintained a stable grasp on the handlebar which can be seen between 32.5 seconds and 35 seconds in Figure 3.7. 200 grasping readings were recorded whenever data was collected.

After the grasping pattern was recorded, the data was labeled with its corresponding marked reference position. The subject was then asked to release the handlebar. Once the sensor had settled, the subject would regrasp the handle aligning their hand with the same marked reference position. This process was repeated three times for each subject at each of the seventeen marked reference positions around the handlebar. Releasing and regrasping the handlebar introduced variability into the training data. When the subjects regrasp the handlebar, it is unlikely for the subject's grasp to be identical to the previous samples due to differences in grasping force and/or finger positioning.

In practical applications, an operator's hand orientation will not be limited to 17 predetermined hand orientations around a cylindrical handlebar. To simulate this, additional datasets were recorded where the subjects would grasp the handlebars at random orientations. After each dataset was collected, the marked reference position closest to the marker on the subject's hand was recorded as the subject's hand orientation for that dataset.

3.2.2 Classification of Hand Orientation

The TMMAS readings consisted of 160 pressure values, each representing the pressure at an individual cell around the cylindrical handlebar. Two classifiers, i.e. SVM and Bayesian Inference, were used to identify the position of the subject's hand. The collected datasets were labeled using the convention shown in Table 3.1 and used as the input to the classifiers. The datasets could be categorized as either a dataset where the subject aligned the marker on their hand with the marked reference positions on the handlebar (LF) or a dataset where the subject grasped the handlebar at random orientations (LR).

TABLE 3.1: Labels being used for the collected datasets. Reproduced from [18].

Label	Description
LF-SX	Dataset collected in a lab, where the marker on the subject's hand is aligned with the fixed reference points on the cylindrical handlebar for subject(s) A, where A can be any number of subjects between 1 & 10. e.g. LF-S1 (one subject) or LF-S12345678 (8 subjects)
LR-SX	Dataset collected in a lab, where the subject A grasped the handlebar at random orientations without aligning the marker on their hand with the reference points on the handlebar.

The output of the classifiers was the estimated hand orientation of the subject. If the identification system is to be implemented in a real-time pHRC scenario, the classifier must have a high accuracy and classification speed. According to previous literature, human reaction time to tactile stimulus is approximately 155*ms* [158] and human response time is approximately 385*ms* [159]. The difference between the two times signifies the time period where the human has felt the stimuli but is unable to react to it. Ideally, the time required for the classification of the hand position should be well below these times.

SVM and Bayesian Inference were selected as the two identification systems used to classify the orientation of the human hand in this thesis. SVM was chosen as it is known to be a powerful tool for non-linear multi-class classification and has been used extensively for pattern recognition and classifying human responses in pHRC [160][161]. It has also been previously implemented in conjunction with the TMMAS to identify the direction in which the subject is pushing when the operator is grasping the handlebar [162]. The libsvm library [163] was implemented in C++ and compiled for Matlab configured with Support Vector Clustering and a one vs. one multi-class approach [164].

Bayesian Inference [165] on the other hand, was selected as the other identification system as it allows the fusing of the prior into the new prediction. This can be relevant when considering the changes in hand orientation over time during pHRC. It has also been used in a number of previous works for real time estimation of robot grasping [166][167]. In this work, the world was modeled as a finite space $s = \{s_1 ... s_n\}$ of states where $1 \leq n \leq 17$ with a finite observation space $z = \{z_1 ... z_m\}$ where $1 \leq m \leq 160$.

The sensor model uses the conditional probability of seeing the pressure reading z_k for the hand orientation (state) s_i, i.e. $P(z_k|s_i)$. A state vector φ is the probabilistic distribution over all hand orientations. Given a prior estimate of the position vector φ_{t-1}, a new estimate for φ_t can be obtained after observing z_k by updating the probability distribution using Bayes' Rule as seen below where N is a normalizing factor:

$$\varphi_t(s_i|z) = \varphi_{t-1} \prod_{k=1}^{k=160} \frac{P(z_k|s_i)}{N} \tag{3.1}$$

The classification of the subject's hand orientation was performed in Matlab, running on a PC with a 3.47 GHz CPU on a Linux Operating System. In this work, training data was generated by randomly sampling 200 TMMAS readings for each marked reference position from the datasets where the reference marker on the subject's hand was aligned with the reference positions on the handlebar. While there is a risk of overfitting with SVM if the amount of training samples is too high, the variability of the data across the 3 data collection instances per position per subject also needs to be accounted for. The number of training data samples was empirically determined by considering the relationship between the number of samples and the accuracy of the classification.

Principal Component Analysis (PCA) [168] is often used as a tool to transform a high-dimensional dataset into a smaller-dimensional subspace [169]. In this research, PCA was used to transform the sensor readings obtained from the TMMAS to reduce the number of inputs for the classifiers. By applying PCA to the input of the classifiers, the time required to identify the human's hand orientation should decrease. In previous works, PCA was adopted as a method to simplify the classification of different human grasp types [170][171]. A result is considered to be statistically significant if its accuracy is above 95% [172][173]. Figure 3.8 shows the number of principal components required to represent 95% of the training data as the number of subjects increases. As training data from more subjects are included, the variety of grasping patterns represented within the training data increases which should improve the accuracy of the classifier in correctly identifying the subject's hand position.

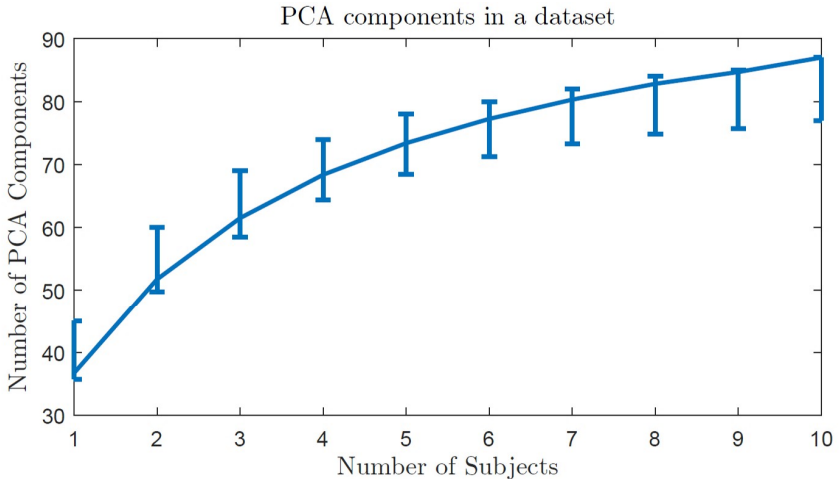

FIGURE 3.8: The number of PCA components required to maintain 95% of the original dataset's information based on the number of subjects included in the dataset. Reproduced from [18].

It can be seen in Figure 3.8 that there is a general trend where the number of required principal components increases as the number of subjects contributing to the training data increases. It can also be seen that the number of principal components begins to plateau with the addition of more subjects. In this work, the test data is classified against the training data, before and after applying PCA in order to verify the effect PCA has on the accuracy and time required for the hand orientation classification.

3.2.3 Experiment Results and Discussion

In this section, an extract of the results from the experiments is provided. The complete results of the experiments can be found in Appendix A. The results from the experiments are split into two categories, accuracy and computation time. In the following tables, Exact refers to the accuracy of the classifier for a correct classification. Within 1 refers to the accuracy of the classifier if the adjacent marked reference position to the subject's actual hand orientation is also considered to be a correct classification. For example, if the subject's hand was at the 15th position but the classifier believed the subject's hand was at the 14th position. The mean refers to the average accuracy of the classifiers for the 10 subjects.

3.2.3.1 Scenario 1 Experimental Results

The purpose of Scenario 1 was to verify that Bayesian Inference and SVM were capable of identifying the position of the subject's hand around a cylindrical handlebar. In this scenario, the training and test data are different but come from the same subject. The training data is comprised of datasets when the subject's hands were aligned with the marked positions on the handlebar and the test data consists of the datasets where the subjects grasped the handlebars at random orientations.

TABLE 3.2: Scenario 1 Example - Classification result of Subject 1 using Subject 1's data as the training data. Reproduced from [18].

Scenario 1 - Subject 1					
Training Data	Test Data	Classifier	Exact Identification	Identification Within 1	Average Time (ms)
LF-S1	LR-S1	SVM Without PCA	76.27%	100.00%	0.31
LF-S1	LR-S1	SVM With PCA	76.92%	100.00%	0.05
LF-S1	LR-S1	Bayesian Without PCA	68.47%	95.17%	0.96
LF-S1	LR-S1	Bayesian With PCA	63.53%	85.03%	0.14

TABLE 3.3: Scenario 1 - Combined Results. The mean and standard deviation of the results for all 10 subjects for Scenario 1. Reproduced from [18].

Classifier	Exact Mean	Exact Std	Within1 Mean	Within1 Std	Time (ms) Mean	Time (ms) Std
SVM Without PCA	69.83%	16.69%	93.79%	6.79%	0.32	0.03
SVM With PCA	70.06%	16.63%	93.67%	6.57%	0.05	0.005
Bayesian Without PCA	49.56%	20.30%	77.35%	18.20%	0.78	0.06
Bayesian With PCA	48.04%	13.48%	67.80%	14.22%	0.15	0.02

Table 3.2 and Table 3.3 show the results from the experiments for Scenario 1. Looking at the average time required for the classification, it is clear that the computational requirements for both identification systems are sufficient for real-time pHRC.

In general, the accuracy of the SVM classifier exceeds that of the Bayesian Inference classifier. The application of PCA had a negligible effect on the accuracy of the SVM classifier but had a negative effect on the accuracy of the Bayesian inference classifier. Most works agree that the accuracy of a Bayesian Inference classifier should increase or be similar after PCA is applied [174][175]; however, that appears to not be the case . One possible explanation is because the same PCA transform was applied to both the training and the test data, which represent the datasets where the human's hand orientation was aligned to the marked reference positions and randomly oriented respectively. In previous works, the training data and the test data used for Bayesian PCA classification were similar, i.e. the expectation is that the test data matches one of the states in the training data. Therefore, even after a PCA transform, the training and test data are still similar. However, in this application, the data used to generate the PCA transform is the dataset where the hand orientation of the subject was aligned with the marked reference positions on the handlebar and the human's hand was randomly oriented in the test data. It is believed that the accuracy of the Bayesian Inference classifier after PCA was similar when the orientation of the subject's hand in the test data was close to a marked reference position but decreased when the marker on the subject's hand was not near a marked reference position. From the tables, it can be seen that the mean accuracy of the classifiers in Scenario 1 increases from $69.83\%(\sigma = 13.48\%)$ to $93.79\%(\sigma = 6.79\%)$ for the SVM classifier and $49.56\%(\sigma = 20.30)$ to $77.35\%(\sigma = 18.20\%)$ for the Bayesian Inference classifier when considering the Exact Mean and Within 1 Mean cases respectively.

During the classification process, the classifiers calculate the probability of the subject's hand being at each of the marked reference positions. Figure 3.9 shows an example of the calculated probabilities when the Exact classification was incorrect but the Within 1 classification was correct. It can be seen from the figure that the classifiers have a strong belief that the orientation of the subject's hand is at either the 9th marked reference position or the 10th marked reference position. The SVM classifiers have an equal certainty for both positions and the difference between the certainty of the Bayesian Inference classifiers for both positions is small. This behavior

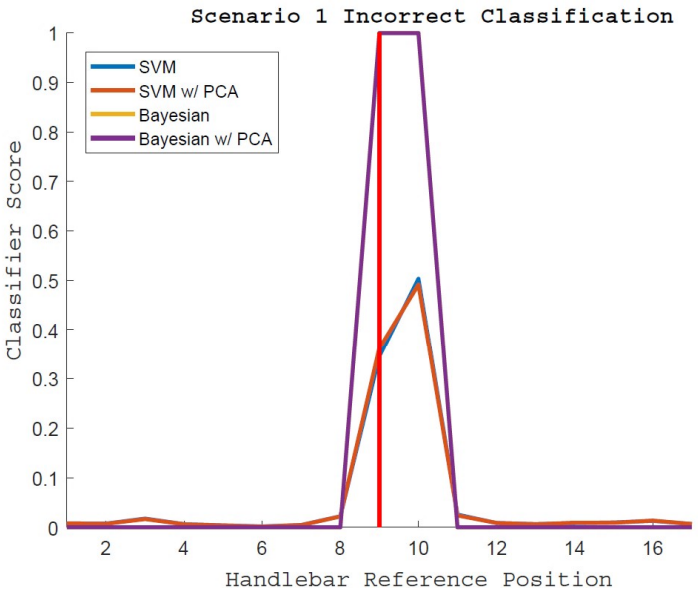

FIGURE 3.9: A example of the probability of the subject's hand being at each marked reference position for an incorrect classification in Scenario 1. The red vertical line represents the labeled position. Reproduced from [18].

is generally true for cases where the classification for Exact Mean was incorrect but the Within 1 Mean classification was correct.

Because the subjects grasped at random orientations for the test data, it is likely that the majority of the hand orientations being classified were not aligned with a marked reference position. Therefore, it is possible that the discrepancy between the accuracies of the Exact Mean and the Within 1 Mean was caused by the incorrect classification of which marked reference position was closer to the subject's hand marker when the subject's hand was between two marked reference positions.

A factor which may have contributed to this discrepancy between the accuracies of the Exact Mean and the Within 1 Mean cases is the webbing on a person's hand between their thumb and forefinger. This webbing deforms slightly during a grasping action which will shift the marker slightly. Although this deformation is much smaller than the distance between two adjacent marked positions on the handlebar, it could be enough for the subject to incorrectly label the orientation of their hand for the test data. This is especially true if the marker is approximately in the middle of two marked reference positions. As the classifiers are able to recognize that the subject's hand orientation is between two marked reference positions, it may be possible that introducing another marked reference position between each of the existing marked reference positions could increase the overall accuracy of the classifiers.

3.2.3.2 Scenario 2 Experimental Results

Scenario 2 verifies whether the two classifiers could be used to identify the hand orientation of a subject using the training data from other subjects. An example result from Scenario 2 can be seen in Table 3.4 where the dataset LF-S10 was used to classify the dataset LR-S1.

TABLE 3.4: Scenario 2 Example - Classification result of Subject 1 when using Subject 10's data as the training data. Reproduced from [18].

Scenario 2 - Subject 1 Example 1					
Training Data	Test Data	Classifier	Exact Identification	Identification Within 1	Average Time (ms)
LF-S10	LR-S1	SVM Without PCA	40.37%	64.53%	0.42
LF-S10	LR-S1	SVM With PCA	36.30%	66.17%	0.07
LF-S10	LR-S1	Bayesian Without PCA	16.35%	29.47%	1.45
LF-S10	LR-S1	Bayesian With PCA	10.00%	23.33%	0.31

From the table it can be seen that there is a drastic drop in the accuracy of the classification compared to the results from Scenario 1. However, by increasing the number of subjects contributing to the training data, the variability in the training data increases may increase the accuracy of the classifiers.

TABLE 3.5: Scenario 2 Example - Classification result of Subject 1 when using the data of all subjects excluding Subject 1 as the training data. Reproduced from [18].

Scenario 2 - Subject 1 Example 2					
Training Data	Test Data	Classifier	Exact Identification	Identification Within 1	Average Time (ms)
LF-S2345678910	LR-S1	SVM Without PCA	64.92%	90.22%	1.65
LF-S2345678910	LR-S1	SVM With PCA	65.10%	90.67%	0.4
LF-S2345678910	LR-S1	Bayesian Without PCA	35.37%	61.57%	1.65
LF-S2345678910	LR-S1	Bayesian With PCA	10.37%	21.62%	0.27

Table 3.5 shows the results of the classifiers when the data of all subjects excluding Subject 1 was used as the training data to identify the orientation of the Subject 1's hand in the dataset LR-S1. It can be seen that by increasing the number of subjects the accuracy of the classifications has increased even though the subject whose hand orientation is being identified is not included in the training data. For the SVM classifier, the accuracy increased from 40.37% and 64.53% to 58.51% and 95.35% for the Exact and Within 1 cases respectively. Similarly, the accuracy of the Bayesian Inference classifier also increased from 16.35% and 29.47% to 45.70% and 85.70% for the Exact and Within 1 cases respectively. The mean accuracies for the classifiers can be seen in Table 3.6.

TABLE 3.6: Scenario 2 - Combined Results. The mean and standard deviation of the results for all 10 subjects for Scenario 2. Reproduced from [18].

Classifier	Exact Mean	Exact Std	Within1 Mean	Within1 Std	Time (ms) Mean	Time (ms) Std
SVM Without PCA	62.00%	14.09%	89.13%	8.93%	1.49	0.07
SVM With PCA	61.68%	12.23%	89.21%	8.46%	0.37	0.03
Bayesian Without PCA	33.52%	7.52%	63.79%	12.72%	1.44	0.11
Bayesian With PCA	7.59%	2.8%	20.16%	6.78%	0.26	0.02

Although the accuracy of the classifications improves with the inclusion of more subjects in the training data, the overall accuracy of the classifiers in Scenario 2 is lower than the accuracy of the classifiers in Scenario 1. The accuracy of the SVM classifier decreased slightly while the accuracy of the Bayesian Inference classifier decreased by a considerable amount.

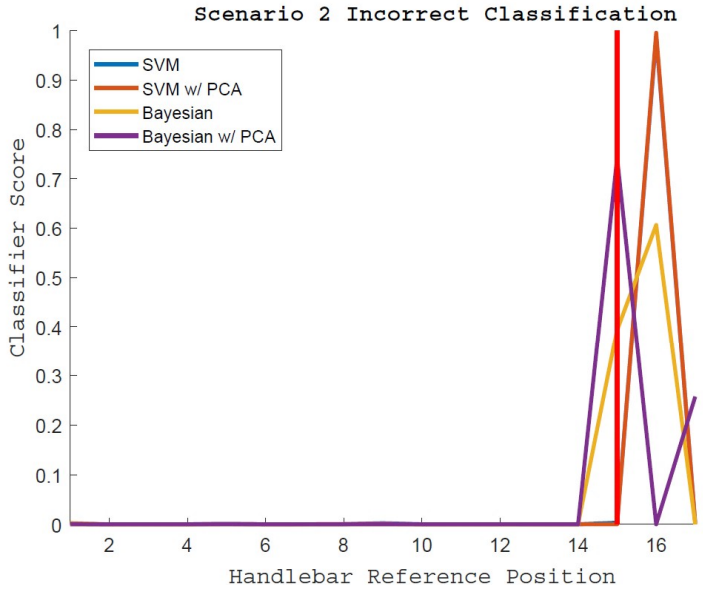

FIGURE 3.10: A example of the probability of the subject's hand being at each marked reference position for an incorrect classification in Scenario 2. The red vertical line represents the labeled position. Reproduced from [18].

Figure 3.10 shows the probability of a subject's hand being at each marked reference position for an incorrect classification. Unlike the sample from Scenario 1 which showed that the orientation of the hand was likely to be between the two marked reference positions, the probabilities in Scenario 2 are generally lower and more spread out. This implies that in Scenario 2, the classifiers can identify the general location of the subject's hand, but the classification of the hand position is less reliable than the classifications in Scenario 1.

One possible explanation for this is the differences in the hand sizes between the subjects. Unlike in Scenario 1, where the hand used for the training and test data is the same, in Scenario 2 the training data is composed of data from other subjects. The difference between the length of the largest and smallest hand sizes of the subjects was 35 mm. As the distance between the reference positions was approximately 6 mm, even if each subject's hand was aligned with the marked reference position, the location a subject's fingers could differ by a number of marked reference positions. As the majority of the forces applied to a handlebar during a grasping action occur at the fingers [149], the corresponding features appearing on the sensor readings would appear to have shifted due to the size of their hands.

3.2.3.3 Discussion

The two classifiers, Bayesian Inference and SVM, were applied to two scenarios which were common in pHRC. Based on the results of the experiments, it was found that the SVM classifier was more suited for the task of identifying the orientation of a person's hand around a cylindrical handlebar than the Bayesian Inference classifier. The effect of PCA on the accuracy of the classifications was negligible in the case of SVM, but did assist in reducing the computational time required by the classifier. Although the Exact accuracy of the SVM classifier is not ideal, the Within 1 classifier results showed that the SVM classifier is able to reliably identity the orientation of the human's hand within 1 adjacent reference position. From the results was shown that in the situations where the Exact classification was incorrect but the Within 1 classification was correct, the marker on the subject's hand was between the identified marked reference position of the SVM classifier and the labeled marked reference position used in the test data. Therefore, it is believed that the Exact accuracy of the SVM classifier can be improved by introducing more marked reference position between each of the existing marked reference positions.

The results also indicate that although training data from other subjects can be used if there is enough variability in the data, the best solution for practical applications is to gather a training dataset from the operator whose hand orientation is being identified. This is because even though the accuracy of the classification is high in Scenario 2, the reliability of the predictions may not be good enough for practical applications. The results also suggest that increasing the number of reference positions around the handlebar may also increase the accuracy of identifying the position

of the operator's hand. In future works, the presented method can be improved by incorporating the dynamic aspects of grasping such as the effects of settling time, the movement of the human's hand, the application of directional forces as inputs in the classifier.

One possible application of this research is in the development of a model for human pose estimation during pHRC. If the human is holding onto the end-effector of a robot, then the position of their hands relative to the robot is known. Previous works have also demonstrated how the human's grasping force on a handlebar is related to the stiffness of their arm [176][177] and arm posture [153][154]. By combining the information on the human's hand position and orientation around the handlebars and the human's grasping strength information, a better estimate of the human's pose may be obtained. Using musculoskeletal models, this information could then be used to gain insight into the operator's strength and fatigue [155] or to adjust the robot's end-effector position during pHRC to a more ergonomic position.

3.3 Human Hand Grasping Strength

Previous research has shown that a human will instinctively tighten their grip when an object is unexpectedly pulled from between their fingers [178][179]. Analyzing how the human responds to physical stimuli and robot misbehavior in pHRC could give insight to a human's instinctive reactions during pHRC.

This section presents the preliminary findings of a study examining the reaction of human during when the robot behaves unexpectedly during pHRC [19]. The focus of the study is on how the grasping strength of the human operator changes during when the robot behaves unexpectedly pHRC and how changes in the human's grasping strength may be an indication of how the human feels about its robot co-worker.

3.3.1 Experimental Design

As the natural reaction of the human when an object is unexpectedly pulled from their fingers is to tighten their grip, the human's reaction to the robot behaving unexpectedly during pHRC is explored by observing the changes in the human's grasping force as the human works collaboratively

with its robot co-worker. This is conducted through two experiments which reflect two scenarios that may occur during pHRC. In the first scenario, the robot co-worker will misbehave at random intervals during the pHRC. In the second scenario, the robot co-worker will not misbehave and support the human during the pHRC. These two scenarios may show a difference in the human's grasping force when the robot's behavior is meets the human operator's expectations and when the robot behaves unexpectedly. In these experiments, the Jexo [180] (Figure 3.11), which is a upper limb exoskeleton designed for collaborative grit-blasting was used.

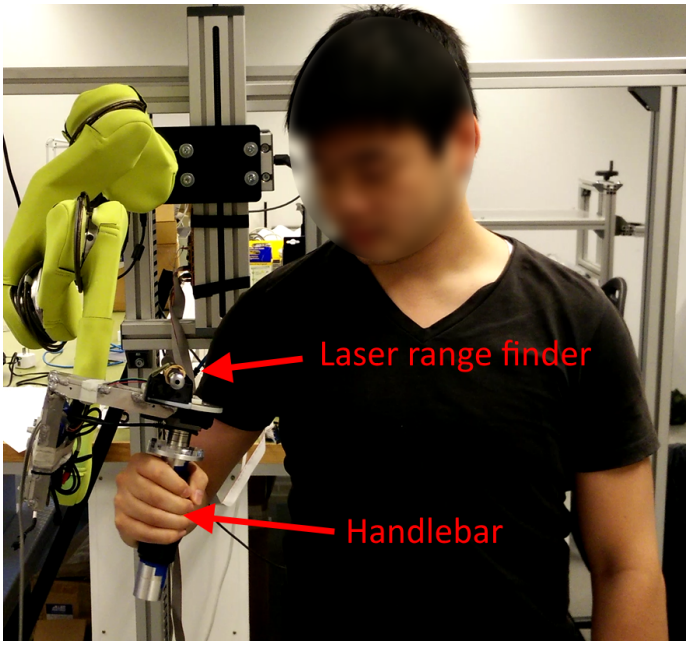

FIGURE 3.11: The Jexo exoskeleton equipped with a handlebar and a laser range finder to emulate an assisted grit-blasting operation.

The Jexo is used to provide physical assistance to the human operator as they complete a collaborative grit-blasting task. Grit-blasting is a physically demanding task where human operators are required to support the blasting nozzle's reaction loads of up to $100N$ for prolonged periods of time [28]. This task is made more challenging due to the limited visibility caused by the dusty environment and the personal protective equipment that are required to be worn by the human operator.

The human operator controls the Jexo through the handlebar mounted to the end of the exoskeleton. The robot detects the forces applied by the human through the load cell which connects the handlebar to the rest of the exoskeleton as seen in Figure 3.2. The robot then uses the detected

forces to infer the human's intention to provide physical assistance during the collaborative grit-blasting task.

The TMMAS that is wrapped around the cylindrical handlebar (Figure 3.2) is used to record the grasping strength of the human operator during the pHRC. In this experiment, the grasping strength of the human operator is collected from the TMMAS through the Sensoray 2608 data acquisition device [181]. The Sensoray 2608 collects TMMAS data at a rate of approximately $50Hz$ and the total pressure applied by the human operator is expressed in millivolts (mV). Each analog input of the Sensoray 2608 is capable of measuring up to $10V$. Based on the grasping information from Section 3.1, it can be inferred that the pressure applied by the human hand will not cause the sensor to saturate. These experiments focus on observing the changes in the grasping strength of the human operator during pHRC. Therefore, it is the relative values of the grasping strength during the pHRC which are important and not the absolute values of the human's grasping strength.

In a collaborative grit-blasting operation, particulate matter would normally be ejected from a nozzle attached to the end-effector of the exoskeleton. However, as the experiments were performed indoors, no particulate matter was released during the experiments. Instead, a laser range finder was fixed onto the end-effector of the Jexo. The laser range finder emits a visible light to simulate the stream of grit and provides the human with a visual representation of where the nozzle would be pointing. The three parameters of interest in these experiments are:

- F_H - The force applied by the human operator to the handlebar on the Jexo's end-effector. This parameter is measured by the load cell attached to the end-effector.
- F_R - The guidance force generated by the Jexo which guides the blasting point along the path or returns the blasting point to the path when the blasting point deviates from the path.
- F_G - The sum of the pressure readings measured by the TMMAS

In the experiments, the goal of the human is to use the laser pointer on the end-effector of the Jexo to follow a path shown on the wall. The control of the exoskeleton utilizes the measured interaction force F_H (the force measured by the load cell in the robot end-effector) to implement an admittance control loop [86]. The robot assists the operator by applying a virtual guidance force

F_R to the admittance control loop which guides the blasting point (the position on the wall projected by the laser range finder) to follow the path that the human operator is currently following. The guidance force of the robot F_R can be decomposed into three components F_{R_x}, F_{R_y} and F_{R_z} which are given by:

$$F_{R_x} = K_N \cdot D_x + K_T \cdot L_x \tag{3.2}$$

$$F_{R_y} = K_N \cdot D_y + K_T \cdot L_y \tag{3.3}$$

$$F_{R_z} = K_P \cdot D_z \tag{3.4}$$

where D_x and D_y is the distance between the blasting point and the path that the human operator is currently following shown in Figure 3.12, D_z is the distance recorded by the laser range finder to the wall, L_x and L_y is the horizontal and vertical distance between the blasting point and the next point of interest (the corners of the path) respectively and K_N, K_T and K_P are constants.

The D component of the equations are introduced to keep the laser pointer on the path and the direction of D is represented as a perpendicular vector between the laser's current position and the path. The further the laser deviates from the path, the larger this component. The second component of the guidance force L is a constant force in the direction of the next point of interest (the corners of the path). The direction of L is represented as a unit vector between the laser's current position on the wall and the next point of interest.

In the experiments, the value of K_T is chosen such that the guidance force has a magnitude of $F_R = 5N$ when the laser is on the path. The value of D_x and D_y should be small to prevent the laser from overshooting when it attempts to return the laser to the path when the position of the laser on the wall deviates. Without human intervention, the robot is able to complete the task on its own. The role of the human in the experiments is to ensure that the laser is following the path.

Before the subjects performed the experiments, the subjects manually followed the paths shown in Figure 3.12 and Figure 3.13 using the blasting point projected by the laser range finder to familiarize themselves with the operation of the exoskeleton. The goal of this step is to ensure that the subjects of the experiment are comfortable with the control of the exoskeleton regardless of their prior experience.

3.3.1.1 Experiment 1 - Unexpected Robot Behavior

In the first experiment, the human uses the laser emitted by the laser range finder to follow the path shown in Figure 3.12 in a clockwise direction.

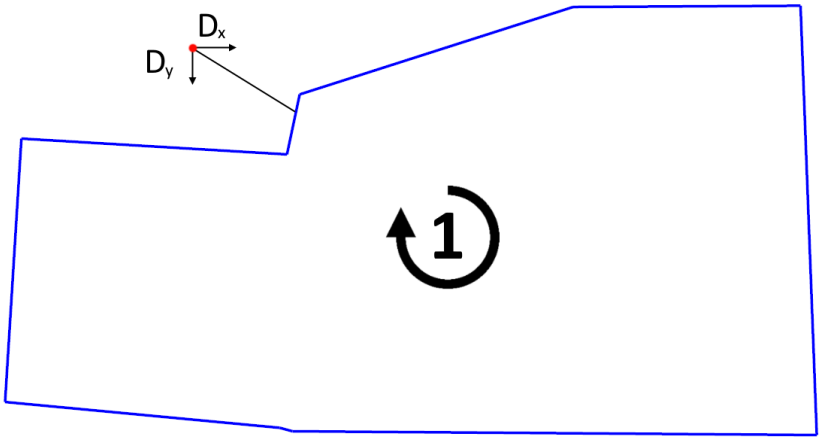

FIGURE 3.12: The blasting path that the subject follows in Scenario 1. The subject moves the laser pointer clockwise around the path in the direction shown. Reproduced from [19].

The goal of the subject during this experiment is to follow the path as accurately as possible. The subject is aware of the guidance force F_R provided by the robot to help them along the path and to reduce the blasting point's deviation from the blasting path.

At random instances during this experiment, the robot create a disturbance and apply a strong force in the direction perpendicular to the blasting path. This will cause the blasting point to shift away from the blasting path which the human is attempting to follow. Prior to the experiments, the subjects practiced the task by following the path on the wall until they are comfortable with controlling the robot. The subjects were not informed that the robot would behave unexpectedly in Experiment 1. This is to prevent their prior knowledge of the robot's unexpected behavior from affecting the subject's initial response to the robot's misbehavior. Following the first disturbance, although the subject may suspect that more disturbances may occur during the rest of the interaction, the subject does not know when they may occur or how strong the disturbances will be. Although the subjects may suspect another disturbance, they may not be expecting another disturbance to occur. It will be interesting to explore in future works how a subject's response to robot misbehavior changes with time and experience.

3.3.1.2 Experiment 2 - Human Initiated Change

In the second experiment, the subject will be the one who initiates changes in the task. The blasting path seen in Figure 3.12 was modified to have two distinct paths which are represented in Figure 3.13 as red lines.

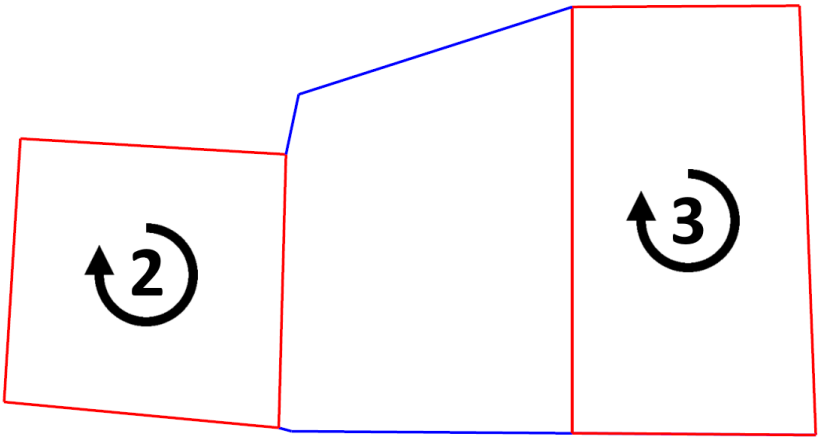

FIGURE 3.13: The blasting path that the subject follows in Scenario 2. The subject moves the laser pointer clockwise in the direction shown around the two paths marked in red and is able to travel between the two paths. Reproduced from [19].

In this experiment, the subject will be following one of the two blasting paths shown in Figure 3.13. Similar to the previous experiment, the robot will apply a guidance force which will help the subject follow the paths. At any point during the pHRC, the subject has the ability to switch from one path to the other.

The subject switches paths by moving the blasting point from one blasting path to the other. Initially, as the subject attempts to change paths, the robot will resist the change in paths as it detects that the subject as deviated from the current blasting path. This resistance force will increase until the new path becomes closer to the blasting point than the previous path. At this point, the robot will recognize that the subject has decided to change paths and the guidance force will change so that the blasting point will follow the new path.

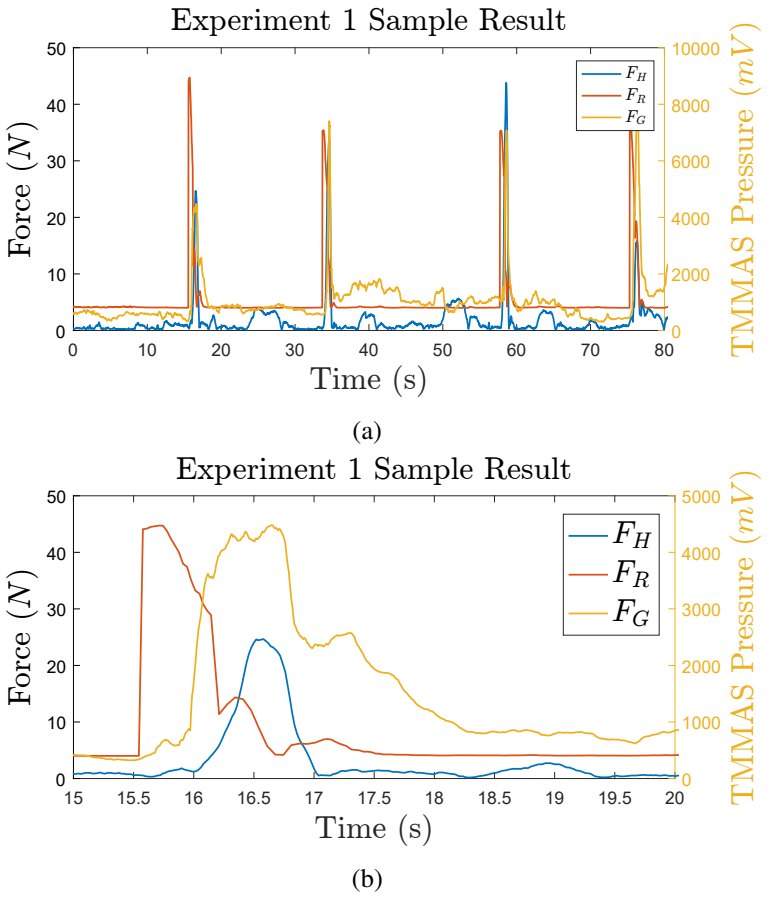

FIGURE 3.14: (a) A sample result from Experiment 1. F_H and F_R are measured in N and the grasping force is measured in mV (b) A magnified view of the forces during robot misbehavior at $t = 15.5$ s from the sample result shown above. Reproduced from [19].

3.3.2 Experimental Results

3.3.2.1 Experiment 1 Experimental Results

A sample result from Experiment 1 can be seen in Figure 3.14a. The characteristics of all the results of Experiment 1 are similar to the one shown. In this experiment, the goal was to observe the reaction of the subject at the handlebar when the robot behaves unexpectedly. Figure 3.14b is a magnified view of one of the disturbances generated by the robot throughout the experiment. The figure shows a sharp increase in F_R followed after a short delay by F_G and F_H. The delay between F_R and the other two forces, can be attributed to the subject's reaction time. However, the time delay between the TMMAS reading (F_G) and the load cell reading (F_H) was not expected prior to the experiment but remained consistent over the course of many experiments.

This phenomenon was originally thought to have been caused by the handlebar on the exoskeleton pushing against the subject's hand when the disturbance generated by F_R occurs. However, if this was the case then the force F_H would have also increased at the same time as F_G. When the force F_G increased, F_H did not increase which indicates that the net force on the handlebar did not change. Although the load cell and the TMMAS poll data at different frequencies, $50Hz$ and $120Hz$ respectively, it does not account for the $200ms$ delay seen Figure 3.14b. The delay shows that prior to the subject pushing the handlebar of the Jexo to return the blasting point to the path, the subject had already increased their grasping force on the handlebar. As the handlebar moved in the subject's hand as a result of the disturbance, the subject's body would react by attempting to prevent the displacement of the handlebar resulting in a stiffening of the subject's hand. In Johansson's work [182], he elaborates on how this automatic grasping force response is a result of the human body's attempt to prevent slippage. If the subject's hand tenses, then it explains why the grasping force F_G measured by the TMMAS would increase prior to the increase in F_H as the handlebar is encompassed by the subject's hand. This implies that before the subject consciously took action, their body had already reacted to the robot's unexpected behavior.

3.3.2.2 Experiment 2 Experimental Results

In Experiment 2, the applied forces of the subject on the handlebar were observed in the situation where the subject was the one who initiated a change in the pHRC. A sample result from Experiment 2 is shown in Figure 3.15a reveals that F_H increases and decreases throughout the experiment. It is interesting to note that this pattern is not present in the subject's grasping force F_G. The sample shown in Figure 3.15a is representative of all the Experiment 2 results as they all reveal similar characteristics. The differences between F_G and F_H indicate that although the force applied to the end-effector is fluctuating, the overall change in the grasping force of the subject is negligible. The small increases and decreases in the grasping force could have been caused by the subject adjusting their grip on the handlebar.

A magnified view of one of the instances where the subject decided to change from the current path to the other path is shown in Figure 3.15b. A closer look at the forces during the change in path reveals a difference between the results from Experiment 1 and Experiment 2. As the subject is the one initiating a change in the pHRC, the expected result for this experiment was for the

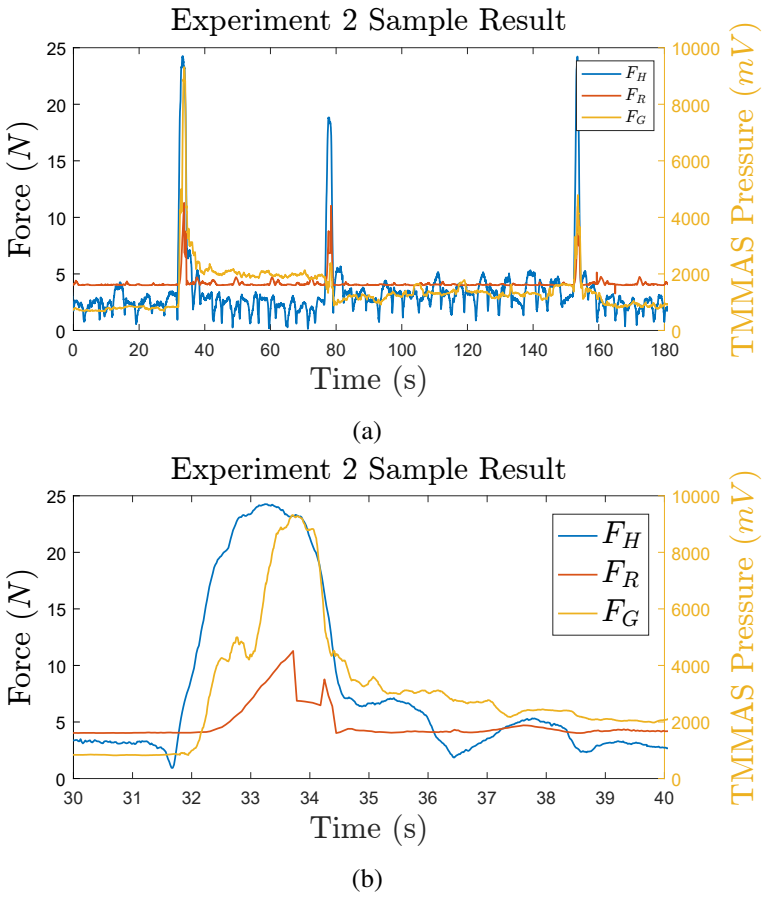

FIGURE 3.15: (a) A sample result from Experiment 1. F_H and F_R are measured in N and the grasping force is measured in mV (b) A magnified view of the forces when the human initiates a change in task at $t \approx 31.5$ s from the sample result shown above. Reproduced from [19].

forces F_H and F_G to increase before F_R as the subject would have to apply forces to the handlebar to initiate a change in the path and the robot would react by producing a guidance force F_R. While this appears to be the case, the reading from the load cell leads the reading from the TMMAS by $300ms$. The time delay implies that although the subject had already applied a large enough force to the handlebar of the Jexo, there was no measurable change in the total grasping force of the subject. This time delay between F_H and F_G when the subject is changing paths is consistent throughout the collected data for this experiment.

This phenomenon can be explained by the redistribution of the grasping force around the handlebar. When the subject wants to change paths, they push the handlebar in the direction that they want to move the blasting point. During the initial pushing action, the forces on one side of the handlebar increases while the forces on the other side of the handlebar decreases. This explains

why there is no change in the F_G when F_H increases. The delayed increase in F_G occurs when the handlebar of the Jexo is already in motion and the human has grasped onto the handlebar. The results indicate that the grasping force of the subject F_G measured by the TMMAS are not always reflected in the force applied to the handlebar F_H measured by a load cell and vice versa. The load cell measures the net forces applied to the handlebar whereas the TMMAS measures the forces applied from all directions to the handlebar.

3.3.3 Discussion

The two experiments presented in this section explored how the grasping strength of the human operator changes during pHRC in response to changes in the task. The first experiment explores how the grasping strength changes when an unexpected event occurs during the interaction while the second experiment explores how the grasping strength of the human changes when they initiate changes within the task. In the first experiment, while the human is performing a path following task, the robot will behave unexpectedly and create a disturbance in the interaction. The disturbance moves the blasting point on the wall off the path and the human must apply a force to the robot end-effector to move the laser back onto the path. In the second experiment, the human has the option to switch between the paths shown in Figure 3.13 which initiates a change in the task. To change paths, the human must apply a force to the robot end-effector which overcomes the guidance force F_R provided by the robot.

Previous works have shown that unexpected occurrences will result in an increase in the human's grip strength in humans [178]. Therefore, the expectation was that when the robot creates a disturbance, the grasping force of the human on the robot end-effector would increase significantly. Figure 3.16 shows an example of the grasping force of the human F_G and the force that the human applies to the end-effector F_H during both Experiment 1 and Experiment 2.

The subject's reaction to the disturbances and the applied forces when the human changes paths is represented by the increases in the value of F_H in Figure 3.16a and Figure 3.16b for Experiment 1 and Experiment 2 respectively. In Experiment 1, the grasping force of the human increases significantly every time the robot creates a disturbance. On the other hand, the grasping force of the human in Experiment 2 does not always increase significantly. In this experiment sample, for the second, fourth and sixth path changes, the grasping force of the human on the handlebar

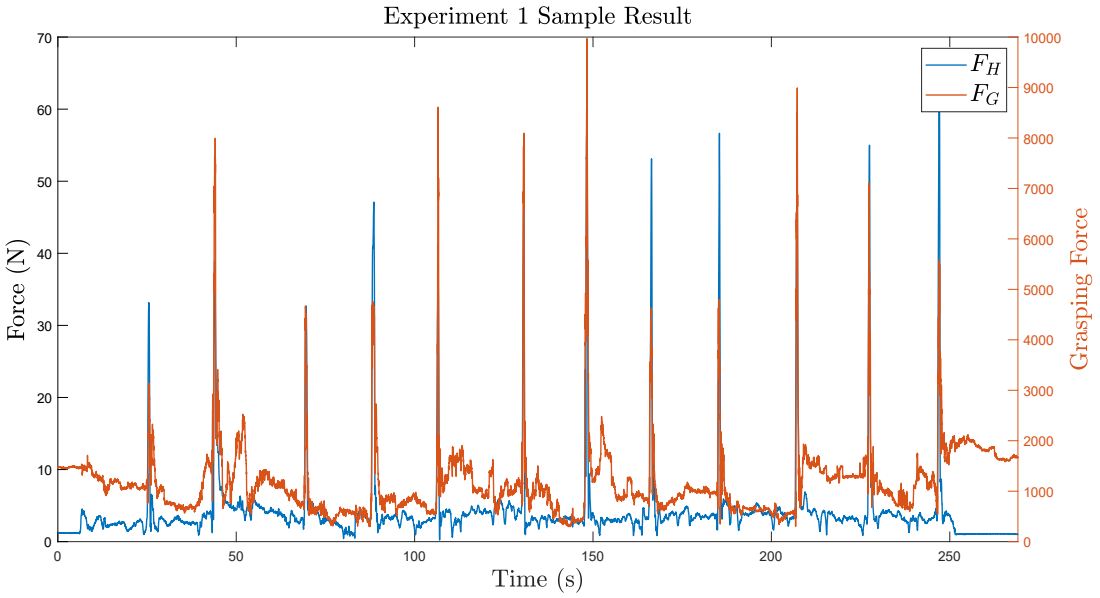

(a)

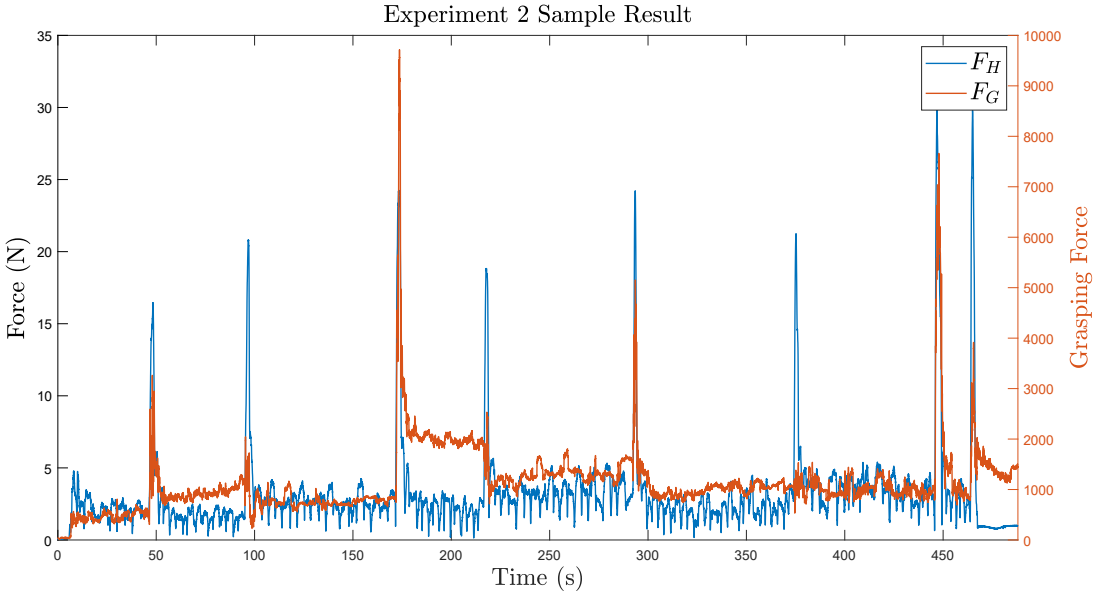

(b)

FIGURE 3.16: (a) A graph depicting the grasping force F_G and the applied operator load F_H during Experiment 1. (b) A graph depicting the grasping force F_G and the applied operator load F_H during Experiment 2.

barely increases and in some cases is actually lower than the force applied by the subject when not initiating a change in path. It would be interesting to explore in future works whether this would change with repeated experiments with the same subjects.

By comparing the average grasping force of the human prior to the disturbance or path change and with the peak grasping force when there is a disturbance or path change, the results in Table 3.7 was obtained. Only the percentage increase in grasping force used to calculate the values in the table as the grasping force before and during a disturbance or path change varies between subjects.

TABLE 3.7: Table shows the statistics concerning the increase a human's grasping strength in response to an unexpected event and a human initiated change in the task in Experiment 1 and Experiment 2 respectively.

	Experiment 1	Experiment 2
Mean Increase (%)	737.63	443.02
Standard Deviation (%)	399.56	335.77
Minimum Increase (%)	294.10	126.80
Maximum Increase (%)	1411.31	1119.24

From the data, it can be seen that there is a larger increase in the grasping force of the human as a result of the robot's disturbance in Experiment 1. Both the mean increase and minimum increase in grasping force is higher in Experiment 1. Despite this, because there were instances in Experiment 2 where the subject changing paths also resulted in a large increase in grasping strength, a large increase in grasping force does not necessarily indicate unexpected robot behavior. However, it can be inferred from the results that a large increase in the grasping strength of the human signifies that there has been a change in the interaction as the grasping force only increases significantly in both experiments when there is a change in the task.

One aspect of the experiments which needs to be explored further is the inconsistency in the increase in the human's grasping forces in Experiment 2. There were no consistent patterns for determining why the subject's grasping strength in Experiment 2 sometimes increased by a large amount. Possible explanations include the subject's unfamiliarity with the robot, the subjects grasping more firmly to prepare themselves to initiate a change in the task or the subjects grasping harder because they know they need to overcome the guidance force of the robot. This will need to be explored in further detail in the future.

One of the possible applications of this research is in industrial pHRC scenarios where the point of contact between the human and robot is a cylindrical handlebar. Currently, for most industrial applications, it is a requirement for devices to incorporate a 3-position switch to break the circuit when the switch is not pressed and when it is fully depressed. If handlebars for pHRC are equipped

with sensors such as the TMMAS, incorporating a 3-position switch into the handlebar may no longer be feasible. Therefore, this research could be used as a replacement for the 3-position switch which can also be used to determine when an unexpected event occurs during the pHRC.

3.4 Summary

In this chapter, the contribution the human's hand orientation and grasping strength towards the robot's perception of its human co-worker during pHRC. The TMMAS sensor was used to record the grasping patterns of human operators as they physically interact with a robot through a cylindrical handlebar mounted onto the end-effector of the robot.

The information derived from the TMMAS sensor showed that it is possible to determine the orientation of the human's hand around the cylindrical handlebar. The human's hand orientation could provide insight into the human's pose. The human's pose during a pHRC can influence a number of factors such as the safety of the human, the energy expenditure of the human and the human's strength during the pHRC. This information provides the robot with more information about the human's current status which can be used by the robot to refine its understanding of the human's actions during pHRC.

The TMMAS was also used to observe the changes in the human's grasping strength during when a robot behaved unexpectedly. The experiments confirmed the hypothesis that a human will instinctively increase their grasping strength when the robot behaves in an unexpected manner during a pHRC. This result also infers that one of the human's responses to unexpected occurrences during pHRC is to tighten their grip. This information could possibly be used by the robot to gain insight into the human's state. As it was shown that the grasping force of the human increased when the robot behaved unexpectedly, it may be possible to use the information for inferring the human's confidence or trust in its robot co-worker during pHRC.

Chapter 4

A Robot Confidence Framework for physical Human-Robot Collaboration

Chapter 3 discussed how the robot's understanding of the human's intention in physical Human-Robot Collaboration (pHRC) can be enriched by utilizing the information from the human's grasping strength and hand orientation. From the robot's perspective, the human's actions and intention can be seen to be either beneficial or detrimental.

Whether an action is beneficial or detrimental to the task goals is dependent on the robot's understanding of the task. The difference between the human's actions and the robot's expectations of the task can provide a measure of the robot's perception of the human's performance in doing a task. In this chapter, a robot confidence framework which uses the robot's perception of its human co-worker's performance is presented.

This chapter is organized as follows. Section 4.2.1 presents a model for calculating the robot's perception of its human co-worker's performance in a task component. This model compares the robot's observations of the human's actions with the robot's understanding of how the task should be performed to calculate the performance of the human. Section 4.2.2 presents a model for calculating the confidence of the robot based on its perception of the human's performance. This model uses the human's performance in the task components and the relative importance of the task components to measure the robot's current confidence in its human co-worker. Section 4.3 presents a robot confidence framework by applying it to three collaborative pHRC scenarios. In

these case studies, the robot monitors the actions of the human during the pHRC and calculates its confidence in its human co-worker in real-time. Section 4.5 discusses limitations of the robot confidence framework.

4.1 Motivation for the Robot Confidence Framework

The goal of the robot confidence framework is to allow a robot to emulate how a human would determine their confidence in their human co-worker. Assume a Human-Human Interaction (HHI) where one of the humans is a supervisor and the other human is a worker. If the worker were to perform poorly, the supervisor's confidence in the worker would decrease. Similarly, if the worker performs well, the supervisor's confidence in the worker would increase. The only exception to these statements is if the supervisor has full confidence or no confidence in the worker, in which case the supervisor's confidence cannot increase or decrease respectively. In the interaction between the supervisor and the worker, it is reasonable to make the assumption that the supervisor will intervene in the worker's actions if the supervisor's confidence in the worker is too low.

Earlier it was mentioned that the cause of the supervisor's confidence in the worker dropping is the worker's decreased performance. A human's confidence is based on their accumulated experiences and prior knowledge. As they observe the state of a task or interaction, they are able to subjectively measure the performance of their co-workers based on their experience and knowledge and there are often many factors which can contribute to the supervisor's perception of the worker's performance. Therefore, a method for modelling the robot's perception of the human's performance is needed. The robot's perception of the human's performance during the task can then be used to calculate the robot's confidence in its human co-worker.

One other aspect to consider is whether the robot's confidence in its human co-worker should change if it cannot observe the human. In the HHI scenario, if the worker performs poorly but the supervisor is unable to observe the worker's poor performance or the results of the worker's poor performance, it is logical to assume that the supervisor's confidence in the worker would not decrease. This is because the supervisor's confidence is based on their perception of the task and as the supervisor could not perceive the poor performance, the supervisor's confidence should not change. By extension, if the worker were to be performing well in the task, but the supervisor was

unable to observe the worker's performance, then the supervisor's confidence should also remain unchanged.

The supervisor's confidence in the worker is also influenced by worker's overall performance in the task. This means that the supervisor's expectations and perception of performance in various components of the task and the contribution of these components to the supervisor's overall confidence must also be taken into account in the robot confidence framework. The following section will describe the robot confidence framework and how these aspects of confidence are modelled within the framework.

4.2 Robot Confidence Framework

The robot confidence framework uses the robot's observations of its human co-worker's actions during pHRC to quantify the robot's confidence in its human co-worker. The presented framework consists of a performance model and a confidence model. In the performance model, the robot decomposes the task into task components. The robot then measures its human co-worker's performance in each of the task components based on its expectations of the human's actions in the task component. In the confidence model, the robot uses the human's performance in each of the task components and the relative importance of each task component to calculate the robot's confidence in its human co-worker. A graphical representation of the flow of information in the robot confidence framework can be seen in Figure 4.1.

4.2.1 Performance Model

4.2.1.1 Decomposing the pHRC into task components

In this thesis, the robot's confidence in its human co-worker is defined as the result of a cost/benefit analysis of the robot's perception of its human co-worker's actions. This is achieved by first modelling the robot's perception of its human co-worker's performance in the pHRC in terms of rewards and penalties. For the robot to measure the performance of its human co-worker during pHRC, the robot must have a method of observing its human co-worker's actions. A robot's perception of the human's actions and its surroundings is limited by the number of sensors and the

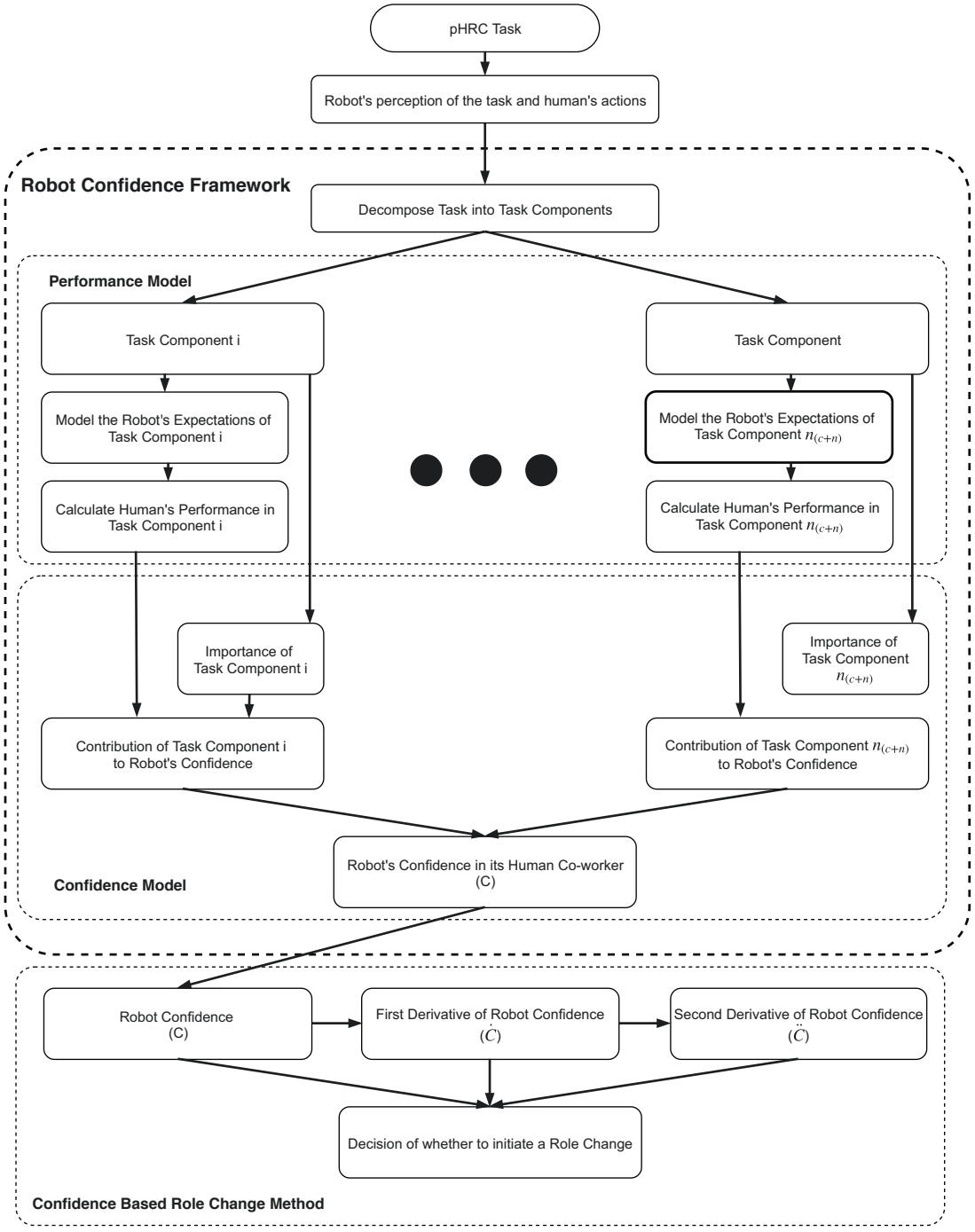

FIGURE 4.1: A flowchart showing the flow of information for the robot confidence framework in a pHRC. The robot confidence framework is composed of $n_{(c+n)}$ task components where $n_{(c+n)}$ is the sum of the number critical and non-critical components in the task.

types of sensors it possesses. Therefore, the robot's perception of its human co-worker's performance during pHRC should be defined in terms of what the robot can observe using its sensors.

This can be done by decomposing the pHRC into task components based on the information that the robot has available to it. These task components are used to measure the human's performance in various aspects of the task. Examples of possible task components in pHRC can include but are not limited to observable phenomenon such as collision avoidance, acceleration, accuracy, applied operator force and operator position. There is no limit to the number of task components; however, the selected task components must be relevant to the task being performed and the robot needs to have a method of observing the human's actions in the task component. The observations of the robot in a task component can be obtained directly or indirectly. A direct observation is what the robot detects through its sensors, while an indirect observation is something which must be inferred from the direct observations. Examples of indirect observations can include intangible aspects of the task such as the completion or accuracy of a task.

Task components can be categorized as either critical components or non-critical components. Critical components are generally task components which have a direct impact on the safety of the robot and/or its human co-worker during the pHRC or are essential to the successful completion of the task being performed collaboratively by the human and the robot. Non-critical components on the other hand are used to assess the performance of the human co-worker in aspects of the task which do not fall into the critical component category. The robot's perception of the human's overall performance in the pHRC can be inferred from the human's performance in the critical and non-critical task components. It must be noted that the categorization of the task components is subjective and can change based on a number of factors such as the purpose of the pHRC or level of risk.

4.2.1.2 Modelling a performance in a task component

In the robot confidence framework, the robot's perception of the human's performance in a task component is modeled as a Fluid Stochastic Petri Net (FSPN) which has been used previously to model accumulated rewards and penalties in Human-Robot Interaction (HRI) [183][184]. FSPN was chosen as it intuitively emulates the process of modelling how a supervisor's perception of performance can change as a result of their expectations and observations. The description of how

the confidence of a human changes during an interaction presented in Section 4.1 also applies to the supervisor's perception of the worker's performance.

At the conceptual level, a FSPN can be envisioned as a container with fluid within it. In the performance model, the fluid level within the container represents the supervisor's perception of the worker's performance. The container has a number of pipes and valves which control the flow of fluid in and out of the container. Fluid entering and leaving the container represents the supervisor's perception of the worker's performance increasing and decreasing respectively. The pipes represent aspects of the task which affect the supervisor's perception of the worker's performance. The flow rate of the fluid and the valves represent how strongly that aspect affects the supervisor's perception of performance and whether the supervisor is able to observe that aspect of the task respectively.

A graphical representation of the FSPN for a generic task component A can be seen in Figure 4.2. The fluid place ϕ_A is modeled as a container with the bounds $0 \leq \phi_A \leq 1$ for all $t \geq 0$. The fluid level inside the fluid place ϕ_A represents the robot's current perception of the human's performance in the task component A.

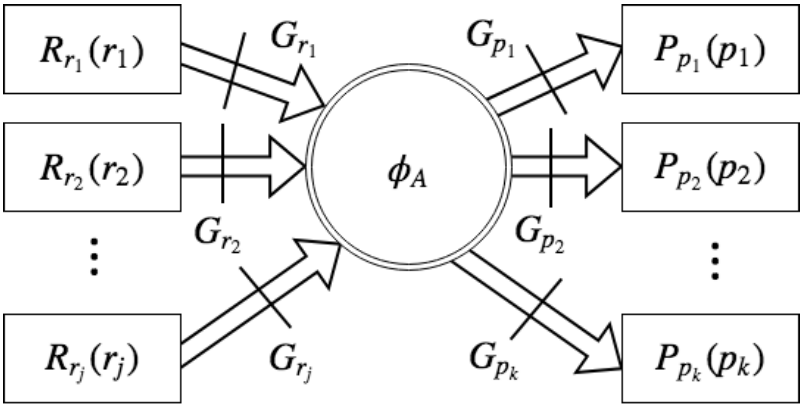

FIGURE 4.2: Example of a FSPN model for a generic task component A.

In the FSPN model for task component A, a change in the fluid level of the fluid place ϕ_A represents a change in the robot's perception of its human co-worker's performance in the task component. Fluid enters and exits the fluid place ϕ_A through fluid arcs which are represented in Figure 4.2 as directional arrows. Fluid can only flow through fluid arcs in the direction that the arrows are pointing. Fluid arcs that increase the fluid within ϕ_A (point towards ϕ_A) and fluid arcs that decrease the fluid within ϕ_A (point away from ϕ_A) are referred to as rewards (R) and penalties (P) respectively.

Rewards and penalties are used to define what the robot considers to be a good performance or a bad performance in the task component and control the flow of fluid in and out of the fluid place ϕ_A. There is no limit to the number of rewards and penalties which can be defined for a pHRC.

For a human, it is their previous experiences and knowledge that shapes their understanding of what they consider to be a good performance or a poor performance. To emulate this in the performance model, the rewards and penalties in the task components reflect the robot's expectations of the human's actions in the task component. The robot's expectations of the human's actions in a task component can be derived from previous collaborative operations between the robot and the human, by identifying acceptable ranges for the observations from the literature or by consulting industry experts. The modelling of a robot's expectations using this information can take any form, from a simple mapping of the observations to a reward or penalty to the output of a machine learning algorithm depending on the complexity of the relationship.

The robot compares its observation of its human co-worker's actions with its expectation of the human's actions during the task. If the observation is within the expected range, then a reward would increase the amount of fluid within the fluid place ϕ_A. However, if the observation is outside the expected range, the amount of fluid entering the fluid place would decrease or cease entirely. Similarly for penalties, if the observation is within the expected range, the fluid level of ϕ_A will not decrease. On the other hand, if the observations are outside the expected range, then the amount of fluid drawn from ϕ_A would increase based on the difference between the robot's observation and the expected range of values.

The magnitude of the penalties and rewards at each time step are not only dependent on the difference between the robot's observations and the robot's expectations of the human's actions but also the rate at which the robot updates its observations. If the robot updates its observations of the human's actions at a faster rate, then the maximum penalty and/or reward at each time step should be smaller. This is especially important for penalties to prevent the robot's perception of the human co-worker's performance in the task component (fluid in ϕ_A) from depleting before its human co-worker has an opportunity to react or correct their errors.

As the rewards and penalties are dependent on the robot's observations, if the robot cannot observe the associated actions of the human for the task component or the observation is not applicable at that point in time, then the robot should not penalize or reward the human co-worker. This behavior

is represented in the FSPN model through enabling functions (G) which are portrayed in Figure 4.2 as lines which bisect the fluid arcs. An enabling function is defined as:

$$G = \prod_{i=1}^{n_B} B_i \tag{4.1}$$

where n_B is the number of enabling conditions (B) for a fluid arc. Each enabling condition is modeled as a Boolean function which describes a condition where fluid would be allowed to flow through the fluid arc. Fluid will only flow through the fluid arc when $G = 1$. If any of the enabling conditions are not fulfilled ($B_i = 0$), then the fluid arc is considered to be disabled and the flow of fluid through the fluid arc is prevented. Common examples of enabling conditions in pHRC can include time restrictions or the presence of forces or motion in the pHRC.

Based on the FSPN model for the generic component A shown in Figure 4.2, the instantaneous change in the robot's perception of the human's performance in the task component A at any time t can be given by:

$$\frac{d\phi_A}{dt} = \sum_{j=1}^{n_R} G_{r_j} \cdot R_j - \sum_{k=1}^{n_P} G_{p_k} \cdot P_k \tag{4.2}$$

where n_R and n_P represent the number of rewards and penalties in the task component respectively. This is intuitive as $\frac{d\phi_A}{dt}$ also represents the instantaneous change in volume of fluid in the fluid place ϕ_A. Therefore the robot's perception of its human co-worker's performance in task component A at any time t during pHRC can be given by:

$$\phi_A = \begin{cases} \phi_{A,0} & t = 0 \\ \phi_A + \frac{d\phi_A}{dt} & t > 0 \\ 1 & \phi_A = 1, \frac{d\phi_A}{dt} \geq 0 \\ 0 & \phi_A = 0, \frac{d\phi_A}{dt} \leq 0 \end{cases} \tag{4.3}$$

where $\phi_{A,0}$ represents the robot's initial perception of its human co-worker's performance in task component A where $0 \leq \phi_{A,0} \leq 1$. If the robot and its human co-worker are in a "trusting relationship" [185], then the robot's trust and/or confidence in its human co-worker's performance should be initially high. In these trusting relationships, a value of $\phi_{A,0} = 1$ represents that the robot begins

the pHRC with a good impression of the human's performance in task component A. However, there are situations where a conservative approach would be more appropriate or the robot may have a negative impression of its human co-worker's capability in a task component. In these task components, the value of $\phi_{A,0}$ should be set to a lower value.

4.2.2 Confidence Model

Once the human's performance in all the task components has been calculated, the confidence of the robot in its human co-worker can be calculated. In the confidence model, the robot's confidence is obtained by combining the robot's perception of its human co-worker's performance in the task components with the robot's perception of how important each task component is to the pHRC. As mentioned previously, each task component is categorized as either a critical component or non-critical component based on their impact on the safety of the human and/or the robot or its effect on the task outcomes. The performance of the human in a generic critical or non-critical component is represented as $\phi_{A,c}$ or $\phi_{A,n}$ respectively.

All critical components, due to the their relationship with the safety of the human and the robot or the successful completion of the task, are considered by the robot to be important and are therefore the largest contributing factor towards the robot's confidence in its human co-worker. The importance of the non-critical components on the other hand is subjective and could change based on the purpose of the pHRC. The relative importance of a non-critical component is represented by γ_A where $\gamma_A \geq 0$ and:

$$\sum_{A=1}^{n_n} \gamma_A = 1 \tag{4.4}$$

where n_n represents the number of non-critical task components in the pHRC. Given this information, the proposed equation which describes the relationship between the robot's perception of the human co-worker's performance in the task components, the importance of the task components and the robot's confidence in its human co-worker is given by:

$$C = \begin{cases} \prod_{j=1}^{n_c} \phi_{j,c} & \text{No } \phi_{A,n} \\ C_{min} + (1 - C_{min}) \cdot \sum_{k=1}^{n_n} \gamma_k \phi_{k,n} & \text{No } \phi_{A,c} \\ \left(C_{min} + (1 - C_{min}) \cdot \sum_{k=1}^{n_n} \gamma_k \phi_{k,n}\right) \cdot \prod_{j=1}^{n_c} \phi_{j,c} & else \end{cases} \tag{4.5}$$

where C_{min} is a constant, n_c and n_n represent the number of critical and non-critical task components in the pHRC respectively. The three forms of the equation presented in (4.5) are used in pHRC with no non-critical task components, pHRC with no critical task components and pHRC with both critical and non-critical task components respectively.

In (4.5), C_{min} defines the overall contribution of the non-critical components to the robot's confidence in its human co-worker and represents a threshold in the robot's confidence. When $C_{min} = 0$, the weighted sum of the human co-worker's performance in the non-critical components emulates a critical component. Conversely, if $C_{min} = 1$ then the human's performance in the non-critical components does not affect the robot's confidence in its human co-worker.

For the confidence to fall below C_{min}, the human's performance in at least one of the critical task components must have decreased from its maximum value. Therefore, C_{min} can be considered as a confidence threshold where the human's performance is poor but is not negatively affecting the outcomes of the task or the safety of the human or the robot. As performance and confidence are both subjective measures, the presented robot confidence framework provides a lot of flexibility in its implementation. The robot confidence framework for a pHRC can be as simple or as complex as necessary based on the requirements and purpose of the pHRC.

4.3 Case Studies

The robot confidence framework is verified using three distinct pHRC case studies. In each case study, the human works collaboratively with the robot to complete a task where the human is in control and the robot observes the actions of its human co-worker. Each of the interactions in the case studies are decomposed into task components and the rewards and penalties for each task component are defined. As task of the human and the robot in each of the interactions is different, the task components selected for each of the interactions will also be different. Even if a task

component is common between the case studies, the rewards and penalties used in each case study will be unique as they are adapted to specific interactions and tasks.

Because the task components for each of the case studies are task specific, the selected task components for each interaction must be related to the information which the robot can observe. In these case studies, the Thrumode Matrix Array Sensor (TMMAS) sensor was not implemented in the robots. Therefore, it is not possible to integrate the human co-worker's grasping strength or hand orientation as task components. However, when the use of the TMMAS in pHRC is explored in future works, the human's grasping information will also be taken into account in the robot's perception of the human's performance during the interactions.

The robot confidence framework is then used to calculate the robot's confidence in its human co-worker during the pHRC. In these case studies, the robot's confidence in its human co-worker was hidden from the human to prevent the information from influencing the human's performance.

For the purpose of succinctness, a limited number of task components were chosen to demonstrate how the robot confidence framework can be applied to various pHRC and how rewards and penalties for task components could be modeled. Although the presented case studies show how the confidence of the robot changes as a result of the selected task components, in actual implementations of the robot confidence framework, it is recommended that a larger number of task components, rewards and penalties be used to model the robot's expectations of its human co-worker's actions during the pHRC. In the following case studies, it is assumed that the robot and human are in a trusting relationship ($\phi_{A,0} = 1$) and that the robot updates its observations of the human's actions at a rate of $100ms$.

In this thesis, the functions modelling the relationship between the robot's observations and the associated rewards and penalties are represented using either a constant or one of the following functions:

$$q_1(o) = \tau\left(\frac{1}{1+e^{b(o-a)}}\right) \tag{4.6}$$

$$q_2(o) = \tau\left(e^{\frac{(o-d)^g}{h}}\right) \tag{4.7}$$

where a, b, d, g, h are constants, τ is the maximum instantaneous reward or penalty, o is the observation of the robot and q_1 and q_2 represent the penalty or reward based on the observation o. The graphs for (4.6) and (4.7) which are used to model the robot's expectations of a human's actions in a task component can be seen in Figure 4.3.

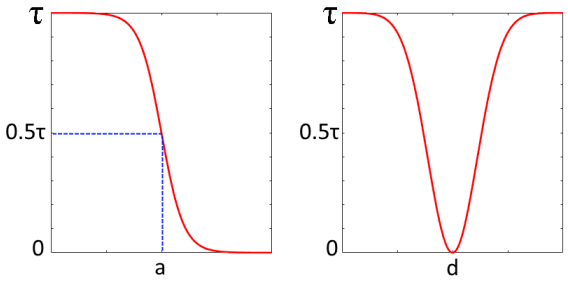

FIGURE 4.3: The equations used in this thesis to model the robot's expectations of its human co-worker's performance in a task component. The graphs display equations (4.6) and (4.7) on the left and right respectively.

Equation (4.6) is useful for modelling rewards and penalties which increase based on the difference between the robot's observation and the expected range of values for the observation. When $o = a$, the corresponding penalty or reward would be equal to half the maximum penalty or reward incurred at each time step. The value of b in the equation determines how quickly the penalty or reward increases or decreases when the observation leaves the expected range of values. In this thesis, when penalties are modeled, the value of a and b are chosen such that the the expected range of values for the observation correspond to a penalty of less than 0.05τ. An example of a task component where (4.6) could be used, is the robot's expectations of the force applied by the human co-worker's during pHRC. If it was modeled as a penalty, then the robot would penalize the human's performance in the task component when the human applies forces outside of the expected range.

The equation (4.7) can be used to model rewards and penalties where the reward or penalty increases based on the deviation of the robot's observation from an ideal value. In this equation, d represents the ideal value for the observation. As the value of the observations deviate from d, the penalty or reward will increase or decrease respectively. The values of g and h determine how quickly the deviation from d increases or decreases the robot's perception of the human's performance in the task component. In this thesis, values of g and h are chosen so that when modelling a penalty, the penalty would be less than 0.05τ when the robot's observation is within the expected range.

In this thesis, the chosen value of τ for most rewards and penalties is generally much smaller than the maximum capacity of the fluid place for each task component. This is so that the human would have time to react to the changes in the task before the fluid place fills or empties.

As the process of modelling a task component always follows the same procedure, a more in-depth explanation of how the performance model of a task component is obtained is provided for the first task component in the first case study. It is assumed that unless otherwise stated, the process of deriving the performance models for all the other task components in this section follows the same process.

4.3.1 Case Study 1: Assistance-as-Needed-roBOT (ANBOT) - Collaborative Grit-Blasting

In a grit-blasting operation, abrasive material such as granite or steel is ejected from a blasting nozzle at high velocities using compressed air. A human grit-blaster would support the reaction forces generated by the nozzle for extended periods of time. As the abrasive material makes contact with the task surface, the abrasive material ricochets and obscures the vision of the human grit-blaster until the particulate matter in the air settles.

In this case study, a human works collaboratively with a robot to complete a grit-blasting operation. The robot used in this case study is the ANBOT developed by the Centre for Autonomous Systems at the University of Technology, Sydney (UTS) [186]. The purpose of the ANBOT is to create a safe platform for collaborative grit-blasting by providing physical assistance to its human co-worker. The ANBOT measures the load generated by the ejected abrasive material so that it can provide the optimal amount of assistance to the human [187]. The majority of the load is supported by the ANBOT, while a small portion of the load is used to provide the human co-worker with tactile feedback of the collaborative grit-blasting operation. The ANBOT shown in Figure 4.4, uses a UR-10 robot arm from Universal Robots and is equipped with a nozzle and hose.

When using the ANBOT for collaborative grit-blasting, the human co-worker stands behind the ANBOT and controls the ANBOT through the two handlebars on the end-effector shown in Figure 4.4. Each handlebar on the ANBOT's end-effector has a three position switch. The switch on

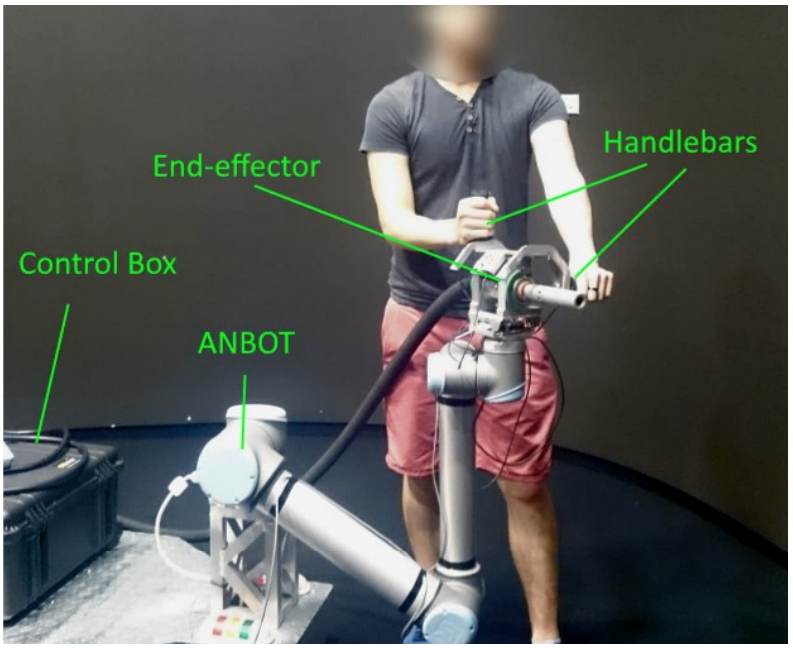

FIGURE 4.4: ANBOT equipped with nozzle and hose mounted for collaborative grit-blasting. Reproduced from [20].

the vertical handlebar (B_m) enables the movement of the ANBOT while the switch on the horizontal handlebar (B_b) enables the flow of abrasive material through the nozzle. The forces applied by the human on the handlebars are detected by a load cell built into the end-effector and are used by the ANBOT to infer the human's intentions. The ANBOT also monitors the human's actions and the environment using an array of RGB-D cameras.

In this case study, the human co-worker used the ANBOT to blast a marked 1.2x1.8m wall section. The ANBOT was positioned approximately 1m away from the wall. As this case study was performed inside a lab, no abrasive material was passed through the nozzle of the ANBOT when the switch B_b was pressed. In Figure 4.5, a flowchart depicting the flow of information in the robot confidence framework configured for the collaborative grit-blasting scenario is shown.

The collaborative grit-blasting task was decomposed into the following task components:

- **Critical Components**
  - Manipulability of the robot (w)
- **Non-Critical Components**

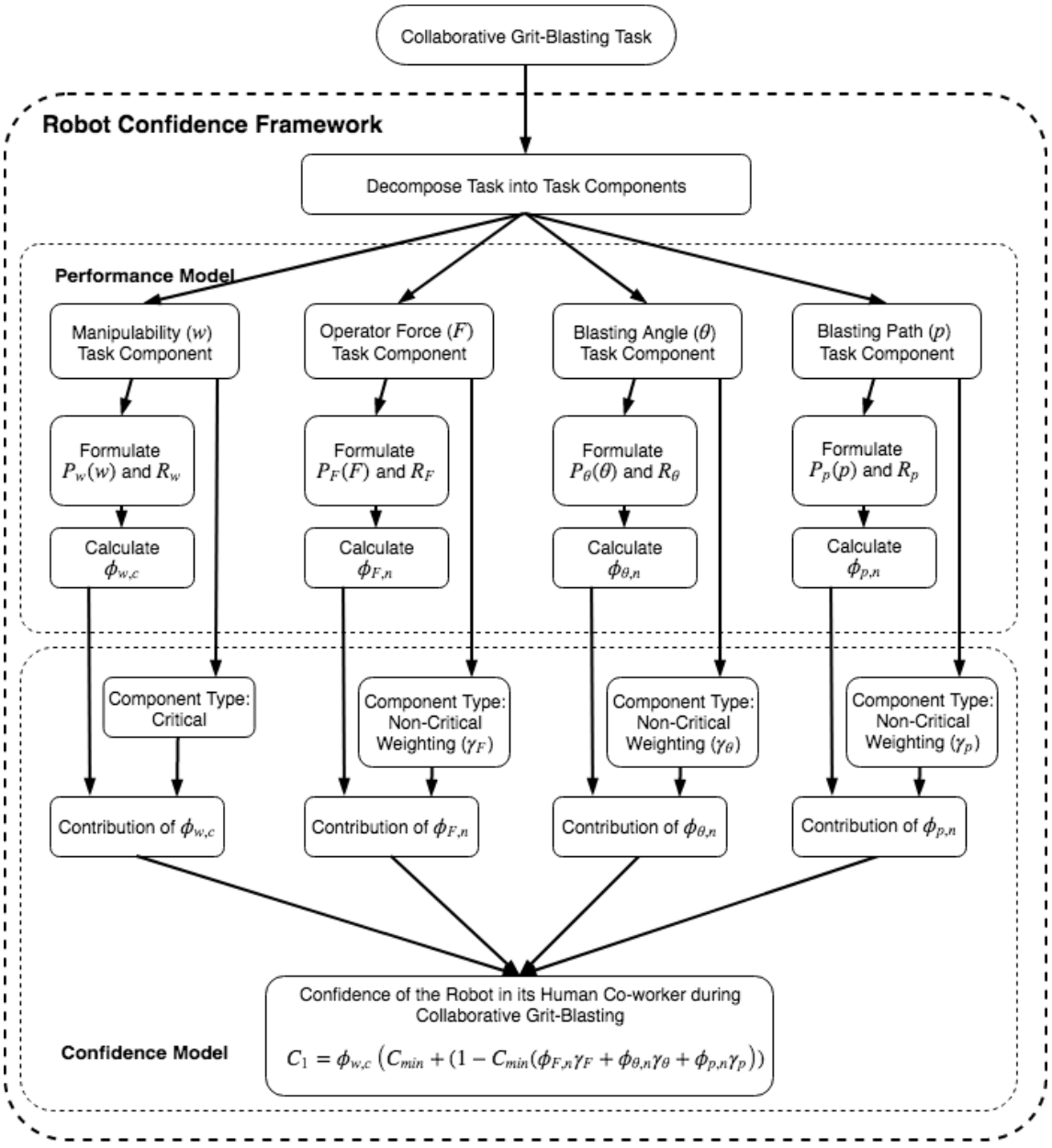

FIGURE 4.5: A flowchart showing the flow of information for the robot confidence framework for Case Study 1: ANBOT - Collaborative Grit-Blasting.

- Operator Force (or force applied to the robot by the human) (F)
- Blasting Angle (θ)
- Variation in Blasting Path (p)

The manipulability task component was selected as a critical component due to its relationship with the likelihood of the robot entering singularity as this may cause the robot to move unpredictably

which may put the safety of the human co-worker at risk. This is especially true when abrasive material is passed through the nozzle of the ANBOT. The non-critical components were selected to measure the human's overall performance in the grit-blasting task as the human operator was expected to maintain a blasting angle and minimize the operator force and variation in blasting path.

The robot observed the human's actions in each of the task components and calculated its perception of its human co-worker's performance in each task component using one reward R_o and two penalties $P_o(o)$ and $P_{\Delta o}(\Delta o)$ where o and Δo represent the current observation in a task component and the average change in the observations for the task component in the previous two seconds respectively. For this case study, a maximum penalty of $\tau = 0.1$ was chosen. This means that the minimum time required for a robot's perception of the human's performance in a task component to go from its maximum value to its minimum value is one second. It was believed that this would provide the human co-worker ample opportunity to react before the fluid place representing the human's performance in a task component emptied. All the rewards in this case study were modeled as a constant inflow of fluid into the fluid place. The chosen reward function for this case study is:

$$R_w = R_F = R_\theta = R_p = 0.01 \tag{4.8}$$

By having a constant reward which is much smaller in magnitude than the maximum penalty, the fluid level in the fluid place will only increase when there is little to no fluid being drawn by the penalties, thus creating a slow positive/ fast negative dynamic to the performance modelling [185]. This dynamic emulates the wariness of the robot following a poor performance from its human co-worker as the human must perform well for an extended period of time to make up for any losses in performance.

In this case study, the switches on the handlebars of the ANBOT are used to define the enabling functions for the task components. A binary representation of the switches is used where 1 represents a pressed state (enabled) and 0 represents a released state (disabled). B_m was selected as the enabling function for the manipulability and operator force components so that the performance measurement would begin when the human co-worker moves the ANBOT.

$$G_{R_w} = G_{P_w} = G_{P_{\Delta w}} = G_{R_F} = G_{P_F} = G_{P_{\Delta F}} = B_m \tag{4.9}$$

Where G_{R_w}, G_{P_w}, $G_{P_{\Delta w}}$ are the enabling functions for the reward and two penalties for the manipulability task component and G_{R_F}, G_{P_F}, $G_{P_{\Delta F}}$ are the enabling functions for the reward and two penalties for the operator force task component. For the blasting angle and blasting path components, a combination of the switches $B_m B_b$ was used for the enabling functions.

$$G_{R_\theta} = G_{P_\theta} = G_{P_{\Delta\theta}} = G_{R_p} = G_{P_p} = G_{P_{\Delta p}} = B_m B_b \tag{4.10}$$

Where G_{R_θ}, G_{P_θ}, $G_{P_{\Delta\theta}}$ are the enabling functions for the reward and two penalties for the blasting angle task component and G_{R_p}, G_{P_p}, $G_{P_{\Delta p}}$ are the enabling functions for the reward and two penalties for the blasting path task component. This is so that the robot's perception of the human's performance in the task components is only considered when both switches are pressed.

4.3.1.1 Performance modelling

Human Performance in the Manipulability Task Component (w)

The manipulability (w) of a robot arm provides a quantitative measure of the robot arm's ability to reposition and reorient its end-effector in its current arm posture [188]. Two experiments were conducted to determine the expected range of values for the manipulability of the ANBOT during a grit-blasting operation. In the first experiment, the human performed the grit-blasting operation normally and in the second experiment the human attempted to put the ANBOT into singularity. At each time step, the Jacobian J of the ANBOT was used to calculate the manipulability using:

$$w = \sqrt{det(J(\theta) \cdot J(\theta)^T))} \tag{4.11}$$

An example of how the manipulability of the ANBOT and the change in manipulability during a collaborative grit-blasting operation is shown in Figure 4.6a and Figure 4.6b. The blue plot represents normal blasting behavior and the orange plot represents a pHRC where the human

attempts to put the ANBOT into singularity. The values of w and Δw used to formulate the penalty functions are obtained by observing the values of w during the two experiments. The value of w is robot specific and will not change between subjects and although there is some variation Δw between subjects, the difference is minimal. Therefore, the data shown in Figure 4.6a and Figure 4.6b is representative of the collected data sets for demonstration purposes in this chapter.

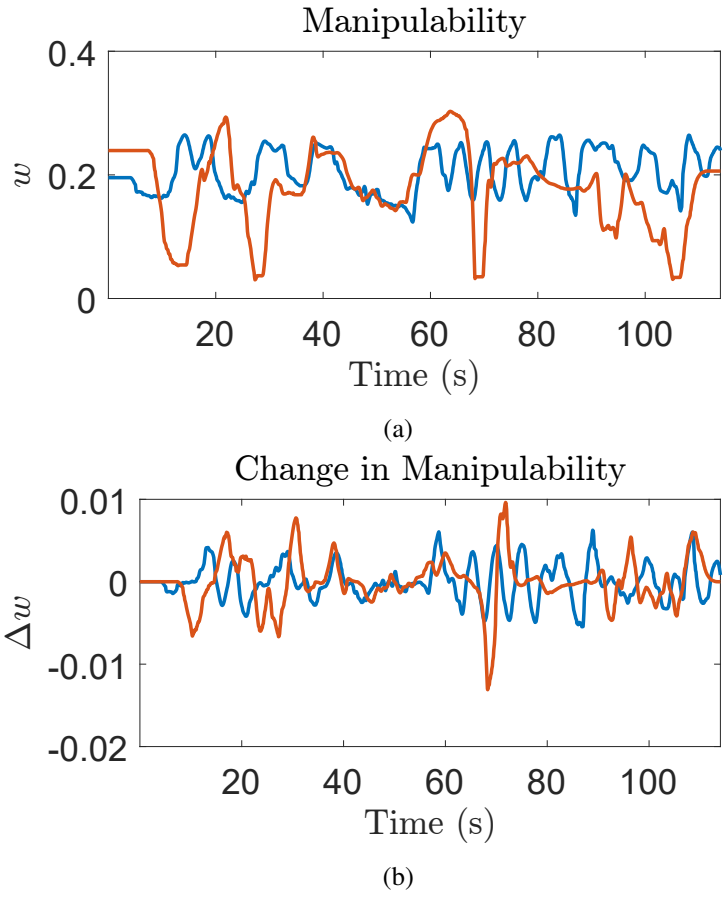

FIGURE 4.6: An example of (a) w and (b) Δw from a previous pHRC using the ANBOT where the human was grit-blasting normally (blue) and attempting to put the ANBOT into singularity (red)

From Figure 4.6a, it can be seen that during normal blasting, the manipulability of the ANBOT was generally in the range $0.15 \leq w \leq 0.25$ and that the manipulability approaches $w = 0.05$ when the ANBOT is close to singularity. This information describes the robot's expectations for the manipulability task component during a normal grit-blasting operation. Therefore, the conditions describing the penalty $P_w(w)$ are:

$$\begin{aligned} w &> 0.15 \qquad \text{No Penalty} \\ w &= 0.05 \quad \text{Maximum Penalty} \end{aligned} \tag{4.12}$$

Because there is no detriment to the task outcomes or the safety of the human and robot when $w > 0.25$, the robot will only penalize the human co-worker's performance when $w < 0.15$ as this represents the observation being outside the expected values for w during normal grit-blasting operations. By combining (4.6) with the previous information, an equation describing $P_w(w)$ can be obtained:

$$P_w(w) = 0.1\left(1 - \frac{1}{1 + e^{58.89(w-0.1)}}\right) \tag{4.13}$$

The second penalty $P_{\Delta w}(\Delta w)$ for the manipulability task component is based on the average change in manipulability of the ANBOT during the grit-blasting operation. An example of the change in manipulability during collaborative grit-blasting can be seen in Figure 4.6b. The average change in manipulability of the ANBOT is defined as:

$$\Delta w = \frac{1}{n}\sum_{j=2}^{n}(w_j - w_{j-1}) \tag{4.14}$$

where n is the number of observations in a previous time horizon of two seconds. A small or positive value of Δw indicates that the human co-worker's manipulation of the ANBOT is stable or improving. A negative Δw indicates that the human's manipulation of the ANBOT has been declining over the previous time horizon, increasing the risk of the ANBOT entering singularity.

Figure 4.6b shows that for the majority of observations during normal grit-blasting, $\Delta w \geq -0.005$. The figure also shows that the minimum value of the average change in manipulability in both experiments was approximately $\Delta w = -0.015$. Based on this information, the conditions used to generate the penalty for Δw were:

$$\begin{aligned} \Delta w &> -0.015 \qquad \text{No Penalty} \\ \Delta w &= -0.005 \quad \text{Maximum Penalty} \end{aligned} \tag{4.15}$$

using these conditions and (4.6), the following function for $P_{\Delta w}(\Delta w)$ was derived:

$$P_{\Delta w}(\Delta w) = 0.1\left(\frac{1}{1+e^{588.89(\Delta w+0.01)}}\right) \tag{4.16}$$

Both penalty functions for the manipulability task component can be seen in Figure 4.7.

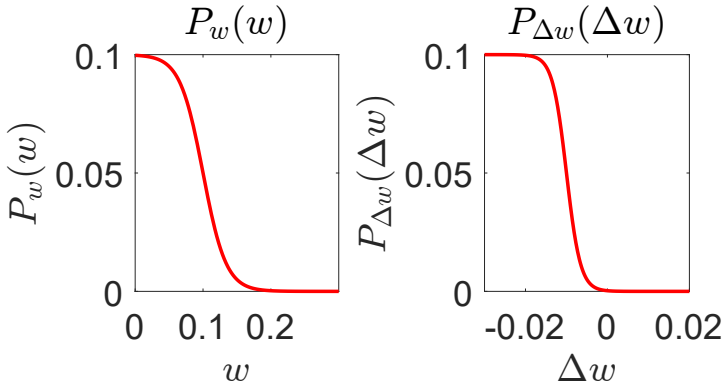

FIGURE 4.7: Penalty functions for the manipulability task component.

The robot updates its perception of its human co-worker's performance in the manipulability task component ($\phi_{w,c}$) when it obtains a new manipulability observation using equation (4.3). The change in the robot's perception of the human's performance in the manipulability task component at each time step can be obtained by substituting the functions for the rewards, penalties and enabling functions into Equation (4.2):

$$\frac{d\phi_A}{dt} = \sum_{j=1}^{n_R} G_{r_j} \cdot R_j - \sum_{k=1}^{n_P} G_{p_k} \cdot P_k$$

$$\frac{d\phi_{w,c}}{dt} = G_{R_w} \cdot R_w - G_{P_w} \cdot P_w(w) - G_{P_{\Delta w}} \cdot P_{\Delta w}(\Delta w) \tag{4.17}$$

$$\frac{d\phi_{w,c}}{dt} = 0.1 \cdot G_{R_w} - G_{P_w} \cdot \left(1 - \frac{0.1}{1+e^{58.89(w-0.1)}}\right) - G_{P_{\Delta w}} \cdot \left(\frac{0.1}{1+e^{588.89(\Delta w+0.01)}}\right) \tag{4.18}$$

Human Performance in the Operator Force Task Component (F)

The purpose of the ANBOT is to reduce the physical strain on the human co-worker during a grit-blasting operation. Therefore, it is expected that the human should not be applying large forces during the pHRC. An example of the force applied by the human on the handlebars mounted on the ANBOT's end-effector during a grit-blasting operation can be seen in Figure 4.8.

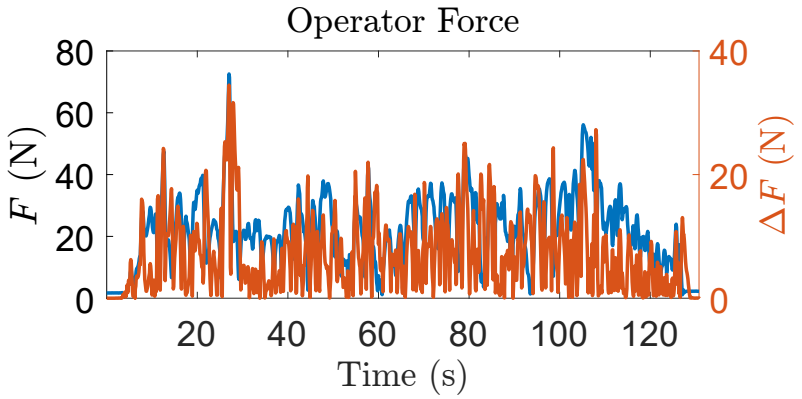

FIGURE 4.8: An example of F and ΔF from a previous experiment where the human was grit-blasting normally.

The figure shows that the operator force applied by this particular subject is generally below $50N$ during a normal grit-blasting operation. Although the applied force varies between subjects, the maximum applied load during the experiments under normal grit-blasting conditions was around $50N$. Because a UR-10 is used, the ANBOT has a maximum allowable payload of $100N$. Therefore, if the human applies a load of $100N$, the maximum penalty should be applied to signify that operator has applied a force which can possibly damage the robot. Thus the following conditions for the penalty function $P_F(F)$ were chosen:

$$\begin{aligned} F < 50N \quad & \text{No Penalty} \\ F = 100N \quad & \text{Maximum Penalty} \end{aligned} \tag{4.19}$$

Combining these conditions with (4.6) results in the following function:

$$P_F(F) = 0.1\left(\frac{1}{1+e^{-0.1178(F-75)}}\right) \tag{4.20}$$

The second penalty for this task component $P_{\Delta F}(\Delta F)$ considers the difference between the current operator force and the average operator force during the previous time horizon of two seconds. This is to allow the robot to differentiate between gradual increases in operator force and spikes in the applied operator force. The observation ΔF is given by:

$$\Delta F = \left| F_n - \frac{1}{n-1} \sum_{j=1}^{n-1} F_j \right| \tag{4.21}$$

where F_n is the current operator force and n is the number of observations in the previous time horizon. From Figure 4.8, it can be seen that the value of ΔF is generally below $20N$ during normal grit-blasting operations and that all values of ΔF were under $40N$. For this penalty, the following conditions were chosen:

$$\begin{aligned} \Delta F &< 20N \quad \text{No Penalty} \\ \Delta F &= 40N \quad \text{Maximum Penalty} \end{aligned} \tag{4.22}$$

$\Delta F = 40N$ was selected as the maximum penalty because it was a value that would not normally be reached during normal blasting conditions and because a sudden increase or decrease of 40% of the maximum payload would be undesirable. Combining these condition with (4.6) results in:

$$P_{\Delta F}(\Delta F) = 0.1 \left(\frac{1}{1 + e^{-0.2944(\Delta F - 30)}} \right) \tag{4.23}$$

The functions for the penalties in the operator force task component can be seen in Figure 4.9. The human's performance in this component ($\phi_{F,n}$) is updated at each time step using (4.3) where:

$$\frac{d\phi_{F,n}}{dt} = G_{R_F} \cdot R_F - G_{P_F} \cdot P_F(F) - G_{P_{\Delta F}} \cdot P_{\Delta F}(\Delta F) \tag{4.24}$$

Human Performance in the Blasting Angle Task Component (θ)

The blasting angle of the nozzle to the surface in a grit-blasting operation has an effect on the efficiency of the task and the quality of the end result. If the blasting angle is too shallow, the

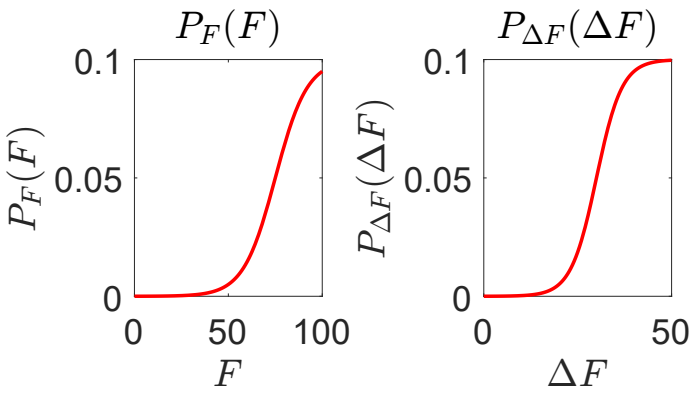

FIGURE 4.9: Penalty functions for the operator force task component.

abrasive material will glance off the blasting surface and if the blasting angle is too close to perpendicular there is an increased risk of injury from the ricocheting abrasive material. For the blasting angle task component, grit-blasting professionals recommended that the appropriate angle for grit-blasting was approximately $\theta = 60°$, where $\theta = 0°$ is parallel to the blasting surface and $\theta = 90°$ is perpendicular to the blasting surface. The range $40° \leq \theta \leq 80°$ was recommended as the allowable blasting angle. Based on this information the following conditions are proposed:

$$\begin{aligned} 40 \leq \theta \leq 80 \qquad & \text{No Penalty} \\ \theta = 0 \qquad & \text{Maximum Penalty} \end{aligned} \tag{4.25}$$

For this penalty, (4.7) was combined with the previous conditions where the curve is centered around $\theta = 60°$. The value $g = 6$ was selected to increase the rate that the penalties increased when the blasting angle was outside of the recommended range. This results in the following equation:

$$P_\theta(\theta) = 0.1\left(1 - e^{\frac{-(\theta-60)^6}{1247730000}}\right) \tag{4.26}$$

The penalty $P_{\Delta\theta}(\Delta\theta)$ considers the average change in blasting angle during the previous two seconds of the pHRC. Ideally, the human co-worker would maintain a constant blasting angle of 60° throughout the grit-blasting operation. However, this would be unintuitive as the human would not be able to pan or tilt the end-effector of the ANBOT during the task. $\Delta\theta$ is given by:

$$\Delta\theta = \frac{1}{n-1}\sum_{j=2}^{n}\left|(\theta_j - \theta_{j-1})\right| \tag{4.27}$$

where n is the number of observations in the previous time horizon. Figure 4.10 shows an example of θ and $\Delta\theta$ during a normal blasting operation.

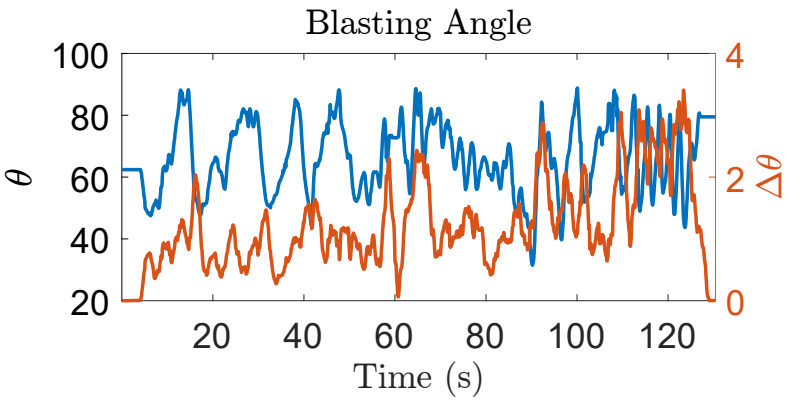

FIGURE 4.10: An example of θ and $\Delta\theta$ from a previous experiment where the human was grit-blasting normally.

From the figure, it can be seen that most values of $\Delta\theta$ fall below 3° with none of the values exceeding $\Delta\theta = 4°$. For this penalty, the chosen conditions were:

$$\begin{aligned} \Delta\theta < 3° \quad & \text{No Penalty} \\ \Delta\theta = 4° \quad & \text{Maximum Penalty} \end{aligned} \tag{4.28}$$

By combining these conditions with (4.6), the following equation for the penalty $P_{\Delta\theta}(\Delta\theta)$ can be obtained:

$$P_{\Delta\theta}(\Delta\theta) = 0.1\left(\frac{1}{1+e^{-5.8889(\Delta\theta-3.5)}}\right) \tag{4.29}$$

The functions representing the penalties for the blasting angle task component can be seen in Figure 4.11.

The robot updates its perception of its human co-worker's performance in the blasting angle task component ($\phi_{\theta,n}$) using (4.3) where:

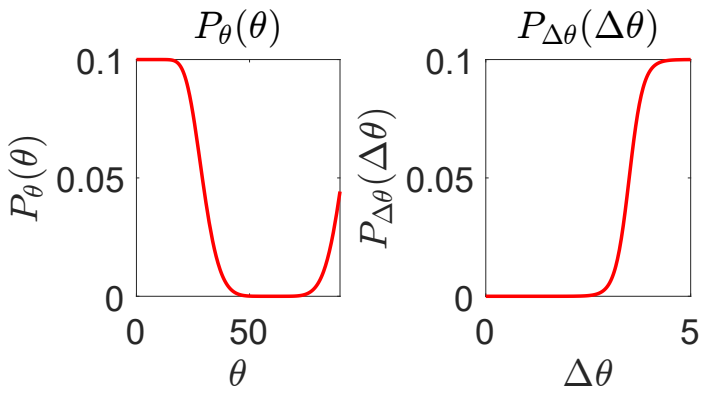

FIGURE 4.11: Penalty functions for the blasting angle task component.

$$\frac{d\phi_{\theta,n}}{dt} = G_{R_\theta} \cdot R_\theta - G_{P_\theta} \cdot P_\theta(\theta) - G_{P_{\Delta\theta}} \cdot P_{\Delta\theta}(\Delta\theta) \tag{4.30}$$

Human Performance in the Variation in Blasting Path Task Component (p)

This task component considers the blasting trajectories and the changes in the direction of the blasting point on the blasting surface during the pHRC. The blasting point refers to the point on the blasting surface obtained by projecting the center of the nozzle onto the blasting surface. The observation p is given by:

$$p = acos(\left| \frac{\vec{v}_t \cdot \vec{v}_{t-1}}{|\vec{v}_t||\vec{v}_{t-1}|} \right|) \tag{4.31}$$

where $\vec{v}_t$ is a vector representing the current trajectory of the blasting point on the blasting surface and $\vec{v}_{t-1}$ represents the previous trajectory. Figure 4.12 shows an example of how p and Δp change during a grit-blasting operation.

From the figure, it can be seen that most values of p fall below 45°. Because $p = 90°$ is the maximum value for p, it was designated as the maximum penalty. This results in the following conditions for the penalty $P_p(p)$:

$$\begin{aligned} p &< 45° \quad \text{No Penalty} \\ p &= 90° \quad \text{Maximum Penalty} \end{aligned} \tag{4.32}$$

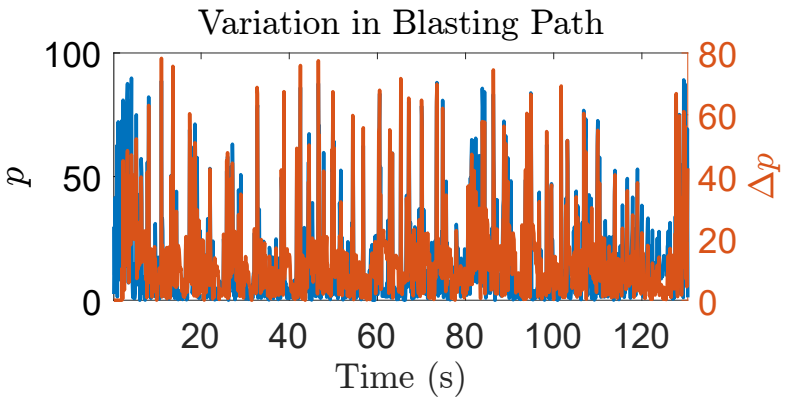

FIGURE 4.12: An example of p and Δp from a previous experiment where the human was grit-blasting normally.

Combining these conditions with (4.6) results in the following formula for the penalty:

$$P_p(p) = 0.1\left(\frac{1}{1+e^{-0.1309(p-67.5)}}\right) \tag{4.33}$$

The second penalty in this task component $P_{\Delta p}(\Delta p)$, adds context to the variations in the blasting path by considering the difference between the current change in blasting path and the average variation in the blasting path. The observation Δp is given by:

$$\Delta p = \left| p_n - \frac{1}{n-1}\sum_{j=1}^{n-1} p_j \right| \tag{4.34}$$

where p_n is the current variation in the blasting path on the blasting surface and n is the number of observations in the previous time horizon. If p is similar to the average change in p in the previous time horizon of two seconds, then the human's blasting can be said to be following a path or a pattern during the previous time horizon. Sporadic blasting path on the other hand would result in a much higher value of Δp which could have adverse effects on the quality of the grit-blasting operation. From Figure 4.12, it can be seen that with the exception of the beginning and the end of the pHRC, most values for Δp fall below 30° during normal blasting conditions. Similar to the previous penalty, $\Delta p = 90°$ is the maximum value of the observation. Therefore the conditions used for the penalty $P_{\Delta p}(\Delta p)$ are:

$$\begin{aligned} \Delta p < 30^\circ \quad & \text{No Penalty} \\ \Delta p = 90^\circ \quad & \text{Maximum Penalty} \end{aligned} \tag{4.35}$$

Using these conditions in conjunction with (4.6) results in the following equation for the penalty:

$$P_{\Delta p}(\Delta p) = 0.1 \left(\frac{1}{1 + e^{-0.09148(\Delta p - 60)}} \right) \tag{4.36}$$

The functions for both $P_p(p)$ and $P_{\Delta p}(\Delta p)$ can be seen in Figure 4.13.

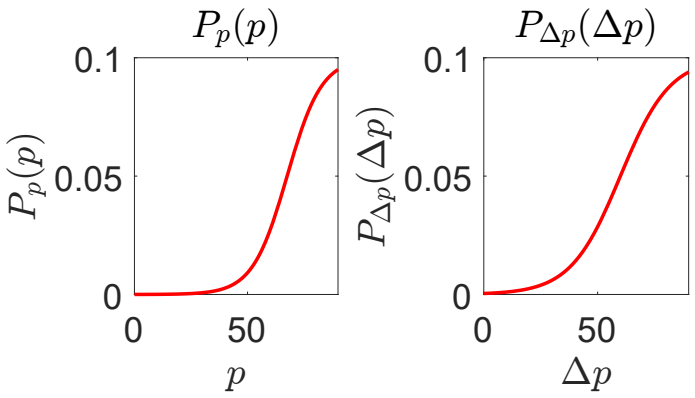

FIGURE 4.13: Penalty functions for the variation in blasting path task component.

The robot's perception of its human co-worker's performance in this task component ($\phi_{p,n}$) is updated at each time step using (4.3) where:

$$\frac{d\phi_{p,n}}{dt} = G_{R_p} \cdot R_p - G_{P_p} \cdot P_p(p) - G_{P_{\Delta p}} \cdot P_{\Delta p}(\Delta p) \tag{4.37}$$

4.3.1.2 Confidence modelling

In this case study, there is a combination of critical and non-critical components. The following equation was used to calculate the confidence of the robot in its human co-worker in the grit-blasting operation:

$$C_1 = \phi_w \left(0.3 + (1 - 0.3)\left(0.4\phi_\theta + 0.4\phi_p + 0.2\phi_F\right)\right) \tag{4.38}$$

The value $C_{1,min} = 0.3$ was chosen to show that emphasis was placed on the non-critical components, but not to the extent of a critical component when combined. ϕ_θ and ϕ_p were given a higher weighting than ϕ_F because the operator force does not directly affect the quality of the grit-blasting operation while the other two components do. Therefore, the weightings of the non-critical task components were set to $\gamma_\theta = 0.4, \gamma_p = 0.4, \gamma_F = 0.2$.

4.3.1.3 Experimental Results

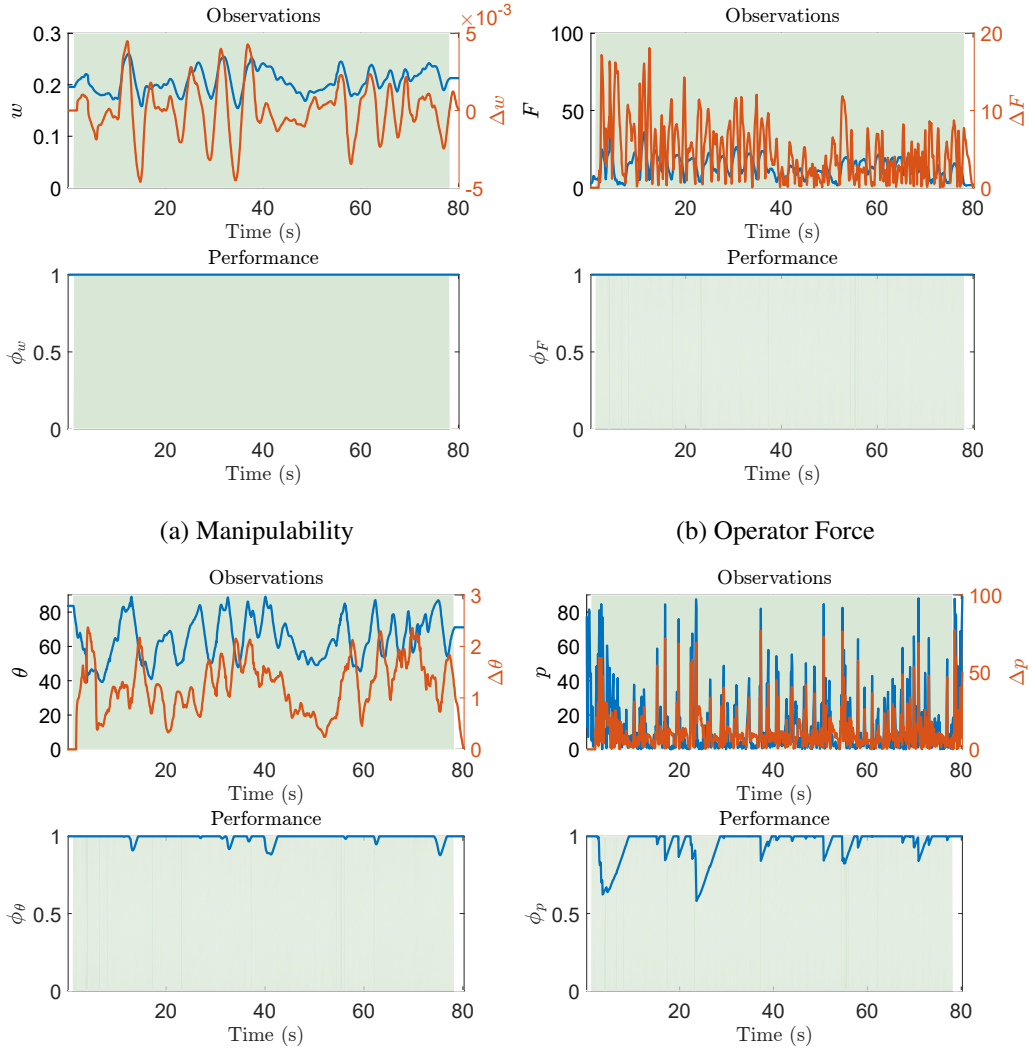

(a) Manipulability

(b) Operator Force

(c) Blasting Angle

(d) Variation in Blasting Path

FIGURE 4.14: The robot's observations (top) and the robot's perception of its human co-worker's performance (bottom) in the (a) manipulability (b) operator force (c) blasting angle (d) variation in blasting path task components.

An example of the robot's observations and the performance of an experienced grit-blaster during a grit-blasting operation in each task component is shown in Figure 4.14. The data recording started when B_m was pressed and ended when B_m was released. The green region represents the period when B_b was pressed. Prior to the switch B_m being pressed, the human is not considered to be in a pHRC with the ANBOT. When the human co-worker releases the switch, the pHRC is considered to have ended and the data recording ceases.

From the figures, it can be seen that there is no decline in the robot's perception of its human co-worker's performance in both the manipulability task component and the operator force task component. This is because the robot's observations of the human's actions in these task components were always within the expected range of values proposed in the previous section. On the other hand, the human's performance was penalized in the variation in blasting path task component and blasting angle task component. In Figure 4.14c, it can be seen that the decrease in the robot's perception of the human's performance in the blasting angle usually occurred when the blasting angle was almost perpendicular to the blasting surface. There are a number of situations during a grit-blasting operation which can cause this. One of the main causes would be when the human co-worker was panning horizontally as during the panning action, the nozzle became perpendicular to the wall for a short period of time.

From the low values of $\Delta\theta$ throughout the grit-blasting operation and the regular decreases in ϕ_p, it can be inferred that the human was blasting slowly but had a tendency to change their blasting trajectory. The importance of the enabling functions is highlighted when considering the robot's observations in Figure 4.14d during the time period where B_m was pressed but B_b was not pressed. During this period, the human co-worker was positioning the ANBOT's nozzle in preparation to begin and end the grit-blasting task. Because, B_b was not pressed, the blasting path of the human should not affect their performance in the task component.

Based on the robot's performance in the task components shown in Figure 4.14 and the equation for the ANBOT's confidence in its human co-worker (4.38), the robot's confidence in its human co-worker during the collaborative grit-blasting operation is shown in Figure 4.15. From the graph it can be seen that the robot's confidence in the human remained fairly high throughout the task as the human's performance was only penalized in non-critical components. If the human co-worker were to be less experienced with the robot or the grit-blasting operation, it is very likely for the

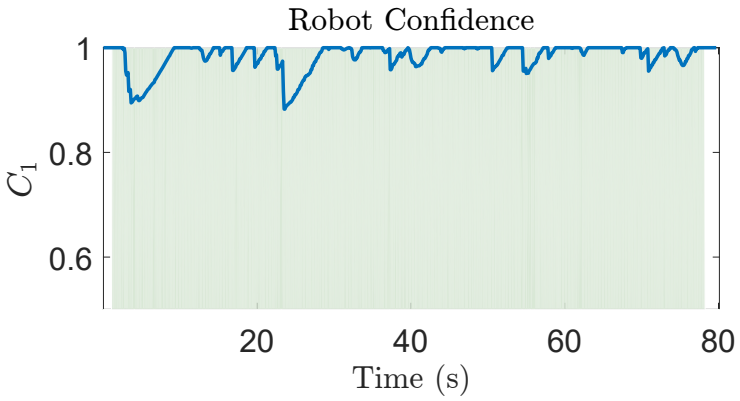

FIGURE 4.15: Confidence of the robot in its human co-worker during the grit-blasting operation.

robot's observations to be outside of the expected ranges more often during the pHRC, resulting in more penalties in the human's performance and a lower robot confidence.

4.3.2 Case Study 2: Smart Hoist - Maneuvering in an Indoor Environment through pHRC

The robot used in this case study is the robotic patient lifter called the Smart Hoist [79][38] shown in Figure 4.16. The Smart Hoist was developed by the Centre for Autonomous Systems at the University of Technology, Sydney with the aim of reducing workplace injuries sustained by nurses and other healthcare workers when transferring non-ambulatory residents (e.g. bed to chair, chair to toilet and bath) in hospitals and nursing homes. Similar to a standard hoist, the Smart Hoist is operated by applying forces on the handlebars which can be seen in the figure. The robot infers the human's intentions through the use of strain gauges to determine the magnitude and direction of the force applied to the handlebars by its human co-worker during the pHRC. The Smart Hoist uses also uses its encoders to measure its velocity and acceleration and has impact sensors that it uses to detect collisions with the environment. A RGB-D camera is used by the Smart Hoist to observe the environment from ground level to detect oncoming obstacles.

In this case study, a patient is seated in the sling of the Smart Hoist. The goal of this task is to transport a patient using the Smart Hoist through pHRC, between two rooms following the path shown in Figure 4.17, while avoiding collisions with the environment. The path that the human must follow during the pHRC is represented in the figure as a red arrow.

FIGURE 4.16: Smart Hoist: A robotic patient lifter designed to assist carers in transporting patients through pHRC.

The task components for this case study were chosen after taking into consideration the sensors the Smart Hoist can use to observe the actions of its human co-worker. The selected task components can be seen below:

- **Critical Components**
  - Impact Detection (i)
  - Acceleration $(\ddot{x})$
- **Non-Critical Components**
  - Distance to walls/obstacles (δ)
  - Velocity $(\dot{x})$
  - Operator Force (F)

FIGURE 4.17: A map of the two rooms being navigated with the path (red line) that the human is expected to maneuver the Smart Hoist.

The impact detection task component checks for collisions between the Smart Hoist and the environment while the acceleration task component concerns the acceleration of the Smart Hoist itself. These were selected as critical components for this interaction as poor performance in either of these task components could result injuries being sustained by the patient sitting in the Smart Hoist's sling. For the non-critical task components, the robot observes the distance between the Smart Hoist and the walls, the velocity of the Smart Hoist and the force applied by the operator. In most circumstances, the velocity task component would also be designated as a critical task component. However, in this particular interaction, the maximum speed the Smart Hoist can reach has been reduced to a safe speed.

A flowchart depicting the flow of information for the robot confidence framework configured for this case study is shown in Figure 4.18. In this case study, the impact detection task component and the acceleration task component were selected as critical components. If the Smart Hoist were

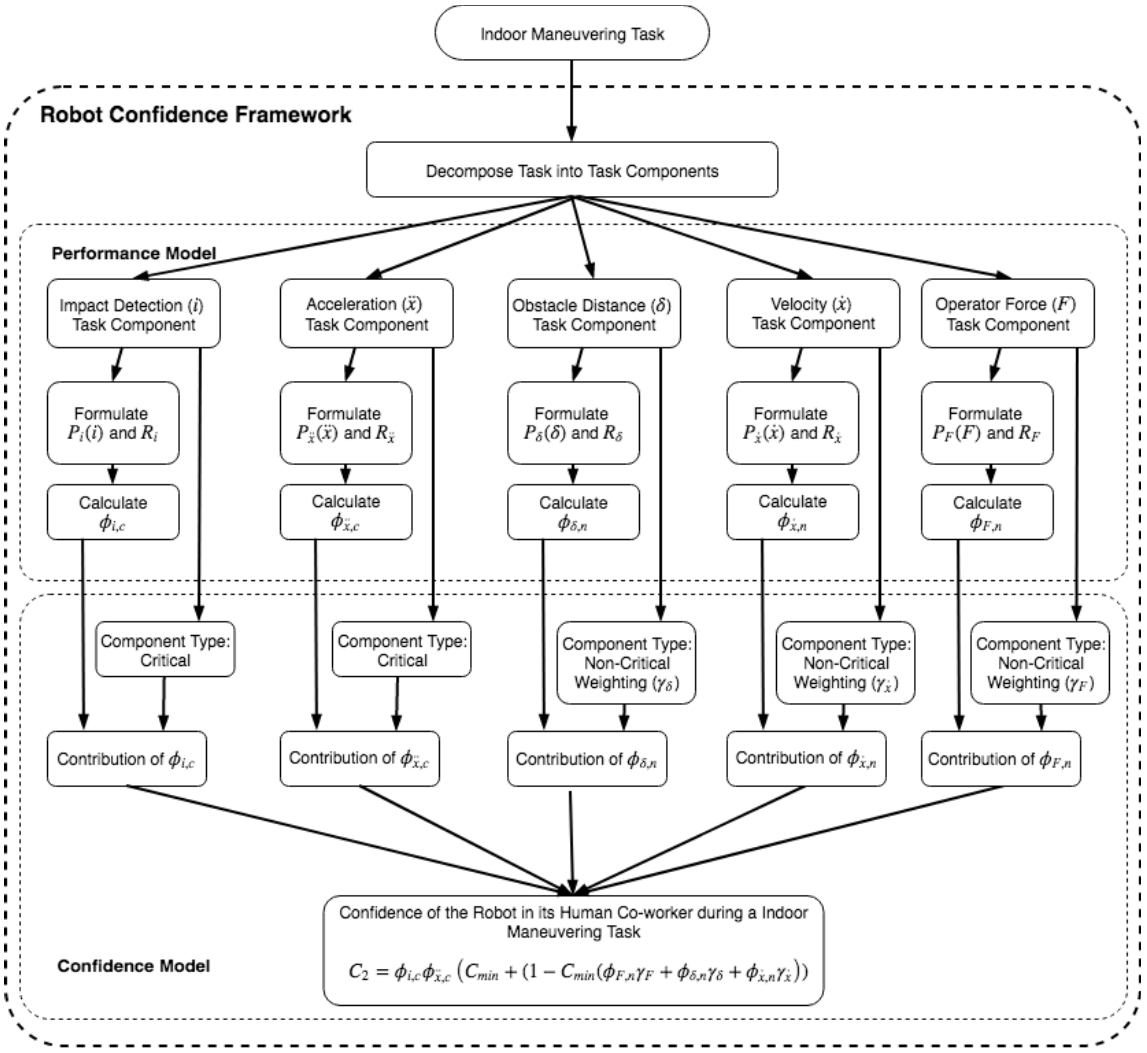

FIGURE 4.18: A flowchart showing the flow of information for the robot confidence framework for Case Study 2: Smart Hoist - Maneuvering in an Indoor Environment through pHRC.

to collide with the environment or undergo large accelerations, then the safety of the patient sitting in the sling would be affected.

4.3.2.1 Performance modelling

Human Performance in the Distance to Obstacle Task Component (δ)

The Smart Hoist measures the distance between the front of each leg of the Smart Hoist and the obstacles it discovers through its RGB-D camera. In pHRC, a distance of $0.5m$ from the robot to the environment is generally considered to be a safe working distance [189]. Therefore, this task

component will penalize the performance of the human when obstacles come within this range. As there are two legs on the Smart Hoist, two penalties are used in this task component. The two penalty functions $P_{\delta_L}(\delta_L)$ and $P_{\delta_R}(\delta_R)$ for this task component assume a maximum penalty when the distance is zero and no penalty when the distance is greater than $0.5m$:

$$P_{\delta_L}(\delta_L) = 0.05\left(\frac{1}{1+e^{(11.78(\delta_L-0.25)))}}\right) \tag{4.39}$$

$$P_{\delta_L}(\delta_R) = 0.05\left(\frac{1}{1+e^{(11.78(\delta_R-0.25)))}}\right) \tag{4.40}$$

where δ_L and δ_R are the distances between the environment and the left and right leg of the Smart Hoist respectively. For this task component, a constant reward of $R_\delta = 0.01$ was chosen. This is so the robot's perception of the human's performance in this task component ($\phi_{\delta,n}$) will increase slowly over time when there are no nearby obstacles. Graphs for the reward and penalty in this task component can be seen in Figure 4.19.

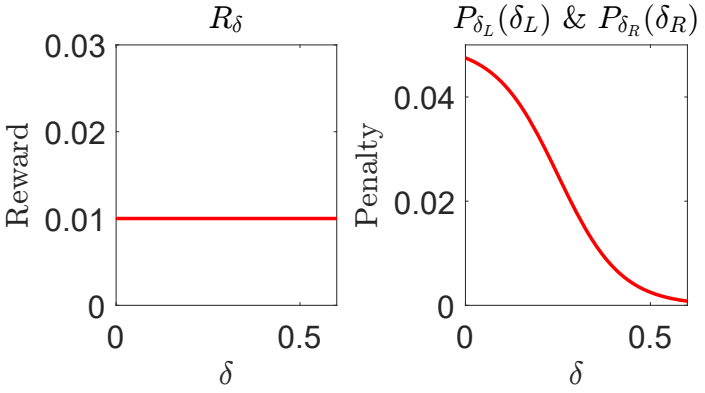

FIGURE 4.19: Graphs representing the functions for the reward (left) and penalty (right) in the distance to walls/obstacles task component.

In this task component, it is intuitive for the rewards and penalties to be enabled when the human co-worker is controlling the Smart Hoist, therefore the enabling function for this task component is given by:

$$G_\delta = \begin{cases} 1 & \text{Force detected} \\ 0 & \text{Force not detected} \end{cases} \tag{4.41}$$

The robot updates its perception of the human's performance in this task component ($\phi_{\delta,n}$) using (4.3) where:

$$\frac{d\phi_{\delta,n}}{dt} = G_\delta R_\delta - G_\delta P_{\delta_L}(\delta_L) - G_\delta P_{\delta_R}(\delta_R) \tag{4.42}$$

Human Performance in the Impact Detection Task Component (i)

For the safety of the patient, the impact detection component was designated as a critical component. This task component utilizes the impact sensors at the front of each leg of the Smart Hoist to detect whether a collision has occurred between the Smart Hoist and the environment. In this component, the robot penalizes the performance of the human whenever the Smart Hoist collides with an obstacle. The penalty for this task component has been modeled as:

$$P_i(i) = 1 \tag{4.43}$$

The penalty is modeled as a constant which will empty the fluid in $\phi_{i,c}$ in a single time step. To control the flow of fluid through the fluid arc for this penalty, the following enabling function was defined:

$$G_i = \begin{cases} 1 & \text{Impact Sensors Triggered} \\ 0 & \text{Impact Sensors Not Triggered} \end{cases} \tag{4.44}$$

Therefore, unless a collision is detected, the robot will not penalize the human's performance in this task component. With the way this penalty function has been designed, it causes the robot's perception of the human's performance in this task component to either be at its maximum or minimum value as the initial value of the fluid place is $\phi_{i,c} = 1$ to represent the human and the robot being in a trusting relationship. Because it is a critical component, it will also cause the confidence of the robot in its human co-worker to be at its minimum value when an impact occurs. For this task component, there is no need for a reward as $\phi_{i,c}$ initially begins at its maximum value and it is assumed that the pHRC ends when the robot's confidence equals zero. Therefore, the

robot updates its perception of the human's performance in this task component ($\phi_{i,c}$) using (4.3) where $\frac{\phi_{i,c}}{dt}$ is given by:

$$\frac{\phi_{i,c}}{dt} = -G_i P_i(i) \tag{4.45}$$

Human Performance in the Velocity Task Component $(\dot{x})$

The maximum allowable speed of a motorized wheelchair is approximately $2.77 m/s$ [190]. As the Smart Hoist is also a motorized device for indoor use, this velocity was used as a reference for the maximum penalty in the velocity task component. Taking into account that the maximum comfortable walking speed for an adult is approximately $1.46 m/s$ [191], the Smart Hoist will penalize the performance of the human when the velocity of the Smart Hoist exceeds $\dot{x} = 1.46 m/s$. Therefore, the function describing the penalty $P_{\dot{x}}(\dot{x})$ is given by:

$$P_{\dot{x}}(\dot{x}) = 0.1\left(\frac{1}{1+e^{(-4.46(\dot{x}-2.12))}}\right) \tag{4.46}$$

A constant reward of $R_{\dot{x}} = 0.01$ was chosen for this task component so that the fluid in $\phi_{\dot{x}}$ would slowly regenerate when the velocity of the Smart Hoist is low. The functions describing the reward and penalty for this task component are shown in Figure 4.20.

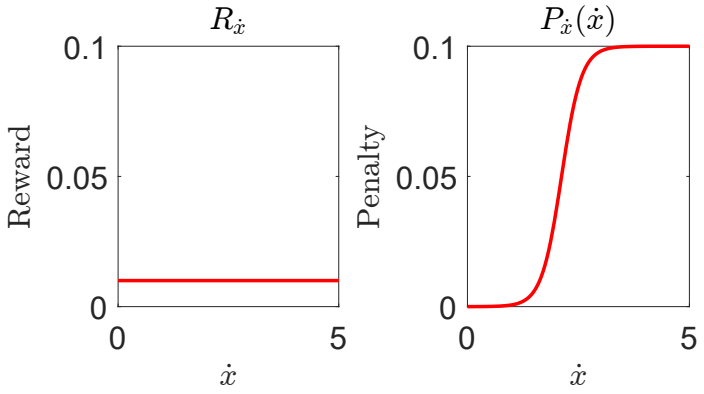

FIGURE 4.20: Graphs representing the functions for the reward (left) and penalty (right) in velocity task component.

The enabling function $G_{\dot{x}} = 1$ was selected for this task component and is considered to be constantly enabled. This is because there are no circumstances where a high velocity should not result

in a penalty in the robot's perception of the human's performance in this task component. The robot updates its perception of the human's performance in this task component ($\phi_{\dot{x},n}$) using (4.3) at each time step where:

$$\frac{d\phi_{\dot{x},n}}{dt} = R_{\dot{x}} - P_{\dot{x}}(\dot{x}) \tag{4.47}$$

Human Performance in the Acceleration Task Component ($\ddot{x}$)

When a patient is seated in the sling of the the Smart Hoist, large accelerations may result in possible injuries as they swing in place. The penalty for the acceleration task component was formulated by examining the acceleration in previous pHRC using the Smart Hoist.

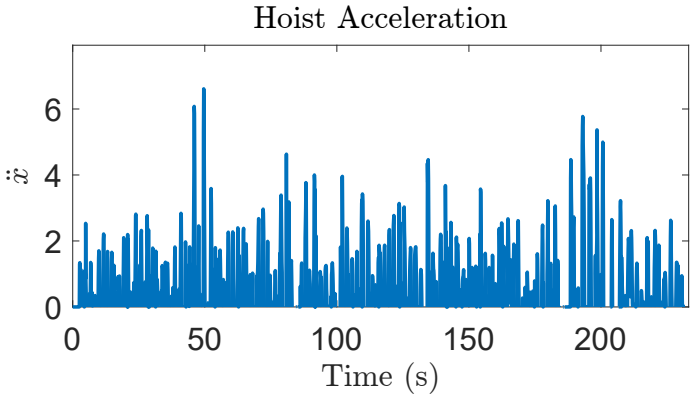

FIGURE 4.21: An example of the acceleration of the Smart Hoist during a previous pHRC.

Figure 4.21 shows an example of the acceleration of the Smart Hoist during a previous pHRC. From the figure, it can be seen that the acceleration of the Smart Hoist would generally be below $2m/s^2$ when a human physically interacts with the Smart Hoist, with high values of acceleration at approximately $4m/s^2$. In this task component, the maximum penalty will occur when the acceleration of the Smart Hoist is above $4m/s^2$ as accelerations above this value are unintentional and could affect the safety of the patient. The penalty function $P_{\ddot{x}}(\ddot{x})$ was formed with this in mind:

$$P_{\ddot{x}}(\ddot{x}) = 0.1\left(\frac{1}{1+e^{(-2.94(|\ddot{x}|-3)))}}\right) \tag{4.48}$$

For this task component, the reward $R_{\ddot{x}} = 0.01$ was selected. The functions representing the penalty and the reward for this task component can be seen in Figure 4.22.

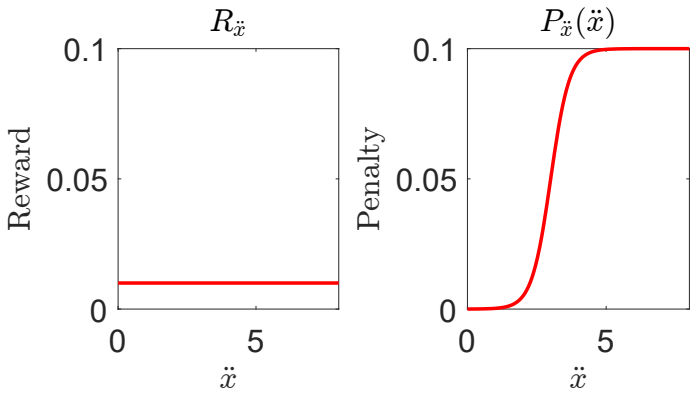

FIGURE 4.22: Graphs representing the functions for the reward (left) and penalty (right) in the acceleration task component.

As with the velocity task component, there are no circumstances where a high acceleration would be appropriate. Therefore, the enabling function $G_{\ddot{x}} = 1$ will always be enabled. The change in the robot's perception of the human's performance in the critical component $\phi_{\ddot{x},c}$ is updated at each time step using (4.3) where:

$$\frac{d\phi_{\ddot{x},c}}{dt} = R_{\ddot{x}} - P_{\ddot{x}}(\ddot{x}) \tag{4.49}$$

Human Performance in the Operator Force Task Component (F)

The purpose of the Smart Hoist is to relieve the physical strain on its human co-worker in order to reduce the likelihood of back injuries during the lifting and transportation of patients. Therefore, the Smart Hoist was designed to be operated with minimal applied forces. It was found that the majority of forces applied by the human during a pHRC using the Smart Hoist was less than 10 N, with a maximum applied load of $20N$. An example of the operator force during a pHRC using the Smart Hoist can be seen in Figure 4.23.

Using this information, the function representing the penalty $P_F(F)$ in this task component was generated:

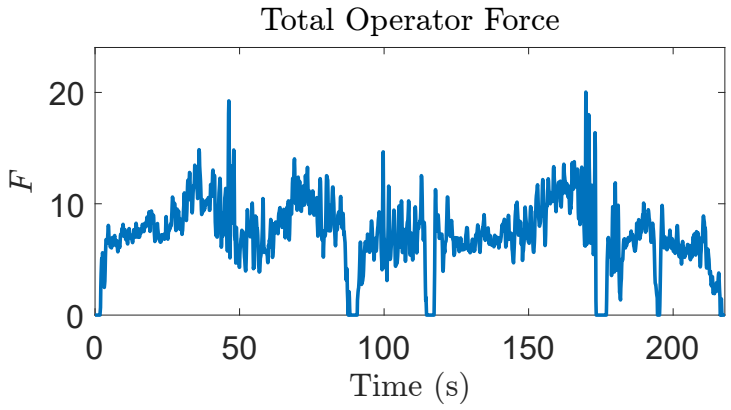

FIGURE 4.23: An example of the operator force applied by the human during a pHRC.

$$P_F(F) = 0.1\left(\frac{1}{1+e^{(-0.588(F-15)))}}\right) \tag{4.50}$$

The reward $R_F = 0.01$ regenerates the fluid in $\phi_{F,n}$ if the human co-worker applies minimal forces or no forces to the handlebars. The functions for the reward and penalty in this task component can be seen in Figure 4.24.

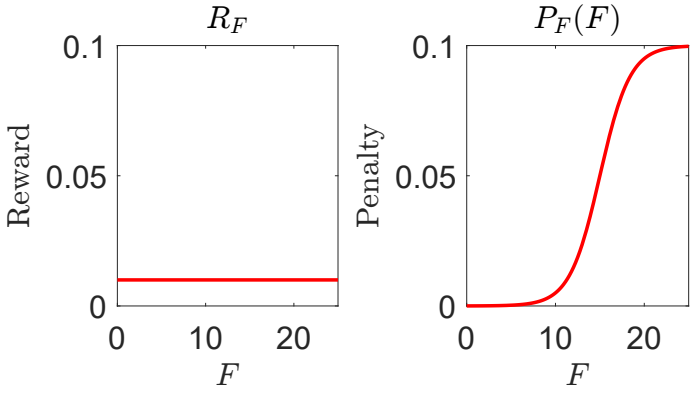

FIGURE 4.24: Graphs representing the functions for the reward (left) and penalty (right) in the operator force task component.

The enabling function $G_F = 1$ for this task component is considered to be permanently enabled. This is because the human should never be applying a large force to the handlebars and accidental contact with the handlebars of the Smart Hoist should not generate enough force to result in a penalized performance. The robot updates its perception of the human's performance in this component $\phi_{F,n}$ at any point in time using (4.3) where:

$$\frac{d\phi_{F,n}}{dt} = R_F - P_F(F) \tag{4.51}$$

4.3.2.2 Confidence modelling

In the Smart Hoist case study, there is a combination of critical and non-critical components. Although a decrease in the human's performance in a non-critical component may not have adverse effects on the safety of the patient, human co-worker or the robot, if human's performance in all of the task components decreases then this may no longer be the case. Therefore, $C_{2,min} = 0$ was chosen so that the human's combined performances in the non-critical components would imitate a critical component. The weightings of the non-critical components were set to $\gamma_{\dot{x}} = 0.2$, $\gamma_F = 0.2$ and $\gamma_\delta = 0.6$ for the velocity, force and distance task components respectively. This distribution was chosen as the Smart Hoist has control strategies in place to deal with higher velocities and forces such as software limitations and scaling but not for obstacle avoidance. This results in the following equation for the robot's confidence in its human co-worker:

$$C_2 = (0.2\phi_{\dot{x},n} + 0.2\phi_{F,n} + 0.6\phi_{\delta,n})\phi_{i,c}\phi_{\ddot{x},c} \tag{4.52}$$

4.3.2.3 Experimental Results

Figure 4.25 depicts the robot's observations of the human's actions and the robot's perception of the human's performance in the task components from a sample pHRC using the Smart Hoist. In the figures, the robot's observations are shown in the top graph while the robot's perception of the human's performance in the corresponding task component is shown in the bottom graph. In the shown pHRC, the impact sensors on the Smart Hoist were not triggered. Therefore, the robot's observations in the task component and the human's performance in the collision detection task component was excluded from Figure 4.26.

From Figure 4.25c, it can be seen that the force applied by the human to the handlebars was generally within the expected range of values. This is because the human's performance in the task component $\phi_{F,n}$ during the pHRC was always at its maximum value. In the acceleration task component, it can be seen that there were a number of occasions during the task where the robot's

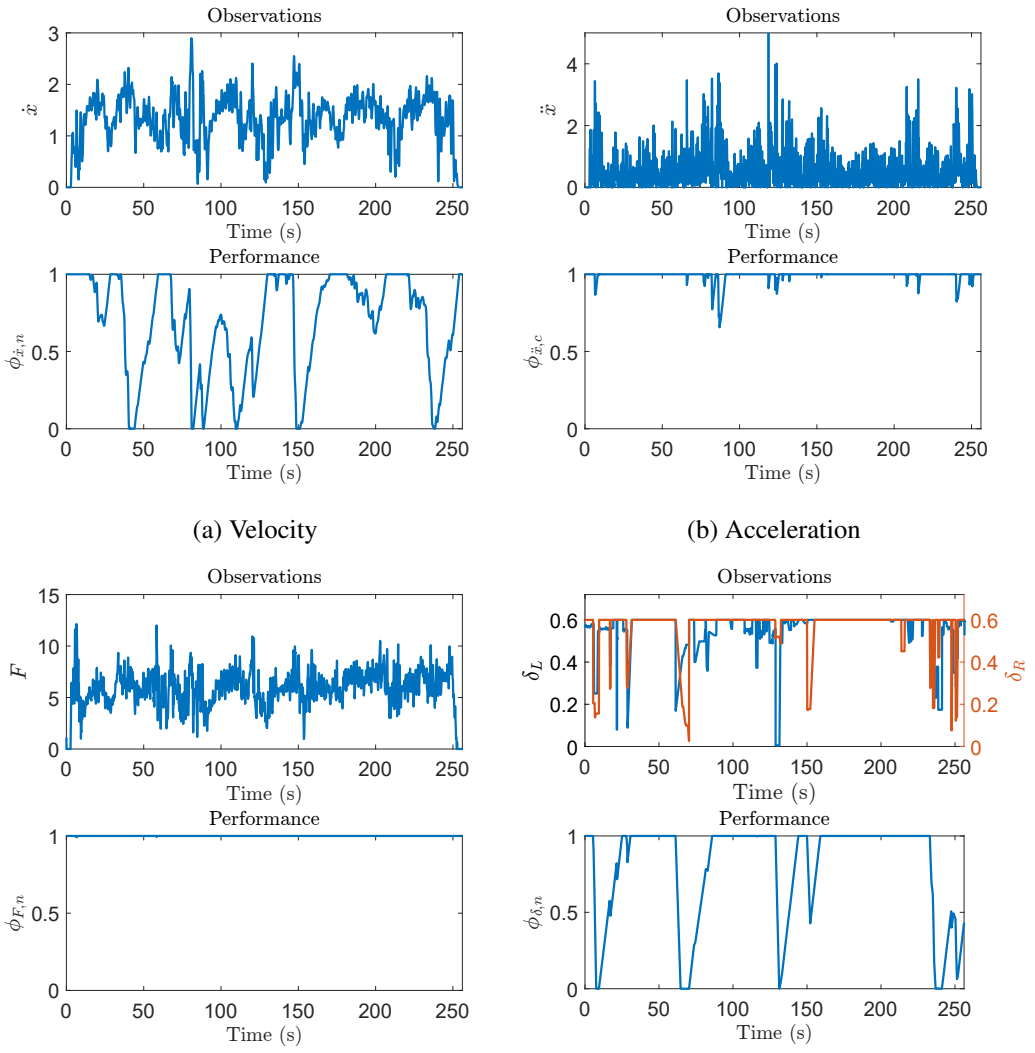

(a) Velocity

(b) Acceleration

(c) Operator Force

(d) Distance to walls/obstacles

FIGURE 4.25: The robot's observations (top) and the robot's perception of its human co-worker's performance (bottom) in the (a) velocity (b) acceleration (c) operator force (d) distance to walls/obstacles task components.

perception of its human co-worker's performance in the task component decreased as the acceleration of the Smart Hoist exceeded the expected range. Comparing the observations of the robot's acceleration to the observations in the distance to walls/obstacles component (Figure 4.25d), it can be seen that these accelerations usually occur when the robot is close to an obstacle. In the context of the task, these obstacles are the door frames which the Smart Hoist must pass through. If a higher acceleration occurs prior to approaching the door frame then it implies that the human was experiencing difficulties in aligning the Smart Hoist.

Because of the way the penalty function P_{δ_L} and P_{δ_R} was formulated, the human's performance in the distance to obstacle component will always decrease when the Smart Hoist approaches a doorway. Although a decrease in confidence is generally the result of a decreased performance, in this particular instance, the decrease in ϕ_δ can also be interpreted as an increased risk towards the safety of the human or the robot or a decrease in the robot's belief that the human co-worker can safely maneuver through the doorways. The impact detection component and the distance to obstacle task components were modeled separately as a critical and non-critical component to distinguish between an actual collision and increased risk of collision.

Other than the distance to walls/obstacle task component, the human's performance in the velocity task component also decreased to its minimum value on numerous occasions during the task. From Figure 4.25a, it can be seen that the velocity of the Smart Hoist during the pHRC would often be above $1.46m/s$ which was defined as the threshold for expected velocity values. Also, it can be seen that the velocity of the Smart Hoist exceeded the maximum indoor speed for motorized vehicles.

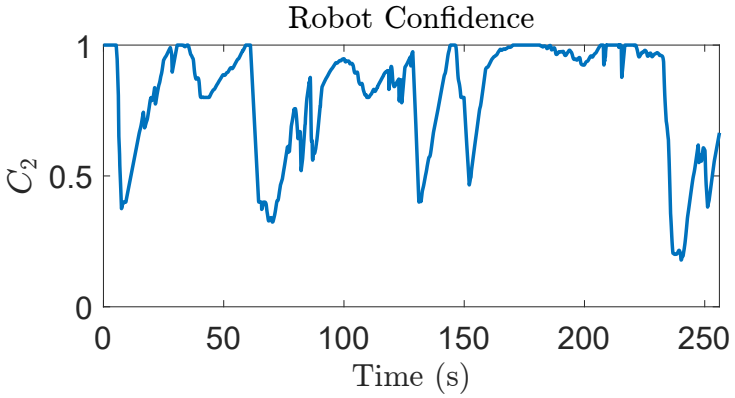

FIGURE 4.26: Confidence of the robot in its human co-worker during a pHRC using the Smart Hoist.

The confidence of the Smart Hoist in its human co-worker can be seen in Figure 4.26. C_2 was calculated using the relationship (4.52) and the performance of the human co-worker in the task components shown in Figure 4.25. In the figure, the confidence of the robot decreased significantly on numerous occasions. Although the human's performance in the distance to walls/obstacles task component and the velocity task component decreased to their minimum values in the pHRC, the confidence of the robot did not fall to zero. This is because those two task components were defined as non-critical components and not critical components. Because the human's performance in the

critical components was high, because of the configuration of confidence defined in (4.52), the results shown in Figure 4.26 can be interpreted as the human having an overall poor performance in the task without affecting the safety of the patient or the task goals.

4.3.3 Case Study 3: Remote Operation of a Robotic Arm's End-Effector in a Complex Simulated Environment

In this case study, the human controls the end-effector of a robot arm in a virtual environment using the Phantom Omni controller seen in Figure 4.27. The Phantom Omni is a portable haptic teleoperation device with six degrees of freedom. The human controls the Phantom Omni by holding onto the pen shaft where the end of the pen shaft corresponds to the end of the robot arm in the virtual environment. When the robot arm in the virtual environment collides with an obstacle, the Phantom Omni provides tactile feedback to the human through vibrations and restricting the actions of the pen shaft in the direction of the obstacle.

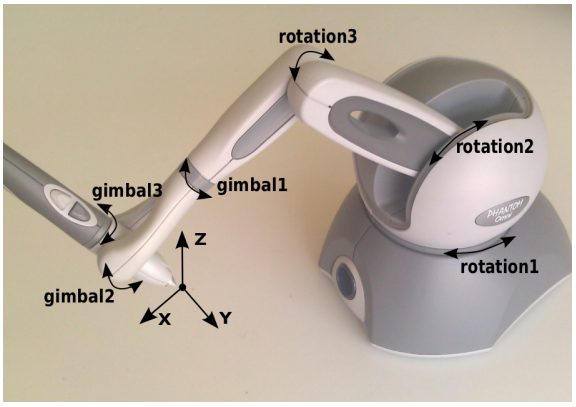

FIGURE 4.27: The Phantom Omni teleoperation input device.

The goal of the human co-worker in this case study is to navigate the robot end-effector through the complex environment seen in Figure 4.28 without colliding with the environment. The human controls the end-effector to enter through the left side, move along the path and then exit through the right side. The task components chosen for this case study were:

- **Non-Critical components**
  - Progress (p)
  - Tactile Feedback (f)

– Control (Δ)

The progress task component measures the human's progress through the complex environment. The longer the human takes the lower the robot's perception of the human's performance. The tactile feedback task component measures the human's performance based on the simulated robot's collisions with the virtual environment and the control task component measures the human's control over the robot in the simulated environment.

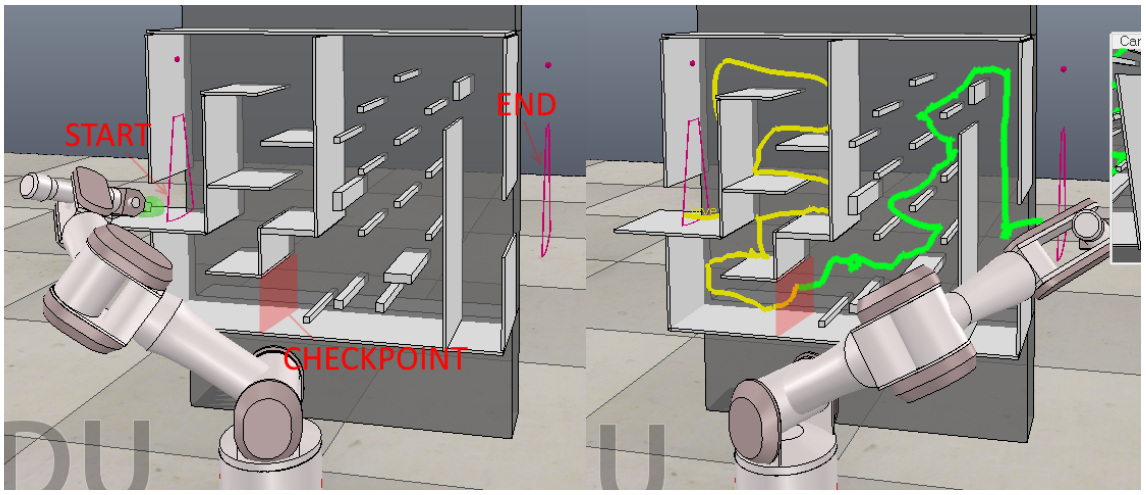

FIGURE 4.28: The simulated environment which the human co-worker attempts to navigate. The path shown in the right image is a recording of a human co-worker's attempt to maneuver through the environment.

Because the human controls the robot arm through tele-operation, both the human co-worker and the robot are not at risk during this pHRC. Therefore, all of the components in this case study were selected as non-critical task components. In this pHRC, the robot is able to monitor the robot arm's position in the virtual environment and infer the human's intention through the Phantom Omni. In this case study, the performance of an experienced operator was used as a benchmark. The penalties and rewards for the task components were modeled using the performance of the experienced operator. A flow chart depicting the flow of information in the robot confidence framework configured for this remote operation case study can be seen in Figure 4.29.

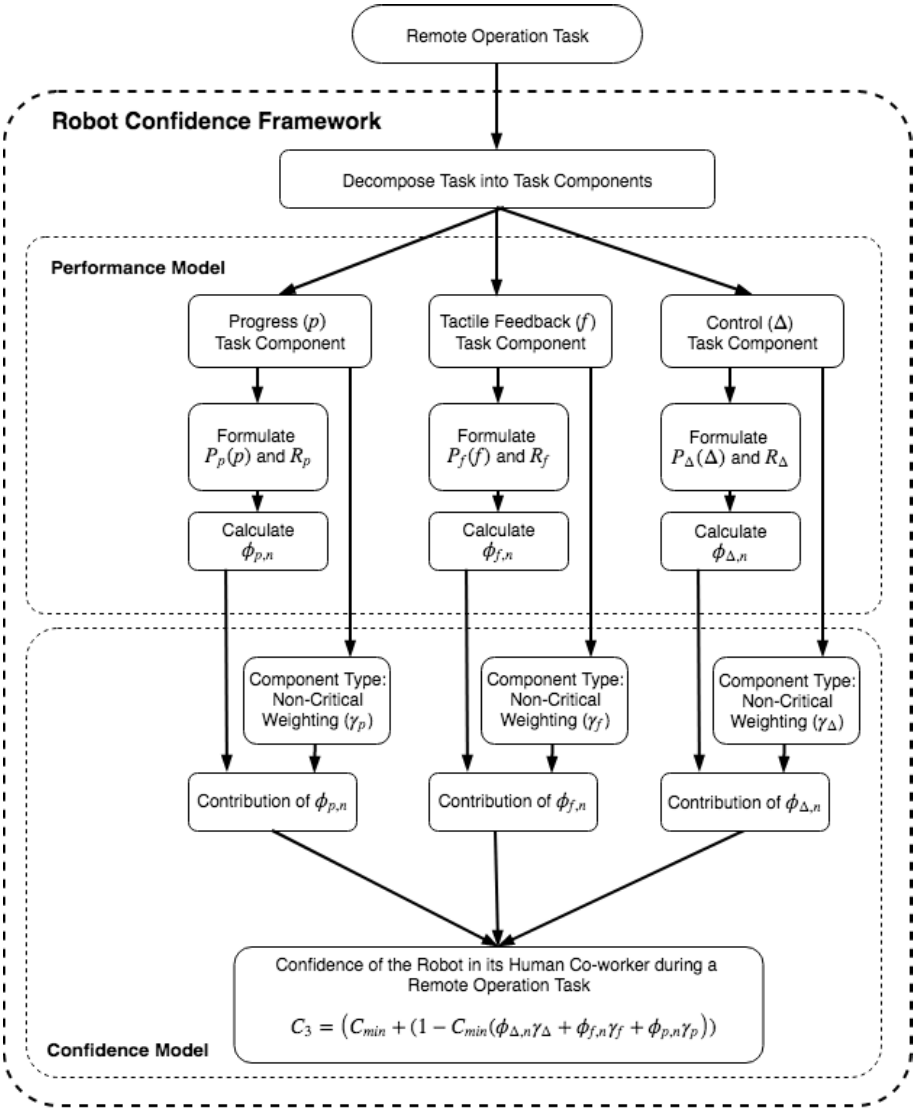

FIGURE 4.29: A flowchart showing the flow of information for the robot confidence framework for Case Study 3: Remote Operation of a Robotic Arm's End-Effector in a Complex Simulated Environment.

4.3.3.1 Performance modelling

Human Performance in the Progress Task Component (p)

The first task component for this case study considers the progress of the robot arm through the virtual environment. As seen in Figure 4.28 the virtual environment has been divided into two different sections. The first section is a simple path with no obstacles (yellow) and the second section requires the human to maneuver around obstacles which hinder the operator's progression

through the environment (green). As the human co-worker maneuvers the robot arm through the virtual environment, the penalty function for this task component:

$$P_p(p) = 0.005 \tag{4.53}$$

penalizes the human's performance when the time taken to finish a section of the virtual environment exceeds the time taken by the experienced operator. As previously mentioned, the robot in this case study updates its observations of the pHRC every $100ms$. This means that the robot's perception of the human's performance in this task component would decreases from its maximum value to its minimum value 20 seconds after the benchmark time has passed. From previous pHRC the experienced operator requires approximately 8 seconds and 16.5 seconds to traverse the first and second sections of the virtual environment respectively.

In this task component, when the human crosses the boundary between the two sections, the robot will reward the human's performance once to signify the robot's acknowledgement of its human co-worker's progress through the environment. The reward for crossing the boundary was set to $R_p = 0.6$.

The enabling function for the penalty in this task component will be different from the enabling function for the reward. The penalty will only penalize the human's performance in this task component when the time taken by its human co-worker exceeds the benchmark. On the other hand, the reward should only increase the fluid in the fluid place $\phi_{p,n}$ if the end-effector moved from the first section to the second section while inside the complex environment. Therefore, the enabling functions for this task component are defined as:

$$G_{p_R} = B_{sec2}B_{trig} \tag{4.54}$$

$$G_{p_P} = \begin{cases} B_{sec1}B_t & \text{Section 1} \\ B_{sec2}B_t & \text{Section 2} \end{cases} \tag{4.55}$$

where $B_{trig} = 1$ represents that the reward has not been awarded before, B_t represents that the time taken by the human co-worker in this section exceeded the time taken by the experienced operator

and $B_{sec1} = 1$ and $B_{sec2} = 1$ represent that the robot arm is currently in the first and second sections of the virtual environment respectively. The functions representing reward and penalty for this task component can be seen in Figure 4.30.

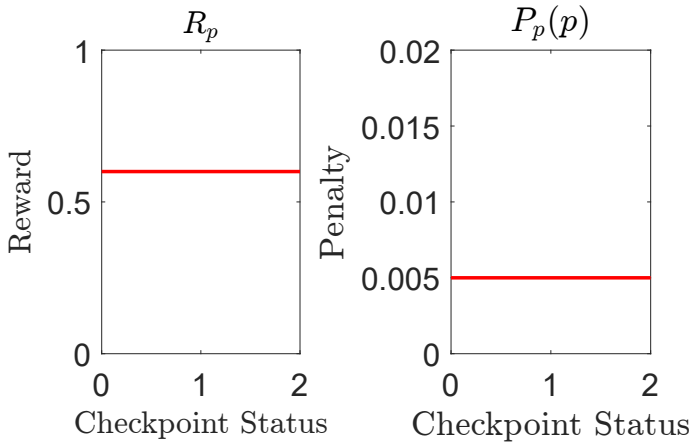

FIGURE 4.30: Graphs representing the functions for the reward (left) and penalty (right) in the progress task component.

The robot updates its perception of the human's performance in the task component $\phi_{p,n}$ at each time step using (4.3) where:

$$\frac{d\phi_{p,n}}{dt} = G_{p_R} R_p - G_{p_P} P_p(p) \tag{4.56}$$

Human Performance in the Tactile Feedback Task Component (f)

The second task component in this case study considers the collisions between the simulated robot end-effector and the complex environment. When the end-effector collides with the environment, the human receives tactile feedback from the Phantom Omni. This tactile feedback takes the form of a vibration in the pen shaft and a resistive force when the human attempts to move in the direction of the walls or obstacles or the intention of the human co-worker would force the robot arm into an unsafe configuration such as self collision or singularity. The observation for this task component f, refers to the strength of the resistive force applied by the Phantom Omni as the human maneuvers the robot arm through the simulated environment.

The tactile feedback received when an experienced operator completes the task is shown in Figure 4.31. From the graph it can be seen that the tactile feedback does not exceed $f = 3$. Therefore,

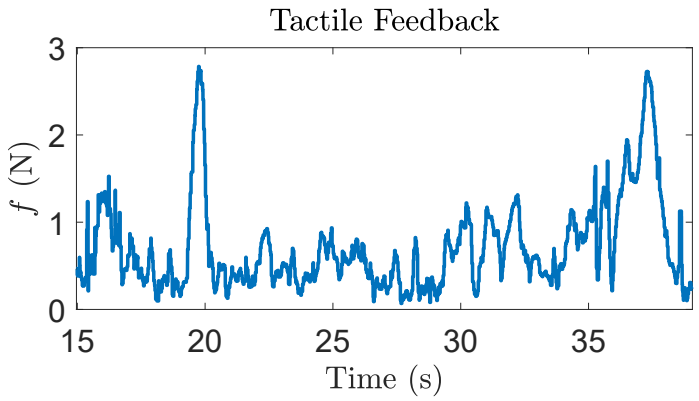

FIGURE 4.31: An example of the tactile feedback received when an experienced operator completes the task.

the penalty for this task component penalizes the human when the tactile feedback exceeds $f = 3$. It was decided that $f = 6$ would correspond with half the maximum penalty and that the maximum penalty would occur when $f = 9$. This results in the following penalty function:

$$P_f(f) = 0.1\left(\frac{1}{1+e^{(-0.98(f-6))}}\right) \tag{4.57}$$

In this task component, the reward $R_f = 0.01$ was chosen to slowly regenerate the fluid in $\phi_{f,n}$ over time. The functions for the penalty and reward can be seen in Figure 4.32.

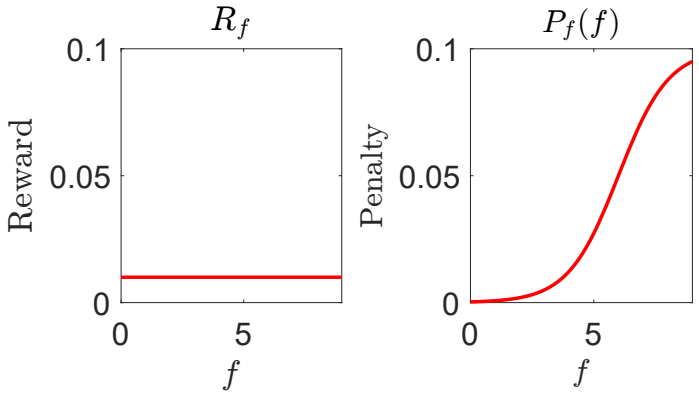

FIGURE 4.32: Graphs representing the functions for the reward (left) and penalty (right) in the tactile feedback task component.

The enabling function $G_f = B_{env}$ was chosen where $B_{env} = 1$ represents that the human is currently inside the complex environment. The robot updates its perception of the human's performance in

this task component $\phi_{f,n}$ using (4.3) where the change in the robot's perception of the human's performance at each time step is given by:

$$\frac{d\phi_{f,n}}{dt} = G_f R_f - G_f P_f(f) \tag{4.58}$$

Human Performance in the Control Task Component (Δ)

The last task component considers the general control aspect of the pHRC. When the human moves the Phantom Omni, a trajectory for the robot end-effector is calculated. The observation Δ is the difference between the distance the virtual end-effector moved and the endpoint of the calculated trajectory. In open spaces, points should be the same; however, inside the simulated environment, this observation provides insight into the human's ability to control the robot arm. As the human co-worker becomes more familiar with the teleoperation of the robot arm in the virtual environment, the expectation is that the value of Δ would become smaller. Smaller values of Δ indicate that the human is familiar with the robot arm's capabilities and is able to make full use of its capabilities without any hindrances to the movement of the robot arm. Larger values of Δ on the other hand, would indicate that the human is attempting to force their way through the complex environment or are unfamiliar with the teleoperation of the robot arm and would require more training to improve their performance.

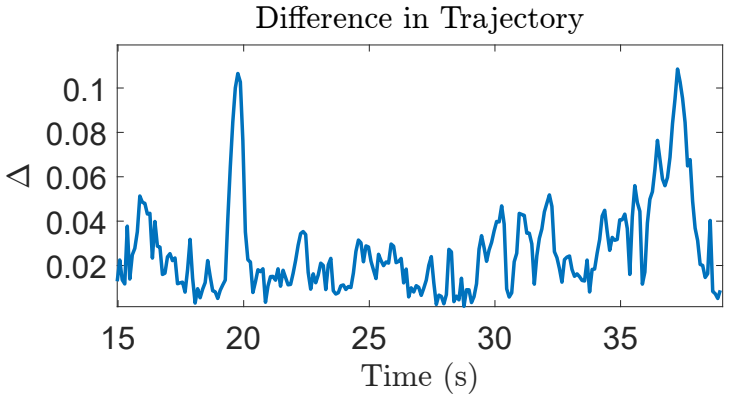

FIGURE 4.33: An example of Δ received when an experienced operator completes the task.

Figure 4.33 shows the value of Δ when an experienced operator completes the task. From the graph, it can be seen that $\Delta \leq 0.1$ when an experienced operator is teleoperating the robot arm through the virtual environment. Therefore, the function which represents the penalty $P_\Delta(\Delta)$ will

penalize the human's performance when $\Delta > 0.1$. The penalty function was designed such that $\Delta = 0.3$ would correspond with the maximum penalty in this task component. The described function is given by:

$$P_{\Delta}(\Delta) = 0.1\left(\frac{1}{1+e^{(-29.44(\Delta-0.2)))}}\right) \tag{4.59}$$

This task component will also be using the reward function $R_{\Delta} = 0.01$ to increase the fluid within the fluid place ϕ_{Δ}. The functions for the reward and penalty in this task component can be seen in Figure 4.34.

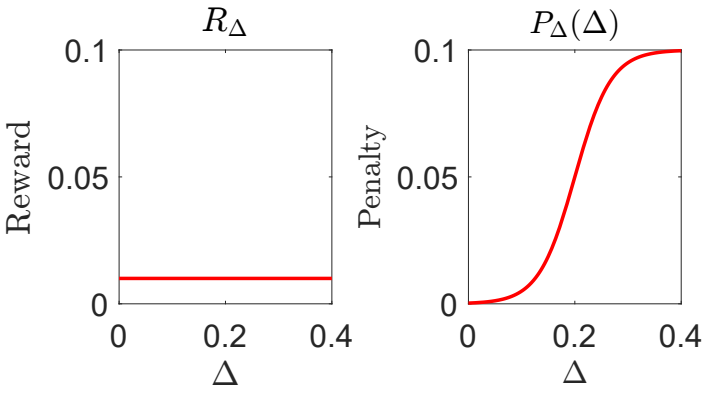

FIGURE 4.34: Graphs representing the functions for the reward (left) and penalty (right) in the control task component.

Similar to the previous task component, the enabling function for this task component will be $G_{\Delta} = B_{env}$. The robot updates its perception of the human's performance in this task component at each time step using (4.3) where:

$$\frac{d\phi_{\Delta,n}}{dt} = R_{\Delta} - P_{\Delta}(\Delta) \tag{4.60}$$

4.3.3.2 Confidence modelling

As there are no critical components in this case study, the calculated confidence purely reflects the robot's overall perception of the human's performance in the task. The confidence will also not fall below $C_{3,min}$. Therefore by setting $C_{3,min} = 0$ the confidence of the robot in its human co-worker will be within the range of $0 \leq C_3 \leq 1$. The weightings of the task components have been set to

$\gamma_\Delta = 0.5$, $\gamma_f = 0.3$, $\gamma_p = 0.2$ for the control, force feedback and operator progress task components respectively. This configuration was chosen as the robot considers the human's ability to control the robot arm more important than the other two task components. γ_p is the lowest of the three weightings as the time required by the human co-worker to complete the task is not as important as their ability to pass through the complex environment with minimal collisions. This results in the following equation for robot's confidence in its human co-worker in this case study:

$$C_3 = 0.5\phi_{\Delta,n} + 0.3\phi_{f,n} + 0.2\phi_{p,n} \tag{4.61}$$

4.3.3.3 Experimental Results

An example of a human co-worker's performance in this case study as they maneuvered the robot arm through the virtual environment with the Phantom Omni is shown in Figure 4.35. The figure depicts the robot's observations of the human's actions in the task components (top) and the robot's perception of the human's performance in the task components (bottom).

From Figure 4.36, it can be seen from the performance graphs that the human co-worker performing the task was not as skilled as the experienced operator. The robot's perception of the human's performance in all the task components decreased with the robot's perception of the human's performance in the tactile feedback task component and the control component reaching their minimum values during the pHRC.

Figure 4.35a shows that although the time required by the human co-worker to complete each section exceeded the benchmark, the human co-worker required a much longer period of time to maneuver the robot arm through the second section than the first section of the task. This was to be expected as the second section of the task is more complex than the first section. It can also be seen from Figure 4.35b that human regularly collided with the environment as they completed the task. Combining this information with the robot's perception of the human's performance in the control task component ($\phi_{\Delta,n}$), it can be inferred that when the human collided with the environment, they had a habit of attempting to force their way through the obstacle. This is largely supported by the observations in the tactile feedback task component which shows that the robot arm was almost in a constant state of collision with the environment as $f \geq 3$ for a large portion of the pHRC.

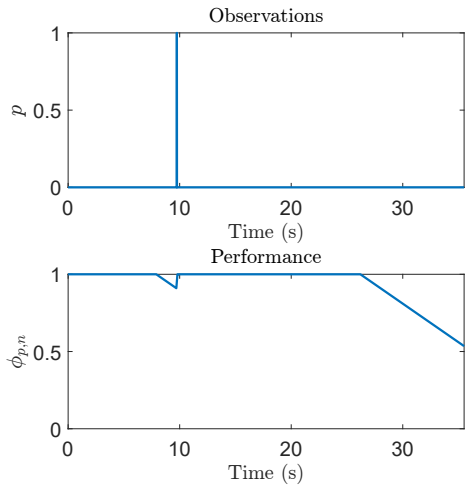

(a) Progress

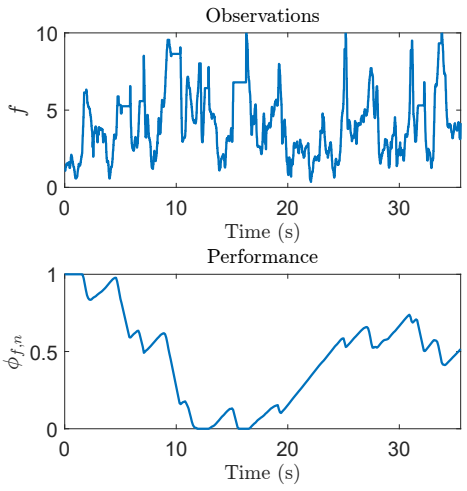

(b) Tactile Feedback

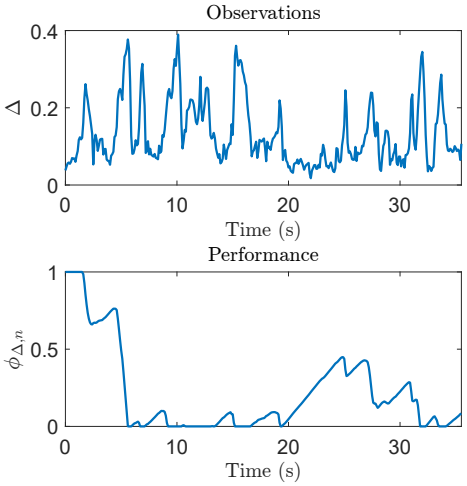

(c) Control

FIGURE 4.35: The robot's observations (top) and the robot's perception of its human co-worker's performance (bottom) in the (a) progress (b) tactile feedback (c) control task components.

The results of this case study showcase how the robot confidence framework can not only be used to quantify the robot's confidence in its human co-worker but also pinpoint areas in the pHRC where the human can improve their performance. The use of the simulated environment is used as a low risk gateway to transition human co-workers towards pHRC using physical robots. If the robot confidence framework from this case study were to be implemented in a physical environment rather than a simulated one, modifications to the implemented framework would be necessary to include task components and rewards and penalties which relate to the physical and safety aspects of the new pHRC.

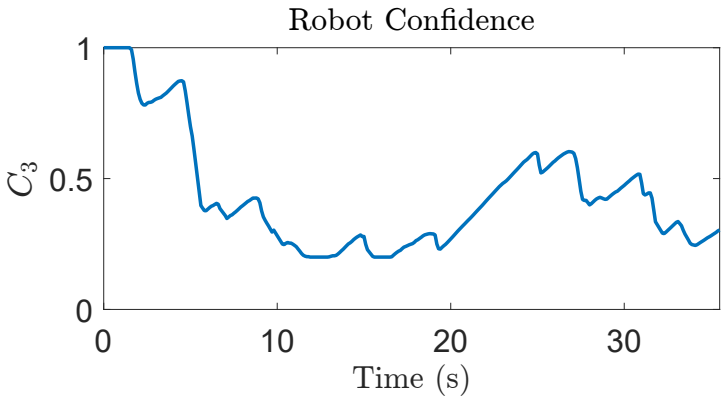

FIGURE 4.36: Confidence of the robot in its human co-worker during a pHRC using the Phantom Omni.

4.4 Further Generalization of the Robot Confidence Framework

The robot confidence framework has the potential to provide many benefits to research on pHRC. The framework could be used by the robot to determine when it should intervene in the interaction. However, this is not the only way the robot confidence framework could be used. Because the robot's confidence in its human co-worker is dependant on the robot's perception of the human's performance in various task aspects, the robot has a record of the human's performance throughout the task. Therefore, it is possible to identify areas where the human's performance could be improved or trends in human performance across multiple human operators which could be used to optimize the interaction. Another possible use for the robot confidence framework is to reduce the speed of the interaction based on the robots confidence in its human co-worker. This could result in improved human performance as the human would have more control over the interaction due to the reduced speed. Once the human's performance increases, the speed of the interaction could return to its initial settings. An example of where this could be useful is in manipulation tasks where the human must guide the robot through complex environments using either physical contact or through tele-operation.

One of the strengths of the robot confidence framework is how it can be easily adapted to any pHRC. In the previous section, three case studies were presented where the robot confidence framework was developed to suit each pHRC scenario. Although the resultant frameworks in each case study differs, the methodology used to develop the framework in each of the case studies was

the same. In this section, an overview of the process for adapting the robot confidence framework for a generic pHRC is provided.

The process of developing a robot confidence framework for a pHRC can be broken into the following steps:

1. Identifying task components for the pHRC.
2. Identify how the robot would observe the human's performance in the task components.
3. Determine the expected values for the robot's observations in each task component.
4. Generate rewards, penalties and enabling functions for each task component.
5. Categorize components into critical and non-critical components.

4.4.1 Identifying task components for the interaction

The first step in formulating the robot confidence framework is to decompose the task into components. Questions to ask include but are not limited to:

- What are the objectives of the task?
- What are the the restrictions or limitations of the task?
- Are there any safety precautions that need to be taken?

Each of these questions should generate a list of task components which could be used for the robot confidence framework. For example, if the task requires the robot or human to reach a position or pose, maintain a speed or state, complete a number of repetitions, navigate an area or find an object, then a portion of the task components should reflect these task requirements. Examples of task oriented task components in the previous case studies include the human maintaining an acceptable blasting angle and the tracking of the human's progress in the task.

In the previous case studies, the majority of the task components were based on safety aspects or limitations of the task. These task components included minimizing applied forces, accelerations and velocities. Theoretically, are no limits to the number of task components which can be defined for a pHRC, at this stage of the framework development, it is best to include as many as possible.

4.4.2 Identifying how the robot would observe the human's performance in the task components

Because the robot's confidence is dependant on the robot's perception of the human's performance and the robot's perception of the human's performance is dependant on its observations of the human's actions, how the robot observes the human's actions is extremely important. If the robot is unable to quantify or observe the human's actions relating to a task component, then it cannot be used as a task component within the robot confidence framework.

For example, assume an interaction where the force applied to the robot end-effector by the human operator was required to be below $10kg$ due to a physical limitation of the robot. If the robot had a load cell built into the robot end-effector, the robot would be able to observe the load applied by the human operator. However, if the robot did not have a load cell and could not observe the force applied by the human, the robot would not be able to measure the human's performance in the task component. Therefore, even though there is no theoretical limit to the number of task components in the robot confidence framework, the number of task components is limited by what the robot can observe through its sensors or other sources of information.

For other task components such as task progression, the robot's ability to observe the human's performance in the task component is dependant on how well defined the task is. As an example, in the grit-blasting case study, the human's progress in blasting the wall section could have been an additional task component. To measure the human's progress in the task component, the robot would need to measure the percentage of the wall that had been blasted. This could be done visually using cameras or by measuring the flow rate of the abrasive material and the trajectory of the nozzle. Observations of task progression in other tasks such as navigation or point-to-point movement could be obtained by implementing a checkpoint system which updates the system state.

4.4.3 Determining expected values for the robot's observations

This step involves defining the robot's expectations for the human's actions in each task component. The robot's perception of the human's performance is dependant on their expectations of

the human's actions. If the robot's expectations for performance are set low, then the robot's perception of the human's performance would be less likely to decrease. Conversely, if the robot's expectations are set high, the robot's perception of the human's performance would be more likely to decrease.

A robot's expectations for a human's actions can be categorized as either expectations resulting from limitations imposed upon the task component or expectations based on prior experience or learning. In Section 4.4.2, the force applied to the robot end-effector was required to be below $10kg$ due to a physical limitation of the robot. Therefore, it is reasonable to assume that the robot's expectations for the force applied by the human operator during the task would be below $10kg$. For the same robot, the robot's expectations of the human's force could refined by modelling the task or analying trends in previous datasets.

For the case studies presented in Section 4.3, the robot's expectations for the task components were obtained by repeating the task with a number of different participants and recording the robot's observations throughout the interactions. Using the observations, the range of values that the robot would expect to observe during an interaction with a generic user was inferred.

4.4.4 Generate rewards, penalties and enabling functions for the task components

Once the robot's expectations for its observations in a task component are identified, the next step is to determine the relationship between the robot's expectations, the robot's observations and the robot's perception of the human's performance in the task components. There are two general rules when defining the rewards and penalties. If the robot's observations of the human are within its expectations, the robot's perception of the human's performance in the task component should increase. However, if the robot's observations of the human are outside of its expectations, then the robot's perception of the human's performance in the task component should decrease.

Intuitively, the further outside the robot's expectations the robot's observations are, the larger the penalty should be. Consider the interaction with the robot end-effector which had a physical limitation of $10kg$. Assume that the robot expects the force applied by the human operator to be less than $5kg$ and consider the three following scenarios; the applied force is less than $5kg$, the applied force is more than $10kg$ and the applied force is more than $5kg$ but less than $10kg$. In the scenario

where the force is below $5kg$, the robot's perception of the human's performance should increase. In the scenario where the force is over $10kg$ the robots perception of the human's performance should decrease. However, in the third scenario where the force applied by the human is between $5kg$ and $10kg$, it can be argued whether the robot's perception of the human's performance should increase, decrease or maintain its current value. The applied force is below the maximum limit of $10kg$ and is therefore safe. However, it is not within the expected range of values for an interaction. Therefore, if the robot's perception of the human's performance were to increase, the increase should be less than the increase in the first scenario where the applied load is less than $5kg$. Similarly, if robot's perception of the human's performance were to decrease, the decrease should be less than the scenario where the applied load is greater than $10kg$. Finally, because the applied load is outside of the expected range but below the maximum load, it may be desirable to maintain the robot's current perception of human performance as the current observation cannot be said to reflect good or bad performance.

The goal of the rewards and penalties is to map the robot's observations to the desired increase or decrease in the robot's perception of the human's performance. This can be done using a variety methods including the use of simple functions, classifications or machine learning algorithms. Using the previous example, two methods for modeling the rewards and penalties for the task component will be presented.

In the first approach one reward and two penalties used. When the applied force is below $5kg$, the reward would increase the robot's perception of the human's performance at a constant rate (fluid within the fluid place would increase at a constant rate). However, if the applied forces were greater than $5kg$ but below $10kg$, one of the penalties would reduce the robot's perception of the human's performance at a constant rate. Finally, if the applied forces were greater than $10kg$, the other penalty would reduce the robot's perception of the human's performance at a faster constant rate. It is also be possible for the rewards and penalties for each range of applied forces to be represented by functions instead of a constant value. From the definition of the reward and penalties, only one of rewards or penalties should be enabled at any given time. In the performance model, the flow of fluid in and out of the fluid place is controlled by the enabling functions. In this case the enabling functions for the rewards and penalties would be enabled when the force applied by the human is within the specified range and would be disabled when the force applied by the human is not within the specified range.

Another approach for modelling the rewards and penalties for the same interaction is to use a single reward and penalty. In this approach, the reward would be set to a constant value and the penalty would be defined by a function. The result in the previous approach can be obtained if the penalty function was represented by three piece-wise functions each representing one of the applied force ranges. However, the values would have to be adjusted to offset the constant reward. Because the robot updates its perception of the human's performance when it receives a new observation, the penalty and reward in this approach would decrease and increase the fluid within the fluid place at the same time. Therefore, unlike the previous approach where each penalty and reward had a distinct enabling function, both the reward and penalty in this approach would have a common enabling function with a condition such as 'the presence of an applied force'. This would ensure that the robot's perception of the human's performance in the task component would only change when the robot detects an applied load. Once again, the reward and penalties do not need to be represented by constant values. In the previous section's case studies, the rewards were generally represented by a constant function while the penalties were generally represented by sigmoid functions.

This step is also used to determine how harsh or lenient the robot is in its judgment of the human's performance. Larger penalties will result in the robot's perception of the human's performance to decrease faster, which will result in a faster decrease in the robot's confidence in the human. Another factor which needs to be taken into account when determining the magnitude of the rewards and penalties, is the rate at which the robot updates its observations. The faster the robot updates its observations, the faster its perception of the human's performance will change. This could result in a small penalty having a large effect on the robot's perception of the human's performance. Therefore, the robot's observations may need to be downsampled or the rewards and penalties scaled appropriately to obtain the desired behavior from the performance model. This step is subjective and the specific values would need to be tuned based on purpose of the task and the framework.

4.4.5 Categorize components into critical and non-critical components

Once the penalties, rewards and their respective enabling functions have been defined for each task component, the final step is to determine the importance of each task component in regards

to the overall task and its importance relative to the other task components. The first part of this step involves categorizing the task components as either critical or non-critical components. If a task component meets any of the following conditions, it should generally be chosen as a critical component:

- Large impact on the safety of the human or robot.
- Large impact on the quality of the task's outputs.
- Large impact on the continuation of the task.
- Requires the robot to quickly intervene in case of poor performance.

From the above list, it can be seen that for a pHRC in an industrial environment, the majority of task components would be designated as critical components. This was not the case in the presented case studies as the tasks were performed within a safe and controlled environment where the safety of the human and the robot were never at risk. An example which highlights the difference between a critical and non-critical component is the categorization of the impact detection and distance to obstacle task components in the Smart Hoist case study which were designated as critical and non-critical task components respectively. The impact detection task component had immediate physical consequences which the robot had to react to immediately whereas being close to walls and obstacles did not necessarily indicate poor performance. In the case study, to pass through doorways, the distance between the Smart Hoist and the environment would be very small due to the width of the Smart Hoist and the doorways. Therefore, poor performance in the distance to obstacle task component does not necessarily indicate that the human is performing poorly in the overall task. Thus the distance to obstacle task component was designated as a non-critical component, so that its influence on the robot's confidence would be significantly smaller when compared to the impact detection task component.

Given that all of the important task components for the interaction have been designated as critical components, all that is left are the non-critical components. An additional weighting needs to be assigned to each of the non-critical components. Similar to how critical components are more important than non-critical components, some non-critical components may be more important than other non-critical components for the interaction. This difference in importance is expressed

through the weightings assigned to each non-critical component. Although this process is subjective, to simplify the process, each non-critical component could be assigned an equal weighting. However, this could result in a problem where the effect of any individual non-critical component on the robot's confidence would be minimal if there are too many non-critical components.

The final variable in the robot confidence framework which needs to be assigned is the C_{min} value. This value specifies the importance of the non-critical components in the task where $C_{min} = 1$ represents the non-critical components having no influence on the robot's confidence and $C_{min} = 0$ represents that the weighted performance of the robot in the non-critical components have the same influence on the robot's confidence as a critical component. It should be noted that in an interaction where there are no non-critical components, $C_{min} = 1$ should not be used as the robot's confidence in the human would not change. For most interactions, that value $C_{min} = 0$ would be used as there are not many situations where decreased performance in non-critical components needs to be dampened. Now that the components of the robot confidence framework are defined, the entire framework can be put together. From the robot's observation of the human's actions, to using the observations to increase and decrease the robot's perception of the human's performance to finally combining the human's performance in the task components to calculate the robot's confidence in its human co-worker.

4.5 Summary

In this chapter, a robot confidence framework was proposed for quantifying the robot's confidence in its human co-worker during pHRC based on its perception of the human's performance. The confidence calculation is application-dependent. Because of this, the framework provides a way of modelling the robot's confidence in its human co-worker based on task specific measures of performance. The rewards and penalties that model the robot's expectations of its human co-worker in the task components are generally created based on what is considered to be best practice for a specific application.

In the case studies presented in this chapter, the calculated confidence of the robot in its human co-worker reflects how confidence should change based on the performance of the human co-worker. The implementation of the framework can be further improved by including more nuanced

rewards and penalties or increasing the number of task components to improve the model of robot's expectations of the human's actions.

The use of the robot confidence framework not only provides the robot with information about its human co-worker's overall performance in the pHRC, it also provides information on aspects of the task where its human co-worker requires improvement. The results of the robot confidence framework can be used as a guide for teaching the human co-worker how to improve their performance in future collaborative operations. In Case Study 3 for example, if a physical robot was used rather than a simulated one, the lessons learned from applying the robot confidence framework can also be applied to the physical robot. However, the robot confidence framework developed in the case study would require modifications to the task components and/or the rewards and penalties to account for the changes in the pHRC.

Chapter 5

Robot Confidence-Based Role Change

In Chapter 4, a robot confidence framework was presented that quantifies the robot's confidence in its human co-worker during physical Human-Robot Collaboration (pHRC). The robot confidence framework was demonstrated by applying it to a number of pHRC case studies. Using the robot's observations of the human's actions and the robot's understanding of the task, the robot's confidence in its human co-worker during pHRC was calculated. A human's confidence in its robot co-worker is one of the factors that determine whether the human would intervene in the robot's actions during an interaction [34][35]. Therefore, using the robot's confidence to determine whether the robot should intervene in the human's actions during pHRC would facilitate a reciprocal interaction dynamic between the human and the robot.

Chapter 5 presents a method that uses the confidence of the robot to determine whether the robot should initiate a role change during pHRC and take control of the interaction away from its human co-worker. In this thesis, a role change is defined as a change in the robot's Level of Autonomy (LoA) which is represented by the robot taking control of an interaction away from its human co-worker. Based on the robot's understanding of the task and its observations of the human's actions, the robot calculates its confidence in its human co-worker using the robot confidence framework presented in Chapter 4. The robot's confidence is then used to determine whether and when the robot take the control away from its human co-worker during pHRC. This method is verified in a case study that uses a collaborative grit-blasting robot.

This chapter is organized as follows. Section 5.1 presents a method for using the robot's confidence in its human co-worker to determine whether the robot should intervene (i.e. take control) in the human's actions during pHRC. The confidence-based role change method takes into account the robot's confidence and the first and second derivatives of the robot's confidence to decide whether it should initiate a role change. Section 5.2 introduces the experiment to verify the role change method. Section 5.3 presents the experimental results where the robot monitors the human's actions during a collaborative grit-blasting task and decides whether it should initiate a role change. Section 5.5 summarizes the experimental results and discusses the limitations of the confidence-based role change method.

5.1 Confidence-Based Role Change Method

The approaches for role change in the literature can be divided into two categories; sliding autonomy and instantaneous role change. In the first category, the change in roles occurs as a gradual relinquishing of control from one of the participants of the interaction [124]. The second category on the other hand, involves an instantaneous change of role in the interaction once a threshold had been exceeded [105]. The confidence-based role change method presented in this chapter is in the second category.

In this chapter, the research is focused on when and whether a robot initiates a role change and assumes that only one of the agents (the human or the robot) has control over the pHRC at any given time. When the robot decides that it should take the control of the pHRC away from its human co-worker, i.e. robot is in control of the pHRC, then the robot will no longer act upon its human co-worker's intentions.

The confidence-based role change method presented in this chapter uses a control value Ω to determine whether it should intervene in the pHRC to take the control away from its human co-worker. The control value Ω determines whether a role change occurs based on the following conditions:

$$\begin{aligned} \Omega \geq 0 \quad & \text{Human co-worker is in control} \\ \Omega < 0 \quad & \text{Robot is in control} \end{aligned} \tag{5.1}$$

The presented confidence-based role change method uses the robot's confidence (C) to calculate the control value Ω. This method also considers the first derivative of the robot's confidence ($\dot{C}$) and the second derivative of the robot's confidence ($\ddot{C}$) when calculating the control value, as each of these values adds contextual value to the robot's decision. It should be noted that the second order term may not be necessary for interactions where the confidence of the robot changes very slowly. The following equation for the control value Ω is proposed:

$$\omega_1(\bar{\ddot{C}}) + \omega_2(\bar{\dot{C}}) + \omega_3(\bar{C}) = \Omega \tag{5.2}$$

where ω_1 is a function of $\bar{\ddot{C}}$, ω_2 is a function of $\bar{\dot{C}}$ and ω_3 is a function of $\bar{C}$. The variables $\bar{\ddot{C}}$, $\bar{\dot{C}}$ and $\bar{C}$ represent the average values of $\ddot{C}$, $\dot{C}$ and C in a time horizon t_H. In the following subsections, the relationship between C, $\dot{C}$, $\ddot{C}$ and the control value Ω will be defined.

5.1.1 Effect of Confidence on Control Value

It is logical that a robot's confidence should contribute to whether the robot should intervene in its human co-worker's actions. The component of the control value, $\omega_3(C)$ is a function of the average confidence of the robot ($\bar{C}$) in its human co-worker in a time horizon (t_H) where $\bar{C}$ is given by:

$$\bar{C} = \frac{1}{n_C} \sum_{i=1}^{n_C} C_i \tag{5.3}$$

where n_C is the number of confidence samples in a time horizon t_H.

When the human co-worker is in control during pHRC, if the robot has confidence in its human co-worker, the robot continues allowing the human to be in control in the pHRC. However, if the confidence of the robot in its human co-worker were to decrease, it is intuitive that the lower the confidence of the robot in its human co-worker, the more the robot wants to take the control of the pHRC away from its human co-worker. In the confidence-based role change method, Ω is increased when the robot's confidence in its human co-worker is high and Ω is decreased when the robot's confidence in its human co-worker is getting low. The proposed equation for the component

ω_3 which describes the effect of the robot's confidence in its human co-worker on the control value is given by:

$$\omega_3(C) = k_A(e^{k_B\bar{C}} - 1) - \omega_{3,max} \tag{5.4}$$

where k_A and k_B are constants and the component ω_3 is modeled within the range $-\omega_{3,max} \leq \omega_3 \leq \omega_{3,max}$. To solve for k_A and k_B, the following conditions should be considered:

$$\omega_3(C) = \begin{cases} 0 & \bar{C} = \bar{C}_{thresh} \\ \omega_{1,max} & \bar{C} = 1 \end{cases} \tag{5.5}$$

where $\bar{C} = \bar{C}_{thresh}$ represents a threshold in the robot's confidence in its human co-worker where the robot's confidence in its human co-worker does not increase or decrease the control value and $\omega_{1,max}$ is the maximum contribution for this component towards the control value. When $\bar{C} < \bar{C}_{thresh}$, the value of ω_3 will be negative which will decrease the control value Ω. This results in the robot becoming more inclined to take the control away from its human co-worker when $\bar{C}$ is lower.

When k_A and k_B can are calculated using (5.4) and (5.5), there are no solutions for k_A and k_B when $\bar{C}_{thresh} = 0$, $\bar{C}_{thresh} = 0.5$ and $\bar{C}_{thresh} = 1$. This divides the possible values for $\bar{C}_{thresh}$ into two ranges, $0 < \bar{C}_{thresh} < 0.5$ and $0.5 < \bar{C}_{thresh} < 1$. For higher values of $\bar{C}_{thresh}$ the robot is more likely to take the control away from its human co-worker during the pHRC, because ω_3 will become negative at a higher value of $\bar{C}$. Therefore, higher values of $\bar{C}_{thresh}$ would be more appropriate for pHRC where the robot's tolerance for poor performance is lower. This is because at a higher value of $\bar{C}_{thresh}$, a smaller decrease in $\bar{C}$ will result in a larger decrease in ω_3 and by extension Ω, making it more likely that the robot will initiate a role change.

Examples of pHRC applications and suggested values of $\bar{C}_{thresh}$ are shown in Table 5.1. To determine the value of $\bar{C}_{thresh}$ that is appropriate for a particular pHRC, factors such as the experience of the human co-worker, the purpose of the interaction and the safety of the human and the robot during the pHRC should be taken into account.

TABLE 5.1: Guidelines for selecting values for $\bar{C}_{thresh}$ based on the type of pHRC.

$\bar{C}_{thresh}$	Description
0.1 - 0.4	When the human co-worker is learning to use the robot in a controlled and safe environment. For these values of $\bar{C}_{thresh}$, the robot is very lenient towards the human and only takes control away from its human co-worker when its confidence in the human is very low. Even when control of the pHRC is taken away, it can be quickly regained if the robot's confidence in its human co-worker increases once more. $\bar{C}_{thresh} = 0.1$ is appropriate when the human co-worker is beginning to interact with the robot for the first time and $\bar{C}_{thresh} = 0.4$ would be used towards the end of the training stage.
0.6	For low risk pHRC such as teleoperation, where the robot and the human are not at risk. Generally used to gauge the performance of the human as the robot would only want to intervene in the pHRC when the human's performance in the task severely decreased.
0.7	Where the robot and human are interacting via direct physical contact should have a threshold of $\bar{C}_{thresh} \geq 0.7$. Working in close proximity with a robot always poses some level of risk to the human which cannot be mitigated. This would be appropriate for pHRC where the robot is only providing physical assistance to its human co-worker in a low risk pHRC.
0.8	At this level there is some risk to the safety of the human or robot, but it is not an immediate danger. This level would be appropriate for pHRC where both agents understand the risks involved and there are safety precautions such as automatic protective stops in place. An example of a pHRC which would use this value of $\bar{C}_{thresh}$ would be controlling a motorized device or vehicle in a cluttered environment.
0.9	Extremely high risk applications, where decreases in the human's performance and the robot's confidence in its human co-worker could have adverse effects on the safety of the human or the robot. For this value of $\bar{C}_{thresh}$, the value of ω_3 would become negative at higher values of $\bar{C}0$. An example of a pHRC where this threshold would be appropriate is when the human and the robot are working in close proximity of heavy machinery or sources of danger.

Taking into consideration the two value ranges for $\bar{C}_{thresh}$, it is reasonable for the higher range of values to be used in interactions where there robot would need to intervene quickly and for the lower range of values for interactions where the robot's intervention is not time sensitive. The higher the value of $\bar{C}_{thresh}$, the more likely it is that the robot will intervene. Interactions which require the robot to quickly intervene include but are not limited to:

- Interactions where the human is in contact with or in close proximity with the robot.
- Interactions where there are large safety risks such as heavy machinery, chemicals, heights or sharp objects.

- Interactions where small mistakes can have a large impact on the task outcomes.

Such interactions should be designated higher $\bar{C}_{thresh}$ values. On the other end of the spectrum, the lower range of $\bar{C}_{thresh}$ values are generally used for training or interactions where there is no risk to the human or the robot. This is because the lower the value of $\bar{C}_{thresh}$, the less likely the robot is to intervene in the interaction. The examples of pHRC in Table 5.1 generally follow this ideology.

The $\bar{C}_{thresh}$ values and their respective applications shown in Table 5.1 are presented as a general guideline. The appropriate value for $\bar{C}_{thresh}$ may differ from those shown in the table based on the specifics of the pHRC. In Chapter 4.3, three pHRC case studies were presented; collaborative grit-blasting, maneuvering an indoor environment and remote operation of a robotic arm's end effector in a complex simulated environment. Using the guidelines presented in Table 5.1, the value of $\bar{C}_{thresh}$ for the three case studies would be $\bar{C}_{thresh} = 0.7$, $\bar{C}_{thresh} = 0.8$, and $\bar{C}_{thresh} = 0.4$ for the grit-blasting, indoor maneuvering and remote operation respectively. Although robot used for the collaborative grit-blasting case study is relatively safe, the human co-worker is in close proximity with the robot which poses a risk to the human if the robot behaves unexpectedly. If this case study were to be performed in an industrial environment where abrasive material is passed through the nozzle on the robot end-effector, the value of $\bar{C}_{thresh}$ should be higher to reflect the increased risk to the human's safety. A value of $\bar{C}_{thresh} = 0.8$ would be suggested as the human would be wearing protective gear during the collaborative grit-blasting task and the robot has in-built fail-safes such as a 3 position switch.

Figure 5.1 shows examples of ω_3 where $\omega_{3,max} = 100$. From the figure, it can be seen that when $\bar{C}_{thresh}$ is small, $\bar{C}$ must be lower for ω_3 to be negative and the rate at which ω_3 decreases with respect to $\bar{C}$ is also decreased. The value of $\bar{C}_{thresh}$ can also be interpreted as the bias or the leniency of the robot where the robot is more forgiving towards the human for lower values of $\bar{C}_{thresh}$ and stricter for higher values of $\bar{C}_{thresh}$.

5.1.2 Effect of the First Derivative of Robot Confidence on Control Value

The second component of the control value $\omega_2(\dot{C})$, considers the effect of the average rate of change of the robot's confidence in its human co-worker on Ω in a time horizon t_H. The value of $\bar{\dot{C}}$ is given by:

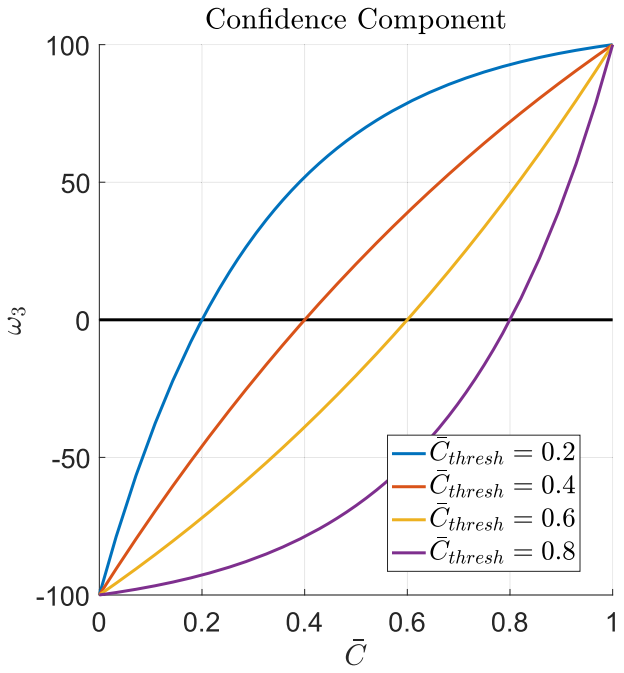

FIGURE 5.1: Examples of ω_3. Where $\omega_{3,max} = 100$, $\bar{C}_{thresh}$ is 0.2 (blue), 0.4 (red), 0.6 (yellow) and 0.8 (purple).

$$\dot{\bar{C}} = \frac{1}{n_C - 1} \sum_{j=2}^{j=n_C} \frac{C_j - C_{j-1}}{t_j - t_{j-1}} \tag{5.6}$$

where n_C is the number of confidence samples in a time horizon t_H and t_j is the time that sample C_j was recorded. Because the magnitude of $\dot{\bar{C}}$ is dependent on the rate at which the robot updates its confidence in its human co-worker, the maximum and minimum value of $\dot{C}$ will change based on the rate that the robot updates its confidence. In the robot confidence framework presented in Chapter 4, the confidence of the robot is defined to be within the range $0 \leq C \leq 1$. If the robot updates its confidence at a constant time interval t_{step}, then the maximum and minimum values of $\dot{\bar{C}}$ can be derived from (5.6).

Consider the robot's confidence in its human co-worker in a time horizon t_H, if the robot's confidence increases from the minimum value to the maximum value in a single time step t_{step}, rate of change in the robot's confidence would be given by:

$$\dot{C}_{max} = \frac{1}{t_{step}} \tag{5.7}$$

This represents the maximum value of $\dot{C}$. Once the robot's confidence reaches its maximum value the confidence of the robot cannot increase further. If the robot's confidence decreases in a subsequent time step during t_H then the value of $\bar{\dot{C}}$ will decrease. Therefore, the maximum value of $\bar{\dot{C}}$ for a time horizon will occur when the robot's confidence increases from the minimum value to the maximum value, without any decreases in the robot's confidence during t_H. This is given by:

$$\bar{\dot{C}}_{max} = \frac{1}{t_{step}(n_C - 1)} \tag{5.8}$$

where n_C is the number of confidence samples in t_H and the robot's confidence in its human co-worker remains at its maximum value for the rest of the time horizon t_H. A similar result can be derived for the minimum value of $\bar{\dot{C}}$.

$$\bar{\dot{C}}_{min} = \frac{-1}{t_{step}(n_C - 1)} \tag{5.9}$$

This results in the following range for $\bar{\dot{C}}$:

$$\frac{-1}{t_{step}(n_C - 1)} \leq \bar{\dot{C}} \leq \frac{1}{t_{step}(n_C - 1)} \tag{5.10}$$

where $\bar{\dot{C}}$ represents the trend of the robot's confidence during t_H. If $\bar{\dot{C}} > 0$ then the robot's confidence in its human co-worker has increased during t_H. $\bar{\dot{C}} < 0$ on the other hand, represents that the robot's confidence has decreased during t_H. If the robot's confidence has been decreasing, the robot is more inclined to take the control away from its human co-worker. On the other hand, if the robot's confidence increased during t_H, then the robot may not feel the need to take control. In the confidence-based role change method, this would be represented as $\omega_2 < 0$ for a decreasing confidence which would decrease the control value Ω, signifying the robot's desire to take the control of the interaction away from its human co-worker, and $\omega_2 > 0$ for an increasing confidence which would increase Ω, representing the robot's willingness to allow its human co-worker to remain in control. The component $\omega_2(\dot{C})$ considers the effect of $\bar{\dot{C}}$ on Ω and is modeled using the following sigmoid function:

$$\omega_2(\dot{C}) = \frac{2\omega_{2,max}}{1+e^{\beta\bar{\dot{C}}}} - \omega_{2,max} \tag{5.11}$$

where β is a constant and ω_2 is within the range $-\omega_{2,max} < \omega_2 < \omega_{2,max}$. The value of $\omega_{2,max}$ determines the maximum and minimum contribution of $\omega_2(\dot{C})$ to the control value Ω. If the values of $\omega_{3,max}$ and $\omega_{2,max}$ are different, then the weighting of each component will also be different when calculating the control value. The value of β determines the sensitivity of ω_2 to the changes in $\bar{\dot{C}}$ where $\beta < 0$.

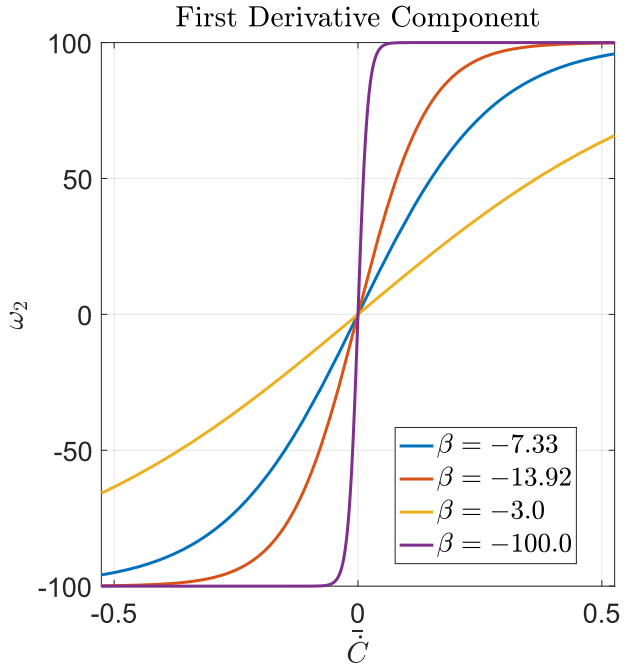

FIGURE 5.2: Examples of ω_2 where $\omega_{2,max} = 100$, $t_{step} = 100ms$, $n_C = 20$. The shape of the ω_2 plots are dependent on the value of β which are -7.33(blue), -13.92(red) -3.0(yellow) and -100.00(purple).

Figure 5.2 shows examples of $\omega_2(\dot{C})$. In the figure, the robot considers the average rate of change in its confidence during a time horizon of $t_H = 2$ seconds where the robot updates its confidence in its human co-worker at a rate of $t_{step} = 100ms$. The plots shown in the figure model the component $\omega_2(\dot{C})$ within the range $-100 \leq \omega_2(\dot{C}) \leq 100$. Under these conditions, the value of $\bar{\dot{C}}$ is within the approximate range $-0.53 \leq \bar{\dot{C}} \leq 0.53$. The figure shows a number of plots, each with different values of β. In the figure, the blue plot ($\beta = -7.33$) shows the relationship between $\omega_2(\dot{C})$ and $\bar{\dot{C}}$ where $\omega_2 = 0.95\omega_{2,max}$ when $\bar{\dot{C}} = 0.95\bar{\dot{C}}_{max}$ and the red plot ($\beta = -13.92$) shows the relationship where $\omega_2 = 0.95\omega_{2,max}$ when $\bar{\dot{C}} = 0.5\bar{\dot{C}}_{max}$. From the figure, it can be seen that when β is small,

a smaller change in $\bar{\dot{C}}$ results in larger changes in ω_2. The yellow ($\beta = -3.0$) and purple plots ($\beta = -100.0$) show relationships between of $\omega_2(\dot{C})$ and $\bar{\dot{C}}$ where ω_2 will not reach its maximum value during the interaction (because $-0.53 \leq \bar{\dot{C}} \leq 0.53$) and where ω_2 will approach $\omega_{2,max}$ when $\bar{\dot{C}}$ is small respectively.

5.1.3 Effect of the Second Derivative of Robot Confidence on Control Value

$\omega_1(\ddot{C})$ considers the average "acceleration" of the robot's confidence ($\bar{\ddot{C}}$) in a time horizon t_H. The value of $\bar{\ddot{C}}$ is defined as:

$$\bar{\ddot{C}} = \frac{1}{n_{\dot{C}} - 1} \sum_{k=2}^{k=n_{\dot{C}}} \frac{\dot{C}_k - \dot{C}_{k-1}}{t_k - t_{k-1}} \tag{5.12}$$

where $n_{\dot{C}}$ represents the number of $\dot{C}$ samples in a time horizon t_H and t_k represents the time at which the sample $\dot{C}_k$ was collected. Similar to $\bar{\dot{C}}$, the range of $\bar{\ddot{C}}$ is dependent on the rate at which the robot updates its confidence in its human co-worker. Assuming that the robot updates its confidence at a constant time interval t_{step} the maximum and minimum range of $\bar{\ddot{C}}$ for a time horizon t_H can be derived from (5.12).

Consider the confidence of the robot during a time horizon t_H. From (5.7), it is known that the maximum value for $\dot{C}$ is given by $\dot{C}_{max} = \frac{1}{t_{step}}$. The maximum value of $\ddot{C}$ occurs when $\dot{C}$ increases from its minimum value to its maximum value in one time step. This is represented as:

$$\bar{\ddot{C}}_{max} = \frac{\dot{C}_{max} - \dot{C}_{min}}{t_{step}} = \frac{2}{t_{step}^2} \tag{5.13}$$

where $\dot{C}_{min} = -\dot{C}_{max}$. For a positive value of $\ddot{C}$, there must be a positive net gain over two successive time steps. Therefore, the maximum average value for the second derivative of robot confidence in a time horizon t_H is given by:

$$\bar{\ddot{C}}_{max} = \frac{2}{t_{step}^2 (n_{\dot{C}} - 1)} \tag{5.14}$$

where $n_{\dot{C}}$ is the number of $\dot{C}$ samples in t_H. A similar approach can be used to derive the minimum value of $\ddot{\bar{C}}$ by considering the situation where $\dot{C}$ decreases from its maximum value to its minimum value in one time step:

$$\ddot{\bar{C}}_{min} = \frac{-2}{t_{step}^2(n_{\dot{C}} - 1)} \tag{5.15}$$

which results in the following range for $\ddot{\bar{C}}$:

$$\frac{-2}{t_{step}^2(n_{\dot{C}} - 1)} \leq \ddot{\bar{C}} \leq \frac{2}{t_{step}^2(n_{\dot{C}} - 1)} \tag{5.16}$$

The magnitude of $\ddot{\bar{C}}$ is a representation of the concavity of C. Positive values of $\ddot{\bar{C}}$ represent an increasing trend in $\dot{C}$ which suggests that the robot's confidence may be more likely to continue to increase. A negative value of $\ddot{\bar{C}}$ on the other hand represents a decreasing trend in $\dot{C}$, which suggests that the confidence of the robot in its human co-worker may decrease. Therefore, if $\ddot{\bar{C}}$ is positive, the value of Ω should increase and if $\ddot{\bar{C}}$ is negative, the value of Ω should decrease. ω_1 represents the effect of $\ddot{\bar{C}}$ on Ω, and can be given by:

$$\omega_1(\ddot{C}) = \frac{2\omega_{1,max}}{1 + e^{\alpha \ddot{\bar{C}}}} - \omega_{1,max} \tag{5.17}$$

where α is a constant and ω_1 is modeled within the range $-\omega_{1,max} < \omega_1 < \omega_{1,max}$. The value of $\omega_{1,max}$ determines the maximum and minimum contribution of ω_1 towards the control value Ω. α represents the sensitivity of ω_1 to the changes in $\ddot{\bar{C}}$ where $\alpha < 0$. Examples of ω_1 are shown in Figure 5.3.

For the example curves shown in the figure, the robot updates its confidence in its human co-worker at a rate of $t_{step} = 100ms$ in a time horizon of $t_H = 2$ seconds with the maximum value of $\omega_{1,max} = 100$. With these parameters, the equation (5.16) can be used to determine the range of $\ddot{\bar{C}}$ ($-11.11 \leq \ddot{\bar{C}} \leq 11.11$). In the figure, the blue plot ($\alpha = -0.366$) represents the relationship between ω_1 and $\ddot{\bar{C}}$ where $\omega_1 = 0.95\omega_{1,max}$ when $\ddot{\bar{C}} = 0.95\ddot{\bar{C}}_{max}$ and the red plot ($\alpha = -0.696$) represents the relationship between ω_1 and $\ddot{\bar{C}}$ where $\omega_1 = 0.95\omega_{1,max}$ when $\ddot{\bar{C}} = 0.5\ddot{\bar{C}}_{max}$. From the figure, it can be seen that when the value of α is small, smaller changes in $\ddot{\bar{C}}$ result in larger

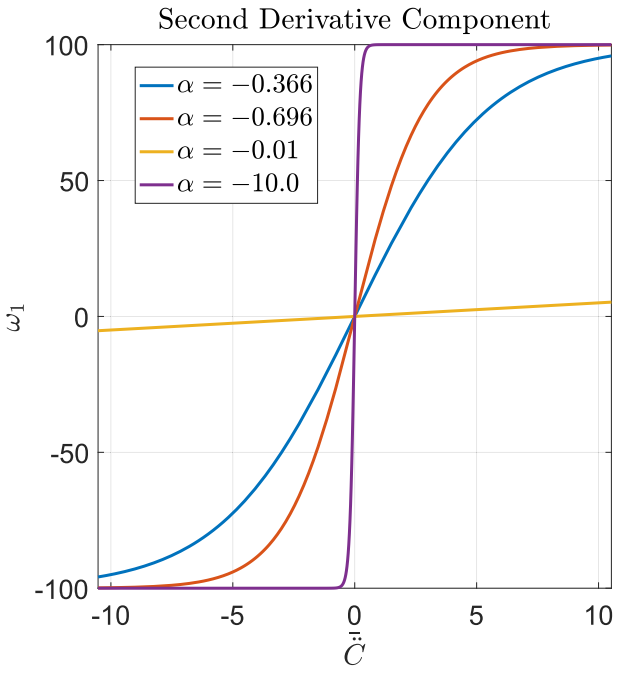

FIGURE 5.3: Examples of ω_1 where $\omega_{1,max} = 100$, $t_{step} = 100ms$, $n_{\dot{C}} = 19$. The shape of the ω_1 plots are dependent on the value of α which are -0.366(blue), -0.696(red) -0.01(yellow) and -10.00(purple).

changes in ω_1. The yellow ($\alpha = -0.01$) and purple plots ($\alpha = -10.0$) represent the relationships of between ω_1 and $\dddot{C}$ where ω_1 will not reach $\omega_{1,max}$ during the interaction (because $-11.11 \leq \dddot{C} \leq 11.11$) and where even a small value of $\dddot{C}$ will cause ω_1 to approach $\omega_{1,max}$ respectively.

5.2 Experiments

To verify the confidence-based role change method, two experiments were conducted using the Assistance-as-Needed-roBOT (ANBOT) described in Section 4.3.1. In the experiments, the robot monitors the performance of its human co-worker as the human uses the ANBOT to move the blasting point along the paths shown in Figure 5.4.

Figure 5.4a shows the experimental setup where the human co-worker moves the ANBOT using the handlebars to conduct a grit-blasting task on the wall. No abrasive material was passed through the nozzle of the ANBOT as the experiments were performed in the lab. Instead, a laser pointer was used to simulate the blasting point on the wall and provide the human co-worker with visual feedback of their accuracy and performance during the grit-blasting task. The task being performed

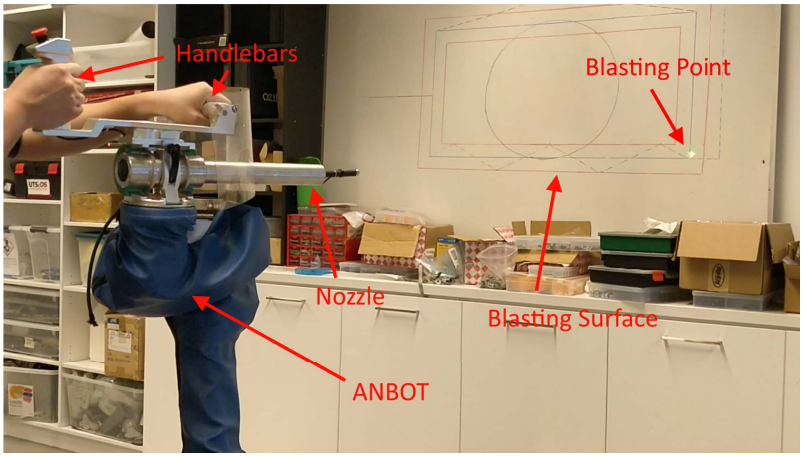

(a)

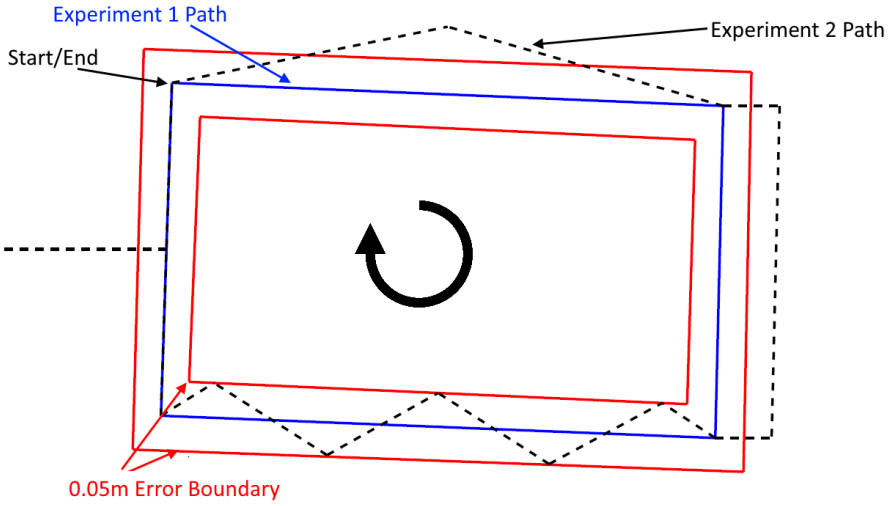

(b)

FIGURE 5.4: (a) The experimental setup where human co-worker uses the ANBOT to complete a collaborative grit-blasting task. (b) The paths on the wall that the human follows using the blasting point projected by a laser pointer mounted on the ANBOT. The human co-worker follows the blue path in the first experiment and the dashed black line in the second experiment.

by the human in the experiments is to follow the paths shown in Figure 5.4b. The human co-worker begins the grit-blasting task in the top left corner and follows the path in a clockwise direction. The task ends when the blasting point on the wall returns to the starting point.

In Experiment 1, the human uses the blasting point to follow the blue path shown in Figure 5.4b. The blue path is a 1x0.5m rectangle and the red lines shown in the figure are spaced 0.05m on either side of the blue path. In this experiment, the robot expects the blasting point to be within the 0.05m error boundary represented by the red lines. As the human co-worker is expected to move the blasting point along the blue path within the error boundary, the robot should not initiate

a role change during this experiment. However, if the blasting point moves outside of the error boundaries, the robot should take the control away from its human co-worker.

In Experiment 2, the human uses the blasting point to follow the dashed black path shown in Figure 5.4b. Like in Experiment 1, the robot expects the human to be following the blue path and remain within the error boundary during Experiment 2. As following the black path will move the blasting point outside of the error boundaries, the robot should initiate a role change and take control away from its human co-worker during Experiment 2.

In the experiments, the robot confidence framework presented in Chapter 4 is used to quantify the robot's confidence in its human co-worker. Although the task components presented in Section 4.3.1 for the ANBOT can also be incorporated into the robot confidence framework used in the experiments, to reduce the experimental variables, only the blasting path accuracy in the grit-blasting task will be used as a task component.

The blasting path accuracy task component is represented as a critical component where $\phi_{a,c}$ represents the robot's perception of its human co-worker's performance in the blasting path accuracy task component. The robot's perception of the human's performance in the blasting path accuracy task component is calculated using one penalty and one reward. The penalty $P_a(a)$ is given by:

$$P_a(a) = \frac{0.2}{1 + e^{-117.778(a-0.075)}} \tag{5.18}$$

where a is the distance (in meters) between the blasting point and the blue path. Because the robot expects its human co-worker to be following the blue path in both Experiment 1 and Experiment 2, the penalty $P_a(a)$ decreases the robot's perception of the human's performance in the blasting path accuracy task component when the blasting point deviates from the blue path. The penalty function was designed such that half the maximum penalty is incurred when the blasting point is $0.075m$ away from the blue path and the maximum penalty is incurred when the blasting point is $0.1m$ from the blue path. As the maximum penalty is 0.2, it would take approximately 0.5 seconds for the fluid place $\phi_{a,c}$ to empty if it was originally full as the robot updates its observations in its human co-worker's actions every $100ms$. The reward R_a is given by:

$$R_a = 0.02 \tag{5.19}$$

By having a constant reward that is much smaller than the maximum penalty, a Slow Positive/Fast Negative dynamic [185] is created. This requires the human co-worker to perform well for a longer period of time to make up for any losses in the robot's perception of the human's performance which emulates the wariness of the robot. In the experiments, good performance is defined as having the blasting point within the error boundary. When the blasting point is within the error boundary, the robot's perception of its human co-worker's performance will increase as $R_a > P_a(a)$ when $a < 0.05$. The plots for the reward and penalty in the blasting path accuracy task component are shown in Figure 5.5.

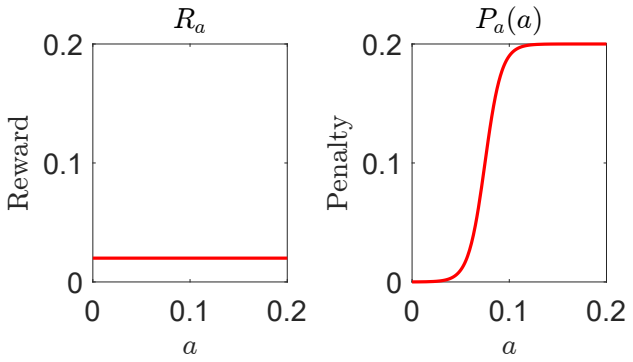

FIGURE 5.5: Graphs representing the functions for the reward R_a and the penalty $P_a(a)$ for the blasting path accuracy task component.

The change in the robot's perception of its human co-worker's performance in the blasting path accuracy task component at each time step is given by:

$$\frac{d\phi_{a,c}}{dt} = B_m B_b \cdot 0.02 - B_m B_b \cdot \frac{0.2}{1 + e^{-117.778(a-0.075)}} \tag{5.20}$$

where B_b and B_m represent the state of the switches on the front and back handlebars of the ANBOT seen in Figure 5.4a respectively. A binary representation is used where 1 represents a pressed state (enabled) and 0 represents a released state (disabled). As no abrasive material is passed through the nozzle during the grit-blasting task, B_b represents the human's intention to blast. B_m on the other hand allows the human co-worker to control the ANBOT when pressed. The robot's perception of the human's performance in the blasting path accuracy task component will only change when both B_b and B_m are pressed. The robot's perception of the human's performance in the blasting path accuracy task component is updated at each time step based on the following rules:

$$\phi_{a,c} = \begin{cases} \phi_{a,0} & t = 0 \\ \phi_{a,c} + \frac{d\phi_{a,c}}{dt} & t > 0 \end{cases} \tag{5.21}$$

where $\phi_{a,0} = 1$ to represent the robot initially having confidence in its human co-worker's ability to perform well in this task component. Because the human's performance in the task component is modeled within the bounds $0 \leq \phi_{a,c} \leq 1$, when the robot updates its perception of the human's performance in the task component, if $\phi_{a,c} > 1$ then $\phi_{a,c} = 1$ and if $\phi_{a,c} < 0$ then $\phi_{a,c} = 0$.

The confidence of the robot in its human co-worker can be derived from (4.5). Because there is only one critical task component and no non-critical components being considered in this experiment, the equation for the robot's confidence is given by:

$$C_4 = \phi_{a,c} \tag{5.22}$$

Once the robot's confidence in the human is calculated, the values of $\bar{C}$, $\dot{\bar{C}}$ and $\ddot{\bar{C}}$ can be obtained using (5.3), (5.6) and (5.12) respectively. In both experiments, the ANBOT updates its confidence in the human at a rate of $100ms$ and considers a time horizon of $t_H = 2$ seconds. The chosen values for $\omega_{1,max}$, $\omega_{2,max}$ and $\omega_{3,max}$ are:

$$\omega_{1,max} = \omega_{2,max} = \omega_{3,max} = 100 \tag{5.23}$$

These values were chosen so that the weighting of each of the components would be equal when calculating Ω. The values $\bar{C}_{thresh} = 0.7$, $\beta = -7.33$ and $\alpha = -0.366$ were chosen for the experiments which results in the following equation for the control value:

$$\frac{200}{1 + e^{-0.366\ddot{\bar{C}}}} + \frac{200}{1 + e^{-7.33\dot{\bar{C}}}} + 39.56(e^{1.801\bar{C}} - 1) - 300 = \Omega \tag{5.24}$$

If the value of Ω becomes negative during the experiments, it signifies that the robot wants to take control of the interaction.

5.3 Experimental Results

In this section, results from experiments where a human performed a collaborative grit-blasting task using the ANBOT are presented. Although no abrasive material was released when B_b was pressed, the human co-worker was given visual feedback of their performance during the experiments through a laser pointer mounted onto the nozzle of the ANBOT which showed the current blasting point on the wall. The colored regions marked$A$, B, C and D in Figure 5.7, Figure 5.8, Figure 5.10, Figure 5.11 and Figure 5.13 represent the presence of the blasting point in the four regions of the blasting path: Section 1 (green), Section 2 (red), Section 3 (blue) and Section 4 (purple) respectively as depicted in Figure 5.6 and Figure 5.9.

5.3.1 Experiment 1 Results

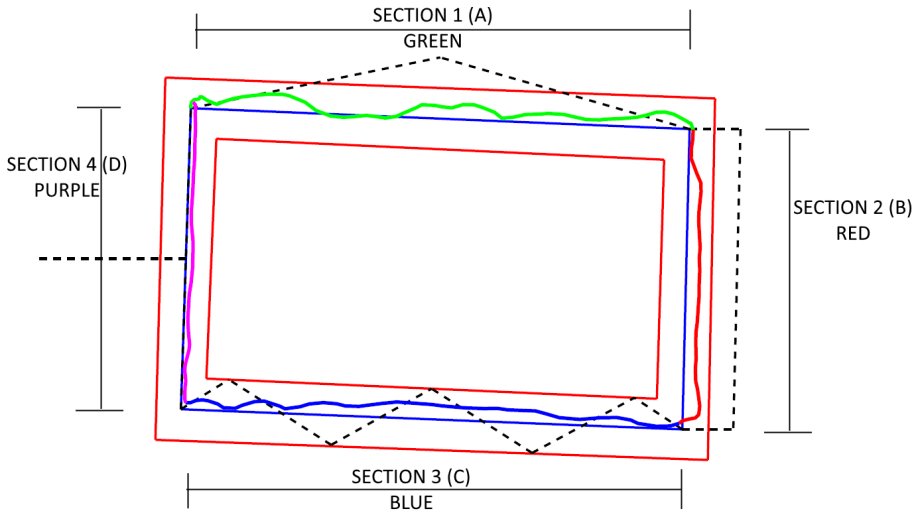

FIGURE 5.6: One example result from Experiment 1 where the human followed the blue path using the ANBOT. The actual blasting path of the human on the wall during the experiment is shown in green, red, blue, purple for Section 1, Section 2, Section 3 and Section 4 respectively.

The human's actual blasting path during Experiment 1 is depicted in Figure 5.6 where the actual blasting path is green, red, blue, purple for Section 1, Section 2, Section 3 and Section 4 respectively. The distance between the blasting point and the blue path during Experiment 1 can be seen in the top graph of Figure 5.7.

The robot's observations of the human's actions during the experiment can be seen in the top graph of Figure 5.7. The graph shows the distance between the blasting point and the blue path during the

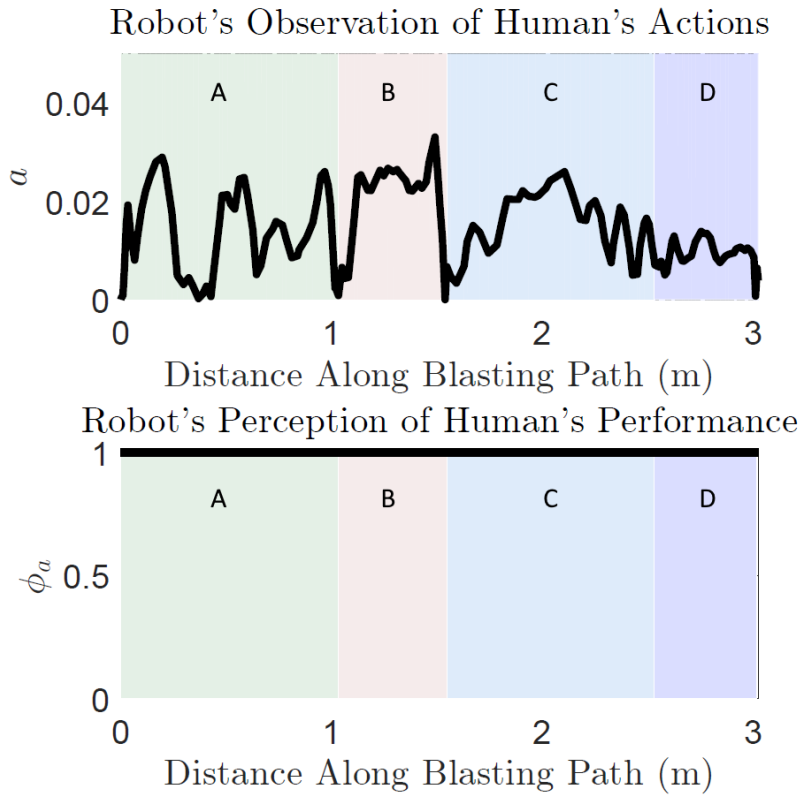

FIGURE 5.7: The distance between the blasting point and the blue path (top) and the robot's perception of the human's performance in the blasting path accuracy task component (bottom) during Experiment 1. The colored regions shown in the graphs represent the time when B_b is pressed and the blasting point was in Section 1 (green), Section 2 (red), Section 3 (blue) and Section 4 (purple) of the blasting path.

experiment as the human completed the collaborative grit-blasting task. The blasting path started from the top right corner and was broken into four sections; top (green), right (red), bottom (blue) and left (purple). From the figure, it can be seen that although the blasting point deviates from the blue path during the experiment, the blasting point is generally within $0.03m$ of the blue path which is within the error boundary of $0.05m$. The robot's perception of the human's performance in the blasting path accuracy task component during the experiment, shown in the bottom graph of Figure 5.7, is calculated using (5.21). Because the blasting point remained within the error boundary during Experiment 1, the robot's perception of its human co-worker's performance did not decrease during the experiment.

As the robot's perception of the human's performance maintained its maximum value, the robot's confidence in its human co-worker also remained at its maximum value. The graphs for Ω, $\bar{C}$, $\dot{\bar{C}}$ and $\ddot{\bar{C}}$ in Experiment 1 can be seen in Figure 5.8. Because the robot's confidence in the subject

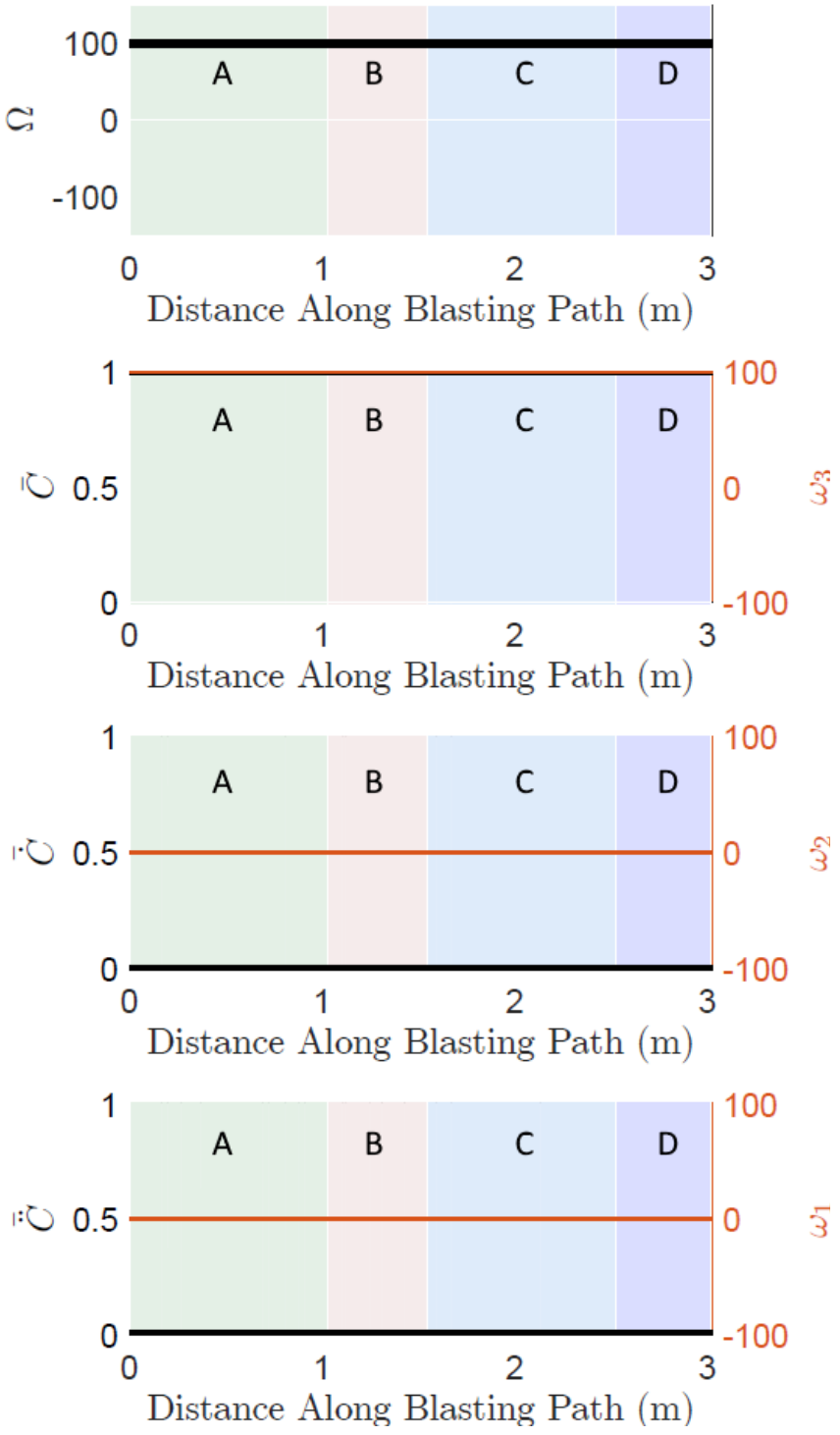

FIGURE 5.8: An example result for Experiment 1 derived from the human's actual blasting path in Figure 5.6 and the robot's perception of the human's performance in Figure 5.7. From top to bottom: The control value Ω, $\ddot{\bar{C}}$ and ω_1, $\dot{\bar{C}}$ and ω_2, $\bar{C}$ and ω_3. The regions shown in the graphs represent the time when B_b is pressed and the blasting point was in Section 1 (green), Section 2 (red), Section 3 (blue) and Section 4 (purple) of the blasting path.

did not change throughout the pHRC, the values of $\dot{\bar{C}}$ and $\ddot{\bar{C}}$ are zero during the experiment. The control value Ω in this experiment also remains constant and is always positive. This indicates that the robot did not feel the need to initiate a role change during the experiment.

5.3.2 Experiment 2

In Experiment 2, the human co-worker followed the path represented by the dashed black line in Figure 5.4b. The black path was designed to verify the confidence-based role change method by artificially inducing what the robot would perceive as poor performance. This is because when the human follows the black path, the blasting point moves outside of the error boundary.

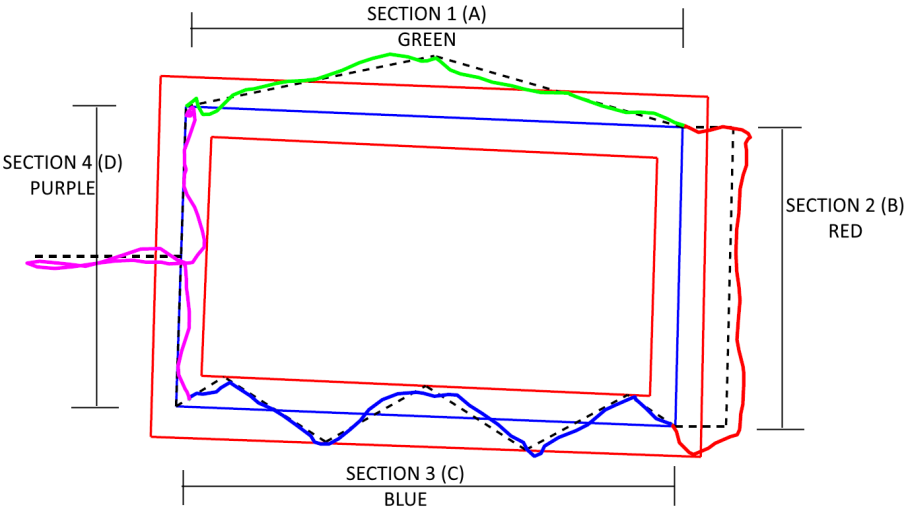

FIGURE 5.9: One example result from Experiment 2 where the human co-worker followed the dashed black path using the ANBOT. The actual blasting path of the human on the wall during Experiment 2 is shown in green, red, blue, purple for Section 1, Section 2, Section 3 and Section 4 respectively.

In Experiment 2, the path that the human is following is longer than the path in Experiment 1 as the black path deviates significantly from the blue path. The length of the black path used in Experiment 2 is approximately $3.88m$. The actual blasting path of the human co-worker from Experiment 2 is shown in Figure 5.9 is approximately $4.14m$ where the green, red, blue, purple portions of the blasting path represent position of the blasting point in Section 1, Section 2, Section 3 and Section 4 respectively. The distance between the blasting point and the blue path during Experiment 2 is shown in the top graph of Figure 5.10. The red horizontal line in the graph represents

the 0.05m error boundary. When the distance between the blasting point and the blue path exceeds the error boundary, the robot's perception of its human co-worker's performance decreases. The robot's perception of its human co-worker's performance in the blasting path accuracy task component during Experiment 2 is shown in the bottom graph of Figure 5.10.

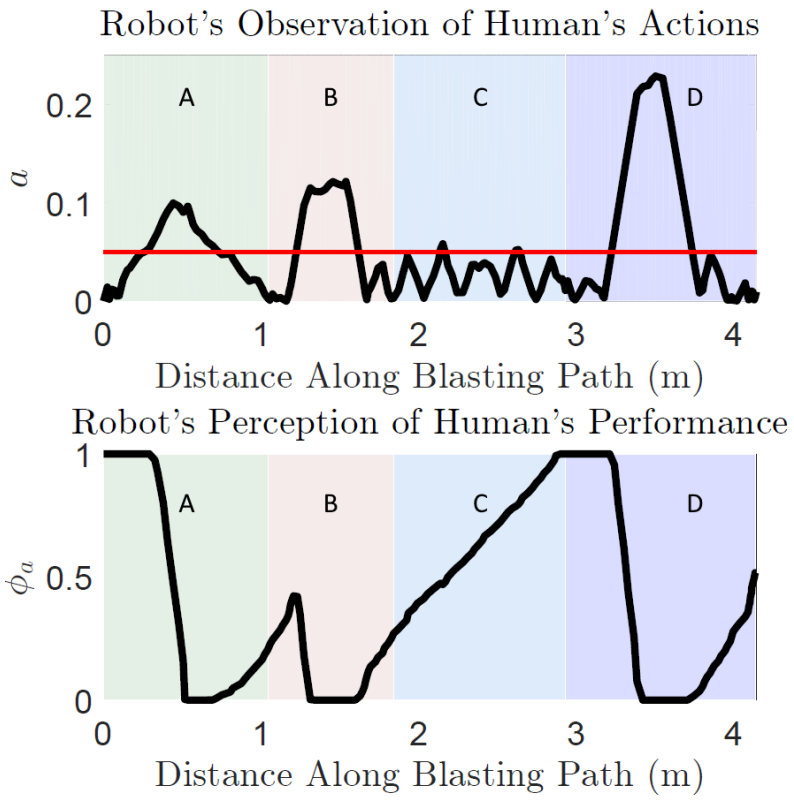

FIGURE 5.10: The distance between the blasting point and the blue path (top) and the robot's perception of the human's performance in the blasting path accuracy task component (bottom) during Experiment 2. The red horizontal line in the top graph represents the error boundary. The colored regions represent when B_b is pressed and the blasting point is in Section 1 (green), Section 2 (red), Section 3 (blue) and Section 4 (purple) of the blasting path.

From the graph it can be seen that the robot's perception in its human co-worker's performance decreases to its minimum value in Section 1 (green), Section 2 (red) and Section 4 (purple). In these sections, the robot's perception of the human's performance decreases as the blasting point deviates from the blue path and increases when the human moves the blasting point closer to the blue path. In Section 3, although the blasting point deviated from the blue path, because the blasting point remained within the error boundary, the robot's perception of the human's performance did not decrease. There were two instances in Section 3 where the blasting point moved outside the error boundary; however, the robot's perception of the human's performance did not decrease

significantly as the blasting point quickly returned inside the error boundary and the loss in the robot's perception in the human's performance was replenished by the reward function R_a.

Using robot's perception of the human's performance in Experiment 2, the values for $\bar{C}$, $\dot{\bar{C}}$ and $\ddot{\bar{C}}$ were calculated. The results of the confidence-based role change method are shown in Figure 5.11. Although the robot did not take control away from its human co-worker during the collaborative grit-blasting operation in Experiment 2, the robot's response to its human co-worker's performance during the pHRC can be derived by examining the value of Ω during the interaction. From the figure, it can be seen that the robot would have initiated a role change in Section 1, taking the control away from its human co-worker when Ω became negative. Then as distance between the actual blasting path and the blue path in Section 1 decreased, the robot's confidence in its human co-worker increased. Although the value of Ω approached zero, the robot did not return control to its human co-worker during Section 1 as value of Ω remained negative. If the value of R_a was higher, or $\bar{C}_{thresh}$ was lower, then the control may have been returned, but that would have also affected when the robot initiated the first role change to take the control away from its human co-worker. The robot would have remained in control until Section 3, where it would return the control to the human when Ω became positive. In Section 4, the decrease the robots confidence would have resulted in the robot initiating another role change and take control of the interaction once again only returning control just before the collaborative grit-blasting task ended.

In Figure 5.12, a graphical representation of when the robot would have initiated role changes during the pHRC is shown. The red circles correspond to the points in the interaction where the robot would take the control away from its human co-worker and the blue circles represent points in the interaction where the robot would have given the human the control. Figure 5.13 shows the distance between the blasting point and the blue path and Ω during the experiment. The role changes which are represented by the vertical red and blue lines for taking away control and giving control respectively. From the figures, it can be seen that even though there is a large deviation between the blasting point and the blue path, the robot would give control back to the human in Section 3. This is because when modeling the human's performance in the blasting path accuracy task component, an error margin of $0.05m$ was defined. Therefore, even though there is a deviation in the human's blasting path, it is still within the robot's expectations for the task. If the error boundary were to be changed to a smaller value, the points in the interaction where the robot would initiate a role change during the interaction would also change. The robot's confidence would

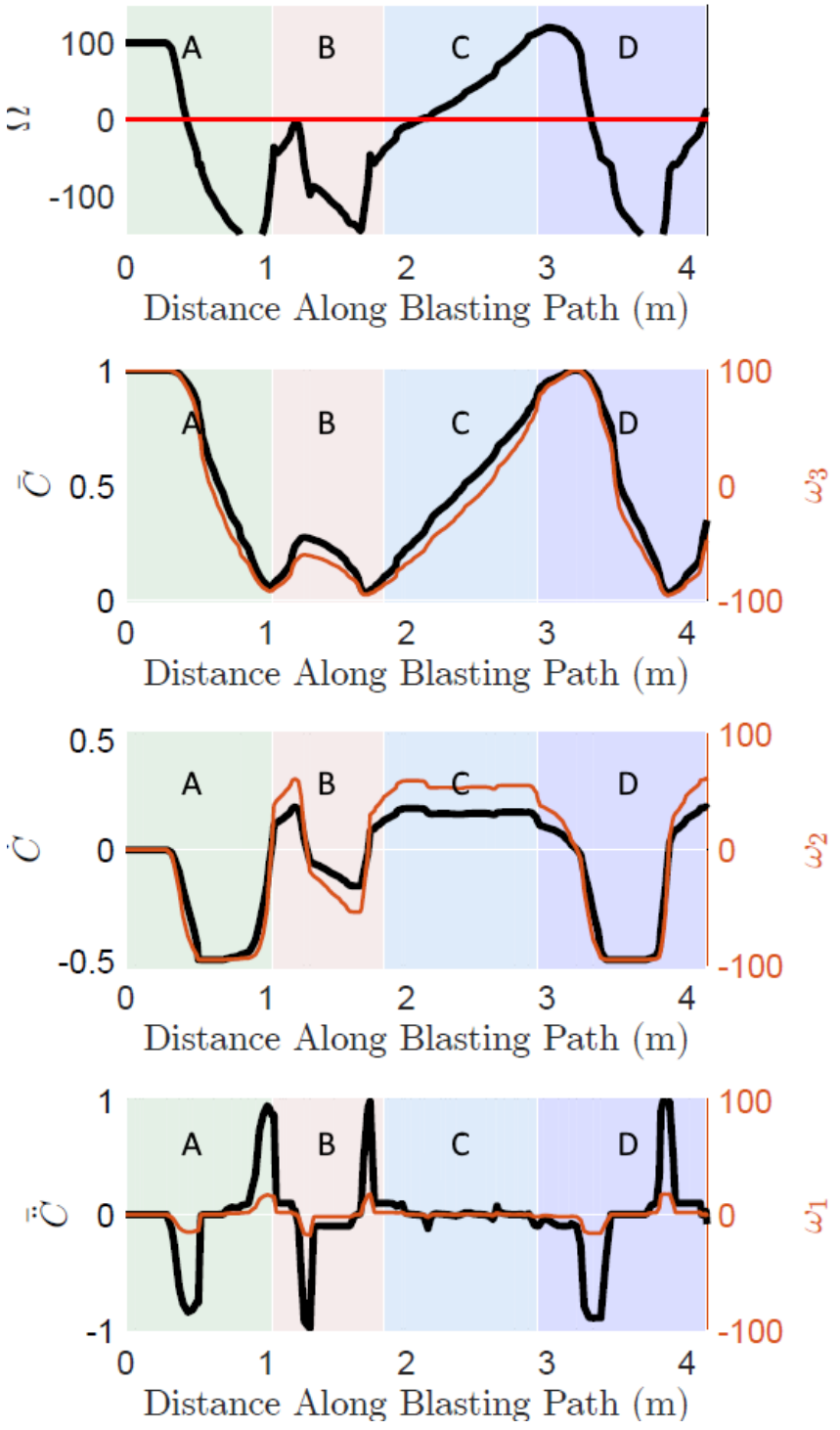

FIGURE 5.11: Example result from Experiment 2 based on the human's blasting path in Figure 5.9 and the human's performance in Figure 5.10. From top to bottom: The control value Ω, $\ddot{\bar{C}}$ and ω_1, $\dot{\bar{C}}$ and ω_2, $\bar{C}$ and ω_3. The regions shown in the graphs represent the time when B_b is pressed and the blasting point was in Section 1 (green), Section 2 (red), Section 3 (blue) and Section 4 (purple) of the blasting path.

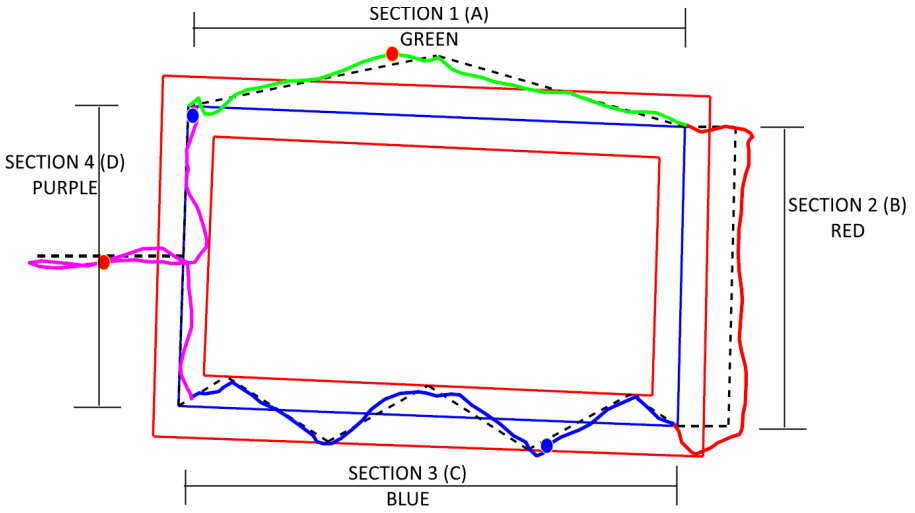

FIGURE 5.12: The points during Experiment 2 where the robot would have initiated a role change based on the control value Ω. The actual blasting path of the human during the experiment is shown in green, red, blue, purple for Section 1, Section 2, Section 3 and Section 4 respectively, and the points where a role change would have occurred are represented as red (robot takes the control away from the human) and blue (robot gives the control to the human) circles.

decrease at smaller values of a and robot's perception of the human's performance in Section 3 would decrease rather than increase.

It can also be seen from the figures that the robot's decision of whether it should initiate a role change is not an instantaneous process and does not occur immediately after the blasting point leaves the error boundary. This is the result of factors such as the selected values for $\bar{C}_{thresh}$ and the maximum penalty at each time step. A higher value of $\bar{C}_{thresh}$ would have resulted in $\omega_3(C)$ becoming negative at a higher value of $\bar{C}$ while a higher maximum penalty would have resulted in ω_1, ω_2 and ω_3 decreasing the value of Ω much more quickly when the blasting path of the human crosses the error boundary.

With the same confidence measurements, it is possible for the role change to occur sooner or later by changing the parameters of the three components of Ω. The values of $\omega_{1,max}$, $\omega_{2,max}$, $\omega_{3,max}$, α, β and $\bar{C}_{thresh}$ heavily influence the conditions under which the robot would initiate a role change. How an event should be interpreted and the appropriate action to take will vary from pHRC to pHRC. Therefore, the confidence-based role change method presented in this chapter offers a lot of flexibility in its implementation.

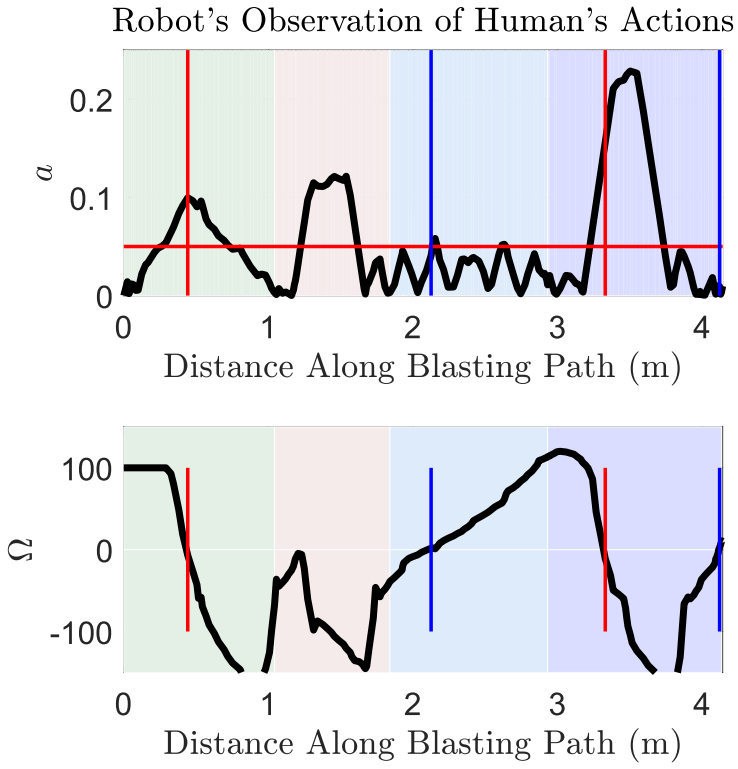

FIGURE 5.13: Graphs showing the distance between the blasting point and the blue path (top) and Ω (bottom) during Experiment 2. The red horizontal line represents the error boundary. The points where the robot would have initiated a role change during the experiment (see also Figure 5.12) are represented as red (robot takes the control away from the human) and blue (robot gives the control to the human) vertical lines.

5.4 Discussion

In the previous section, an example of how the confidence-based role change method could be applied to an interaction was shown. In the experiment, the robot confidence model used one task component (accuracy) to demonstrate when the robot would intervene in the human's actions during the interaction. One of the strengths of the robot confidence framework and confidence based role change method is how they can be adapted to any pHRC. As long as there is a relationship between the robot's observations of the human and the robot's expectations of the task, any number of performance measures could be used to calculate the robot's confidence in the human. In an industrial setting, more aspects of the interaction such as the force applied by the human, the manipulability of the robot and the efficiency of the human operator would be modeled and the human's performance in each aspect or component of the interaction would be taken into account

when determining the robot's confidence.

To simplify the robot confidence framework for the experiment, only the accuracy of the human was considered as a task component. Normally, the operator force would be selected as a task component due to the physical contact between the human and robot. However, the purpose of the task was for the human to follow the paths as accurately as possible. Therefore, the human's blasting accuracy was selected as the task component as it best represents the human's overall performance in this case study. It is proposed that it may be more beneficial to select a number of focused task components that are representative of the robot's perception of the human's performance in the task rather than defining too many task components.

If there are too many task components contributing to the confidence measurement, it can result in undesired behavior if the robot confidence framework is ill-defined. If there are too many critical components, it is possible for the robot's confidence to be extremely sensitive to changes in the task as the robot's confidence would fluctuate if human's performance in a large number of critical components were to increase or decrease by small amounts. On the other hand, if there were too many non-critical components, the effect of each component on the robot's overall confidence in its human co-worker would be negligible as its individual weighting would be too low. Both scenarios do not reflect how the confidence of a human or robot should change over the course of an interaction.

In regards to the robot initiating a role change during the interaction, the robot's own ability to complete the task is not taken into consideration in the robot confidence framework or the confidence-based role change method. The robot's decision to intervene is based on its confidence which is dependant on its observations of the human's actions and its knowledge of the task, not its ability to perform the task. The intervention of the robot does not necessarily have to involve the robot taking over the task from the human. For example, the robot could also stop the interaction to advise its human co-worker on how their performance can be improved or call for a supervisor to troubleshoot any problems the robot cannot handle. The robot's ability to perform the task should be taken into account after the robot has intervened to take the control of the interaction away from the human. The robot's ability to perform the task should determine how the robot would react after gaining control of the system. This aspect of the interaction is outside the scope of this thesis.

5.5 Summary

In this chapter, a confidence-based role change method for pHRC was presented. This method uses the robot's confidence in its human co-worker to determine whether the robot should initiate a role change during pHRC and take the control away from its human co-worker. The method considers the effects of the robot's confidence and the first and second derivatives of the robot's confidence in its human co-worker to determine whether a role change should be initiated.

This method was verified using two experiments involving a collaborative grit-blasting robot. The robot observed the actions of its human co-worker during the experiments to determine whether it should initiate a role change and take the control away from the the human. Using its confidence in its human co-worker, the robot was able to identify the human co-worker's poor performance and identify logical points where it should initiate a role change during the pHRC.

Chapter 6

Conclusion

This thesis aimed at addressing three research challenges in physical Human-Robot Collaboration (pHRC) including: robot perception of the human co-worker's intention during pHRC, modeling of the robot's confidence in its human co-worker and how a robot would decide whether and when it should intervene (by taking control) in its human co-worker's actions during pHRC. This Chapter summarizes the research outcomes and discusses the limitations and future works.

6.1 Summary of Contributions

6.1.1 A Method for Identifying the Human Hand Orientation when grasping a handlebar

A method for identifying the orientation of a human operator's hand around a cylindrical handlebar during pHRC was developed. The grasping pattern of the human hand was obtained using the Thrumode Matrix Array Sensor (TMMAS) that was wrapped around a cylindrical handlebar. Using the grasping patterns, the human's hand orientation around the handlebar was identified using Support Vector Machine (SVM) and Bayesian Inference. Principal Component Analysis (PCA) was also implemented to reduce the number of inputs for the classifiers. Two experiments were conducted to verify the effectiveness of the method. In the first experiment, the data obtained was from the same subjects but different experiments. In the second experiment, the subject's hand

orientation was classified using data from other subjects. The results of the experiments showed that the grasping pattern of the human operator can be used to identify the orientation of their hand around a cylindrical handlebar. The SVM classifier had a higher accuracy when identifying the hand orientation and this difference in accuracy became more pronounced when PCA was applied to the grasping patterns.

6.1.2 A Method for Detecting the Human's Reaction to Unexpected Events During pHRC

A method for detecting human co-worker's reaction to unexpected events during pHRC was developed. The grasping strength of the human hand during pHRC was recorded using the TMMAS that was wrapped around a cylindrical handlebar. The handlebar was attached to an upper limb exoskeleton. The exoskeleton measures the forces applied by the human hand to the handlebar through a load cell. Two experiments were conducted to observe differences in the human's grasping strength when the human initiates changes in the task and when the robot behaves unexpectedly. In the experiments, the subjects followed a predefined path using a laser pointer mounted to the exoskeleton. In the first experiment, the robot applied a large force in the direction perpendicular to the path at random intervals to disrupt the task. In the second experiment, there were two separate paths that the subjects could follow and the subjects may move between the two paths during the pHRC. The results of the experiments showed that the subjects instinctively increased their grasping strength when the robot behaved unexpectedly. The grasping force measured by the TMMAS would increase before the force detected by the load cell. Furthermore, when the subject initiated the change in the task, the grasping force of the subject increased after the forces were detected by the load cell.

6.1.3 A Framework for Modeling a Robot's Confidence in its Human Co-worker during pHRC

A robot confidence framework was developed for quantifying the robot's confidence in its human co-worker during pHRC. In the performance model, a pHRC task is decomposed into task components which represent different aspects of the task from which the robot can observe the actions

of its human co-worker. A Fluid Stochastic Petri Net (FSPN) model is used to model the robot's perception of its human co-worker's performance. A series of reward and penalty functions are used to calculate the robot's perception of the human co-worker's performance in the task component. A confidence model is developed to calculate the robot's confidence in the human by utilizing the robot's perception of the human's performance in the task components. The robot confidence framework was verified using three pHRC case studies where the human and robot worked collaboratively to complete a task. In each case study, the pHRC was decomposed into task components and the robot calculated its perception of the human's performance based on its observations of the human's actions. The robot then used the human's performance to calculate the robot confidence in its human co-worker in real-time. The results of the case studies showed that the robot's confidence in its human co-worker changed intuitively, increasing and decreasing as the human performed well or poorly respectively.

6.1.4 A Robot Confidence-Based Role Change Method

A method for using the robot's confidence in its human co-worker to determine whether the robot should initiate a role change was presented. The confidence-based role change method considers the robot's confidence, the first derivative and the second derivative of the robot's confidence over a time horizon to determine whether the robot should intervene in its human co-worker's actions. This role change model was verified using two experiments where the human and robot worked collaboratively to follow a path. In the first experiment, the human co-worker tried to follow a path marked on the wall. In the second experiment, the human followed a different path which deviated from the expected path. Using the robot confidence framework, the robot's confidence in its human co-worker was calculated during the experiments. The robot then used the confidence-based role change method to successfully identify points where it would be appropriate for the robot to initiate a role change.

6.2 Discussion and Limitations

The work presented in this thesis was designed to improve the robot's understanding of its human co-workers during pHRC and to determine whether the robot should initiate a role change during

pHRC. The crux of the research lies in the robot's ability to observe and interpret the human's actions and intentions in the context of the interaction. There are a number of limitations which must be considered when implementing the work presented in this thesis. This section discusses the limitations in the use of the human's grasping information during pHRC, robot confidence framework and the confidence-based role change method.

6.2.1 Grasp Sensor Integration

In this thesis, the TMMAS was wrapped around a cylindrical handlebar to obtain the human hand's grasping information. This approach poses some practical limitations when applied outside of a lab environment. One of the limitations is that in pHRC, the handlebar may not always be cylindrical. Non-cylindrical handlebars tend to be common in applications where the human and the robot are expected to interact for extended periods of time. These interactions often use a more ergonomic handlebar [192, 193]. Although the polyurethane layer covering the TMMAS could be molded into a more ergonomic shape, most ergonomic handlebars do not allow the human co-worker to grasp comfortably in a large range of orientations due to the shape of the handlebar [194, 195]. This undermines the practical applicability of the hand orientation classification method for a subset of pHRC.

6.2.2 Observability of the Human's Actions and Performance

The performance model used in the robot confidence framework relies on the robot being able to observe the actions of its human co-worker during the pHRC. A limitation of the performance model is that it cannot measure the performance of the human in task components which it cannot observe. If the robot cannot observe the actions of the human in a task component, its perception of its human co-worker's performance in the task component will not change. Although this dynamic is intuitive and is in line with the definition of confidence used in this thesis, it prevents the robot confidence framework from incorporating factors which the robot does not have sensors for. Therefore, the assumption is that the robot has the capability to observe its human co-worker's performance. This needs to be considered when decomposing a pHRC task into task components as well.

6.2.3 Subjectivity of the models for Performance and Confidence measurement

The confidence-based role change method is task/application dependent or subjective; from the model of the human co-worker's performance to the robot's confidence model and to the decision on whether the robot should intervene in the pHRC. In any Human-Human Interaction (HHI), the perception and decision of whether to intervene during an interaction are also task and human dependent. A human's decision of whether to intervene in their co-worker's actions is the result of the cumulation of their experience and knowledge. The confidence-based role change was designed to replicate the role change dynamic seen in HHI from a robot's perspective. The parameters used in the confidence-based role change method inevitably have bias when implemented.

The bias in the performance model can be offset by taking into account safety standards and protocols when designing the rewards and penalties in task components [196]. This has the effect of making the robot's measure of confidence in its human co-worker more objective. However, the rate of increase and decrease of the robot's perception of the human's performance is left to the discretion of the integrator. This is also true for whether a task component is categorized as a critical or non-critical component and the relative weighting of the non-critical components. These decisions are left to the integrator as each pHRC differs and the task components, rewards, penalties and definition of the task components are task specific.

The presented method can be adapted to suit the needs of individual pHRC. The sensitivity of the performance model, confidence model and control value presented in this thesis are fully adjustable so that the robot's intervention during pHRC can be more nuanced.

6.3 Future Work

6.3.1 Incorporating Hand Grasping Information to improve the Robot's Model of the Human during pHRC

Using the TMMAS or possibly an array of individual sensors such as the takktile [197] to record the grasping pattern of the handlebar could prove to be a viable replacement for a load cell in pHRC. A load cell can only measure the net forces and torques applied to the handlebar by the

human co-worker. By detracting the grasping force on the handlebar from the human's grasping pattern, it is possible to determine both the magnitude and the direction of the forces applied by the human on the handlebar by implementing the method proposed by Wu [162]. Other works have also shown that it is possible to measure the sheer forces using an array of sensors such as the takktile sensors, which could be used to estimate the torque applied by the handlebar [198].

Furthermore, because the grasping pattern of the human hand can be obtained, the force applied by different parts of the hand can be obtained. It would be possible to develop a model which can determine not only the orientation of the human hand, but also the contact points of each part of the hand using the distribution of forces during grasping, pulling and pushing actions on the handlebar [149, 199]. If the entire hand can be mapped, then the human's hand size can be inferred using biomechanical models of the human hand [150, 200, 201]. From these models, the size of the human hand can also be used to estimate the height of the human [202, 203] which could be used in conjunction with musculoskeletal models of the human body for pose and strength predictions during pHRC.

Finally, the incorporation of the human's grasping information such as their hand orientation and their grasping strength also needs to be investigated. In this thesis, the robots presented in the case studies were not equipped with the TMMAS sensor which was used in Chapter 3 to obtain the human's grasping information. Therefore, it was not able to be incorporated into the robot confidence frameworks in Chapters 4 and 5 as task components to measure the human's performance during the interactions.

6.3.2 Discussion on the Robot Confidence Framework

In this work, a robot confidence framework for quantifying the robot's confidence in its human co-worker was proposed as well as a method for using the robot's confidence to initiate a role change during an interaction. Case studies and experiments were presented which verified the usefulness of the robot confidence framework and the confidence-based role change method, however, a more rigorous statistical analysis is required. Exploration into the degree to which the implementation of the robot confidence method and the confidence-based role change method improve the performance of the human, the efficiency of the task and the safety of the interaction need to be considered across a range of different pHRC scenarios. It would be interesting to generate a robot

confidence framework using a subset of subjects and use the generated framework to measure the robots confidence in another subset of subjects to observe how the robots confidence changes from subject to subject.

6.3.3 Confidence-Based Role Change in non-physical Human-Robot Interaction (HRI)

The confidence-based role change method presented in this work focused specifically on the robot intervening in the human co-worker's actions during pHRC based on its perception of the human's performance.

Expanding the scope of this research to include non-physical interaction information can improve the performance model used in the robot confidence framework. As more task components or aspects of the interaction are taken into account, a more complete model can be obtained.

For example, including cognitive, social or cultural factors which may influence the human's actions or the robot's perception of the human's performance in a task would add additional context to the robot's decision of whether it should intervene in the human's actions. Some of these factors may not be observable during an interaction or be difficult to model. Many of these factors cannot currently be measured or quantified through sensor-based observation. Even if it is possible to measure in a lab, it may not be possible in industrial applications.

6.3.4 Confidence-Based Role Change Method for Sliding Autonomy

In the confidence-based role change method presented in this thesis, a control value was used to initiate an instant role change. One future work is to explore whether the role change method can also be applied in sliding autonomy where the control of the pHRC is gradually transfered between the human and robot.

In the confidence-based role change method presented in this thesis, positive and negative values of the control value represent a human controlled interaction and a robot controlled interaction respectively. The work in this thesis focuses on role change from the robot's perspective. When the robot initiates a role change, the human co-worker becomes aware of the robot's decision only

after the intervention has occurred. If the robot's confidence in its human co-worker decreases, it would be helpful if the human could get feedback such as encountering resistance in their control of the robot.

6.3.5 Human Confidence-Based Role Change in pHRC

Although the confidence-based role change method was designed for the robot to determine whether the robot should initiate a role change, whether this method can be used to model the human co-worker's decision during pHRC would also be interesting to explore. If a method for modeling the human's confidence in its robot co-worker is developed, then the human's confidence in its robot co-worker can be used as an input for the confidence-based role change method. If the robot's confidence is used by the method to determine whether the robot should take control of the interaction, then the human's confidence would be used to determine whether the robot should relinquish its control (i.e. human takes control).

6.3.6 Negotiation of Control and Role Change in pHRC

The confidence-based role change method presented in this thesis is for the robot to decide whether and when to initiate a role change during pHRC. Like HHI, any role change should ideally be negotiated between the human and the robot. Many factors need to be considered in this negotiation including the robot's desire for role change, the human's desire for role change, the resistance of the robot and the human to role change and the confidence of the robot and the human. Game theory may prove a useful method for the negotiation [204–207]. Part of the future work is to investigate how game theory can be applied for role change negotiation in pHRC.

Appendix A

Hand Orientation Identification Complete Results

In this appendix, the full results from the experiments performed in Section 3.2 are shown. In the experiments, the

A.1 Scenario 1

TABLE A.1: Complete results for Scenario 1 using the SVM classifier without PCA from Section 3.2.

Scenario 1 - SVM without PCA				
Training Data	**Test Data**	**Exact Accuracy**	**Within 1 Accuracy**	**Time (ms)**
LF-S1	LR-S1	76.25%	100.00%	0.31
LF-S2	LR-S2	82.58%	100.00%	0.37
LF-S3	LR-S3	79.28%	99.58%	0.27
LF-S4	LR-S4	91.95%	98.55%	0.29
LF-S5	LR-S5	84.52%	96.07%	0.33
LF-S6	LR-S6	59.27%	90.43%	0.37
LF-S7	LR-S7	69.00%	85.00%	0.30
LF-S8	LR-S8	60.88%	97.83%	0.30
LF-S9	LR-S9	35.03%	88.75%	0.39
LF-S10	LR-S10	59.52%	81.72%	0.31
Average Values		**69.83%**	**93.79%**	**0.32**
Standard Deviation		**16.69%**	**6.79%**	**0.04**

TABLE A.2: Complete results for Scenario 1 using the SVM classifier with PCA from Section 3.2.

Scenario 1 - SVM with PCA				
Training Data	**Test Data**	**Exact Accuracy**	**Within 1 Accuracy**	**Time (ms)**
LF-S1	LR-S1	76.92%	100.00%	0.05
LF-S2	LR-S2	83.03%	100.00%	0.05
LF-S3	LR-S3	79.07%	99.55%	0.04
LF-S4	LR-S4	91.23%	98.68%	0.05
LF-S5	LR-S5	85.27%	96.18%	0.05
LF-S6	LR-S6	58.87%	90.35%	0.05
LF-S7	LR-S7	70.57%	84.95%	0.05
LF-S8	LR-S8	59.33%	95.78%	0.05
LF-S9	LR-S9	35.63%	88.83%	0.06
LF-S10	LR-S10	60.72%	82.40%	0.05
Average Values		**70.06%**	**93.67%**	**0.05**
Standard Deviation		**16.63%**	**6.57%**	**0.005**

TABLE A.3: Complete results for Scenario 1 using the Bayesian Inference classifier without PCA from Section 3.2.

Scenario 1 - Bayesian Inference without PCA				
Training Data	**Test Data**	**Exact Accuracy**	**Within 1 Accuracy**	**Time (ms)**
LF-S1	LR-S1	68.47%	95.17%	0.89
LF-S2	LR-S2	68.55%	91.20%	0.83
LF-S3	LR-S3	78.25%	95.53%	0.72
LF-S4	LR-S4	71.38%	95.02%	0.71
LF-S5	LR-S5	32.28%	56.30%	0.76
LF-S6	LR-S6	44.42%	77.03%	0.77
LF-S7	LR-S7	33.98%	58.00%	0.74
LF-S8	LR-S8	45.55%	84.90%	0.78
LF-S9	LR-S9	30.30%	73.65%	0.86
LF-S10	LR-S10	22.42%	46.67%	0.78
Average Values		**49.56%**	**77.35%**	**0.78**
Standard Deviation		**20.30%**	**18.20%**	**0.06**

TABLE A.4: Complete results for Scenario 1 using the Bayesian Inference classifier with PCA from Section 3.2.

Scenario 1 - Bayesian Inference with PCA				
Training Data	**Test Data**	**Exact Accuracy**	**Within 1 Accuracy**	**Time (ms)**
LF-S2345678910	LR-S1	63.53%	85.03%	0.14
LF-S1345678910	LR-S2	46.60%	60.73%	0.12
LF-S1245678910	LR-S3	55.70%	74.00%	0.15
LF-S1235678910	LR-S4	74.82%	95.50%	0.17
LF-S1234678910	LR-S5	41.65%	69.00%	0.12
LF-S1234578910	LR-S6	36.87%	61.13%	0.17
LF-S1234568910	LR-S7	38.50%	44.95%	0.17
LF-S1234567910	LR-S8	47.93%	65.82%	0.14
LF-S1234567810	LR-S9	29.23%	61.40%	0.18
LF-S123456789	LR-S10	45.57%	60.47%	0.15
Average Values		**48.04%**	**67.80%**	**0.15**
Standard Deviation		**13.48%**	**14.22%**	**0.02**

A.2 Scenario 2

TABLE A.5: Complete results for Scenario 2 using the SVM classifier without PCA from Section 3.2.

Scenario 2 - SVM without PCA				
Training Data	**Test Data**	**Exact Accuracy**	**Within 1 Accuracy**	**Time (ms)**
LF-S2345678910	LR-S1	64.92%	90.22%	1.65
LF-S1345678910	LR-S2	68.82%	96.83%	1.56
LF-S1245678910	LR-S3	82.62%	96.15%	1.53
LF-S1235678910	LR-S4	66.57%	83.68%	1.43
LF-S1234678910	LR-S5	79.08%	92.58%	1.47
LF-S1234578910	LR-S6	55.15%	94.10%	1.45
LF-S1234568910	LR-S7	50.43%	67.93%	1.45
LF-S1234567910	LR-S8	54.97%	92.83%	1.49
LF-S1234567810	LR-S9	34.38%	82.27%	1.42
LF-S123456789	LR-S10	63.02%	94.67%	1.47
Average Values		**62.00%**	**89.13%**	**1.49**
Standard Deviation		**14.01%**	**8.93%**	**0.07**

TABLE A.6: Complete results for Scenario 2 using the SVM classifier with PCA from Section 3.2.

Scenario 2 - SVM with PCA				
Training Data	**Test Data**	**Exact Accuracy**	**Within 1 Accuracy**	**Time (ms)**
LF-S2345678910	LR-S1	65.10%	90.67%	0.40
LF-S1345678910	LR-S2	67.90%	96.90%	0.38
LF-S1245678910	LR-S3	79.18%	95.47%	0.42
LF-S1235678910	LR-S4	67.07%	82.02%	0.40
LF-S1234678910	LR-S5	76.33%	89.93%	0.35
LF-S1234578910	LR-S6	55.58%	94.32%	0.34
LF-S1234568910	LR-S7	53.20%	70.08%	0.35
LF-S1234567910	LR-S8	51.90%	92.32%	0.36
LF-S1234567810	LR-S9	38.42%	83.55%	0.35
LF-S123456789	LR-S10	62.08%	96.85%	0.35
Average Values		**61.68%**	**89.21%**	**0.37**
Standard Deviation		**12.23%**	**8.46%**	**0.03**

TABLE A.7: Complete results for Scenario 2 using the Bayesian Inference classifier without PCA from Section 3.2.

Scenario 2 - Bayesian Inference without PCA				
Training Data	**Test Data**	**Exact Accuracy**	**Within 1 Accuracy**	**Time (ms)**
LF-S2345678910	LR-S1	35.37%	61.57%	1.65
LF-S1345678910	LR-S2	49.18%	75.97%	1.62
LF-S1245678910	LR-S3	42.37%	78.77%	1.49
LF-S1235678910	LR-S4	31.42%	58.18%	1.41
LF-S1234678910	LR-S5	36.65%	58.70%	1.41
LF-S1234578910	LR-S6	29.17%	81.37%	1.34
LF-S1234568910	LR-S7	28.50%	41.28%	1.37
LF-S1234567910	LR-S8	29.30%	69.20%	1.36
LF-S1234567810	LR-S9	24.28%	50.62%	1.40
LF-S123456789	LR-S10	29.00%	62.20%	1.39
Average Values		**33.52%**	**63.79%**	**1.44**
Standard Deviation		**7.52%**	**12.72%**	**0.11**

TABLE A.8: Complete results for Scenario 2 using the Bayesian Inference classifier with PCA from Section 3.2.

Scenario 2 - Bayesian Inference without PCA				
Training Data	**Test Data**	**Exact Accuracy**	**Within 1 Accuracy**	**Time (ms)**
LF-S2345678910	LR-S1	10.37%	21.62%	0.27
LF-S1345678910	LR-S2	8.50%	34.05%	0.29
LF-S1245678910	LR-S3	9.80%	20.97%	0.27
LF-S1235678910	LR-S4	2.83%	12.15%	0.27
LF-S1234678910	LR-S5	9.42%	24.83%	0.24
LF-S1234578910	LR-S6	3.42%	15.87%	0.24
LF-S1234568910	LR-S7	8.02%	15.97%	0.25
LF-S1234567910	LR-S8	8.22%	25.72%	0.26
LF-S1234567810	LR-S9	5.10%	12.37%	0.25
LF-S123456789	LR-S10	10.25%	18.08%	0.28
Average Values		**7.59%**	**20.16%**	**0.26**
Standard Deviation		**2.80%**	**6.78%**	**0.02**

Bibliography

[1] A. Ajoudani. Human-Robot Interfaces and physical Interaction, 2016. URL https://goo.gl/dWD8EA.

[2] T. Lee. Robotic Exoskeleton Lets Workers Lift Heavy Objects Effortlessly, 2014. URL https://goo.gl/5PPbmT.

[3] F. Bimmer. Rise of the robots, 2014. URL https://goo.gl/VNcWLm.

[4] HumaRobotics. Cobot Sawyer - Interaction homme robot, 2016. URL https://goo.gl/v6zZfk.

[5] Australian Government. Intergenerational Report 2007 (the second intergenerational report). Technical report, Treasury, 2007. URL https://goo.gl/XZphft.

[6] F. Maggi, D. Quarta, M. Pogliani, M. Polino, A. M. Zanchettin, S. Zanero, and P. Di Milano. Rogue Robots: Testing the Limits of an Industrial Robot's Security. Technical report, Trend Micro, Politecnico di Milano, 2017. URL https://documents.trendmicro.com/assets/wp/wp-industrial-robot-security.pdf.

[7] G. Nichols. Robots are coming to work. Are they safe?, 2017. URL https://goo.gl/sNaNho.

[8] UTS:NEWSROOM. Robotics lab promises a new world for people with disabilities, 2011. URL https://goo.gl/nehcHV.

[9] Burke Neurological Institute. ARMEO®SPRING by Hocoma, 2018. URL https://goo.gl/hJt4Wo.

[10] P. A. Hancock, D. R. Billings, K. E. Schaefer, J. Y. C. Chen, E. J. de Visser, and R. Parasuraman. A Meta-Analysis of Factors Affecting Trust in Human-Robot Interaction. *Human Factors*, 53(5):517–527, 10 2011. ISSN 0018-7208. doi: 10.1177/0018720811417254.

[11] K. E. Schaefer. Measuring Trust in Human Robot Interactions: Development of the Trust Perception Scale-HRI. In *Robust Intelligence and Trust in Autonomous Systems*, pages 191–218. Springer US, Boston, MA, 2016. ISBN 9781489976680. doi: 10.1007/978-1-4899-7668-0_10.

[12] J. Lee and N. Moray. Trust, Control Strategies and Allocation of Function in Human-Machine Systems. *Ergonomics*, 35(March):1243–1270, 1992. ISSN 0014-0139. doi: 10.1080/00140139208967392.

[13] J. M. Beer, S. Carolina, A. D. Fisk, and W. A. Rogers. Toward a Framework for Levels of Robot Autonomy in Human - Robot Interaction. *Journal of Human-Robot Interaction*, 3 (2):74–99, 2014. doi: 10.5898/JHRI.3.2.Beer.

[14] F. Flemisch, M. Heesen, T. Hesse, J. Kelsch, A. Schieben, and J. Beller. Towards a dynamic balance between humans and automation: authority, ability, responsibility and control in shared and cooperative control situations. *Cognition, Technology & Work*, 14(1):3–18, 11 2011. ISSN 1435-5558. doi: 10.1007/s10111-011-0191-6.

[15] S. O. Oguz, A. Kucukyilmaz, T. M. Sezgin, and C. Basdogan. Haptic negotiation and role exchange for collaboration in virtual environments. In *2010 IEEE Haptics Symposium*, pages 371–378. IEEE, 3 2010. ISBN 978-1-4244-6821-8. doi: 10.1109/HAPTIC.2010.5444628.

[16] F. O. Flemisch, K. Bengler, H. Bubb, H. Winner, and R. Bruder. Towards cooperative guidance and control of highly automated vehicles: H-Mode and Conduct-by-Wire. *Ergonomics*, 57(3):343–60, 3 2014. ISSN 1366-5847. doi: 10.1080/00140139.2013.869355.

[17] S. M. Rahman, Y. Wang, I. D. Walker, L. Mears, R. Pak, and S. Remy. Trust-based compliant robot-human handovers of payloads in collaborative assembly in flexible manufacturing. In *IEEE International Conference on Automation Science and Engineering*, volume 2016-Novem, pages 355–360. IEEE, 8 2016. ISBN 9781509024094. doi: 10.1109/COASE.2016.7743428.

[18] A. Tran, D. Liu, R. Ranasinghe, and M. Carmichael. Identifying Human Hand Orientation around a Cylindrical Handlebar for physical Human-Robot Interaction. In *IEEE International Symposium on Robotics*, pages 427–434, 2018.

[19] A. Tran, D. Liu, R. Ranasinghe, M. Carmichael, and C. Liu. Analysis of Human Grip Strength in Physical Human Robot Interaction. In *International Conference on Applied Human Factors and Ergonomics*, volume 3, pages 1442–1449. Elsevier B.V., 2015. doi: 10.1016/j.promfg.2015.07.320.

[20] A. Tran, D. Liu, R. Ranasinghe, and M. Carmichael. A Method for Quantifying a Robots Confidence in its Human Co-worker in Human-Robot Cooperative Grit-Blasting. In *IEEE International Symposium on Robotics*, pages 474–481, 2018. ISBN 9783800746996.

[21] B. Vanderborght, R. Van Ham, D. Lefeber, T. G. Sugar, and K. W. Hollander. Comparison of Mechanical Design and Energy Consumption of Adaptable, Passive-compliant Actuators. *The International Journal of Robotics Research*, 28(1):90–103, 1 2009. ISSN 0278-3649. doi: 10.1177/0278364908095333.

[22] N. Elkmann, M. Fritzsche, and E. Schulenburg. Tactile Sensing for Safe Physical Human-Robot Interaction. In *International Conference on Advances in Computer-Human Interactions*, pages 212–217, 2011. ISBN 9781612081175.

[23] J. Drury, J. Scholtz, and H. Yanco. Awareness in human-robot interactions. In *IEEE International Conference on Systems, Man and Cybernetics*, pages 912–918, 2003. ISBN 0-7803-7952-7. doi: 10.1109/ICSMC.2003.1243931.

[24] B. Lacevic, P. Rocco, and A. M. Zanchettin. Safety assessment and control of robotic manipulators using danger field. *IEEE Transactions on Robotics*, 29(5):1257–1270, 2013. ISSN 15523098. doi: 10.1109/TRO.2013.2271097.

[25] A. De Luca and F. Flacco. Integrated control for pHRI: Collision avoidance, detection, reaction and collaboration. In *IEEE International Conference on Biomedical Robotics and Biomechatronics*, pages 288–295. IEEE, 6 2012. ISBN 978-1-4577-1200-5. doi: 10.1109/BioRob.2012.6290917.

[26] P. A. Lasota, T. Fong, and J. A. Shah. A Survey of Methods for Safe Human-Robot Interaction. *Foundations and Trends in Robotics*, 5(3):261–349, 2017. ISSN 1935-8253. doi: 10.1561/2300000052.

[27] Investing Answers. Industrial Goods Sector, 2018. URL `https://goo.gl/Lk4Adp`.

[28] D. K. Liu, G. Dissayanake, P. B. Manamperi, P. a. Brooks, G. Fang, G. Paul, S. Webb, N. Kirchner, P. Chotiprayanakul, N. M. Kwok, and T. R. Ren. A Robotic System for Steel Bridge Maintenance: Research Challenges and System Design. In *Australasian Conference on Robotics and Automation*, pages 1–7, 2008. ISBN 9780646506432.

[29] G. Paul, S. Webb, D. Liu, and G. Dissanayake. Autonomous robot manipulator-based exploration and mapping system for bridge maintenance. *Robotics and Autonomous Systems*, 59(7-8):543–554, 2011. ISSN 09218890. doi: 10.1016/j.robot.2011.04.001.

[30] B. Sadrfaridpour, H. Saeidi, and Y. Wang. An integrated framework for human-robot collaborative assembly in hybrid manufacturing cells. In *2016 IEEE International Conference on Automation Science and Engineering (CASE)*, pages 462–467. IEEE, 8 2016. ISBN 978-1-5090-2409-4. doi: 10.1109/COASE.2016.7743441.

[31] Investing Answers. Healthcare Sector, 2018. URL `https://goo.gl/3mwzko`.

[32] Australian Bureau of Statistics. Population by Age and Sex, Regions of Australia, 2016. URL `https://goo.gl/Rcce2N`.

[33] Australian Government. Australia to 2050: future challenges. Technical report, Treasury, 2010. URL `https://goo.gl/CT3qgp`.

[34] A. Freedy, E. DeVisser, G. Weltman, and N. Coeyman. Measurement of trust in human-robot collaboration. In *IEEE International Symposium on Collaborative Technologies and Systems*, pages 106–114. IEEE, 5 2007. ISBN 0978569911. doi: 10.1109/CTS.2007.4621745.

[35] B. M. Muir and N. Moray. Trust in automation. Part II. Experimental studies of trust and human intervention in a process control simulation. *Ergonomics*, 39(3):429–460, 3 1996. ISSN 0014-0139. doi: 10.1080/00140139608964474.

[36] B. D. Adams. Trust vs. Confidence. Technical report, Humansystems Incorporated, Toronto, 2005. URL `https://goo.gl/vzcxdV`.

[37] H. Ding, M. Schipper, and B. Matthias. Collaborative behavior design of industrial robots for multiple human-robot collaboration. In *IEEE International Symposium on Robotics*, pages 1–6. IEEE, 10 2013. ISBN 978-1-4799-1173-8. doi: 10.1109/ISR.2013.6695707.

[38] L. Dantanarayana, R. Ranasinghe, A. Tran, A. Liu, and G. Dissanayake. A Novel Collaboratively Designed Robot to Assist Carers. In *International Conference on Social Robotics*, pages 105–114, 2014. ISBN 9783319119724. doi: 10.1007/978-3-319-11973-1_11.

[39] S. Sakai, M. Iida, and M. Umeda. Heavy material handling manipulator for agricultural robot. In *IEEE International Conference on Robotics and Automation*, pages 1062–1068. IEEE, 2002. ISBN 0-7803-7272-7. doi: 10.1109/ROBOT.2002.1013496.

[40] H. M. Do, C. Park, and J. H. Kyung. Dual arm robot for packaging and assembling of IT products. *IEEE International Conference on Automation Science and Engineering*, pages 1067–1070, 2012. ISSN 21618070. doi: 10.1109/CoASE.2012.6386417.

[41] A. Bicchi, M. Bavaro, G. Boccadamo, D. De Carli, R. Filippini, G. Grioli, M. Piccigallo, A. Rosi, R. Schiavi, Soumen Sen, and G. Tonietti. Physical human-robot interaction: Dependability, safety, and performance. In *IEEE International Workshop on Advanced Motion Control*, pages 9–14. IEEE, 3 2008. ISBN 978-1-4244-1702-5. doi: 10.1109/AMC.2008.4516033.

[42] L. O'Sullivan, R. Nugent, and J. van der Vorm. Standards for the Safety of Exoskeletons Used by Industrial Workers Performing Manual Handling Activities: A Contribution from the Robo-Mate Project to their Future Development. *Procedia Manufacturing*, 3:1418–1425, 2015. ISSN 23519789. doi: 10.1016/j.promfg.2015.07.306.

[43] T. Brogårdh. Present and future robot control development - An industrial perspective. *Annual Reviews in Control*, 31(1):69–79, 1 2007. ISSN 1367-5788. doi: 10.1016/J.ARCONTROL.2007.01.002.

[44] J. Fryman and B. Matthias. Safety of Industrial Robots: From Conventional to Collaborative Applications. In *ROBOTIK*, pages 51–55, 2012. ISBN 9783800734184.

[45] M. Vasic and A. Billard. Safety issues in human-robot interactions. In *IEEE International Conference on Robotics and Automation*, pages 197–204. IEEE, 5 2013. ISBN 978-1-4673-5643-5. doi: 10.1109/ICRA.2013.6630576.

[46] G. Tonietti and A. Bicchi. Adaptive simultaneous position and stiffness control for a soft robot arm. In *IEEE International Conference on Intelligent Robots and Systems*, pages 1992–1997. IEEE, 2002. ISBN 0-7803-7398-7. doi: 10.1109/IRDS.2002.1044048.

[47] A. Bicchi and G. Tonietti. Fast and "soft-arm" tactics. *IEEE Robotics and Automation Magazine*, 11(2):22–33, 6 2004. ISSN 10709932. doi: 10.1109/MRA.2004.1310939.

[48] A. Albu-Schaffer, O. Eiberger, M. Grebenstein, S. Haddadin, C. Ott, T. Wimböck, S. Wolf, and G. Hirzinger. Soft robotics. *IEEE Robotics and Automation Magazine*, 15(3):20–30, 9 2008. ISSN 10709932. doi: 10.1109/MRA.2008.927979.

[49] R. Bischoff, J. Kurth, G. Schreiber, R. Koeppe, A. Albu-Schaffer, A.-D. Beyer, O. Eiberger, S. Haddadin, G. Stemmer, Andreas Grunwald, and Others. The KUKA-DLR Lightweight Robot arm-a new reference platform for robotics research and manufacturing. In *IEEE International Symposium on Robotics*, pages 1–8, 2010. ISBN 978-3-8007-3273-9. doi: 10.1108/01439910710774386.

[50] E. Cheung and V. Lumelsky. A sensitive skin system for motion control of robot arm manipulators. *Robotics and Autonomous Systems*, 10(1):9–32, 1 1992. ISSN 09218890. doi: 10.1016/0921-8890(92)90012-N.

[51] K. Kosuge, H. Takeuchi, and K. Furuta. Motion Control of a Robot Arm Joint Torque Sensor. *IEEE Transactions on Robotics and Automation*, 6(2):258–263, 4 1990. ISSN 1042296X. doi: 10.1109/70.54743.

[52] R. Woodman, A. F. Winfield, C. Harper, and M. Fraser. Building safer robots: Safety driven control. *The International Journal of Robotics Research*, 31(13):1603–1626, 11 2012. ISSN 0278-3649. doi: 10.1177/0278364912459665.

[53] D. Ebert and D. Henrich. Safe human-robot-cooperation: image-based collision detection for industrial robots. In *IEEE International Conference on Intelligent Robots and System*, volume 2, pages 1826–1831. IEEE, 2002. ISBN 0-7803-7398-7. doi: 10.1109/IRDS.2002.1044021.

[54] P. A. Lasota, G. F. Rossano, and J. A. Shah. Toward safe close-proximity human-robot interaction with standard industrial robots. In *IEEE International Conference on Automation Science and Engineering*, pages 339–344. IEEE, 8 2014. ISBN 978-1-4799-5283-0. doi: 10.1109/CoASE.2014.6899348.

[55] Y.-H. Weng, C.-H. Chen, and C.-T. Sun. Toward the HumanRobot Co-Existence Society: On Safety Intelligence for Next Generation Robots. *International Journal of Social Robotics*, 1(4):267–282, 11 2009. ISSN 1875-4791. doi: 10.1007/s12369-009-0019-1.

[56] C. Lenz, S. Nair, M. Rickert, A. Knoll, W. Rosel, J. Gast, A. Bannat, and F. Wallhoff. Joint-action for humans and industrial robots for assembly tasks. In *IEEE International Symposium on Robot and Human Interactive Communication*, pages 130–135. IEEE, 8 2008. ISBN 978-1-4244-2212-8. doi: 10.1109/ROMAN.2008.4600655.

[57] A. Cherubini, R. Passama, A. Crosnier, A. Lasnier, and P. Fraisse. Collaborative manufacturing with physical humanrobot interaction. *Robotics and Computer-Integrated Manufacturing*, 40:1–13, 8 2016. ISSN 0736-5845. doi: 10.1016/J.RCIM.2015.12.007.

[58] B. Mutlu, A. Terrell, and C.-M. Huang. Coordination Mechanisms in Human-Robot Collaboration. *International Conference on Human-Robot Interaction - Workshop on Collaborative Manipulation*, pages 1–6, 2013.

[59] C.-M. Huang, M. Cakmak, and B. Mutlu. Adaptive Coordination Strategies for Human-Robot Handovers. In *Robotics: Science and Systems XI*, 2015. ISBN 9780992374716. doi: 10.15607/RSS.2015.XI.031.

[60] A. Edsinger and C. C. Kemp. Human-robot interaction for cooperative manipulation: Handing objects to one another. In *IEEE International Workshop on Robot and Human Interactive Communication*, pages 1167–1172. IEEE, 2007. ISBN 1424416345. doi: 10.1109/ROMAN.2007.4415256.

[61] H. Robinson, B. MacDonald, and E. Broadbent. The Role of Healthcare Robots for Older People at Home: A Review. *International Journal of Social Robotics*, 6(4):575–591, 11 2014. ISSN 18754805. doi: 10.1007/s12369-014-0242-2.

[62] S. Yi, D. Moon, Y. Yang, and K. Kim. Healthcare robot technology development. In *The International Federation of Automatic Control*, volume 17, pages 5318–5323. Elsevier, 1 2008. ISBN 9783902661005. doi: 10.3182/20080706-5-KR-1001.0938.

[63] E. Broadbent, I. H. Kuo, Y. I. Lee, J. Rabindran, N. Kerse, R. Stafford, and B. A. MacDonald. Attitudes and Reactions to a Healthcare Robot. *Telemedicine and e-Health*, 16(5): 608–613, 6 2010. ISSN 1530-5627. doi: 10.1089/tmj.2009.0171.

[64] M. Njah and M. Jallouli. Wheelchair obstacle avoidance based on fuzzy controller and ultrasonic sensors. In *International Conference on Computer Applications Technology*, pages 423–436, 2013. ISBN 9781467352857. doi: 10.1109/ICCAT.2013.6522062.

[65] J. B. Richey and T. D. Wakefield. Motorized wheelchairs, 7 1999. URL `https://patents.google.com/patent/US6202773B1/en`.

[66] J. Pineau and A. Atrash. SmartWheeler: A robotic wheelchair test-bed for investigating new models of human-robot interaction. *AAAI Spring Symposium - Technical Report*, SS-07-07: 59–64, 2007.

[67] L. Kitagawa, T. Kobayashi, T. Beppu, and K. Terashima. Semi-autonomous obstacle avoidance of omnidirectional wheelchair by joystick impedance control. In *IEEE International Conference on Intelligent Robots and Systems*, volume 4, pages 2148–2153. IEEE, 2001. ISBN 0-7803-6612-3. doi: 10.1109/IROS.2001.976388.

[68] G. Quaglia, W. Franco, and R. Oderio. Wheelchair.q, a motorized wheelchair with stair climbing ability. *Mechanism and Machine Theory*, 46(11):1601–1609, 11 2011. ISSN 0094114X. doi: 10.1016/j.mechmachtheory.2011.07.005.

[69] H. Seki, T. Iijima, H. Minakata, and S. Tadakuma. Novel step climbing control for power assisted wheelchair based on driving mode switching. In *Industrial Electronics Conference*, pages 3827–3832. IEEE, 11 2006. ISBN 1424401364. doi: 10.1109/IECON.2006.347574.

[70] C. Gao, M. Sands, and J. R. Spletzer. Towards Autonomous Wheelchair Systems in Urban Environments. In *Field and Service Robotics*, pages 13–23. Springer, Berlin, Heidelberg, 2010. ISBN 978-3-642-13408-1. doi: 10.1007/978-3-642-13408-1_2.

[71] C. De La Cruz, T. F. Bastos, F. A. A. Cheein, and R. Carelli. SLAM-based robotic wheelchair navigation system designed for confined spaces. In *IEEE International Symposium on Industrial Electronics*, pages 2331–2336. IEEE, 7 2010. ISBN 9781424463916. doi: 10.1109/ISIE.2010.5637760.

[72] T. Taha, J. V. Miró, and G. Dissanayake. POMDP-based long-term user intention prediction for wheelchair navigation. In *IEEE International Conference on Robotics and Automation*, pages 3920–3925. IEEE, 5 2008. ISBN 9781424416479. doi: 10.1109/ROBOT.2008.4543813.

[73] D. Craig and H. Nguyen. Wireless Real-Time Head Movement System Using a Personal Digital Assistant (PDA) for Control of a Power Wheelchair. In *2005 IEEE Engineering in Medicine and Biology 27th Annual Conference*, pages 772–775. IEEE, 2005. ISBN 0-7803-8741-4. doi: 10.1109/IEMBS.2005.1616529.

[74] P. Jia, H. H. Hu, T. Lu, and K. Yuan. Head gesture recognition for handsfree control of an intelligent wheelchair. *Industrial Robot: An International Journal*, 34(1):60–68, 1 2007. ISSN 0143-991X. doi: 10.1108/01439910710718469.

[75] Q. Nguyen and S. Jo. Electric wheelchair control using head pose free eye-gaze tracker. *Electronics Letters*, 48(13):750, 2012. ISSN 00135194. doi: 10.1049/el.2012.1530.

[76] R. C. Simpson and S. P. Levine. Voice control of a powered wheelchair. *IEEE Transactions on Neural Systems and Rehabilitation Engineering*, 10(2):122–125, 6 2002. ISSN 15344320. doi: 10.1109/TNSRE.2002.1031981.

[77] M. Martins, C. Santos, A. Frizera, and R. Ceres. A review of the functionalities of smart walkers, 10 2015. ISSN 18734030. URL `http://www.ncbi.nlm.nih.gov/pubmed/26307456`.

[78] J. Shin, A. Rusakov, and B. Meyer. SmartWalker: An intelligent robotic walker. *Journal of Ambient Intelligence and Smart Environments*, 8(4):383–398, 7 2016. ISSN 18761364. doi: 10.3233/AIS-160383.

[79] R. Ranasinghe, L. Dantanarayana, A. Tran, S. Lie, M. Behrens, and L. Liu. Smart hoist: An assistive robot to aid carers. In *IEEE International Conference on Control Automation*

Robotics & Vision, pages 1285–1291. IEEE, 12 2014. ISBN 978-1-4799-5199-4. doi: 10.1109/ICARCV.2014.7064501.

[80] C. N. Schabowsky, S. B. Godfrey, R. J. Holley, and P. S. Lum. Development and pilot testing of HEXORR: Hand exoskeleton rehabilitation robot. *Journal of NeuroEngineering and Rehabilitation*, 7(1):36, 7 2010. ISSN 17430003. doi: 10.1186/1743-0003-7-36.

[81] Z. Song and S. Guo. Design process of exoskeleton rehabilitation device and implementation of bilateral upper limb motor movement. *Journal of Medical and Biological Engineering*, 32(5):323–330, 2012. ISSN 16090985. doi: 10.5405/jmbe.987.

[82] H. S. Lo and S. Q. Xie. Exoskeleton robots for upper-limb rehabilitation: State of the art and future prospects. In *Medical Engineering & Physics*, pages 261–268. Elsevier, 4 2012. ISBN 1350-4533. doi: 10.1016/j.medengphy.2011.10.004.

[83] P. Heo, G. M. Gu, S. j. Lee, K. Rhee, and J. Kim. Current hand exoskeleton technologies for rehabilitation and assistive engineering, 5 2012. ISSN 12298557. URL `http://link.springer.com/10.1007/s12541-012-0107-2`.

[84] N. Hogan, H. I. Krebs, B. Rohrer, J. J. Palazzolo, L. Dipietro, S. E. Fasoli, J. Stein, R. Hughs, W. R. Frontera, D. Lynch, and B. T. Volpe. Motions or muscles? Some behavioral factors underlying robotic assistance of motor recovery. *The Journal of Rehabilitation Research and Development*, 43(5):605, 2006. ISSN 0748-7711. doi: 10.1682/JRRD.2005.06.0103.

[85] M. G. Carmichael and D. Liu. Estimating physical assistance need using a musculoskeletal model. *IEEE Transactions on Biomedical Engineering*, 60(7):1912–1919, 7 2013. ISSN 00189294. doi: 10.1109/TBME.2013.2244889.

[86] M. G. Carmichael and D. Liu. Admittance control scheme for implementing model-based assistance-as-needed on a robot. In *International Conference of the IEEE Engineering in Medicine and Biology Society*, pages 870–873. IEEE, 7 2013. ISBN 9781457702167. doi: 10.1109/EMBC.2013.6609639.

[87] A. Bicchi, M. A. Peshkin, and J. E. Colgate. Safety for Physical HumanRobot Interaction. *Springer Handbook of Robotics*, pages 1335–1348, 2008. doi: 10.1007/978-3-540-30301-5_58.

[88] R. Alami, A. Bicchi, R. Bischoff, R. Chatila, a. D. Luca, and a. D. Santis. Safe and Dependable Physical Human-Robot Interaction in Anthropic Domains : State of the Art and Challenges. *Society*, 6(1):15, 2006. doi: 10.1.1.74.5133.

[89] A. De Santis, B. Siciliano, A. De Luca, and A. Bicchi. An atlas of physical humanrobot interaction. *Mechanism and Machine Theory*, 43(3):253–270, 3 2008. ISSN 0094114X. doi: 10.1016/j.mechmachtheory.2007.03.003.

[90] T. L. Sanders, T. Wixon, K. E. Schafer, J. Y. C. Chen, and P. A. Hancock. The influence of modality and transparency on trust in human-robot interaction. *2014 IEEE International Inter-Disciplinary Conference on Cognitive Methods in Situation Awareness and Decision Support, CogSIMA 2014*, pages 156–159, 2014. doi: 10.1109/CogSIMA.2014.6816556.

[91] T. Helldin. *Transparency for Future Semi-Automated Systems*. PhD thesis, Orebro University, 2014.

[92] T. Munzer, Y. Mollard, and M. Lopes. Impact of Robot Initiative on Human-Robot Collaboration. In *Proceedings of the Companion of the 2017 ACM/IEEE International Conference on Human-Robot Interaction - HRI '17*, pages 217–218, New York, New York, USA, 2017. ACM Press. ISBN 9781450348850. doi: 10.1145/3029798.3038373.

[93] Y. Wang and J. Vassileva. Trust and reputation model in peer-to-peer networks. In *Proceedings Third International Conference on Peer-to-Peer Computing (P2P2003)*, pages 150–157. IEEE Comput. Soc, 2003. ISBN 0-7695-2023-5. doi: 10.1109/PTP.2003.1231515.

[94] R. Mittu, D. Sofge, A. Wagner, and W. F. Lawless. *Robust intelligence and trust in autonomous systems*. Springer US, Boston, MA, 2016. ISBN 9781489976680. doi: 10.1007/978-1-4899-7668-0.

[95] M. Hoogendoorn, S. W. Jaffry, and J. Treur. An Adaptive Agent Model Estimating Human Trust in Information Sources. In *2009 IEEE/WIC/ACM International Joint Conference on Web Intelligence and Intelligent Agent Technology*, pages 458–465. IEEE, 2009. ISBN 978-0-7695-3801-3. doi: 10.1109/WI-IAT.2009.195.

[96] K. Akash, Wan-Lin Hu, T. Reid, and N. Jain. Dynamic modeling of trust in human-machine interactions. In *2017 American Control Conference (ACC)*, pages 1542–1548. IEEE, 5 2017. ISBN 978-1-5090-5992-8. doi: 10.23919/ACC.2017.7963172.

[97] J.-Y. Jian, A. M. Bisantz, and C. G. Drury. Foundations for an Empirically Determined Scale of Trust in Automated Systems. *International Journal of Cognitive Ergonomics*, 4 (1):53–71, 3 2000. ISSN 1088-6362. doi: 10.1207/S15327566IJCE0401_04.

[98] M. Madsen, M. Madsen, and S. Gregor. Measuring human-computer trust. In *Australasian Conference on Information Systems*, pages 6–8, 2000.

[99] R. Yagoda. WHAT! You Want Me to Trust a ROBOT? The Development of a Human Robot Interaction (HRI) Trust Scale. *International Journal of Social Robotics*, 4(3):235–248, 2 2011.

[100] M. Lewis, S. Katia, and P. Walker. The Role of Trust in Human-Robot Interaction. In *Foundations of Trusted Autonomy*, pages 135–159. Springer, Cham, 2018.

[101] D. A. Sanders, B. J. Sanders, A. Gegov, and D. Ndzi. Using confidence factors to share control between a mobile robot tele-operater and ultrasonic sensors. In *2017 Intelligent Systems Conference (IntelliSys)*, pages 1026–1033. IEEE, 9 2017. ISBN 978-1-5090-6435-9. doi: 10.1109/IntelliSys.2017.8324255.

[102] M. Hoogendoorn, S. W. Jaffry, P. P. Van Maanen, and J. Treur. Modelling biased human trust dynamics. *Web Intelligence and Agent Systems*, 11(1):21–40, 1 2013. ISSN 15701263. doi: 10.3233/WIA-130260.

[103] C. Basu and M. Singhal. Trust Dynamics in Human Autonomous Vehicle Interaction : A Review of Trust Models. *2016 AAAI Spring Symposium Series*, pages 85–91, 2016.

[104] J. Urbano, A. P. Rocha, and E. Oliveira. Computing confidence values: Does trust dynamics matter? *Lecture Notes in Computer Science (including subseries Lecture Notes in Artificial Intelligence and Lecture Notes in Bioinformatics)*, 5816 LNAI(2002):520–531, 2009. ISSN 03029743. doi: 10.1007/978-3-642-04686-5_43.

[105] I. D. Walker, L. Mears, R. S. M. Mizanoor, R. Pak, S. Remy, and Y. Wang. Robot-Human Handovers Based on Trust. *Proceedings - 2015 2nd International Conference on Mathematics and Computers in Sciences and in Industry, MCSI 2015*, pages 119–124, 2016. doi: 10.1109/MCSI.2015.50.

[106] B. Sadrfaridpour and Y. Wang. Collaborative Assembly in Hybrid Manufacturing Cells: An Integrated Framework for HumanRobot Interaction. *IEEE Transactions on Automation Science and Engineering*, 15(3):1178–1192, 7 2018. ISSN 1545-5955. doi: 10.1109/TASE.2017.2748386.

[107] J. Guiochet, M. Machin, and H. Waeselynck. Safety-critical advanced robots: A survey. *Robotics and Autonomous Systems*, 94:43–52, 8 2017. ISSN 0921-8890. doi: 10.1016/J.ROBOT.2017.04.004.

[108] S. Haddadin. Physical Safety in Robotics. In *Formal Modeling and Verification of Cyber-Physical Systems*, pages 249–271. Springer Fachmedien Wiesbaden, Wiesbaden, 2015. doi: 10.1007/978-3-658-09994-7_9.

[109] P. Tsarouchi, S. Makris, and G. Chryssolouris. Human-robot interaction review and challenges on task planning and programming. *International Journal of Computer Integrated Manufacturing*, 29(8):916–931, 8 2016. ISSN 13623052. doi: 10.1080/0951192X.2015.1130251.

[110] G. Charalambous, S. Fletcher, and P. Webb. Identifying the key organisational human factors for introducing human-robot collaboration in industry: an exploratory study. *The International Journal of Advanced Manufacturing Technology*, 81(9-12):2143–2155, 12 2015. ISSN 0268-3768. doi: 10.1007/s00170-015-7335-4.

[111] M. Coeckelbergh, C. Pop, R. Simut, A. Peca, S. Pintea, D. David, and B. Vanderborght. A Survey of Expectations About the Role of Robots in Robot-Assisted Therapy for Children with ASD: Ethical Acceptability, Trust, Sociability, Appearance, and Attachment. *Science and Engineering Ethics*, 22(1):47–65, 2 2016. ISSN 1353-3452. doi: 10.1007/s11948-015-9649-x.

[112] F. Ferland and A. Tapus. User profiling and behavioral adaptation for HRI: A survey. *Pattern Recognition Letters*, 99:3–12, 11 2017. ISSN 0167-8655. doi: 10.1016/J.PATREC.2017.06.002.

[113] N. Jarrassé, T. Charalambous, and E. Burdet. A framework to describe, analyze and generate interactive motor behaviors. *PloS one*, 7(11):e49945, 2012. ISSN 1932-6203. doi: 10.1371/journal.pone.0049945.

[114] a.-B. Karami, L. Jeanpierre, and A.-I. Mouaddib. Human-robot collaboration for a shared mission. *Human-Robot Interaction (HRI), 2010 5th ACM/IEEE International Conference on*, pages 155–156, 2010. doi: 10.1109/HRI.2010.5453219.

[115] P. Evrard and A. Kheddar. Homotopy switching model for dyad haptic interaction in physical collaborative tasks. *Proceedings - 3rd Joint EuroHaptics Conference and Symposium on Haptic Interfaces for Virtual Environment and Teleoperator Systems, World Haptics 2009*, pages 45–50, 2009. doi: 10.1109/WHC.2009.4810879.

[116] N. Côté, A. Canu, M. Bouzid, and A.-I. Mouaddib. Humans-Robots Sliding Collaboration Control in Complex Environments with Adjustable Autonomy. In *IEEE International Conferences on Web Intelligence and Intelligent Agent Technology*, pages 146–153, 2012.

[117] J. C. Perry, J. Rosen, and S. Burns. Upper-Limb Powered Exoskeleton Design. *IEEE/ASME Transactions on Mechatronics*, 12(4):408–417, 8 2007. ISSN 1083-4435. doi: 10.1109/TMECH.2007.901934.

[118] S. Balasubramanian, M. Perez, B. Shepard, E. Koeneman, and J. Koeneman. RUPERT: An exoskeleton robot for assisting rehabilitation of arm functions. In *2008 Virtual Rehabilitation*, pages 163–167. IEEE, 8 2008. ISBN 978-1-4244-2700-0. doi: 10.1109/ICVR.2008.4625154.

[119] T. Lenzi, N. Vitiello, S. M. M. De Rossi, S. Roccella, F. Vecchi, and M. C. Carrozza. NEUROExos: A variable impedance powered elbow exoskeleton. In *2011 IEEE International Conference on Robotics and Automation*, pages 1419–1426. IEEE, 5 2011. ISBN 978-1-61284-386-5. doi: 10.1109/ICRA.2011.5979866.

[120] M. Lohse, M. Hanheide, and H. Zender. Expectations, Intentions, and Actions in Human-Robot Interaction. *International Journal of Social Robotics*, 4(2):219, 2010.

[121] T. Iqbal and L. D. Riek. Role Distribution in Synchronous Human-Robot Joint Action. In *IEEE International Conference on Robot and Human Interactive Communication*, pages 1–4, 2014.

[122] S. Scheggi, M. Aggravi, F. Morbidi, and D. Prattichizzo. Cooperative human-robot haptic navigation. In *2014 IEEE International Conference on Robotics and Automation*

(ICRA), pages 2693–2698. IEEE, 5 2014. ISBN 978-1-4799-3685-4. doi: 10.1109/ICRA.2014.6907245.

[123] X. Lamy, F. Colledani, F. Geffard, Y. Measson, and G. Morel. Overcoming human force amplification limitations in comanipulation tasks with industrial robot. *Intelligent Control and Automation (WCICA), 2010 8th World Congress on*, pages 592–598, 2010. doi: 10.1109/WCICA.2010.5553839.

[124] D. a. Abbink, M. Mulder, and E. R. Boer. Haptic shared control: smoothly shifting control authority? *Cognition, Technology & Work*, 14(1):19–28, 11 2011. ISSN 1435-5558. doi: 10.1007/s10111-011-0192-5.

[125] J. W. Crandall, M. A. Goodrich, D. R. Olsen, and C. W. Nielsen. Validating human-robot interaction schemes in multitasking environments. *IEEE Transactions on Systems, Man, and Cybernetics Part A:Systems and Humans.*, 35(4):438–449, 2005. ISSN 10834427. doi: 10.1109/TSMCA.2005.850587.

[126] T. B. Sheridan and W. L. Verplank. Human and Computer Control of Undersea Teleoperators, 1978. URL `http://www.dtic.mil/docs/citations/ADA057655`.

[127] R. Parasuraman, T. B. Sheridan, and C. D. Wickens. A model for types and levels of human interaction with automation. *IEEE transactions on systems, man, and cybernetics. Part A, Systems and humans : a publication of the IEEE Systems, Man, and Cybernetics Society*, 30(3):286–97, 5 2000. ISSN 1083-4427.

[128] M. a. Goodrich and A. C. Schultz. Human-Robot Interaction: A Survey. *Foundations and Trends® in Human-Computer Interaction*, 1(3):203–275, 2007. ISSN 1551-3955. doi: 10.1561/1100000005.

[129] a. Phatak and G. Bekey. Model of the Adaptive Behavior of the Human Operator in Response to a Sudden Change in the Control Situation. *IEEE Transactions on Man-Machine Systems*, 10(3):72–80, 1969. ISSN 0536-1540. doi: 10.1109/TMMS.1969.299886.

[130] Y. Li, K. P. Tee, W. L. Chan, R. Yan, Y. Chua, and D. K. Limbu. Role Adaptation of Human and Robot in Collaborative Tasks. *International Conference on Robotics and Automation*, pages 5602–5607, 2015.

[131] K. W. Strabala, M. K. Lee, A. D. Dragan, J. L. Forlizzi, S. Srinivasa, M. Cakmak, and V. Micelli. Towards Seamless Human-Robot Handovers. *Journal of Human-Robot Interaction*, 2 (1):112–132, 3 2013. ISSN 21630364. doi: 10.5898/JHRI.2.1.Strabala.

[132] F. Mars, M. Deroo, and J.-M. Hoc. Analysis of human-machine cooperation when driving with different degrees of haptic shared control. *IEEE Transactions on Haptics*, 1412(c): 1–1, 2014. ISSN 1939-1412. doi: 10.1109/TOH.2013.2295095.

[133] S. Lyu and C. C. Cheah. Adaptive robot control for human-dominant interactions using a general task function. In *2016 IEEE International Conference on Real-Time Computing and Robotics, RCAR 2016*, pages 39–44. IEEE, 6 2016. ISBN 9781467389594. doi: 10.1109/RCAR.2016.7783998.

[134] N. Stefanov, A. Peer, and M. Buss. Role determination in human-human interaction. *Proceedings - 3rd Joint EuroHaptics Conference and Symposium on Haptic Interfaces for Virtual Environment and Teleoperator Systems, World Haptics 2009*, pages 51–56, 2009. doi: 10.1109/WHC.2009.4810846.

[135] B. Whitsell and P. Artemiadis. On the Role Duality and Switching in Human-Robot Cooperation: An adaptive approach. *International Conference on Robotics and Automation*, pages 3770–3775, 2015.

[136] M. Awais and D. Henrich. Human-robot collaboration by intention recognition using probabilistic state machines. *19th International Workshop on Robotics in Alpe-Adria-Danube Region (RAAD 2010)*, pages 75–80, 6 2010. doi: 10.1109/RAAD.2010.5524605.

[137] Y. Li, K. P. Tee, R. Yan, D. K. Limbu, and S. S. Ge. Shared Control of Human and Robot by Approximate Dynamic Programming. In *Acc 2015*, pages 1167–1172, 2015. ISBN 9781479986866.

[138] D. Bell, J. Borenstein, S. Levine, Y. Koren, and J. Jaros. An assistive navigation system for wheelchairs based upon mobile robot obstacle avoidance. In *Proceedings of the 1994 IEEE International Conference on Robotics and Automation*, pages 2018–2022. IEEE Comput. Soc. Press, 1994. ISBN 0-8186-5330-2. doi: 10.1109/ROBOT.1994.351167.

[139] M. B. Dias, B. Kannan, B. Browning, E. G. Jones, B. Argall, M. F. B. Dias, M. Zinck, M. M. Veloso, and A. J. Stentz. Sliding Autonomy for Peer-To-Peer Human-Robot Teams.

In *International Conference on Intelligent Autonomous Systems*, pages 332–341, 12 2008. doi: 10.3233/978-1-58603-887-8-332.

[140] J. Brookshire, S. Singh, and R. Simmons. Preliminary results in sliding autonomy for assembly by coordinated teams. In *IEEE International Conference on Intelligent Robots and Systems*, volume 1, pages 706–711. IEEE, 2004. ISBN 0-7803-8463-6. doi: 10.1109/IROS.2004.1389435.

[141] M. T. Long and R. R. Murphy. The Impact of Autonomy and Reasoning on Social Roles for Robotics. *Journal of Artificial Intelligence Research*, 1:1–10, 2006.

[142] M. Johnson, J. M. Bradshaw, P. J. Feltovich, C. M. Jonker, B. V. Riemsdijk, and M. Sierhuis. The Fundamental Principle of Coactive Design : Interdependence Must Shape Autonomy. In *Coordination, Organizations, Institutions, and Norms in Agent Systems VI*, pages 172–191. Springer International Publishing, 2011. ISBN 978-3-642-21267-3.

[143] Y. Li, K. P. Tee, R. Yan, W. L. Chan, and Y. Wu. A Framework of HumanRobot Coordination Based on Game Theory and Policy Iteration. *IEEE Transactions on Robotics*, 32(6): 1408–1418, 12 2016. ISSN 1552-3098. doi: 10.1109/TRO.2016.2597322.

[144] H. Kazerooni. Human power extender: an example of human-machine interaction via the transfer of power and information signals. *AMC'98 - Coimbra. 1998 5th International Workshop on Advanced Motion Control. Proceedings (Cat. No.98TH8354)*, pages 565–572, 1998. doi: 10.1109/AMC.1998.743598.

[145] M. Geravand, F. Flacco, and A. De Luca. Human-robot physical interaction and collaboration using an industrial robot with a closed control architecture. In *2013 IEEE International Conference on Robotics and Automation*, pages 4000–4007. IEEE, 5 2013. ISBN 978-1-4673-5643-5. doi: 10.1109/ICRA.2013.6631141.

[146] Sensitronics. ThruMode Matrix Array, 2018. URL `http://www.sensitronics.com/products-thru-mode-matrix-array.php`.

[147] F. M. Perna, K. Coa, R. P. Troiano, H. G. Lawman, C.-Y. Wang, Y. Li, R. P. Moser, J. T. Ciccolo, B. A. Comstock, and W. J. Kraemer. Muscular Grip Strength Estimates of the U.S. Population From the National Health and Nutrition Examination Survey 20112012.

Journal of Strength and Conditioning Research, 30(3):867–874, 2016. ISSN 1064-8011. doi: 10.1519/JSC.0000000000001104.

[148] R. G. Dong, J. Z. Wu, D. E. Welcome, and T. W. McDowell. A new approach to characterize grip force applied to a cylindrical handle. *Medical Engineering and Physics*, 30(1):20–33, 2008. ISSN 13504533. doi: 10.1016/j.medengphy.2007.01.002.

[149] J. W. Nicholas, R. J. Corvese, C. Woolley, and T. J. Armstrong. Quantification of hand grasp force using a pressure mapping system. *Work*, 41(SUPPL.1):605–612, 2012. ISSN 10519815. doi: 10.3233/WOR-2012-0217-605.

[150] N. J. N. J. Seo, T. J. Armstrong, and A. Arbor. Investigation of Grip Force , Normal Force , Contact Area , Hand Size , and Handle Size for Cylindrical Handles. *Human Factors: The Journal of the Human Factors and Ergonomics Society*, 50(5):734–744, 10 2008. ISSN 0018-7208. doi: 10.1518/001872008X354192.

[151] Kitronyx. Snowboard, 2018. URL `http://sites.kitronyx.com/wiki/snowboard`.

[152] E. J. Carey and T. J. Gallwey. Effects of wrist posture, pace and exertion on discomfort. *International Journal of Industrial Ergonomics*, 29(2):85–94, 2002. ISSN 01698141. doi: 10.1016/S0169-8141(01)00053-1.

[153] E. A. Kuzala and M. C. Vargo. The relationship between elbow position and grip strength. *The American journal of occupational therapy. : official publication of the American Occupational Therapy Association*, 46(6):509–512, 1992. ISSN 02729490. doi: 10.5014/ajot.46.6.509.

[154] J. Mogk and P. Keir. The effects of posture on forearm muscle loading during gripping. *Ergonomics*, 46(9):956–975, 2003. ISSN 0014-0139. doi: 10.1080/0014013031000107595.

[155] J. L. Morse, M. C. Jung, G. R. Bashford, and M. S. Hallbeck. Maximal dynamic grip force and wrist torque: The effects of gender, exertion direction, angular velocity, and wrist angle. *Applied Ergonomics*, 37(6):737–742, 2006. ISSN 00036870. doi: 10.1016/j.apergo.2005.11.008.

[156] T. Feix, J. Romero, H. B. Schmiedmayer, A. M. Dollar, and D. Kragic. The GRASP Taxonomy of Human Grasp Types. *IEEE Transactions on Human-Machine Systems*, 46(1): 66–77, 2015. ISSN 21682291. doi: 10.1109/THMS.2015.2470657.

[157] H. Forssberg, A. C. Eliasson, H. Kinoshita, R. S. Johansson, and G. Westling. Development of human precision grip I: Basic coordination of force. *Experimental Brain Research*, 85 (2):451–457, 1991. ISSN 00144819. doi: 10.1007/BF00229422.

[158] E. S. Robinson. *Work of the Integrated Organism.* Clark University Press, Worcester, MA, 1934.

[159] A. W. Y. Ng and A. H. S. Chan. Finger Response Times to Visual, Auditory and Tactile Modality Stimuli. *Proceedings of the International MultiConference of Engineers and Computer Scientists*, II:1449–1454, 2012. ISSN 20780958.

[160] R. C. Luo and Y.-C. Wu. Hand gesture recognition for Human-Robot Interaction for service robot. *2012 IEEE International Conference on Multisensor Fusion and Integration for Intelligent Systems (MFI)*, pages 318–323, 2012. doi: 10.1109/MFI.2012.6343059.

[161] N. Li, S. Wei, M. Wei, and B. Liu. Hand Motion Recognition Based on Pressure Distribution Maps and LS-SVM. In *International Conference on Mechatronics and Control*, pages 1027–1031, 2014. ISBN 9781479925384.

[162] H. Wu, H. Liu, and D. Liu. Two-Dimensional Direction Recognition Using Uniaxial Tactile Arrays. *IEEE Sensors Journal*, 13(12):4897–4903, 12 2013. ISSN 1530-437X. doi: 10.1109/JSEN.2013.2277736.

[163] C.-C. Chang and C.-J. Lin. LIBSVM: a library for support vector machines, 2001. URL `https://www.csie.ntu.edu.tw/~cjlin/libsvm/`.

[164] D. Wang, L. Shi, D. S. Yeung, P.-A. Heng, T.-T. Wong, and E. C. C. Tsang. Support vector clustering for brain activation detection. *Medical image computing and computer-assisted intervention : MICCAI ... International Conference on Medical Image Computing and Computer-Assisted Intervention*, 8(Pt 1):572–579, 2005. ISSN 0003-6951. doi: 10.1162/15324430260185565.

[165] G. E. Box and G. C. Tiao. *Bayesian Inference in Statistical Analysis*. John Wiley & Sons, Inc., Hoboken, NJ, USA, 4 1992. ISBN 9781118033197. doi: 10.1002/9781118033197.

[166] L. Zhang, S. Lyu, and J. Trinkle. A dynamic Bayesian approach to real-time estimation and filtering in grasp acquisition. *Robotics and Automation (ICRA), 2013 IEEE International Conference on*, pages 85–92, 2013. ISSN 1050-4729. doi: 10.1109/ICRA.2013.6630560.

[167] Y. Bekiroglu, D. Song, L. Wang, and D. Kragic. A probabilistic framework for task-oriented grasp stability assessment. *Proceedings - IEEE International Conference on Robotics and Automation*, pages 3040–3047, 2013. ISSN 10504729. doi: 10.1109/ICRA.2013.6630999.

[168] I. T. Jolliffe. Principal component analysis. *Applied Optics*, 44(May):6486, 2005. doi: 10.1007/SpringerReference_205537.

[169] C. Isbell and M. Littman. Introduction to Principal Component Analysis (PCA), 2014. URL `http://www.lauradhamilton.com/introduction-to-principal-component-analysis-pca`.

[170] J. Park and J. Cheong. Analysis of collective behavior and grasp motion in human hand. *2010 International Conference on Control, Automation and Systems (ICCAS)*, pages 2514–2518, 2010.

[171] N. M. Kakoty and S. M. Hazarika. Recognition of grasp types through principal components of DWT based EMG features. *IEEE ... International Conference on Rehabilitation Robotics : [proceedings]*, 2011:5975398, 2011. ISSN 1945-7901. doi: 10.1109/ICORR.2011.5975398.

[172] M. E. Payton, M. H. Greenstone, and N. Schenker. Overlapping confidence intervals or standard error intervals: What do they mean in terms of statistical significance? *Journal of Insect Science*, 3(1), 1 2003. ISSN 1536-2442. doi: 10.1093/jis/3.1.34.

[173] P. Koehn. Statistical significance tests for machine translation evaluation. *Proceedings of the Conference on Empirical Methods in Natural Language Processing*, 4:388–395, 2004. doi: 10.1145/2063576.2063688.

[174] M. N. Nounou, B. R. Bakshi, P. K. Goel, and X. Shen. Bayesian principal component analysis. *Journal of Chemometrics*, 16(11):576–595, 11 2002. ISSN 08869383. doi: 10.1002/cem.759.

[175] T. Howley, M. G. Madden, M.-L. OConnell, and A. G. Ryder. The effect of principal component analysis on machine learning accuracy with high-dimensional spectral data. *Knowledge-Based Systems*, 19(5):363–370, 2006. ISSN 09507051. doi: 10.1016/j.knosys.2005.11.014.

[176] M. J. Hoozemans and J. H. van Dieën. Prediction of handgrip forces using surface EMG of forearm muscles. *Journal of Electromyography and Kinesiology*, 15(4):358–366, 2005. ISSN 10506411. doi: 10.1016/j.jelekin.2004.09.001.

[177] J. Duque, D. Masset, and J. Malchaire. Evaluation of handgrip force from EMG measurements. *Applied ergonomics*, 26(1):61–66, 1995. ISSN 00036870. doi: 10.1016/0003-6870(94)00003-H.

[178] R. S. Johansson, C. Häger, and R. Riso. Somatosensory control of precision grip during unpredictable pulling loads: I Changes in load force amplitude. *Experimental Brain Research*, 89(1):181–191, 4 1992. ISSN 0014-4819. doi: 10.1007/BF00229016.

[179] R. S. Johansson, C. Häger, R. Riso, C. Häger, L. Bäckström, and R. Riso. Somatosensory control of precision grip during unpredictable pulling loads: II Changes in load force rate. *Experimental Brain Research*, 89(1):192–203, 4 1992. ISSN 0014-4819. doi: 10.1007/BF00229016.

[180] M. G. Carmichael, B. Moutrie, and D. Liu. A framework for task-based evaluation of robotic coworkers. In *IEEE International Conference on Control Automation Robotics & Vision*, pages 1362–1367. IEEE, 12 2014. ISBN 978-1-4799-5199-4. doi: 10.1109/ICARCV.2014.7064514.

[181] Sensoray - Embedded Electronics. Analog I/O Module — Model 2608, 2018. URL `http://www.sensoray.com/Ethernet_16_analog_input_2608.htm`.

[182] R. S. Johansson. How Is Grasping Modified by Somatosensory Input? In *Motor Control: Concepts and Issues*, pages 331–355, 1991. ISBN 0471929190. doi: doi=10.1.1.570.8128.

[183] G. Horton, V. Kulkarni, D. Nicol, and K. S. Trivedi. {F}luid {S}tochastic {P}etri nets: {T}heory, {A}pplication and {S}olution. *European Journal of Operational Research*, 105 (97):184–201, 1998.

[184] K. Wolter and A. Zisowsky. On Markov reward modelling with FSPNs. *Performance Evaluation*, 44(1-4):165–186, 2001. ISSN 01665316. doi: 10.1016/S0166-5316(00)00056-0.

[185] C. M. Jonker and J. Treur. Formal analysis of models for the dynamics of trust based on experiences. *Lecture Notes in Computer Science (including subseries Lecture Notes in Artificial Intelligence and Lecture Notes in Bioinformatics)*, 1647:221–231, 1999. ISSN 16113349. doi: 10.1007/3-540-48437-X_18.

[186] Center for Autonomous Systems University of Technology Sydney. ANBOT - From the lab to the workplace - YouTube, 2018. URL `https://goo.gl/FdemnJ`.

[187] M. G. Carmichael and D. Liu. Estimating physical assistance need using a musculoskeletal model. *IEEE Transactions on Biomedical Engineering*, 60(7):1912–1919, 2013. ISSN 00189294. doi: 10.1109/TBME.2013.2244889.

[188] T. Yoshikawa. Manipulability of Robotic Mechanisms. *The International Journal of Robotics Research*, 4(2):3–9, 6 1985. ISSN 0278-3649. doi: 10.1177/027836498500400201.

[189] International Organization for Standardization. *Robots and robotic devices – Safety requirements for industrial robots - Part 2: Robot systems and integration*. International Organization for Standardization, 2011. URL `https://www.iso.org/standard/41571.html`.

[190] Transport for New South Wales. Motorised Wheelchairs, 2017. URL `http://roadsafety.transport.nsw.gov.au/stayingsafe/pedestrians/motorisedwheelchairs/`.

[191] R. W. Bohannon. Comfortable and maximum walking speed of adults aged 20 - 79 years: reference values and determinants. *Age and Ageing*, 26(1):15–19, 1997. ISSN 0002-0729. doi: 10.1093/ageing/26.1.15.

[192] H. C. Wu and M. J. J. Wang. Relationship between maximum acceptable work time and physical workload. *Ergonomics*, 45(4):280–289, 3 2002. ISSN 00140139. doi: 10.1080/00140130210123499.

[193] N. Stylopoulos and D. Rattner. Robotics and ergonomics, 12 2003. ISSN 00396109. URL `http://www.ncbi.nlm.nih.gov/pubmed/14712869`.

[194] P. Examiner and B. L. Eland. Ergonomic Handle, 10 2011. URL `https://patents.google.com/patent/US20100018007A1/en`.

[195] P. Examiner and B. L. Eland. Ergonomic Handle, 10 2011. URL `https://patents.google.com/patent/US7028581B2/en`.

[196] International Organization for Standardization. ISO 10218:2011. Robots and robotic devices - Safety requirements for industrial robots. *ISO International Standard*, 2011, 2011.

[197] TakkTile. TakkStrip - TakkTile, 2018. URL `http://www.takktile.com/product:takkstrip`.

[198] C. Reeks, M. G. Carmichael, Dikai Liu, and K. J. Waldron. Angled sensor configuration capable of measuring tri-axial forces for pHRI. In *2016 IEEE International Conference on Robotics and Automation (ICRA)*, pages 3089–3094. IEEE, 5 2016. ISBN 978-1-4673-8026-3. doi: 10.1109/ICRA.2016.7487475.

[199] D. Welcome, S. Rakheja, R. Dong, J. Z. Wu, and a. W. Schopper. An investigation on the relationship between grip, push and contact forces applied to a tool handle. *International Journal of Industrial Ergonomics*, 34(6):507–518, 2004. ISSN 01698141. doi: 10.1016/j.ergon.2004.06.005.

[200] M. Kouchi, N. Miyata, and M. Mochimaru. An Analysis of Hand Measurements for Obtaining Representative Japanese Hand Models. In *Digital Human Modeling for Design and Engineering Symposium*, pages 1–7, Japan, 6 2005. ISBN 2005012734. doi: 10.4271/2005-01-2734.

[201] C. S. Edgren, R. G. Radwin, and C. B. Irwin. Grip Force Vectors for Varying Handle Diameters and Hand Sizes. *Human Factors: The Journal of the Human Factors and Ergonomics Society*, 46(2):244–251, 6 2004. ISSN 0018-7208. doi: 10.1518/hfes.46.2.244.37337.

[202] R. S. Guerra, I. Fonseca, F. Pichel, M. T. Restivo, and T. F. Amaral. Hand length as an alternative measurement of height. *European Journal of Clinical Nutrition*, 68(2):229–233, 2 2014. ISSN 09543007. doi: 10.1038/ejcn.2013.220.

[203] D. P. Bhatnagar, S. P. Thapar, and M. K. Batish. Identification of personal height from the somatometry of the hand in Punjabi males. *Forensic Science International*, 24(2):137–141, 2 1984. ISSN 03790738. doi: 10.1016/0379-0738(84)90093-8.

[204] M. B. Mathur and D. B. Reichling. An uncanny game of trust. In *Proceedings of the 4th ACM/IEEE international conference on Human robot interaction - HRI '09*, page 313, New York, New York, USA, 2009. ACM Press. ISBN 9781605584041. doi: 10.1145/1514095.1514192.

[205] S. Nikolaidis, S. Nath, A. D. Procaccia, and S. Srinivasa. Game-Theoretic Modeling of Human Adaptation in Human-Robot Collaboration. *Proceedings of the 2017 ACM/IEEE International Conference on Human-Robot Interaction - HRI '17*, pages 323–331, 2017. ISSN 21672148. doi: 10.1145/2909824.3020253.

[206] R. Spica, D. Falanga, E. Cristofalo, E. Montijano, D. Scaramuzza, and M. Schwager. A Real-Time Game Theoretic Planner for Autonomous Two-Player Drone Racing. In *Robotics: Science and Systems*, pages 1–9, 1 2018.

[207] L. Peternel, T. Petric, S. Gopinathan, S. K. Ötting, and J. J. Steil. a User study on Personalized stiffness control and Task specificity in Physical humanrobot interaction. *Front. Robot. AI*, 4(4), 2017. doi: 10.3389/frobt.2017.00058.